Current Research and Development in Chemistry
Vol. 4

Book Publisher International

Current Research and Development in Chemistry

Vol. 4

Current Research and Development in Chemistry

Vol. 4

India ▪ United Kingdom

Book Publisher International

Editor(s)

Dr. Syed A. A. Rizvi

Assistant Professor,
Department of Pharmaceutical Sciences, Nova Southeastern University, USA and
Department of Pharmaceutical Sciences, Hampton University School of Pharmacy, USA.
Email: srizvi@nova.edu, syed.rizvi@hamptonu.edu;

FIRST EDITION 2020

ISBN 978-93-90206-41-4 (Print)
ISBN 978-93-90206-42-1 (eBook)
DOI: 10.9734/bpi/crdc/v4

© Copyright (2020): Authors. The licensee is the publisher (Book Publisher International).

Contents

Preface i

Chapter 1 1-23
Study on the Adsorption of Pb, Zn, Cu, Ni, and Cd by Modified Ligand in a Single Component Aqueous Solution: Equilibrium, Kinetic, Thermodynamic, and Desorption Studies
E. Igberase, P. Osifo and A. Ofomaja

Chapter 2 24-38
Substituent, Temperature and Solvent Effects on the Keto-Enol Equilibrium in β-Ketoamides: An NMR and Theoretical Study
Diego D. Colasurdo, Patricia E. Allegretti and Sergio L. Laurella

Chapter 3 39-51
Recent Observations on Preparation of Novel Chitosan-Starch Blends as a Multi-function Thickening Agent and Their Application in Textile Printing
E. S. Abdou, H. M. El-Hennawi and K. A. Ahmed

Chapter 4 52-65
Research on Efficient One Pot Synthesis of TiO_2-induced Nanoparticles via Microwave Irradiation and Its Application in Cotton Dyeing with Some Acid Dyes
N. S. Elshemy, S. A. Mahmoud, H. M. Mashaly and K. Haggag

Chapter 5 66-76
Cu^{II} Complexes with (2-benzylidenehydrazinyl)- 4-Phenylthiazole Ligands: An Experimental and Theoretical Study
Emanoel Hottes, Thiago Moreira Pereira, Arthur Eugen Kummerle, Amanda Porto Neves, Clarissa Oliveira da Silva and Marcelo H. Herbst

Chapter 6 77-101
Acetamide Derivatives of N-Methyl-4-Hydroxyaniliniumsulfate: Design, Synthesis, Spectral Characterization and in silico Study to Report them as Therapeutic Agents
Misbah Irshad, Muhammad Athar Abbasi and Aziz-Ur-Rehman

Chapter 7 102-111
Critical Research on Enhancement of the Inhibitor Efficiency of 4-Phenyl-1,2-dithiol-3-thione on Corrosion of Mild Steel for 20% Sulphuric Acid
M. Dakmouche, M. Saidi, M. Hadjadj, M. Yousfi and Z. Rahmani

Chapter 8 112-124
The Use of Spectrophotometric and Thermodynamic Methods for the Determination of Glibenclamide
Nwanisobi Gloria and Ukoha Pius

Chapter 9 125-134
Studies on the Characterisation, Phytochemical and Functional Groups Assay of a Tropical Timber (Bombax brevicuspe) Stem
I. P. Udeozo, C. M. Ejikeme, A. N. Eboatu and H. I. Kelle

Chapter 10 135-142
Studies on the Characterisation of Poly blend-Nanofilms of Cellulose Acetate and Poly Styrene
S. Srilalitha and K. N. Jayaveera

Chapter 11 143-161
Investigation on in vitro Evaluation of Antioxidant and Anti-inflammatory Properties of Methanol and Dichloromethane Extracts of the Leaf of Globimetula oreophila
Esther O. Faboro, Idowu J. Olawuni, Bolajoko A. Akinpelu, Oluokun O. Oyedapo, Ezekiel O. Iwalewa and Craig A. Obafemi

Chapter 12 162-170
Studies on UV Spectrophotometric Analysis of Drugs Terbinafine Hydrochloride and Clarithromycin
R. Mrutyunjaya Rao and C. S. P. Sastry

Chapter 13 171-177
Recent Research on Kinetics and Mechanism of Oxidation of Ethyl Diethylene Glycol by Ce(IV) Catalyzed by Ir(III) in Aqueous Sulphuric Acid Media
Kamini Singh, Ashish Kumar Singh, Jaya Jaiswal and R. A. Singh

Chapter 14 178-182
Application of Antioxidants as Effective Remedies at Hepatotoxic Action of Carbon Tetrachloride
Karlen Hovnanyan, Vardan Mamikonyan, Anahit Margaryan, Kristine Sargsyan, Margarita Hovnanyan, Maria Karagyozyan and Konstantin Karageuzyan

Preface

This book covers key areas of Research and Development in Chemistry. The contributions by the authors include Adsorption, aqueous solution, equilibrium, kinetic, thermodynamic, ß-Ketoamides, keto-enol equilibrium, NMR spectroscopy, theoretical calculations, Solvent Effects, p(x)-Laplacian equation, existence, uniqueness, numerical blow-up, variable exponents, difference method, Chitosan-Starch Blends, Multi-function Thickening Agent, Textile Printing, hiazole, Cu II complexes, EPR, conformational analysis, (2-benzylidenehydrazinyl)- 4Phenylthiazole Ligands, Titanium di-oxide, nanoparticles, cotton treatment, microwave heating, antimicrobial, self-cleaning, 2,3-Dihydro-1,4-benzodioxin-6-amine, antibacterial activity, enzyme inhibition, planetol, Therapeutic Agents, Acid, corrosion, inhibition, dithiole thione, mild steel, electrochemical impedance spectroscopy, 4-Phenyl-1,2-dithiol-3-thione, Glibenclamide, spectrophotometry, thermodynamics, charge transfer, DDQ, Bombax brevicuspe, tropical timber, thermal characteristics, phytochemical and functional groups, Polymeric materials, blending technique, cellulose acetate, polystyrene, SEM analysis, phase morphology, Antioxidant, membrane stabilization, anti-inflammatory, red blood cells, G. oreophila, Methanol and Dichloromethane Extract, Terbenafine hydrochloride, clarithromycin, spectrophotometer and picric acid Analysis of Drugs, Kinetics, mechanism, oxidant Ce(IV), ethyl diethylene glycol, Ir(III) catalyst and suplhuric acid, CCl4, GSE, a-tocopherol, ultrastructural changes, intoxicated hepatocytes, electron microscopy etc. This book contains various materials suitable for students, researchers and academicians in the field of Research and Development in Chemistry.

Chapter 1
Print ISBN: 978-93-90206-41-4, eBook ISBN: 978-93-90206-42-1

Study on the Adsorption of Pb, Zn, Cu, Ni, and Cd by Modified Ligand in a Single Component Aqueous Solution: Equilibrium, Kinetic, Thermodynamic, and Desorption Studies

E. Igberase[1*], P. Osifo[1] and A. Ofomaja[1]

DOI: 10.9734/bpi/crdc/v4

ABSTRACT

In this investigation, an amino functionalized adsorbent was developed by grafting 4-aminobenzoic acid onto the backbone of cross-linked chitosan beads. The 3 sets of beads including chitosan (CX), glutaraldehyde cross-linked chitosan (CCX), and 4-aminobenzoic acid grafted cross-linked chitosan (FGCX) were characterized by FTIR, XRD, SEM, and TGA. The water content and amine concentration of FGCX were determined. The effect of adsorption parameters was studied and the optimum was used for further studies. Equilibrium data was obtained from the adsorption experiment carried out at different initial concentration; the data were applied in isotherm, thermodynamics, and kinetic studies. The Langmuir and Dubinin-Kaganer-Radushkevich (DKR) models were successful in describing the isotherm data for the considered metal ions while the Freundlich and Temkin model fit some of the considered metal ions. Pseudo-second-order and intraparticle model described the kinetic data quite well. Thermodynamic parameters such as Gibb's free energy change ($\Delta G°$), enthalpy change ($\Delta H°$), and entropy change ($\Delta S°$) were calculated and the results showed that the adsorption of Pb, Cu, Ni, Zn, and Cd ions onto FGCX is spontaneous and endothermic in nature. Regeneration of the spent adsorbent was efficient for the considered metal ions.

Keywords: Adsorption; aqueous solution; equilibrium; kinetic; thermodynamic.

1. INTRODUCTION

Metals used across chemical, electroplating, leather, tan-nery, galvanizing, mining, pigment, and dye industries are regarded as the major toxic unbiodegradable elements present in the world today. This becomes a treat as the industrial effluents containing a reasonable amount of harm-ful metal ions are discharged into the environment without possible remediation which resulted in environmental issues; hence the environmental protection agency (USEPA) has considered certain metals as carcinogenic and bioaccumula-tive element. Among the most toxic metals are Cu, Cd, Pb, Zn, and Ni. These metals have been reported by researchers to have negative health effect on humans, aquatic life, plant, and the environment at large [1–4]. Various techniques have been applied for the removal of metal ions from industrial wastewaters including chemical precipitation, membrane separation, reverse osmosis, ion exchange, and nanofiltration [5] These methods can be applied alone or integrating more than one method together, such as chemical precipitation prior to nanofiltration [1]. This procedure has been reported to be disadvantaged due to incomplete removal, high energy requirements, and production of toxic waste sludge which needs to be treated and disposed [6]. Recently, researchers have developed a more cost effective method to reduce or completely remove the metal ions to its allowable limit as given by USEPA. T hus, increasing the quality of the treated wastewater. Adsorption has proven to be of high standard due to its simple design and operation, low

[1]*Department of Chemical Engineering, Vaal University of Technology, Private Mail Bag X021, Vanderbijlpark 1900, South Africa.*
**Corresponding author: E-mail: mychoice2009@yahoo.com;*

cost, effectiveness, and outstanding chelating behaviour and can be regenerated by some desorption techniques [7–9].

However, in providing cheaper and cleaner technology for the treatment of wastewater with toxic metal ions, chitosan is considered the solution. Chitosan is a derivative of N-deacetylation of chitin and chitin is a naturally occurring polysaccharide found in crustacean and microbial biomass [8]. The presence of amine ($–NH_2$) and hydroxyl functional group in the back bone of chitosan gives the polymer its distinctive adsorption quality. Amine groups are mainly responsible for the binding of Cu, Cd, Pb, Zn, and Ni cations as shown in

$$-NH_3^+ + M^{2+} \rightarrow NH_3M^{2+} + H^+ \quad (1)$$

However, the adaptability of chitosan allows the polymer to be simply modified; hence, chemical modification techniques such as cross-linking and grafting become necessary. Cross-linking happens when a chemical or compound referred to as the cross-linker makes intermolecular covalent bridge between chains (Fig. 1). The mechanism involves the for-mation of Schiff base via nucleophilic attack by the nitrogen of the amino group (from chitosan) on the carbon of the glutaraldehyde which displaces the oxygen of the aldehyde resulting in the C=N bond [10]. Cross-linking results in insolubility as the chains are attached together by strong covalent bond [11]. Consequently, cross-linking also has its short comings. Authors such as Gyananath and Balhal [12] and Igberase et al. [5] reported that cross-linking reduces the adsorption capacity of adsorbents Table 2; hence grafting of some functionality onto the cross-linked material becomes important. Grafting of chitosan allows the formation of functional derivatives by covalent binding of a molecule onto chitosan backbone. Fig. 2 shows the proposed grafting reaction of 4-aminobenzoic acid onto cross-linked chitosan. However, in this Figure the grafting material binds to the amino and hydroxyl group in the polymeric chain leading to a large number of adsorption sites.

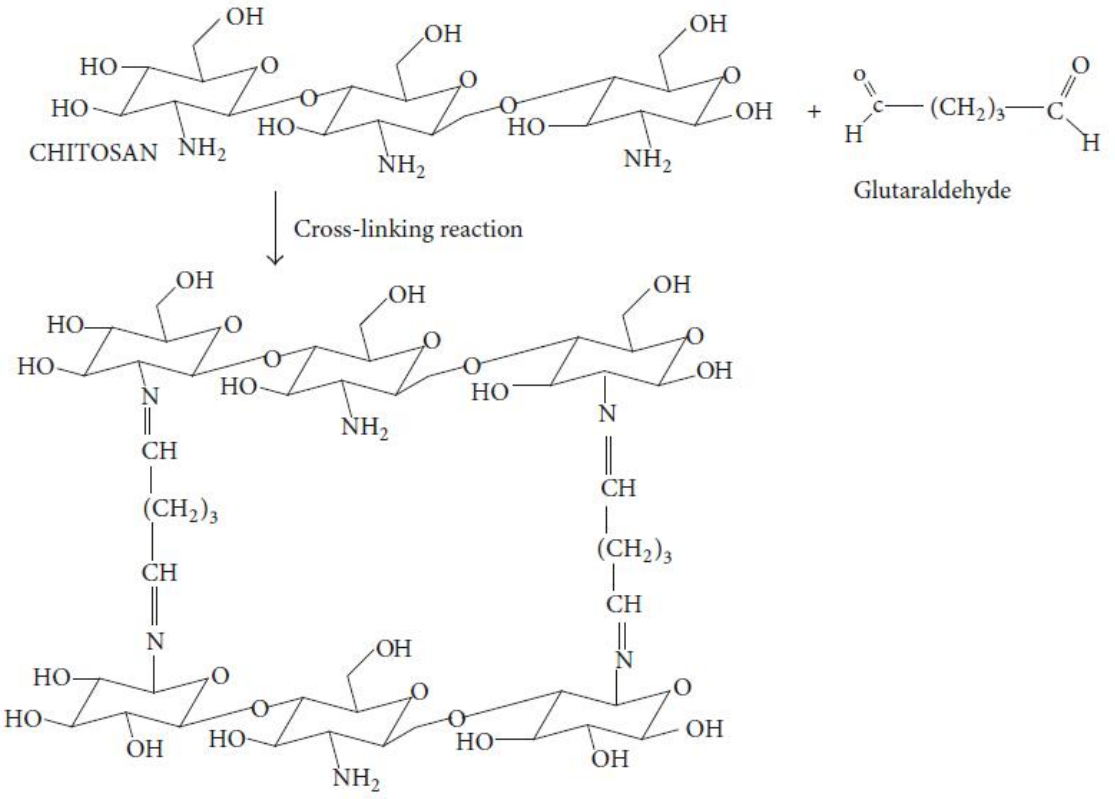

Fig. 1. Schematic representation of the cross-linking process of chitosan

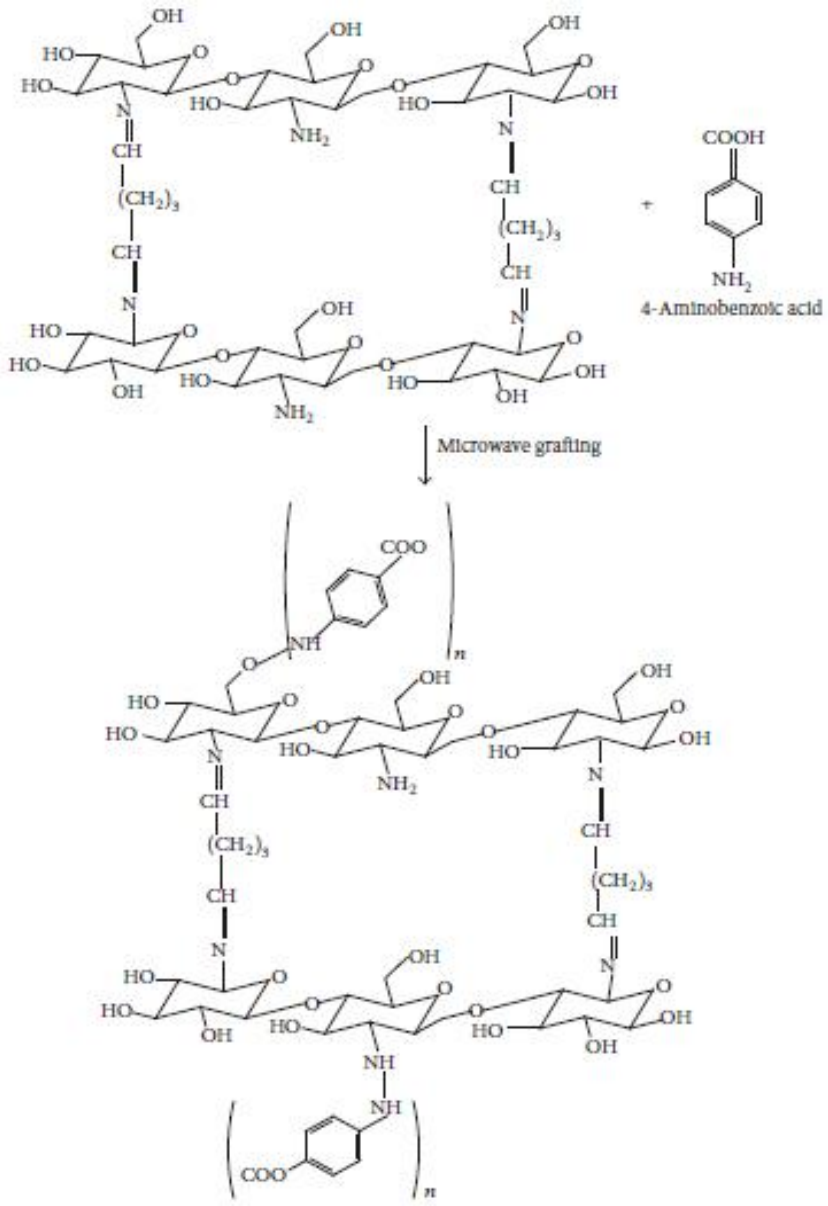

Fig. 2. Schematic representation of the proposed structure of the grafting process of the cross-linked chitosan beads

The focus of this study is to consider the possible appli-cation of a modified ligand for the effective removal of metal ions in batch mode. On this note, chitosan solution was cross-linked with 2.5% glutaraldehyde concentration (Fig. 1). The cross-linked solution was used in preparing the beads and then grafted with 4-aminobenzoic acid to produce FGCX (Fig. 2). The water content amine concentration in the developed ligand was determined. The beads were characterized by Fourier transform infrared spectroscopy (FTIR), X-ray diffraction (XRD), thermogravimetric analysis (TGA), and scanning electron microscope (SEM) to provide evidence of successful modification process. The effect of adsorp-tion parameters on the binding of metal ions onto FGCX was investigated. FGCX was used in adsorption studies. Adsorption/desorption studies were investigated in others to determine the cost effectiveness of the produced FGCX.

2. EXPERIMENTAL

2.1 Materials and Equipment

Materials used in this study were of analytical grade. Chitosan powder with a degree of deacetylation of 74% was obtained from China. The powder was used in preparing chitosan beads. Glutaraldehyde and 4-amino-benzoic acid (>99.5%) were purchased from Sigma-Aldrich. Domestic oven was used in the grafting of the cross-linked beads. Hydrochloric acid (>99%), acetic acid (>99%), and sodium hydroxide (>99%) were all purchased from Sigma-Aldrich. The pH of the solution was adjusted with a pH meter (Hanna HI 8421) and was purchased from Sigma-Aldrich. Distilled water was produced with a pure water distiller (Ultima 888 water distiller) in the school laboratory. A shaker (labcon incubator) was used for adsorption studies.

Atomic adsorption spectrophotometer (Varian SpectrAA-10) was applied in determining the amount of metal ions adsorbed.

2.2 Adsorbate Preparation

The stock solutions of Cu^{2+}, Cd^{2+}, Zn^{2+}, Pb^{2+}, and Ni^{2+} were obtained by separately preparing a calculated mass of $CuSO_4{\cdot}5H_2O$, $CdCl_2 \cdot H_2O$, $Zn(NO_3)_2{\cdot}6H_2O$, $Pb(NO_3)_2$, and $NiSO_4{\cdot}6H_2O$. This stock solution produced was again diluted with distilled water to obtain the relevant initial concentrations of 0.5 to 2.5 mmol/l.

2.3 Preparation of Ligand and Possible Modification

Chitosan solution was prepared by dissolving 30 g of chitosan powder in 1 L of 5.0% (v/v) acetic acid solution. The dissolved solution was mixed with 2.5% glutaraldehyde solution and stirred with a magnetic stirrer for 2 hrs in others to achieve cross-linking reaction. The cross-linked solution was then passed through a glass pipette with the aid of a peristaltic pump to a 1 M solution of sodium hydroxide; this proce-dure results in the formation of glutaraldehyde-cross-linked chitosan gel beads. The gel beads were rinsed with distilled water several times to remove any residue sodium hydroxide. T he beads produced by this method have mean diameter of 3.3 mm. Consequently, the cross-linked beads were grafted by microwave irradiation. This was actualised by mixing 4 g of the cross-linked beads in 0.1 g/l of 4-aminobenzoic acid in an open neck flask. This flask was then placed in a domestic microwave oven with a medium-low power for 20 mins.

The grafted-cross-linked beads were again rinsed with distilled water and ready to be applied for studies. The water content (W_c) present in the FGCX was determine using

$$W_c = \frac{W_1 - W_2}{W_2}, \tag{2}$$

where W_1 and W_2 denote the weights of wet FGCX and dry FGCX, respectively.

2.4 Determination of Amine Concentration of the Grafted-Cross-Linked Beads

10.0 g of the grafted cross-linked beads was weighed and ground with an 18mm Teflon pestle; the grounded beads were mixed with distilled water up to a 100 ml.The solutionwas stirred continuously with amagnetic stirrer and titrated with 1M of HCl. The pH of the solution was recorded at time interval; the result obtained from the experiment was used to determine the amine concentration in mmol/g of adsorbent.

2.5 Characterization of the Beads

Approximately 1.0 g of CX, CCX, and FGCX was separately weighed and oven dried at 60°C and blended to its powdered form. The infrared measurement was done with a Shimadzu FTIR model 8300 Kyoto, Japan; the spectra were recorded in the range of 500–4000 cm^{-1}. The crystallinity of the beads was studied with a Shimadzu XRD model 7000; the intensities were recorded in the range of

10–90° (2θ). The weight loss of the beads at different temperatures was studied with a Shimadzu TGA 8000 Japan.

The SEM analysis was done by separately bisecting CX, CCX, and FGCX in other to get a distinct vision of the inner fibres. The bisected beads were then coated with gold and the morphology of the coated beads was studied with a Jeol 733 super probe.

2.6 Adsorption Studies

A known mass of FGCX was transferred into a series of Erlenmeyer flasks; then samples of 100mL having a known concentration were measured into each flask. The pH of the samples was adjusted by 0.1M HCl and 0.1M NaOH. The effect of adsorption parameters was observed under the following conditions: pH (2–8), contact time (10–80) min, initial concentration (0.5–2.5)mmol/L, adsorbent dosage (2–10) g/L, temperature (25–55)°C, and ionic strength (0.05–0.2) M. The experiment was carried out in duplicate and the average result was shown in this study.

Isotherm studies were carried out by transferring 6 g/L of FGCX, separately into a series of 250mL Erlenmeyer flasks; each of the flaskswas filled with 100mL of eachmetal solution with different initial concentrations of 0.5–2.5mmol/L and at temperature of 45°C. These initial concentrations were prepared from a stock solution and then adjusted to optimum pH. In other to attain equilibrium, the Erlenmeyer flasks were placed in a labcon incubator for 60 min; the agitation speedwas at 150rpm.Thermodynamics was carried out at an initial concentration of 0.5mmol/L. Kinetics was investigated upon by mixing 6 g/L of FGCX with 100mL of metal ions solution in a series of 250mL Erlenmeyer flasks having initial concentration of 0.5mmol/L. In order to attain equilibrium, the Erlenmeyer flasks were placed in a labcon incubator, the solution was shaken at 150rpm, and the temperature was fixed at 45°C. Samples were taken at interval of 10–60 min and analysed for metal ions removal. This procedure was observed for Pb, Cu, Ni, Cd, and Zn.

To determine the amount of metal ion adsorbed, the equilibrium adsorption capacity was calculated from the mass balance equation as shown in

$$q_e = \frac{(C_o - C_e)\,XV}{M}, \tag{3}$$

where q_e (mmol/g) is the equilibrium adsorption capacity, C_o and C_e are the initial and equilibriumconcentration (mmol/l) of heavy metal ion in solution, respectively, while V (mL) is the volume and M (g) is the weight of the adsorbent. The percentage removal of metal ions from the single component mixture was calculated by

$$\%\,R\ = \frac{(C_o - C_e)}{C_o} \times\ 100. \tag{4}$$

2.7 Theory of Evaluation of Data

2.7.1 Isotherm model

Equilibrium is reached when the capacity of the binding material is achieved and the rate of binding corresponds with the rate of desorption [12]. Basically, the binding capacity of an adsorbent can be obtained from isotherms such as Langmuir, Freundlich, Temkin, and DKR model. The constants from the model are measures of binding capacity of adsorbent for the considered metal ions.

The Langmuir model is based on the fact that every adsorption site is identical and energetically equivalent and assumes that the adsorption occurs at specific homogeneous sites on the adsorbent and this is used successfully in monolayer adsorption processes [13]. Thismodel is described in the linear form in

$$\frac{C_e}{q_e} = \frac{C_e}{Q_m} + \frac{1}{Q_m K_L} \quad \text{(Linear form)} \tag{5}$$

The Langmuir constant Q_m (mmol/g) represents the maximum adsorption capacity and K_L (l/mmol) relates to the rate of adsorption. Higher values of K_L indicate much stronger affinity of metal ion adsorption [14]. The parameters of the Langmuir model can be estimated from the slope and intercepts of C_e/q_e versus C_e. The basic characteristics of Langmuir model can be shown in terms of a dimensionless constant known as separation factor (R_L) which is used to project if an adsorption systemis favourable or not favourable [15], as shown in (6).Theconditions of R_L > 1, R_L = 1 and R_L between 0 and 1 signify unfavourable, linear, and favourable, respectively,

$$R_L = \frac{1}{1 + K_L C_O}. \tag{6}$$

The empirical Freundlich isotherm is based on the equilibrium relationship between heterogeneous surfaces. This isotherm is derived from the assumption that the adsorption sites are distributed exponentially with respect to the heat of adsorption [16].This model is described in the linear form in

$$log\ q_e = log\ K_F + \frac{1}{n}\ log\ C_e \text{ (Linear form)}. \tag{7}$$

K_F and n are constants representing the adsorption capacity and adsorption intensity, respectively. The parameters of this model can be calculated from the slope and intercepts of $log\ q_e$ versus $log\ C_e$ plot; under normal adsorption conditions, the values of n should be in the range of 1 to 10 [17].

The derivation of the Temkin model is based on the heat of adsorption of metal ions which assumes the relationship between metal ions and adsorbent is linear and is described by

$$q_e = \frac{RT}{b}\ (ln\ A\ +\ ln\ C_e), \tag{8}$$

$$\frac{RT}{b} = B, \tag{9}$$

where R (8.314 Jmol/K) is the universal gas constant, T (K) is the temperature, and C_e (mmol/L) is the equilibrium concentration of metal ions. A (L/mmol) and B (J/mol) are Temkin isotherm constants associated with equilibrium adsorption constant and intensity of adsorption (9), respectively. Alinear plot of amount adsorbed q_e versus ln C_e gives the values of the constant A and b from the slope and intercept of the graph, respectively.

The unique feature of DKR model is that it is temperature dependent [18]; this model has been applied to study the adsorption of metal ions onto adsorbent [19]. The model equation is shown in

$$ln\ q_e = ln\ X_m - K_{ad}\varepsilon^2, \tag{10}$$

where K_{ad} (mol^2/KJ^2) and X_m (mmol/g) are the DKR isotherm constants and ε is the Polanyi potential which is defined by

$$\varepsilon = RT \ln\left(1 + \frac{1}{C_e}\right). \tag{11}$$

The slope and intercept of the plot of $ln\ q_e$ versus ε give K_{ad} and X_m, respectively. However, the adsorption energy required to remove each molecule of metal ions from its position into the adsorption site can be calculated using the relation in

$$E\ = \frac{1}{\sqrt{-2K_{ad}}}. \tag{12}$$

The value of E is vital and can be applied in obtaining the nature of adsorption process; if the value of E is <8 kJ/mol, then the adsorption process is physical in nature but if it is between 8 and 16kJ/mol then it can explain by ion exchange mechanism [20].

2.7.2 Thermodynamic parameters of adsorption

The original ideal of thermodynamics is based on the assumption that in a system that is kept isolated, where energy cannot be gained or lost to the surroundings, the entropy change is the driving force. In environmental engineering practice, both energy and entropy factors must be considered to decide what processes will occur spontaneously [21]. The entropy and enthalpy change, associated with the process, can be calculated from

$$ln\,K = -\frac{\Delta H^\circ}{RT} + \frac{\Delta S^\circ}{R}. \quad (13)$$

The Gibbs free energy change, ΔG°, is the fundamental criterion of spontaneity. Reactions occur spontaneously at a given temperature if ΔG° is a negative quantity [21]. The free energy of the adsorption reaction, considering the adsorption equilibrium constant, K, is given by

$$\Delta G^\circ = -RT\ ln\,K. \quad (14)$$

The equilibrium constant "K" as defined mathematically by Liu et al. [17] is given in

$$K = \frac{q_e}{C_e}. \quad (15)$$

ΔS° is the entropy change while ΔH° is the enthalpy change. ΔH° and ΔS° can be calculated from the slope and intercept of a plot of $ln\,K$ as a function of $1/T$.

2.8 Adsorption Kinetics

The evaluation of kinetics of a system can disclose the mechanism of binding. Most researchers apply the pseudo-first-order kinetics of Lagergren [22], the pseudo-second-order kinetic model that was introduced by Ho & McKay [23], and the intraparticle diffusion model as shown in (16)–(18) to describe kinetic data. These models are used to investigate the controlling mechanism of adsorption process

$$log(q_e - q_t) = log(q_e) - t\frac{K_1}{2.30\ 3}, \quad (16)$$

where q_e and q_t represents the amount of copper ions absorbed on the adsorbent (mmol/g) at equilibrium and time t, respectively. K_1 (min^{-1}) is the rate constant of the pseudofirst-order kinetics. The value of adsorption rate constant, K_1 can be calculated from the straight-line plot of $log(q_e - q_t)$ versus t

$$\frac{t}{q_t} = \frac{1}{K_2 q_e^2} + \frac{1}{q_e}t, \quad (17)$$

where K_2 (g/mmol·min) is the rate constant for a pseudosecond-order model and the definitions of q_e and q_t remain the same. The slope and intercept of the linear plot of t/q_t versus t give the values of q_e and K_2, respectively.

Intraparticle diffusion model is very vital in that it is the rate determining step in any liquid adsorption system [14]. In a properly stirred batch adsorption system, the intraparticle diffusion model has been applied in analysing the adsorption process taking place in the porous adsorbent [24].

Intraparticle diffusion model varies directly with the rate constant and also the square root of time

$$q_t = K_{idm}\sqrt{t} \quad (18)$$

where t is the time (min) and K_{idm} (mmol/gmin$^{1/2}$) is the intraparticle diffusion rate constant. The slope of the linear plot of q_t against $t^{1/2}$ gives the value of K_{idm}.

3. RESULTS AND DISCUSSION

3.1 Characterization

3.1.1 Determination of water and amine content in FGCX

The water content present in GFCX was found to be 74.6%. This water content is vital for the effective transport of metal ions to adsorption site. Consequently, in determining the amine concentration of FGCX the pH as a function of the amount of acid added was studied and the point of inflection from the graph directed to the x-axis gave the value of amine concentration. The amine concentration of FGCX was found to be 5.3 mmol/g.

3.2 XRD Result

The crystallinity of the three sets of beads was studied with X-ray diffraction analyser. Fig. 3(a), 3(b), and 3(c) show the diffraction pattern of chitosan, crosslinked chitosan and grafted cross-linked chitosan beads, respectively. The non-cross-linked chitosan is said to be crystalline in nature; this crystalline nature prevents the amine group from binding efficiently with adsorbate [9]. A common feature of 2θ = 20° which corresponds to 110 planes of chitosan was observed in Fig. 3(a) and 3(b); this is because it is possible to modify chitosan and still retain some of its properties. However, in Fig. 1(c) there was a slight shift in the peak to 2θ = 25° due to copolymer formation which provides evidence of successful grafting. A similar trend was reported by Igberase et al. [5]. Also in Fig. 3(c), the intensity reduced drastically because some of the crystalline chains have been eliminated during grafting process.

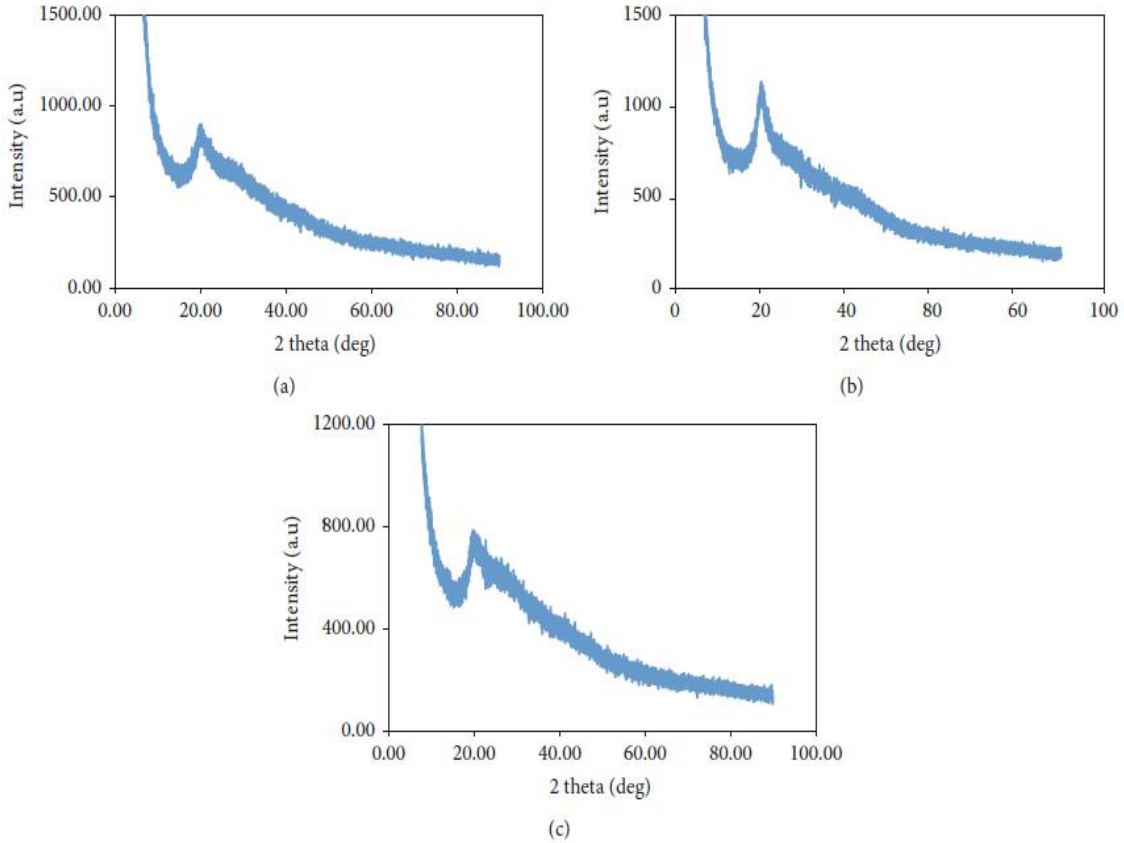

Fig. 3. XRD of CX, CCX, and FGCX, respectively

3.3 SEM Result

SEM was utilized to analyse the morphology and changes of chitosan after cross-linking and grafting. SEM images of the different set of beads are presented in Fig. 4(a), 4(b), and 4(c). The surface of CCX appears to be more visible and smooth as compared to CX due to the reaction between native chitosan beads and glutaraldehyde and as such glutaraldehyde has been chemically bonded with chitosan. The grafting of 4-aminobenzoic acid onto the backbone of cross-linked beads lead to the evenness of the surface.

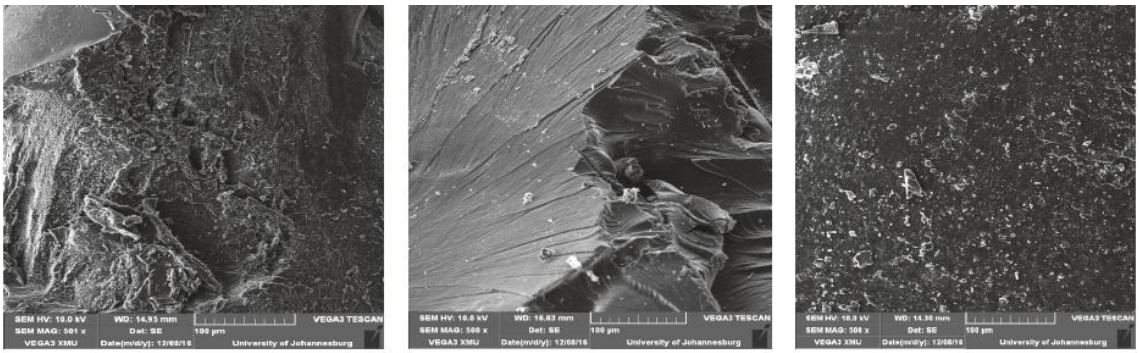

Fig. 4. SEM analysis of chitosan, cross-linked chitosan and grafted cross-linked chitosan beads, respectively

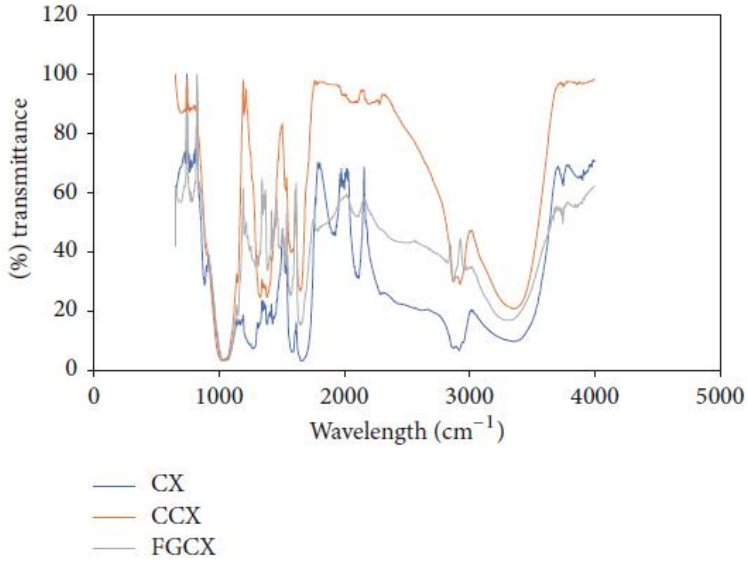

Fig. 5. FTIR of chitosan and cross-linked chitosan beads

3.4 FTIR Result

The infrared spectroscopy was used to pro-vide evidence of comparable difference between the three sets of beads which are CX, CCX, and FGCX (Fig. 5). T he broad band of chitosan, cross-linked chitosan, and grafted cross-linked chitosan at wavelengths 3384 cm^{-1}, 3385 cm^{-1}, and 3389 cm^{-1} indicates the presence of exchangeable protons which is from alcohol and amine group. The slight shift in band may be due to exchangeable protons in the modifica-tion process. The C–H stretch at wavelengths of 2918 cm^{-1}, 2926 cm^{-1}, and 2875 cm^{-1} corresponds to chitosan, cross-linked chitosan,

and grafted cross-linked chitosan, respec-tively [30]. All three sets of beads had a common wavelength of 1000 cm^{-1} which indicates C–O stretching vibration, since it is possible for an adsorbent to retain some of its properties after modification [5]. The sharp peaks at wave-length 1217 cm^{-1} and 1508 cm^{-1} in the cross-linked chitosan beads correspond to C–N stretching vibration and N=O stretching vibration, respectively. The IR spectra of the cross-linked chitosan beads showed increase in intensity between wavelength 1217 cm^{-1} and 1653 cm^{-1} as compared to chitosan beads. Subsequently the grafted cross-linked chitosan showed increase in intensity between wavelength 1195 cm^{-1} and 1653 cm^{-1}. This provides evidence of successful modification.

3.5 TGA Result

TGA was used to study the thermal prop-erties when heat is applied in the three set of beads. A plot of weight % versus temperature was done to study the thermal stability of the set of beads. Fig. 6 depicts the stages involved in the thermal degradation of the sets of beads. The decomposition of CX took place in 3 stages; in the first stage there was 6% weight loss between temperatures of 34 and 148°C which corresponds to the removal of water from the adsorbent [31]. The second stage started at 250°C up to 320◦C with 36% weight loss. This loss of weight is ascribed to the dehydration of the saccharide rings, depolymerisation, and decomposition of the acetylated and deacetylated units of adsorbent [32]. In the third stage there was 51% loss of weight above 400°C. This stage is the decomposition of non-cross-linked chitosan.

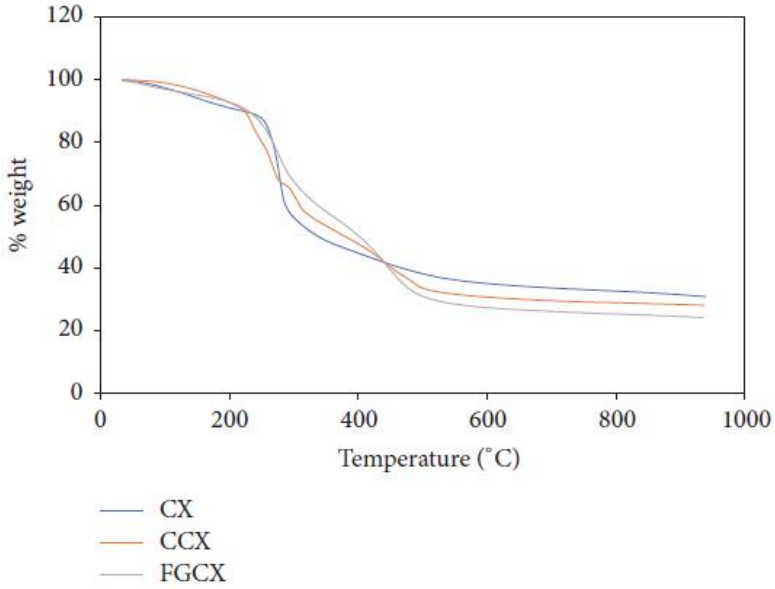

Fig. 6. TGA of CX, CCX, and FGCX

The CCX showed a 5% weight loss at temperatures between 34 and 141°C during the first stage. The second stage started at 227°C and continued up to 330°C with 31% weight loss. In the third stage, there was 10% weight loss above 500°C. This loss of weight in the 1st, 2nd, and 3rd stages corresponds to removal of surface water, depolymerisation, and decomposition of the acetylated and deacetylated units of adsorbent and decomposition of cross-linked chitosan, respectively [31,32].

The FGCX showed a 10% weight loss at temperatures between 51 and 150°C in the first stage of degradation. The second stage started at 280°C and continued up to 398°C with 24% weight loss. In the third stage, there was 15% weight loss above 500°C. This loss of weight in the 1st, 2nd, and 3rd stages corresponds to removal of surface water, depolymerisation, and decomposition of the acetylated and deacetylated units of adsorbent and decomposition of grafted cross-linked chitosan, respectively [31,32].

3.6 Effect of Solution pH

Metal binding efficiency of amino-functionalized ligand is greatly affected by pH, since it influences the surface charge of ligands and ionisation degree [33]. It also impacts on the level of adsorbate precipitation and the nature of structures formed between adsorbate and adsorbents. A plot of percentage removal against solution pH was made to obtain the optimum pH for the binding of heavy metal ions onto grafted cross-linked chitosan beads, as presented in Fig. 7. In this figure there was a noticeable reduction in percentage removal at lower pH values which is mainly due to the protonation of the amine group that creates an electrostatic repulsion between the metal ions in solution and the amine group of chitosan. As the pH is increased the surface of the beads becomes negatively charged due to deprotonation reaction [9]. Consequently, the repulsive force that exists between metal ions in solution and the amine group of chitosan decreases, thus increasing the removal of metal ions in solution until an optimum value is achieved. At pH above the optimum value insoluble metal hydroxide begins to precipitate from the solution resulting in the decrease of metal ions removal from the solution.

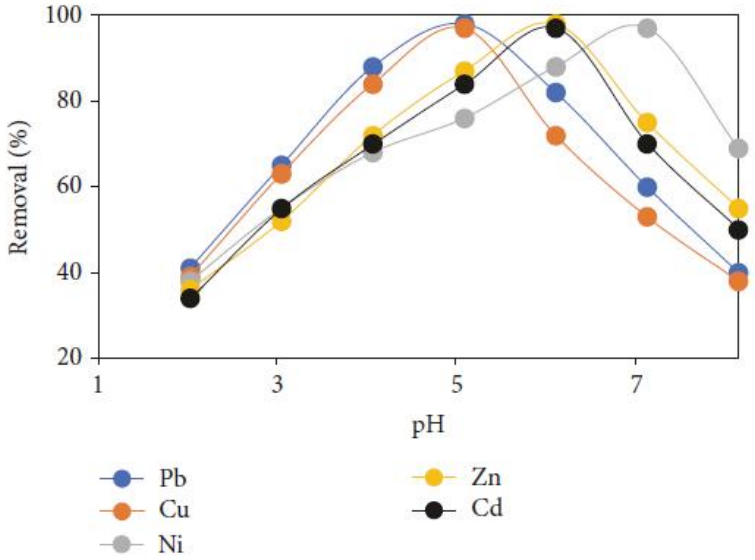

Fig. 7. Effect of pH on percentage removal of heavy metal ions by FGCX (conditions: 7 g/l FGCX; contact time: 70 min; Temperature: 25°C; initial concentration: 0.8 mmol/L; agitation speed: 120 rpm)

3.7 Effect of Contact Time

In any given adsorption system it is vital to establish the time dependence of the system in achieving equilibrium. Fig. 8 depicts the effect of contact time on the adsorption of heavy metals from a single component solution and time range of 10–80 mins. It was observed that 45 min was sufficient to establish equilibrium for Pb, Cu, and Ni while it took 55 min for Zn and Cd. The adsorption was very fast at the initial stage for all metal ions investigated due to sufficient and well aligned site available for the binding of the considered metal ions but became slower until equilibrium is reached since the binding sites have been covered with metal ions which causes repulsion with increase in time [9,34]. This result is important because longer contact time between the beads and metal ions in solu-tion can consume energy and hence increase cost of treatment.

3.8 Effect of Temperature

Temperature as an important parameter in adsorption process is directly linked to the kinetic energy of adsorbent in the solution [35]. The effect of temperature was studied at a temperature range of 25–

65◦C and a plot of percentage removal against temperature (Fig. 9) was made to elucidate the observation. It was shown that a rise in temperature expedites the binding of metal ions until an optimum of 45◦C is reached. This finding is due to the fact that as the temperature rises the kinetic energy also rises which then promotes the accessibility of metal ions onto adsorbents and, in the process, reduces the time to reach adsorption equilibrium [36,37]. Also, the reaction of amino groups with ions is exothermic and the process for the dis-tribution of metal ions into the FGCX pores is endothermic and this positive enthalpy change is greater than the negative enthalpy change due to the formation of complexes between the amino group of FGCX and considered metal ions in solution leading to an overall positive enthalpy change [25]. Hence a rise in temperature is vital for the adsorption of metal ions onto FGCX. Consequently, as the temperature exceeds that of the optimum, deterioration of the adsorbent may occur leading to reduced removal of metal ions. This result is favourable by virtue of cost effectiveness.

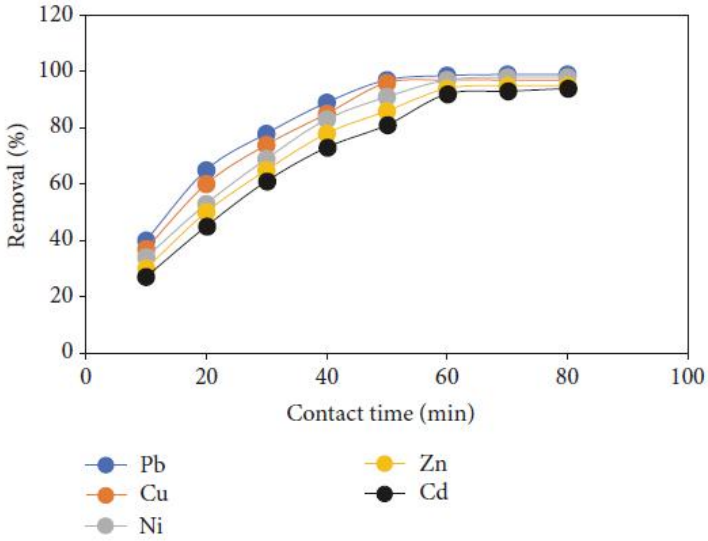

Fig. 8. Effect of contact time on percentage removal of heavy metal ions by FGCX (conditions: 7 g/l FGCX; pH: Pb = 5, Cu = 5, Ni = 7, Zn = 6, and Cd = 6; Temperature: 25°C; initial concentration: 0.8 mmol/L; agitation speed: 120 rpm)

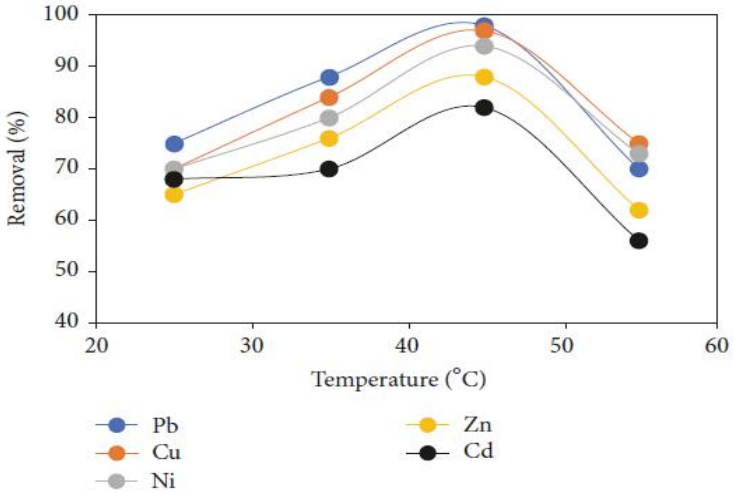

Fig. 9. Effect of contact time on percentage removal of heavy metal ions by FGCX (conditions: 7 g/l FGCX; pH: Pb = 5, Cu = 5, Ni = 7, Zn = 6, and Cd = 6; contact time: 60 min; initial concentration: 0.8 mmol/L; agitation speed: 120 rpm)

3.9 Effect of Initial Concentration

The effect of initial metal concentration is of significance in adsorption studies, since it depends on several parameters such as the type of metal and the liquid medium, the presence of competing cations, the availability of the functional groups in the adsorbent surface, and the ability of these groups to attach metal ions [38–40]. Fig. 10 explores the percentage removal of heavy metal ions as a function of initial concentration. It was observed that at lower initial concentration of 0.5 mmol/L the % *R* of Pb, Cu, Ni, Zn, and Cd were 99.9, 99.5, 98.6, 98, and 97.8%, respectively. At higher initial concentration of 2.5 mmol/L the % *R* were Pb (58%), Cu (55%), Ni (55%), Zn (42%), and Cd (32%). This may be due to the fact that at lower initial concentration the ratio of metal cations to FGCX mass is low; a rise in initial concentration implies that additional metal ions are present in the mixture and hence more ions are attached to same quantity of FGCX which results in saturation of the FGCX adsorbent causing a decrease in % *R*. Also, at higher initial concentration the driving force to overcome the mass transfer opposition for the movement of the metal ions from the mixture to the adsorbent surface increases and, in this case, higher concentration would lead to saturation of the adsorbent surface [41].

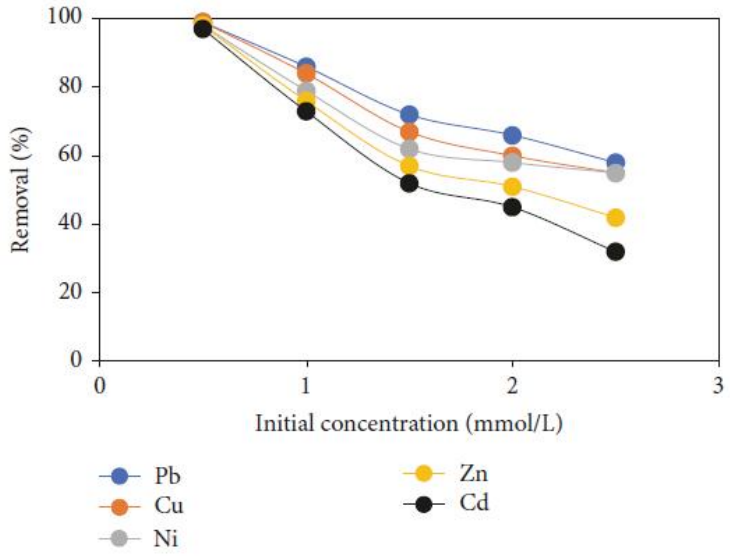

Fig. 10. Effect of initial concentration on percentage removal of heavy metal ions by FGCX (conditions: 6 g/l FGCX; pH: Pb = 5, Cu = 5,Ni = 7, Zn = 6, and Cd = 6; contact time: 60 min; agitation speed: 120 rpm; temperature: 45°C)

3.10 Effect of Adsorbent Dose

The adsorbent type and func-tional group present in the adsorbent has intense effect on adsorption, since it determines the availability of binding sites. Fig. 11 illustrates the effect of FGCX dose on the % *R* of metal ions. There was a sharp increase in % *R* of metal ions at FGCX dose range of 2 to 6 g/l and increasing the FGCX dose above 6 g/l did not cause any further changes in the % *R* of metal ions. The observed behaviour occurred because at the initial stage there were sufficient binding sites for the complexation of metal ions and increasing the dose beyond 6 g/l resulted in the establishment of equilibrium between the metal ions bounded to FGCX and those remaining unabsorbed in the mixture [9,42].

3.11 Effect of Agitation Speed

Agitation speed is an important parameter that is mostly neglected by some researchers in adsorption studies. Park et al. [43], reported that the application of appropriate agitation speed increases the

movement of metal ions in the mixture, reducing the mass transfer resistance in the process. Fig. 12 depicts the impact of agitation speed on % *R* of metal ions by FGCX at agitation speed range of 50–250 rpm. It was observed that agitation speed has a positive impact on metal ions removal by FGCX. Consequently, there was a fast increase in metal ions removal up to 150 rpm and thereafter it became constant. This is because at high agitation speed the boundary layer becomes thinner which eventually influence the speed of distribution of metal ions through the boundary layers [44]. However, a further increase beyond 150 rpm would lead to saturation of the adsorption site.

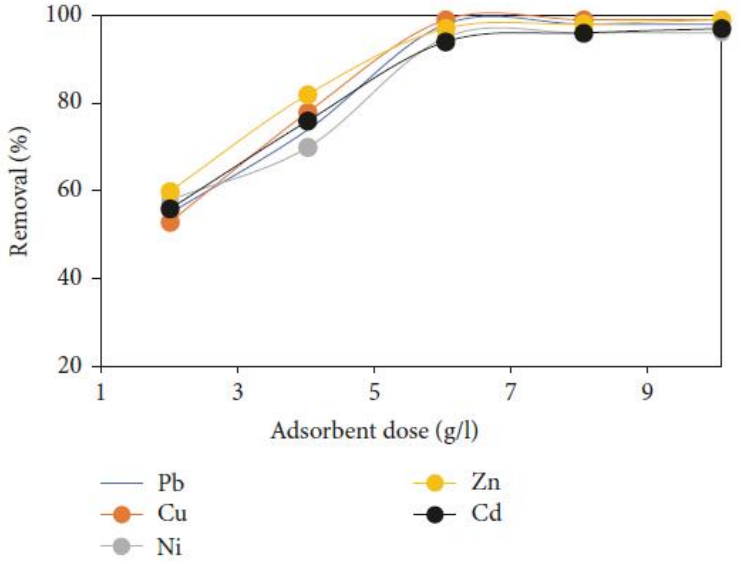

Fig. 11. Effect of FGCX dose on percentage removal of heavy metal ions (conditions: pH: Pb = 5, Cu = 5, Ni = 7, Zn = 6, and Cd = 6; contact time: 60 min; initial concentration: 0.5 mmol/L; agitation speed: 120 rpm; temperature: 45°C)

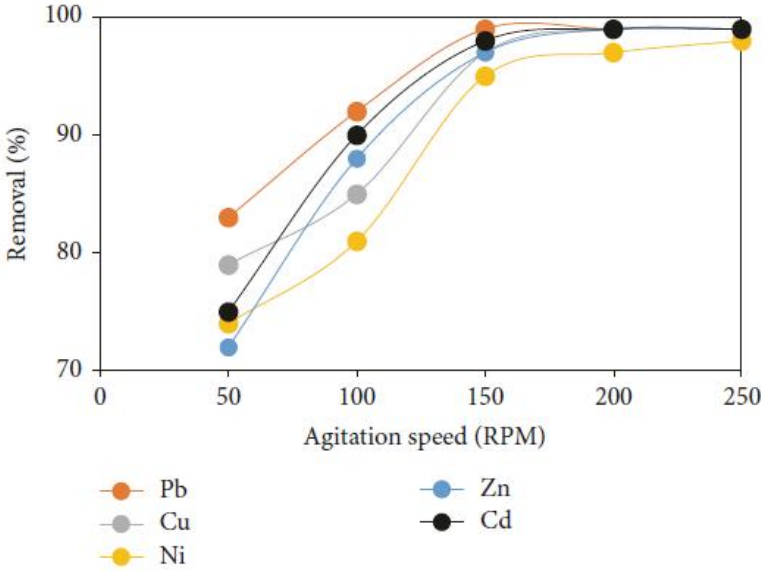

Fig. 12. Effect of agitation speed on percentage removal of heavy metal ions by FGCX (conditions: 6 g/l FGCX; pH: Pb = 5, Cu = 5, Ni = 7, Zn = 6, and Cd = 6; contact time: 60 min; initial concentration 0.5mmol/L; temperature: 45°C)

3.12 Effect of Ionic Strength

Wastewater usually comprises different cations and anions that can hinder the efficient binding of metal ions in solution. Fig. 13 elucidates the effect of ionic strength on the adsorption of metal ions onto FGCX. In this plot there was a decrease in % *R* with increase in the concentration of $NaNO_3$. This observation shows that the interaction between the amine group of FGCX and the metal cations is ionic in nature and raising the ionic strength reduces their movement to the solid surface [4]. Among the five metals investigated Pb and Cu proved to have higher binding strength even when the concentration of Na^+ was increased. This may be because some binding sites have the potential to attach specific metal ions [45].

Table 1. Langmuir, Freundlich, Temkin, and DKR isotherm parameters for binding of considered metal ions onto FGCX at temperature of 45°C

Ions	Langmuir parameters			Freundlich parameters			Temkin parameters			DKR parameters		
	Q_m (mmol/g)	K_L (l/mmol)	R^2	n	K_f (mmol/g)	R^2	A (l/mmol)	B (J/mol)	R^2	X_m (mmol/g)	E (kJ/mol)	R^2
Pb	3.96	2	0.99	2.70	1.79	0.86	2.99	9.11	0.98	3.92	14.55	0.99
Cu	2.88	3.71	0.99	2.22	1.70	0.86	3.42	10.33	0.85	2.75	13.42	0.99
Ni	2.80	1.33	0.98	3.42	2.13	0.98	1.52	11.21	0.98	2.85	13.11	0.97
Cd	1.82	1.08	0.99	1.98	1.46	0.87	1.20	10.56	0.88	1.79	10.21	0.99
Zn	1.76	0.86	0.99	2.5	2.05	0.99	0.92	9.98	0.99	1.77	9.82	0.99

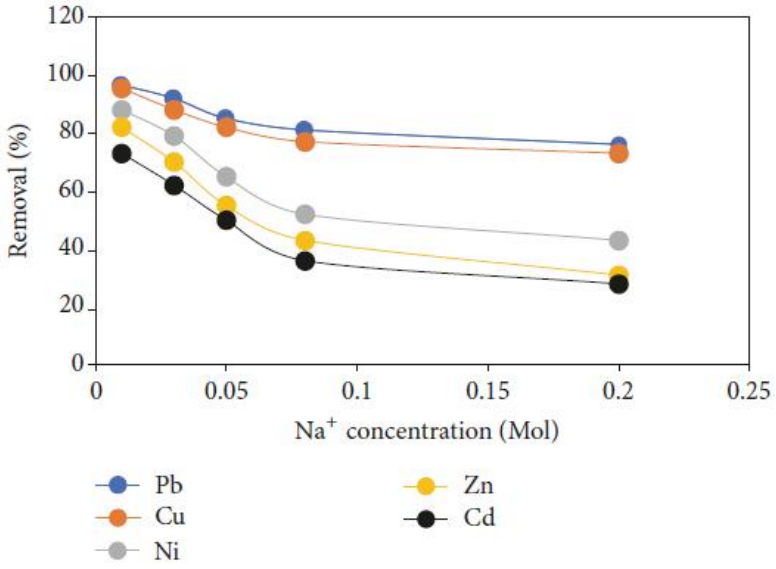

Fig. 13. Effect of ionic strength on percentage removal of heavy metal ions by FGCX (conditions: 6 g/l FGCX; pH: Pb = 5, Cu = 5, Ni = 7, Zn = 6, and Cd = 6; contact time: 60 min; initial concentration 0.5mmol/L; temperature: 45°C; agitation speed: 150 RPM)

3.13 Isotherm Result

The closer R^2 values are to one the best the model fits [9]. The parameters of the models are presented in Table 1, while Fig. 14(a), 14(b), 14(c), and 14(d) depict the plot for Langmuir, Freundlich, Temkin, and DKR models, respectively.

The Langmuir model was efficient in analysing adsorp-tion data of all the metal ions studied with R^2 values ≥0.98. Q_m values for the binding of metal ions onto FGCX followed a decreasing sequence of

Pb (3.96) > Cu (2.89) > Ni (2.8) > Cd (1.82) >Zn (1.76 mmol/g), whereas which determines the affinity of binding proved that the GFCX sites had greater affinity for Cu and the trend followed a decreasing order of Cu (3.71) >Pb (2) >Ni (1.33) >Cd (1.08) >Zn (0.86 l/mmol). This trend can be explained in terms of electronegativity of metal ions, since adsorption of these metal ions is also due to ion exchange at the surface. Therefore, more electronegative metal ions will exhibit a higher tendency of adsorption. The electronegativities of Pb, Cu, Ni, Cd, and Zn per Pauling scale are 1.87, 1.9, 1.8, 1.7, and 1.6, respectively, which agrees with the order of affinity. Based on this study it can be said that the affinity of metal ions onto FGCX is also believed to be a function of electronegativity. The R_L values for Cu, Pb, Ni, Cd, and Zn were 0.35, 0.5, 0.6, 0.65, and 0.7, respectively, and these values signify favourable adsorption process.

The Freundlich model was successful in analysing experimental data of Ni and Zn ions onto FGCX while that of Pb, Cu, and Cd did not fit the model very well. The K_f values decreased in the order of Ni (2.13) > Zn (2.05) > Pb (1.79) > Cu (1.7) >Cd (1.46 mmol/g); the n values indicated favourable adsorption for the considered metal ions.

The data for the adsorption of Pb, Ni and Zn onto FGCX was in agreement with Temkin model with R^2 value ≥ 0.98 in contrast to the R^2 value (≥0.85) obtained for the adsorption of Cu and Cd.

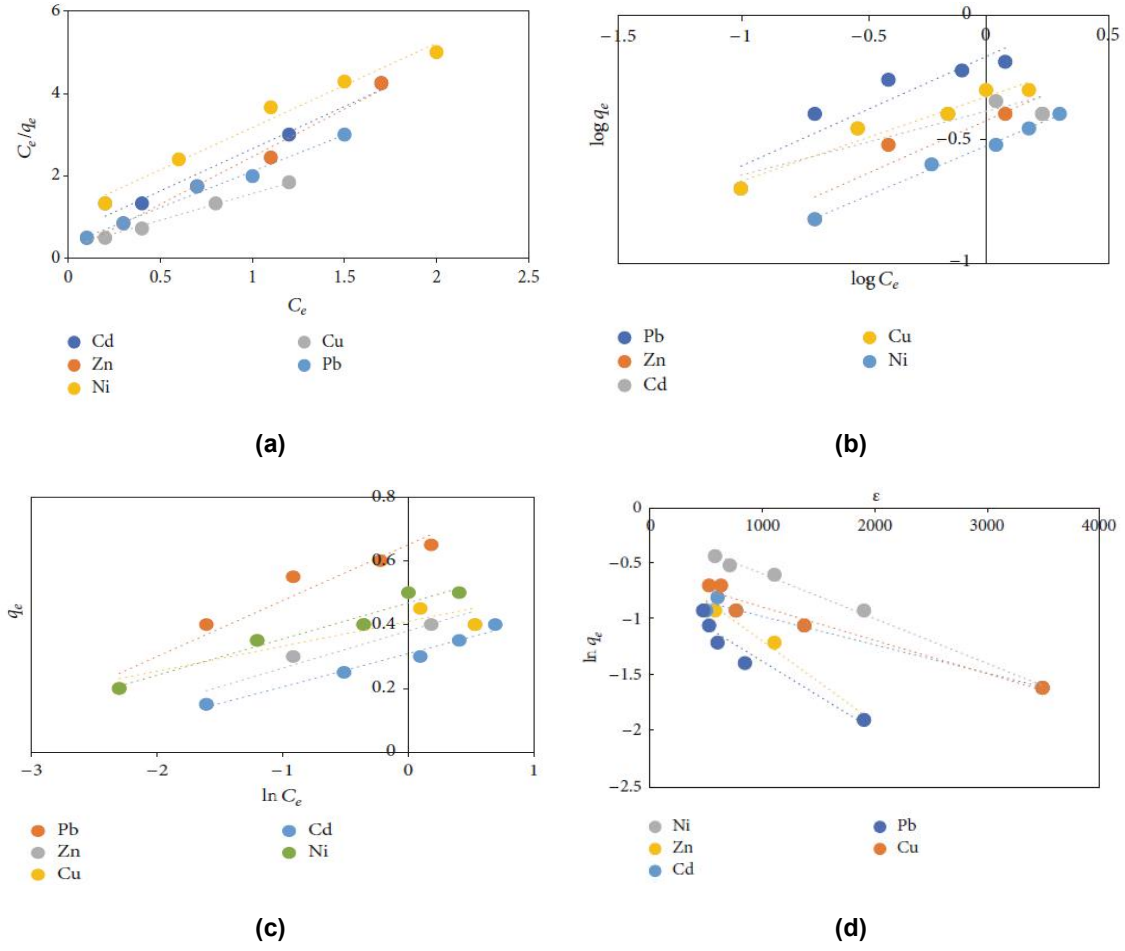

Fig. 14. Langmuir, Freundlich, Temkin, and DKR isotherm models, respectively, at temperature of 45°C

The DKR model was successful in describing experimental data for the considered metal ions with R^2 value ≥0.98. The adsorption capacity (X_m) was found to be 3.92, 2.75, 2.85, 1.79, and 1.77mmol/g for Pb, Cu, Ni, Zn, and Cd, respectively. The adsorption energy values for these ions are, respectively, 14.55, 13.42, 13.11, 10.21, and 9.82 kJ/mol. These values indicate the process can also be described by ion exchange mechanism.

Table 2. Comparison of adsorption capacity of FGCX onto Pb, Cu, Ni, Cd, and Zn with other absorbent

Heavy metal ions	Adsorbent	Q_m(mmol/g)	Temperature	Reference
Lead	Mesoporous silicas	2.86	25	[25]
	Romania peat	0.20	20	[26]
	Lignin	0.43	20	[27]
	Cross-linked CMCS resin	1.89	25	[28]
	FGCX	3.96	45	This study
Copper	Mesoporous silicas	2.34	25	[25]
	Cross-linked CMCS resin	1.82	25	[28]
	Lignin	0.36	20	[27]
	FGCX	2.88	45	This study
Nickel	Lignin	0.10	20	[27]
	Cross-linked CMCS resin	0.78	25	[28]
	Alginate microcapsules	0.52		[29]
	FGCX	2.80	45	This study
Cadmium	Mesoporous silicas	1.71	25	[25]
	Romania peat	0.39	20	[26]
	Lignin	0.23	20	[27]
	FGCX	1.82	45	This study
Zinc	Mesoporous silicas	1.36	25	[25]
	Lignin	0.17	20	[27]
	Cross-linked CMCS resin	0.74	25	[28]
	FGCX	1.76	45	This study

3.14 Thermodynamic Parameters

The plot of $In\ K$ versus 1/*T* for the adsorption of Pb, Cu, Ni, Zn, and Cd onto FGCX is presented in Fig. 15. Table 3 provides the parameters for thermodynamic studies. The free energy change ($\Delta G°$) obtained during the absorption reaction at temperatures of 25, 35, 45, and 55◦C was all negative and this indicates that the adsorption of heavy metals onto FGCX is spontaneous and favourable. A similar finding was reported by Zawani et al. [46] Also, increase in negative values of $\Delta G°$ as temperature increases indicates greater driving force for binding of metal ions. The positive value of $\Delta H°$ indicates that the adsorption process is endothermic in nature. This finding is in agreement with the result presented by Liu et al. [17]. The positive value of $\Delta S°$ indicates the increased randomness at the solid-solution interface during the adsorption of heavy metal ions onto FGCX [17].

Table 3. Thermodynamic parameters for the adsorption of heavy metal ions onto FGCX at an initial concentration of 0.5mmol/l

Metal ions	ΔS^o (kJ/mol/k)	ΔH^o (kJ/mol)	ΔG^o (kJ/mol)				R^2
			T=298K	T=303K	T=318K	T=328K	
Pb	57.23	0.23	-1.52	-1.34	-4.45	-4.98	0.99
Cu	64.78	0.26	-1.25	-1.65	-3.97	-4.91	0.99
Ni	67.12	0.20	-2.31	-6.92	-8.78	-9.56	0.98
Zn	54.26	0.32	-1.20	-2.32	-4.75	-6.43	0.99
Cd	68.45	0.27	-2.58	-4.41	-8.54	-9.43	0.97

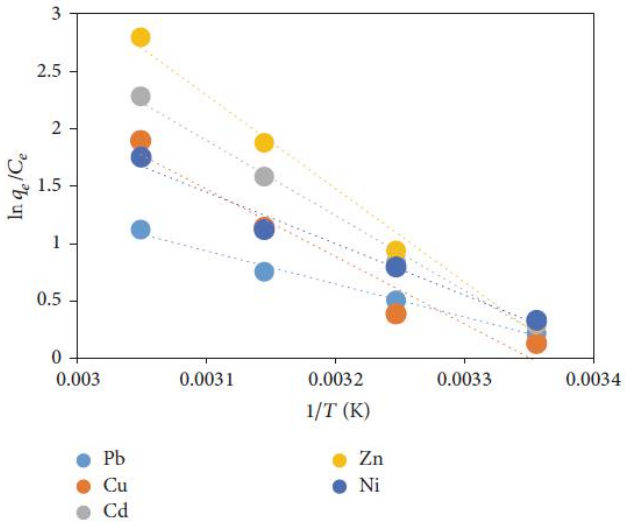

Fig. 15. Thermodynamic plot of $ln\ K$ versus $1/T$ for metal ions binding onto FGCX

3.15 Kinetic Parameters

The straight-line plot of the pseudo-first- and pseudo-second-order and intraparticle diffusion model for the binding of assessed metal ions (Pb, Cu, Cd, Zn, and Ni) onto FGCX is presented in Figs. 16(a), 16(b), and 16(c), and the values of the parameters in each case are presented in Table 4. It is evident that the R^2 values for the pseudo-second-order and intraparticle model are higher and closer to one in comparison with pseudo-first-order model. This observation indicates that the pseudo-second-order and intraparticle model best describe the kinetic data of the assessed metal ions binding onto FGCX. Also, the pseudo-second rate constant (K_2) followed a decreasing sequence of Pb (7.34) > Cu (5.82) > Ni (5.12) > Zn (3.21) > Cd (2.56) in g/mmol·min. This suggests that the chemical interaction is dependent on the affinity of metal ions to interact with the amino group of FGCX. A similar report was presented by Bulgariu et al. [26].

Table 4. Kinetic parameters for the binding of considered metal ions onto FGCX

Metal ions	Pseudo-first-order parameters			Pseudo-second-order parameters			Intra-particle diffusion parameters	
	K_1 (min^{-1})	q_e (mmol/g)	R^2	K_2 (g/mmol.min)	q_e (mmol/g)	R^2	K_{idm} ($mmol/gmin^{1/2}$)	R^2
Pb	0.03	1.59	0.88	7.34	3.54	0.98	3.43	0.97
Cu	0.01	1.16	0.81	5.28	3.87	0.99	4.18	0.99
Ni	0.02	1.90	0.83	5.12	3.12	1.00	2.97	0.99
Zn	0.03	2.2	0.83	3.21	3.99	0.99	2.56	0.98
Cd	0.05	1.85	0.73	2.56	3.52	0.99	3.78	0.99

3.16 Reusability of the Spent FGCX

Adsorbent reuse is an important aspect of adsorption studies in that its reusability helps lower the processing cost. The recovery of the consid-ered metal ions and subsequent usage of the adsorbent were made possible with 0.5 M HCl and contact time of 180 min; the recovery efficiencies of the metal ions from its spent FGCX were 98.8, 97.5, 97.9, 98.3, and 97.7 for Pb, Cu, Ni, Zn, and Cd, respectively. There was no loss in the mass of the regenerated beads.

3.17 Reaction Mechanism of Chitosan

Most researchers support that the amine group of chitosan is the main reactive site for metal ions, though hydroxyl groups may contribute to binding of metal ions [9]. However, of the free amino groups only some are accessible to metal binding, since some of these amine sites interact with hydrogen ions at lower pH. These reactive groups may react with metal ions through different mechanisms such as chelation and electrostatic depending on factors such as the type of metal, the pH, fraction of deacetylated units (free amine groups), polymer chain length, crystallinity, molecular weight, conditioning of polymers, physical form of chitosan, solution pH, type and concentration of the acid used for solution, composition of solution, metal ion selectivity and speciation, and the matrix of the solution [47]. The amine group initiates a coordinate bond with the metal ions; the bond is formed between the free electron pairs of the nitrogen in the amine group and the void orbitals of the metal. Also, the free electron doublet of nitrogen on amine groups is responsible for the adsorption of metal cations at pH near neutrality and at lower pH value, where protonation of the amine group takes place; the poly-mer attains cationic groups which can bind anions through electrostatic interactions [48].

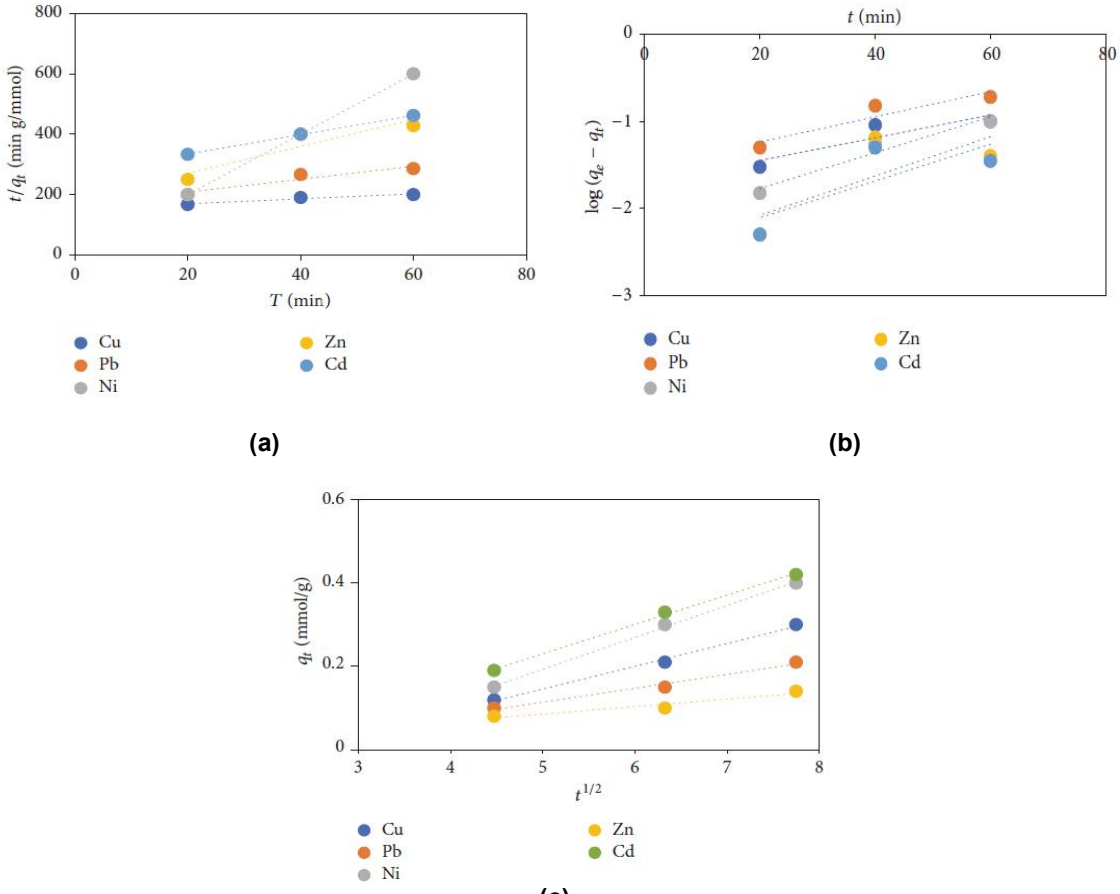

Fig. 16. Pseudo-first-, pseudo-second-, and intraparticle diffusion plot, respectively

4. CONCLUSION

A promising adsorbent was developed by grafting 4-amino-benzoic acid onto the backbone of cross-linked chitosan beads which reduced its crystallinity and expanded the polymer network for easy accessibility of the considered metal ions to binding site. Comprehensive investigation was performed in order to access the effect adsorption parameters have on the binding of metal ions onto FGCX. The

adsorption of Pb, Cu, Ni, Zn, and Cd was dependent on pH, contact time, adsorbent dosage, initial concentration, agitation speed, and ionic strength. The binding of these metal ions was observed to be a feasible, spontaneous, and endothermic process and corresponds with the Langmuir and DKR isotherm model, while some metals were in agreement with Freundlich and Temkin model. The binding was also observed to be in agreement with pseudo-second-order and intraparticle diffusion model. The result indicated that binding of these metal ions is mainly controlled by chemisorption, electrostatic attraction, or ion exchange. At industrial level, this developed adsorbent with high amino content can be an excellent candidate for the adsorption of metal ions even the ions not mentioned in this study.

COMPETING INTERESTS

Authors have declared that no competing interests exist.

REFERENCES

1. Ramos S, Pedrosa A, Teodoroa X, et al. Modeling mono-and multi-component adsorption of cobalt(II), copper(II), and nickel(II) metal ions from aqueous solution onto a new carboxylated sugarcane bagasse. Part I: Batch adsorption study," Industrial Crops and Products. 2015;74: 357–371.
2. Zhang L, Zeng Y, Cheng Z. Removal of heavy metal ions using chitosan and modified chitosan: A review. Journal of Molecular Liquids. 2016;214:175–191.
3. Luo X, Zhang Z, Zhou P, Liu Y, Ma G, Lei Z. Synergic adsorption of acid blue 80 and heavy metal ions (Cu^{2+}/Ni^{2+}) onto activated carbon and its mechanisms. Journal of Industrial and Engineering Chemistry. 2015;27:164–174.
4. Mittal A, Naushad M, Sharma G, Alothman ZA, Wabaidur SM, Alam M. Fabrication of MWCNTs/ThO_2 nano-composite and its adsorption behavior for the removal of Pb(II) metal from aqueous medium. Desalination and Water Treatment. 2016;57(46):21863–21869.
5. Igberase E, Osifo P, Ofomaja A. The adsorption of copper (II) ions by polyaniline graft chitosan beads from aqueous solu-tion: equilibrium, kinetic and desorption studies. Journal of Environmental Chemical Engineering. 2014;2(1):362–369.
6. Barakat MA. New trends in removing heavy metals from industrial wastewater. Arabian Journal of Chemistry. 2011;4(4):361–377.
7. Mohamed Z, Abdelkarim A, Ziat K, Mohamed S. Adsorption of Cu(II) onto natural clay: Equilibrium and thermodynamic studies. Journal of Materials and Environmental Science. 2016; 7(2):566–570.
8. Naushad M, Ahamad T, Alothman ZA, Shar MA, AlHokbany NS, Alshehri SM. Synthesis, characterization and application of curcumin formaldehyde resin for the removal of Cd^{2+} from wastewater: Kinetics, isotherms and thermodynamic studies. Journal of Industrial and Engineering Chemistry. 2015;29:78–86.
9. Igberase E, Osifo P. Equilibrium, kinetic, thermodynamic and desorption studies of cadmium and lead by polyaniline grafted cross-linked chitosan beads from aqueous solution. Journal of Industrial and Engineering Chemistry. 2015;26:340–347.
10. Berger J, Reist M, Mayer JM, Felt O, Peppas NA, Gurny R. Structure and interactions in covalently and ionically crosslinked chitosan hydrogels for biomedical applications. European Journal of Pharmaceutics and Biopharmaceutics. 2004;57(1):19–34.
11. Maitra Y, Shukla VK. Cross-linking in hydrogels. American Journal of Polymer Science. 2014;4: 25–31.
12. Gyananath G, Balhal DK. Removal of lead (II) from aqueous solutions by adsorption onto chitosan beads. Cellulose Chemistry and Technology. 2012;46(1-2):121–124.
13. Payne KB, Abdel-Fattah TM. Adsorption of divalent lead ions by zeolites and activated carbon: Effects of pH, temperature and ionic strength. Journal of Environmental Science and Health. 2004;39(9):2275–2291.
14. Hena S. Removal of chromium hexavalent ion from aqueous solutions using biopolymer chitosan coated with poly 3-methyl thiophene polymer. Journal of Hazardous Materials. 2010; 181(1-3):474–479.

15. Mohammed RK. Determination of the degree of N-acetylation for chitin and chitosan by various NMR spectroscopy techniques: A review. Carbohydrate Polymers. 2011;79(4):801–810.
16. Ola A. Kinetic and isotherm studies of copper (ii) removal from wastewater using various adsorbents. Egyptian Journal of Aquatic Research. 2007;33:125–143.
17. Liu D, Sun D, Li Y. Removal of Cu(II) and Cd(II) from aqueous solutions by polyaniline on sawdust. Separation Science and Technology. 2011;46(2):321–329.
18. Dada AO, Olalekan AP, Olatunya AM, Dada O. Langmuir, freundlich, temkin and dubinin–radushkevich isotherms studies of equilibrium sorption of Zn^{2+} unto phosphoric acid modified rice husk. Journal of Applied Chemistry. 2012;3(1):38–45.
19. Erdem B, Ozcan A, Gok O,¨ Ozcan AS. Immobilization of 2,2 -dipyridyl onto bentonite and its adsorption behavior of copper(II) ions. Journal of Hazardous Materials. 2009;163(1):418–426.
20. Ngah WSW, Fatinathan S. Adsorption characterization of Pb(II) and Cu(II) ions onto chitosantripolyphosphate beads: Kinetic, equilibrium and thermodynamic studies. Journal of Environmental Management. 2010;91(4):958–969.
21. Ho YS, Ofomaja AE. Kinetics and thermodynamics of lead ion sorption on palm kernel fibre from aqueous solution. Process Biochemistry. 2005;40(11):3455–3461.
22. Lagergren S. Zur theorie der sogenannten adsorption geloster stoffe, Kungliga Svenska Vetenskapsakademiens. Handlingar. 1898;24:596.
23. Ho YS, McKay G. Sorption of dye from aqueous solution by peat. Chemical Engineering Journal. 1998;70(2):115–124.
24. Itodo AU, Abdulrahman FW, Hassan LG, Maigandi SA, Happiness UO. T hermodynamic, equilibrium, kinetics and adsorption mechanism of industrial dye removal by chemically modified poultry droppings activated carbon. Nigerian Journal of Basic and Applied Sciences. 2009;17:38–43.
25. Hao S, Antonio V, Aprea P, Pepe F, Caputo D, Zhu W. Optimal synthesis of amino-functionalized mesoporous silicas for the adsorption of heavy metal ions. Microporous and Mesoporous Materials. 2016;236:250–259.
26. Bulgariu L, Balan C, Bulgariu D, Macoveanu M. Valorisation of romanian peat for the removal of some heavy metals from aqueous media. Desalination and Water Treatment. 2014;52:31-33,5891–5899.
27. Guo X, Zhang S, Shan XQ. Adsorption of metal ions on lignin. Journal of Hazardous Materials. 2008;151(1):134–142.
28. Sun S, Wang A. Adsorption properties and mechanism of cross-linked carboxymethyl-chitosan resin with Zn(II) as template ion. Reactive and Functional Polymers. 2006;66(8):819–826.
29. Ngomsik AF, Bee A, Siaugue JM, Cabuil V, Cote G. Nickel adsorption by magnetic alginate microcapsules containing an extractant. Water Research. 2006;40(9):1848–1856.
30. Rao MM, Rao GPC, Seshaiah K, Choudary NV, Wang MC. Activated carbon from *Ceiba pentandra* hulls, an agricultural waste, as an adsorbent in the removal of lead and zinc from aqueous solutions.. Waste Management. 2008;28(5):849–858.
31. Srivastava A, Mishra DK, Behari K. Graf t copolymerization of N-vinyl-2-pyrrolidone onto chitosan: Synthesis, characterization and study of physicochemical properties. Carbohydrate Polymers. 2010;80(3):790–798.
32. Omorogie MO, Babalola JO, Unuabonah EI, Song W, Gong, JR. Efficient chromium abstraction from aqueous solution using a low-cost biosorbent: Nauclea diderrichii seed biomass waste. Journal of Saudi Chemical Society. 2016;20(1):49–57.
33. Malamis S, Katsou E. A review on zinc and nickel adsorption on natural and modified zeolite, bentonite and vermiculite: Examination of process parameters, kinetics and isotherms. Journal of Hazardous Materials. 2013;252-253:428–461.
34. Shanmugapriya A, Hemalatha M, Scholastica B, Augustine TB. Adsorption studies of lead (II) and nickel (II) ions on chitosan-G-polyacrylonitrile. Der Pharma Chemica. 2013;5(3):141–155.
35. Nouri L, Ghodbane I, Hamdaoui O, Chiha M. Batch sorption dynamics and equilibrium for the removal of cadmium ions from aqueous phase using wheat bran. Journal of Hazardous Materials. 2007;149(1):115–125.
36. Crini G, Badot PM. Application of chitosan, a natural aminopolysaccharide, for dye removal from aqueous solutions by adsorption processes using batch studies: A review of recent literature. Progress in Polymer Science. 2008;33(4):399–447.

37. Dong C, Zhang F, Pang Z, Yang G. Efficient and selective adsorption of multimetal ions using sulfonated cellulose as adsorbent. Carbohydrate Polymers. 2016;151:230–236.
38. C¸oruh S, Ergun ON. $Ni2^{+}$ removal from aqueous solutions using conditioned clinoptilolites: Kinetic and isotherm studies. Environmental Progress and Sustainable Energy. 2009;28(1): 162–172.
39. Erdem E, Karapinar N, Donat R. The removal of heavy metal cations by natural zeolites. Journal of Colloid and Inter-face Science. 2004;280(2):309–314.
40. Wu D, Sui Y, He S, Wang X, Li C, Kong H. Removal of trivalent chromium from aqueous solution by zeolite synthesized from coal fly ash. Journal of Hazardous Materials. 2008;155(3): 415–423.
41. Gupta SS, Bhattacharyya KG. Immobilization of Pb(II), Cd(II) and Ni(II) ions on kaolinite and montmorillonite surfaces from aqueous medium. Journal of Environmental Management. 2008; 87(1):46–58.
42. Ozer A, Ozer D, Ozer A. The adsorption of copper(II) ions on to dehydrated wheat bran (DWB): Determination of the equilibrium and thermodynamic parameters. Process Bio-chemistry. 2004; 39(12):2183–2191.
43. Park D, Yun YS, Park JM. T he past, present, and future trends of biosorption. Biotechnology and Bioprocess Engineering. 2010;15(1):86–102.
44. Evans JR, Davids WG, MacRae JD, Amirbahman A. Kinetics of cadmium uptake by chitosan-based crab shells. Water Research. 2002;36(13):3219–3226.
45. Katsou E, Malamis S, Haralambous K. Examination of zinc uptake in a combined system using sludge, minerals and ultrafiltration membranes. Journal of Hazardous Materials. 2010;182(1-3):27–38.
46. Zawani Z, Luqman CA, Thomas SYC. Equilibrium, kinetics and thermodynamic studies: Adsorption of remazol black 5 on the palm kernel shell activated carbon (PKS-AC). European Journal of Scientific Research. 2009;37:63–71.
47. Mourya VK, Inamdar NN, Tiwari A. Carboxymethyl chitosan and its applications. Advanced Materials Letters. 2010;1:11–33.
48. Guibal E. Interactions of metal ions with chitosan-based sorbents: A review. Separation and Purification Technology. 2004;38(1):43–74.

Biography of author(s)

Dr. E. Igberase
Department of Chemical Engineering, Vaal University of Technology, Private Mail Bag X021, Vanderbijlpark 1900, South Africa.

He holds a B.Sc. in Chemical and Polymer Engineering from Lagos State University, Lagos, Nigeria and Magister Technologiae in Chemical Engineering from Vaal University of Technology. He also obtained his Ph. D in Chemical Engineering from the Vaal University of Technology in the broad areas of wastewater treatment, and he is employed as a lecturer in the Chemical Engineering Department. He has attended local conferences where he gave both oral and poster presentations and has published nine research articles in well-known peer reviewed journals. Ephraim is a Member of Water Institute of South Africa, (WISA, 2017) and a registered Candidate of Engineering Council of South Africa (ECSA 2017). Ephraim is also a reviewer for certain journals such as International Journal of Biological Macromolecule, Journal of Environmental Chemical Engineering and Environmental Technology and Innovation. Ephraim have extended his studies to the development of novel polymeric beads for the removal of organic dyes, rare earth elementals, and hazardous metals from aqueous solutions due to their hazardous impact on the environment. The primary aim of his research is the chemical modification of chitosan for the preparation of new materials with novel applications. He had the opportunity to co-supervising research students.

Prof. P. Osifo
Department of Chemical Engineering, Vaal University of Technology, Private Mail Bag X021, Vanderbijlpark 1900, South Africa.

He currently holds the position of an Acting Executive Dean in the faculty of Engineering and Technology at the Vaal University of Technology (VUT), Vanderbijlpark, South Africa. In 1991 He has received a Bachelor of Engineering Degree in Chemical Engineering from the University of Benin, Nigeria. In 1992, he joined the Oil Test Services, a petroleum servicing company, in Port-Harcourt, Nigeria. After several years of working, he started research in the department of Biotechnology for Master of Technology degree at Durban University of Technology in South Africa, where he has graduated in 2001. After which he started his doctorate programmes at the North-West University, South Africa and received his PhD in chemical engineering in 2007. He joined the Vaal University of Technology as a lecturer since 2003 and, in January 2008 to August 2015 he became the Head of department of Chemical Engineering. His teaching focuses primarily on reactor technology, process optimization and control and fluid mechanics. His current research programmes include clean technology of wastewater treatment through biodegradation of domestic and industrial wastewater involving membrane filtration, and heavy metals removal from contaminated water using biosorbents. Others include membrane development from bioresourses materials for applications in fuel cells. He has published over 20 paper in accredited journals, 8 books chapters and attended several local and international conferences. He has examined more than 10 dissertations from various universities in South Africa and have graduated 5 masters' and 1 PhD students.

© Copyright (2020): Author(s). The licensee is the publisher (Book Publisher International).

DISCLAIMER
This chapter is an extended version of the article published by the same author(s) in the following journal.
International Journal of Analytical Chemistry, 2017: 15, 2017, Article ID 6150209.

Chapter 2
Print ISBN: 978-93-90206-41-4, eBook ISBN: 978-93-90206-42-1

Substituent, Temperature and Solvent Effects on the Keto-Enol Equilibrium in β-Ketoamides: An NMR and Theoretical Study

Diego D. Colasurdo[1,2], Patricia E. Allegretti[1,3*] and Sergio L. Laurella[1,3]

DOI: 10.9734/bpi/crdc/v4

ABSTRACT

Substituent, temperature and solvent effects on tautomeric equilibria in several β-ketoamides have been investigated by means of nuclear magnetic resonance spectroscopy (NMR). Keto-enol tautomerism is observed and amide-imidol equilibrium is not detectable in this series of β-ketoamides. In solution, these compounds exist mainly as ketoamide and *Z*-enolamide tautomers, both forming intramolecular hydrogen bonds. The relative stability of the individual tautomers and the corresponding equilibrium shifts are explained considering electronic and steric effects and tautomer stabilization *via* internal hydrogen bonds. These assumptions are supported by theoretical calculations.

Keywords: β-Ketoamides; keto-enol equilibrium; NMR spectroscopy; theoretical calculations.

1. INTRODUCTION

Keto-enol tautomerism in β-ketoesters, β-diketones and β-ketonitriles is a topic that has been extensively studied from several angles and using a variety of experimental methods [1-3]. However, the occurrence of this phenomenon in β-ketoamides has not been studied deeply, with exception of a few previous works [4,5]. It is usual to describe them only as keto forms [6], although it has been demonstrated that some of them exist as a tautomeric mixture in which the enol form is the major tautomer.

The importance of studying β-ketoamides arises from their versatility as intermediates in the synthesis of several heterocycles: 3-acyltetramic acids [7] (used in the total synthesis of tirandamycin and other related natural antibiotics [8]), pyrans [9], alkaloids [10], lactams and spirolactams [11], azetidin-2-ones [12], as well as several 3-hydroxyisothiazol bioisoesters of glutamic acid and analogs of the AMPA receptor agonist [13]. Moreover, some β-ketoamides have been converted into γ-ketoamides, a class of compounds having to do with a wide variety of relevant biological systems [14].

The reactivity of β-ketoamides is related to their structure and their tautomeric equilibria; that is why it should be useful to determine their spectral behaviour in different conditions in order to study their tautomeric distribution.

Keto-enol tautomerism has attracted much interest for more than fifty years. Since the equilibrium involved is sufficiently slow to permit keto and enol tautomeric forms to be detected by nuclear magnetic resonance spectroscopy (NMR), many investigations on tautomerism have been carried out using this technique [15].

[1]CEDECOR (Centro de Estudio de Compuestos Orgánicos), Facultad de Ciencias Exactas, Universidad Nacional de La Plata (UNLP), Calle 115 y 47, (1900) La Plata, Argentina.
[2]CONICET (Consejo Nacional de Investigaciones Científicas y Técnicas), Argentina.
[3]CIC-BA (Comisión de Investigaciones Científicas de la Provincia de Buenos Aires), Argentina.
**Corresponding author: E-mail: pallegre@quimica.unlp.edu.ar;*

The tautomeric equilibrium of some β-ketobutanamides in solution has been investigated by means of ^{1}HNMR and ^{13}CNMR. Their chemical shifts were compared with those of related β-hydroxybutanamides. Equilibrium populations of the keto and enol forms were measured and substituent effects on the chemical shifts were discussed [16].

Intramolecular hydrogen bond is one of the main factors that govern tautomerism kinetics and influence the structure of tautomers in solution. Regarding β-ketoamides, internal hydrogen bonds can be formed in several tautomers. This point has been particularly studied for a series of 3-oxo-2-phenylbutanamides [17].

In this chapter, different factors affecting the tautomeric equilibrium of eleven β-ketoamides are analyzed: differential solvation, electronic and steric substituents effects and temperature variations.

2. EXPERIMENTAL

Synthesis of β-Ketoamides: The eleven β-ketoamides **1**-**11** (Scheme 1) were synthesized and purified according to procedures found in literature or their modified versions [18]. They were identified by ^{1}HNMR and ^{13}CNMR in DMSO-d_6, in which the peaks corresponding to the enol forms are depleted. Experimental chemical shifts are summarized in a previous work [19].

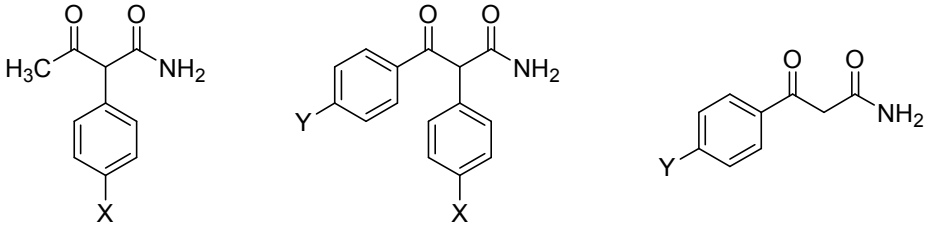

1. X= H
2. X= OCH_3
3. X= Cl
4. X= Y= H
5. X= H; Y= OCH_3
6. X= H; Y= Cl
7. X= OCH_3; Y= H
8. X= Cl; Y= H
9. Y= H
10. Y= OCH_3
11. Y= Cl

Scheme 1. Structure of the eleven studied β-ketoamides

NMR Experiments: ^{1}HNMR spectra were recorded in $CDCl_3$ and DMSO-d_6 using a Bruker 300 spectrometer, 300.13 MHz, grad Z and temperature control. The typical spectral conditions were as follows: spectral width 5000 Hz, acquisition time 2 s and 8-16 scans per spectrum. Digital resolution was 0.39 Hz per point, TMS was used as internal standard. Sample concentration was 0.05 M. Spectra were taken at 25, 30, 35, 40 and 45°C.

^{13}CNMR proton decoupled spectra were recorded with a Bruker 300 spectrometer operating at 75.4MHz from DMSO-d_6 solutions at 25°C. The spectral conditions were as follows: spectral width 16 500 Hz, acquisition times 1.303 s and 512-1000 scans per spectrum.

Theoretical Calculations: Theoretical calculations were carried out following several steps. The energy of different conformations of each tautomer were evaluated using the DFT method [20] by rotation of all unrestrained bonds in each structure. To this end, Gaussian 03 package [21] was used to apply the B3LYP hybrid exchange-correlation functional [22] together with the 6-31G basis set. The molecular structures of minimum energy were re-optimized by means of B3LYP/6-31G(d,p). These re-optimized structures were then used for calculation of reaction enthalpy (ΔH) at the same level of theory. Solvent effects were evaluated by means of the polarization continuum model SCRF-PCM [23].

3. TAUTOMERIC EQUILIBRIUM in β-Ketoamides

In order to study the tautomeric equilibrium in β-ketoamides, eleven compounds were synthesized trying to achieve some variety in substituents and reach some conclusions on the influence of such radicals on the equilibrium (steric and electronic effects). The structures and numbers of the ketoamides under study are given in Scheme 1.

At first, several tautomeric structures can be thought for β-ketoamides, since it has been proven that ketones and amides participate in tautomeric equilibria (keto-enol and amide-imidol, respectively). Scheme 2 shows the possible tautomeric structures for β-ketoamides **1** to **11**.

Ketoamide | Enolamide (E and Z) | Ketoimidol | Enolimidol (E and Z)

Scheme 2. Possible tautomeric structures for β-ketoamides

When tautomerism occurs, the observed NMR spectrum is the superposition of the several spectra, since the tautomers are altogether in equilibrium. As an example, Fig. 1 shows the ^{1}HNMR spectrum of **1** (3-oxo-2-phenylbutanamide) in $CDCl_3$ at 25°C. Values at the top correspond to the chemical shifts and the ones at the bottom, to the integration of each peak.

In order to assign the ^{1}HNMR signals to the corresponding tautomers, the peaks can be separated into two groups whose integration values are related by simple ratios.

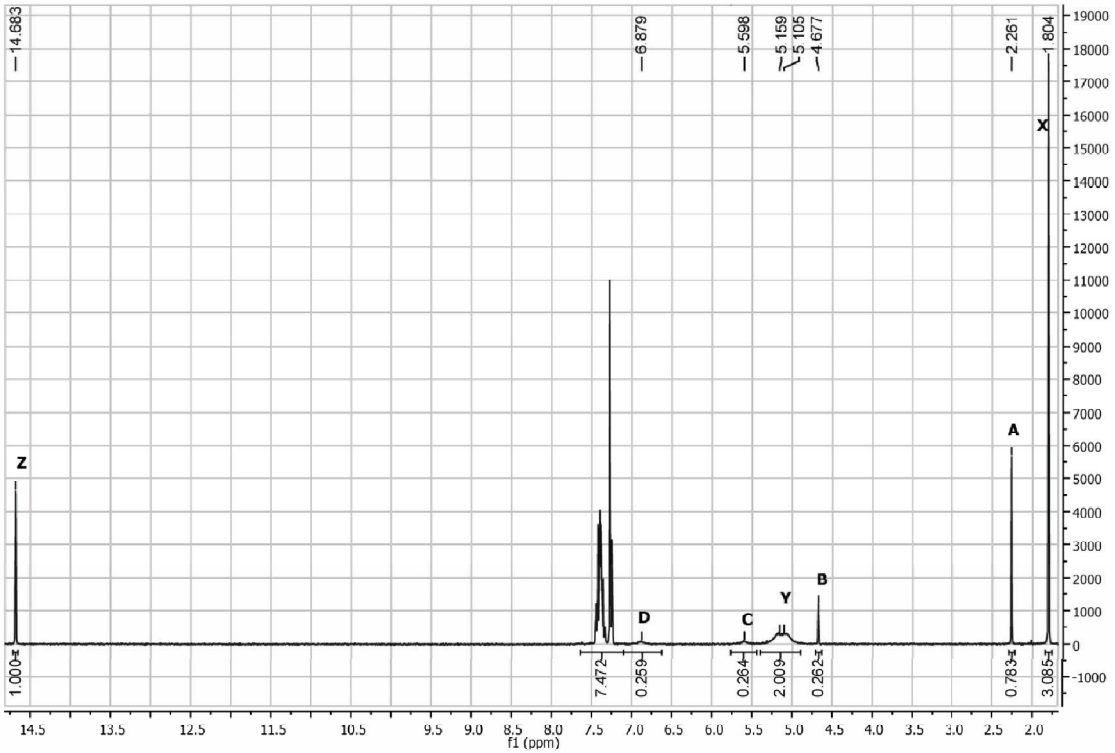

Fig. 1. ^{1}HNMR spectrum of compound 1 in $CDCl_3$ at 25°C

Peaks A, B, C and D appear to be in 3:1:1:1 ratio, while peaks X, Y and Z show a ratio of 3:2:1. Table 1 shows the expected number of non-aromatic signals and their integration for each tautomer. It is important to remark that, in some cases, internal hydrogen bonds can be formed and affect chemical shift.

At this point, theoretical calculations were carried out in vacuum in order to make a first approach to the most stable structures. Even when this order is only tentative (since it does not consider the solvent that surrounds the molecules), it is useful for discarding very unstable structures. Internal hydrogen bonds are observed in all minimum energy structures (when permitted by geometry). Results are shown in Table 1.

Regarding the data given in Table 1, peaks X, Y and Z can be assigned to the *Z*-enolamide hydrogens (CH_3, NH_2 and OH respectively), whereas peaks A, B, C and D can assigned to the ketoamide hydrogens (CH_3, CH, NH and NH respectively). The rest of the tautomeric forms could not be detected, and this fact indicates that they are absent or in very low concentration. Therefore, keto-enol tautomerism is observed and amide-imidol equilibrium is not detectable.

The assignment of the peaks to their corresponding protons was made keeping in mind not only signal integration but also theoretical displacements. Even when a 3:1:1:1 integration is expected for ketoimidol and enolimidol tautomers, their existence is discarded regarding their high energy. This assumption agrees with previous studies which also include theoretical calculations on this type of compounds [24].

Table 1. Structures, expected integrations in ^{1}HNMR and calculated energy (kcal/mol) for β-ketoamide tautomers

Tautomer		Expected integration	Relative energy (kcal/mol)
ketoamide	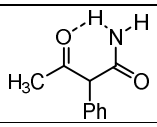	3:1:1:1	0.00
E-enolamide	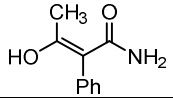	3:2:1	+9.51
Z-enolamide	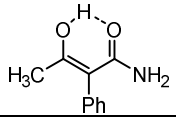	3:2:1	-4.52
ketoimidol	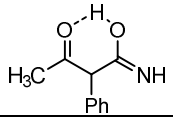	3:1:1:1	+19.84
E-enolimidol	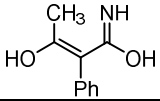	3:1:1:1	+22.80
Z-enolimidol	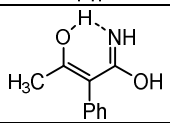	3:1:1:1	+25.02

Intramolecular hydrogen bond appears to be a key factor that influences tautomeric equilibrium in solution. In the case of β-ketoamides, the two tautomers of major concentration (ketoamide and *Z*-enolamide) form internal hydrogen bonds. This stabilizing factor explains the following spectral observations:

1) The high relative concentration of these tautomers,
2) The high value of δ observed for the hydroxyl proton in the enolamide form (peak Z, Fig. 1),

3) The two different δ values of the hydrogen atoms bonded to nitrogen in the ketoamide form (peaks C and D, Fig. 1).

Table 2 shows the ^{1}H chemical shifts of the eleven β-ketoamides in $CDCl_3$ and DMSO-d_6. In many cases, hydrogens attached to N were observed as very broad and low peaks in DMSO-d_6 (due to the fact that they form hydrogen bonds with the solvent causing a significant signal broadening). For this reason, their chemical shifts could not be determined properly.

The integrated spectra made possible to calculate the enol ratio considering the peaks of CH or CH_2 (ketoamide tautomer) and those of OH group (*Z*-enolamide tautomer) by following Equations 1 and 2.

$$\%\text{enol} = \frac{\text{OH integration}}{\text{OH integration + CH integration}} \cdot 100 \qquad \text{compounds } \mathbf{1}\text{-}\mathbf{8} \tag{1}$$

$$\%\text{enol} = \frac{\text{OH integration}}{\text{OH integration + } \frac{1}{2}\text{CH}_2 \text{ integration}} \cdot 100 \qquad \text{compounds } \mathbf{9}\text{-}\mathbf{11} \tag{2}$$

Then, the equilibrium constant (K = [enol]/[keto] = (%enol)/(%keto)) and the corresponding free energies at 25°C ($\Delta G^0 = -RT \ln K$) for the keto-enol equilibria were determined and they are shown in Table 3.

Table 2. ^{1}H chemical shifts (δ, ppm) for compounds 1-11

Compound	Solvent	Chemical shifts δ_H (ppm)
1	$CDCl_3$	1.80 (CH_3 enol); 2.26 (CH_3 keto); 4.68 (CH keto); 5.10/5.16 (NH_2 enol); 5.60/6.88 (NH_2 keto); 7.2 - 7.5 (aromatics); 14.68 (OH enol).
	DMSO-d_6	1.66 (CH_3 enol); 2.13 (CH_3 keto); 4.58 (CH keto); 7.2 - 7.4 (aromatics); 15.7 (OH enol).
2	$CDCl_3$	1.79 (CH_3 enol); 2.24 (CH_3 keto); 3.82 (OCH_3 keto); 3.84 (OCH_3 enol); 4.61 (CH keto); 5.10/5.31 (NH_2 enol); 5.73/6.81 (NH_2 keto); 6.9 - 7.4 (aromatics); 14.63 (OH enol).
	DMSO-d_6	1.71 (CH_3 enol); 2.10 (CH_3 keto); 3.85 (OCH_3 keto); 3.89 (OCH_3 enol); 4.51 (CH keto); 6.8 - 7.2 (aromatics) 15.67 (OH enol).
3	$CDCl_3$	1.80 (CH_3 enol); 2.26 (CH_3 keto); 4.63 (CH keto); 5.02/5.21 (NH_2 enol); 5.63/6.89 (NH_2 keto); 7.2 - 7.5 (aromatics); 14.72 (OH enol).
	DMSO-d_6	1.66 (CH_3 enol); 2.16 (CH_3 keto); 4.65 (CH keto); 7.2 - 7.5 (aromatics); 15.79 (OH enol).
4	$CDCl_3$	5.30 (NH_2 enol); 5.61 (CH keto); 5.53/6.98 (NH_2 keto); 7.1 - 8.0 (aromatics); 15.25 (OH enol).
	DMSO-d_6	5.75 (CH keto); 7.2 - 7.9 (aromatics)
5	$CDCl_3$	3.90 (OCH_3 keto); 3.93 (OCH_3 enol); 5.31 (NH_2 enol); 5.49 (CH keto); 5.63/7.18 (NH_2 keto); 6.9 - 8.0 (aromatics); 14.31 (OH enol).
	DMSO-d_6	3.83 (OCH_3 keto); 5.69 (CH keto); 7.1 - 7.9 (aromatics)
6	$CDCl_3$	5.37/5.46 (NH_2 enol); 5.54 (CH keto); 5.72/6.93 (NH_2 keto); 7.0 - 8.0 (aromatics); 15.30 (OH enol).
	DMSO-d_6	5.74 (CH keto); 7.2 - 8.0 (aromatics)
7	$CDCl_3$	3.76 (OCH_3 keto); 3.76 (OCH_3 enol); 5.38 (NH_2 enol); 5.54 (CH keto); 5.66/6.9[1] (NH_2 keto); 6.8 - 8.0 (aromatics); 15.22 (OH enol).
	DMSO-d_6	3.73 (OCH_3 keto); 5.68 (CH keto); 7.1 - 7.9 (aromatics)
8	$CDCl_3$	5.33 (NH_2 enol); 5.58 (CH keto); 5.62/7.2[1] (NH_2 keto); 7.0 - 8.0 (aromatics); 15.32 (OH enol).
	DMSO-d_6	5.79 (CH keto); 7.3 - 7.9 (aromatics)
9	$CDCl_3$	3.99 (CH_2 keto); 5.26 (NH_2 enol); 5.57 (CH enol); 5.55/7.02 (NH_2 keto); 7.2 - 8.1 (aromatics); 14.22 (OH enol).
	DMSO-d_6	3.90 (CH_2 keto); 7.15 (NH_2 enol); 5.78 (CH enol); 7.36 (NH_2 keto); 7.4 - 8.1 (aromatics); 15.31 (OH enol).

Compound	Solvent	Chemical shifts δ_H (ppm)
10	$CDCl_3$	3.86 (OCH_3 enol); 3.90 (OCH_3 keto); 3.93 (CH_2 keto); 5.49 (CH enol); 5.64/7.2[1] (NH_2 keto); 6.9 - 8.0 (aromatics); 14.31 (OH enol).
	DMSO-d_6	3.78 (CH_2 keto); 3.80 (OCH_3 enol); 3.84 (OCH_3 keto); 5.63 (CH enol); 7.0 - 8.0 (aromatics); 15.27 (OH enol).
11	$CDCl_3$	3.96 (CH_2 keto); 5.34 (NH_2 enol); 5.54 (CH enol); 5.68/7.00 (NH_2 keto); 7.2 - 8.0 (aromatics); 14.28 (OH enol).
	DMSO-d_6	3.86 (CH_2 keto); 5.74 (CH enol); 7.1 - 8.0 (aromatics); 15.31 (OH enol).

[1]*In compounds **7**, **8** and **10**, the peak corresponding to the ketoamide NH_2 overlaps the aromatic signals and its value cannot be determined precisely*

The relative stability of individual tautomers and the corresponding equilibrium shifts are explained below considering several factors, such as electronic substituent effects, steric effects introduced by bulky groups, differential solvation and tautomer stabilization *via* internal hydrogen bonds.

Table 3. Keto-enol content, equilibrium constant *K* and ΔG^0 in $CDCl_3$ and DMSO-d_6 at 25°C for compounds 1-11

Compound		Solvent	% enol	% keto	*K*	ΔG^0 (kcal·mol^{-1})
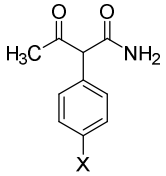	**1**	$CDCl_3$	79.2	20.8	3.82	−0.79 ± 0.06
	X = H	DMSO-d_6	17.3	82.7	0.210	0.97 ± 0.06
	2	$CDCl_3$	75.5	24.5	3.09	−0.67 ± 0.06
	X = OCH_3	DMSO-d_6	16.5	83.5	0.198	0.96 ± 0.06
	3	$CDCl_3$	79.5	20.5	3.88	−0.80 ± 0.06
	X = Cl	DMSO-d_6	18.0	82.0	0.220	0.90 ± 0.06
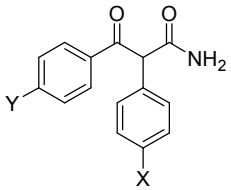	**4**	$CDCl_3$	28.0	72.0	0.389	0.56 ± 0.06
	X = Y = H	DMSO-d_6	0.0	100.0	0.0	-
	5	$CDCl_3$	9.0	91.0	0.099	1.79 ± 0.06
	X = H/Y = OCH_3	DMSO-d_6	0.0	100.0	0.0	-
	6	$CDCl_3$	40.6	59.4	0.684	0.22 ± 0.06
	X = H/Y = Cl	DMSO-d_6	0.0	100.0	0.0	-
	7	$CDCl_3$	25.0	75.0	0.333	0.65 ± 0.06
	X = OCH_3/Y = H	DMSO-d_6	0.0	100.0	0.0	-
	8	$CDCl_3$	28.8	71.2	0.404	0.54 ± 0.06
	X = Cl/Y = H	DMSO-d_6	0.0	100.0	0.0	-
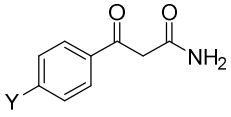	**9**	$CDCl_3$	12.2	87.8	0.139	1.17 ± 0.06
	Y = H	DMSO-d_6	29.1	70.9	0.411	0.53 ± 0.06
	10	$CDCl_3$	3.8	96.2	0.0393	1.94 ± 0.06
	Y = OCH_3	DMSO-d_6	14.7	85.3	0.173	1.58 ± 0.06
	11	$CDCl_3$	16.7	83.3	0.200	0.95 ± 0.06
	Y = Cl	DMSO-d_6	39.4	60.6	0.650	0.26 ± 0.06

Steric effects: Steric repulsion caused by bulky groups lowers the stability of both tautomers in different degree. In the case of *Z*-enolamide forms, compounds having two phenyl groups (**4**-**8**) exhibit greater steric repulsion than those having phenyl and methyl groups (**1**-**3**), and, therefore, the enol concentration is reduced in this kind of compounds. When considering ketoamide tautomers, such steric repulsion is reduced because of the rotation around the C2─C3 bond, letting the two phenyl groups to get further from each other.

On the other hand, bulky phenyl groups at C2 position increase the enolic content (compare compounds **9**-**11** with **1**-**3** and **4**-**8**). This fact is in concordance with previous studies where it has been demonstrated that bulky radicals in alpha position increase the enol content [25,26].

Electronic effects: The substituents may donate or withdraw electrons through resonance or inductive effects. An electron donating methoxy group and an electron withdrawing chlorine atom,

both placed at the *para*-position of phenyl rings, produce opposite effects: the presence of chlorine atoms (compounds **3**, **6**, **8** and **11**) make the enol content higher, whereas methoxy groups (compounds **2**, **5**, **7** and **10**) shift the equilibrium towards the keto tautomer. These effects are more pronounced if the substituent is attached to C3 (compare **5**-**7**/**6**-**8**).

These observations could be explained considering the influence of the substituents on the internal hydrogen bonds formed in each tautomer:

- An electron acceptor at C2 or C3 position (compounds **3**, **6**, **8** and **11**) strengthens the hydrogen bond in the enol tautomer stabilizing it, and destabilizes the keto form by weakening its hydrogen bond. Both facts increase the enolic content.
- An electron donor at C2 position (compounds **2** and **7**) weakens the hydrogen bond in the enol tautomer causing destabilization, while it stabilizes the keto form by enhancement of its hydrogen bond. These two facts decrease the enolic content.
- An electron donor at C3 position (compounds **5** and **10**) stabilizes the enol tautomer by strengthening its internal hydrogen bond, but it stabilizes the keto form even more by a stronger reinforcing of its internal hydrogen bond. Both facts decrease the enolic content.

At C2 position, the stabilizing effects in keto and enol form would be, ultimately, inductive. That is why in this position the effects are weaker than at C3, where inductive and mesomeric effects are affecting the keto and enol form. These assumptions are supported by previous works in gas phase [24] (where the same behaviour was observed and supported by theoretical calculations) and the analysis of the dependence of δ with temperature in the last section (Internal hydrogen bonds).

Solvent effects: Differential solvation effects generally produce equilibrium shifts in tautomeric systems. The data shown in Table 3 demonstrate that a higher solvent polarity produces an increase in keto forms concentration for compounds **1**-**8**, whereas in the case of compounds **9**-**11** the effect is opposite. This behaviour can be explained considering the values of Δ*H* and Δ*S* of each compound, discussed in the next section.

Temperature effects: Enol contents and equilibrium constants *K* were determined for compounds **1**-**11** in $CDCl_3$ and DMSO-d_6 at five different temperatures between 25°C and 45°C. Equation 3 provides a simple method for determining Δ*H* and Δ*S* in keto-enol tautomerization for the studied compounds.

$$\ln\left(\frac{[\text{enol}]}{[\text{keto}]}\right) = \ln K = -\frac{\Delta G^0}{RT} = -\frac{\Delta H}{R}\cdot\frac{1}{T} + \frac{\Delta S}{R} \qquad (3)$$

Figs. 2 and 3 show the ln*K* *vs* 1/*T* plots for β-ketoamides **1-11** in both solvents. The calculated slopes and y-intercepts obtained by linear fitting of these graphics can be used to determine the enthalpy and entropy of the tautomeric equilibrium of each compound. Unfortunately, this procedure could not be applied to compounds **4**-**8** in DMSO-d_6, since the enol tautomer could not be detected within the experimental temperature range. Results are shown in Table 4.

As expected, compounds including an electron donating moiety (compounds **2**, **5**, **7** and **10**), which have lower enolic contents (Table 3), show higher values of Δ*H* compared to the reference compounds (**1**, **4** and **9**). On the other hand, β-ketoamides having electron withdrawing groups (compounds **3**, **6, 8** and **11**) exhibit higher enolic contents and lower Δ*H* values.

The Δ*H* values shown in Table 4 are more negative in DMSO-d_6 than in $CDCl_3$, indicating that, in this solvent, the enol form would be more stabilized than the keto form. This effect can be explained considering that one molecule of *Z*-enolamide tautomer can form two intermolecular hydrogen bonds with DMSO, while in the ketoamide tautomer only one intermolecular hydrogen bond is possible (Scheme 3).

On the other hand, Δ*S* values are more negative in DMSO-d_6 compared with $CDCl_3$, what would shift the equilibrium towards the keto tautomer. This fact can be explained considering the different molecular arrangements that are set when the tautomers form hydrogen bonds with DMSO-d_6.

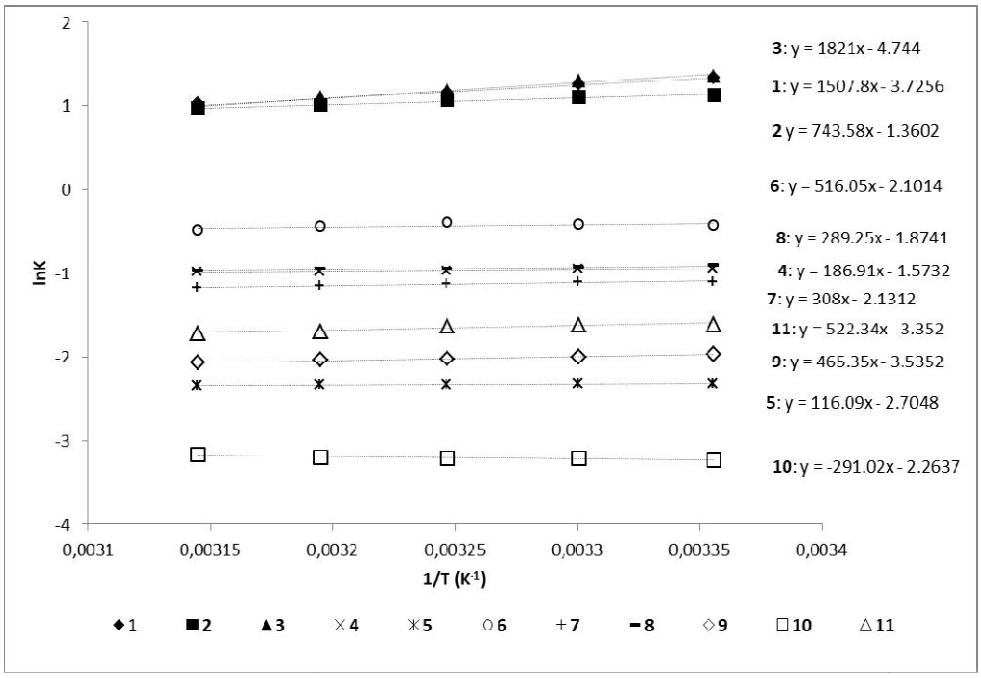

Fig. 2. ln*K vs* 1/*T* plot for compounds 1-11 in $CDCl_3$. Linear fitting equations shown on the right

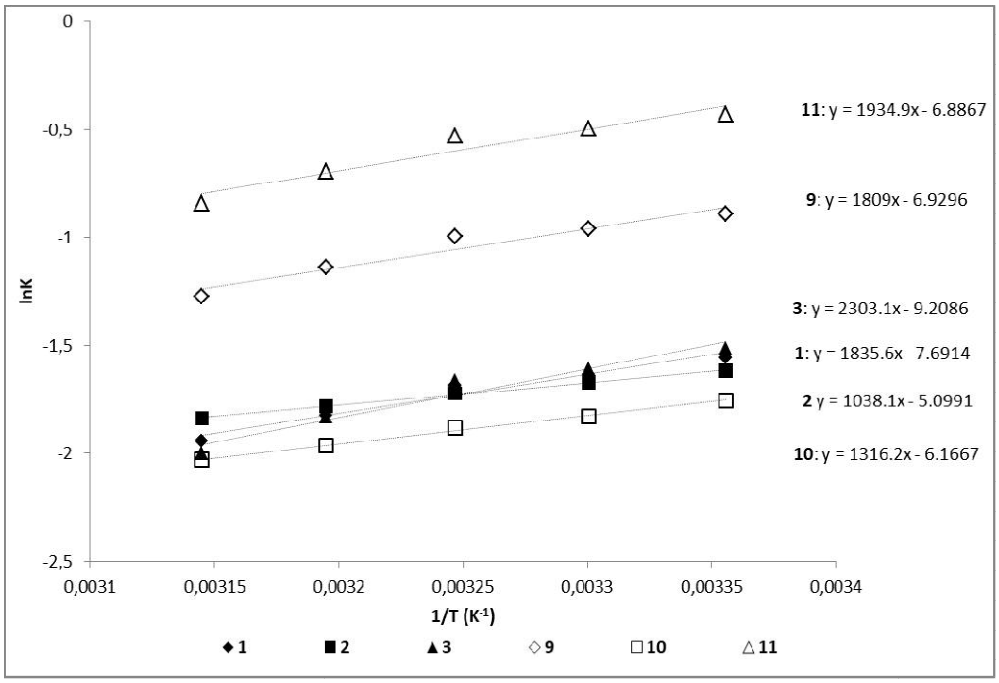

Fig. 3. ln*K vs* 1/*T* plot for compounds 1-3 and 9-11 in DMSO-d_6. Linear fitting equations shown on the right

Table 4. Thermodynamic parameters in $CDCl_3$ and in DMSO-d_6 for compounds 1-11

Compound		$CDCl_3$		DMSO-d_6	
		Δ*H* **(kcal/mol)**	**Δ*S*** **(cal/mol·K)**	**Δ*H*** **(kcal/mol)**	**Δ*S*** **(cal/mol·K)**
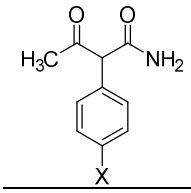	**1** X = H	−3.0 ± 0.2	−7.4 ± 0.7	−3.6 ± 0.8	−15 ± 3
	2 X = OCH_3	−1.6 ± 0.2	−3.0 ± 0.7	−2.0 ± 0.2	−10.0 ± 0.5
	3 X = Cl	−3.1 ± 0.1	−7.6 ± 0.3	−5 ± 1	−18 ± 4
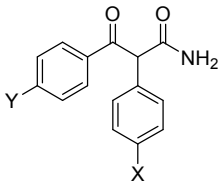	**4** X = Y = H	−0.40 ± 0.02	−3.20 ± 0.05	-	-
	5 X = H/Y = OCH_3	−0.23 ± 0.08	−6.7 ± 0.3	-	-
	6 X = H/Y = Cl	−1.0 ± 0.3	−4 ± 1	-	-
	7 X = OCH_3/Y = H	−0.32 ± 0.07	−3.3 ± 0.3	-	-
	8 X = Cl/Y = H	−0.58 ± 0.08	−3.7 ± 0.5	-	-
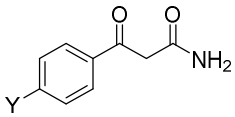	**9** Y = H	−0.92 ± 0.01	−7.02 ± 0.04	−3.6 ± 0.9	−14 ± 3
	10 Y = OCH_3	+0.5 ± 0.3	−4.9 ± 0.9	−2.7 ± 0.2	−14.4 ± 0.5
	11 Y = Cl	−1.1 ± 0.3	−7 ± 1	−4 ± 1	−14 ± 4

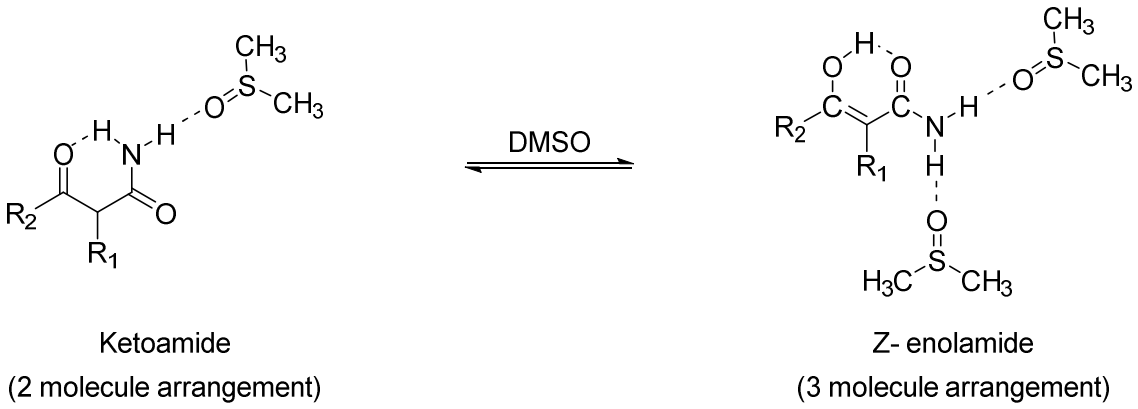

Scheme 3. Solvent-tautomer interaction in ketoamide-enolamide equilibrium

The result of these two contrary effects is explained by experimental determinations, and the overall equilibrium shift (which depends ultimately on Δ*G*, Table 3) indicates that in compounds **1**-**8** the entropic effect predominates over the enthalpic effect. On the other hand, in compounds **9**-**11** the enthalpic effect is the one that rules the situation. This difference can be explained considering that in compounds **1**-**8** (in which R_1 = Ar) the solvation of one NH hydrogen is sterically hindered by the phenyl group. In the case of compounds **9**-**11** (in which R_1 = *H*) both NH hydrogens are easily solvated. These assumptions are supported by the different decrease in Δ*H* in DMSO-d_6 respecting to $CDCl_3$ (approximately a decrease of 1 kcal/mol for compounds **1**-**3** and 3 kcal/mol for compounds **9**-**11**).

Data obtained from these experiments also show a linear relation between ln*K* at different temperatures. Fig. 4 shows the plot of ln*K* at 45°C *vs* ln*K* at 25°C, where the linear fitting suggests a common mechanism underlying all the studied equilibria [27].

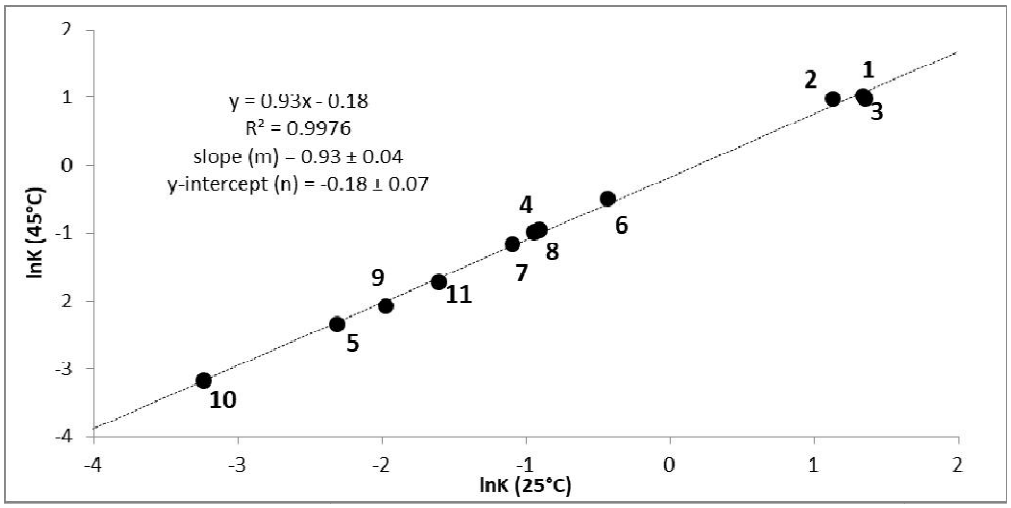

Fig. 4. ln*K* (45°C) *vs* ln*K* (25°C) plot for compounds 1-11 in $CDCl_3$

Enthalpies of reaction ΔH were calculated in order to support the previous assumptions. In the case of DMSO, two types of calculations were made: considering the solvent as PCM model (i.e. homogeneous polarizable medium surrounding the molecule) and adding explicit solvent molecules. Figs. 5 and 6 show the calculated *vs* the experimental *ΔH* plots in chloroform and DMSO, respectively.

In $CDCl_3$, the calculated values are close to the experimental ones, within a medium deviation of 0.3 kcal/mol. In the case of DMSO-d_6, calculations are improved when considering explicit solvent molecules (medium deviations are 1.5 kcal/mol and 0.6 kcal/mol for calculations using PCM model and PCM + explicit solvent molecules, respectively). This results support the previous assumptions regarding solvation of tautomers by DMSO *via* hydrogen bonds.

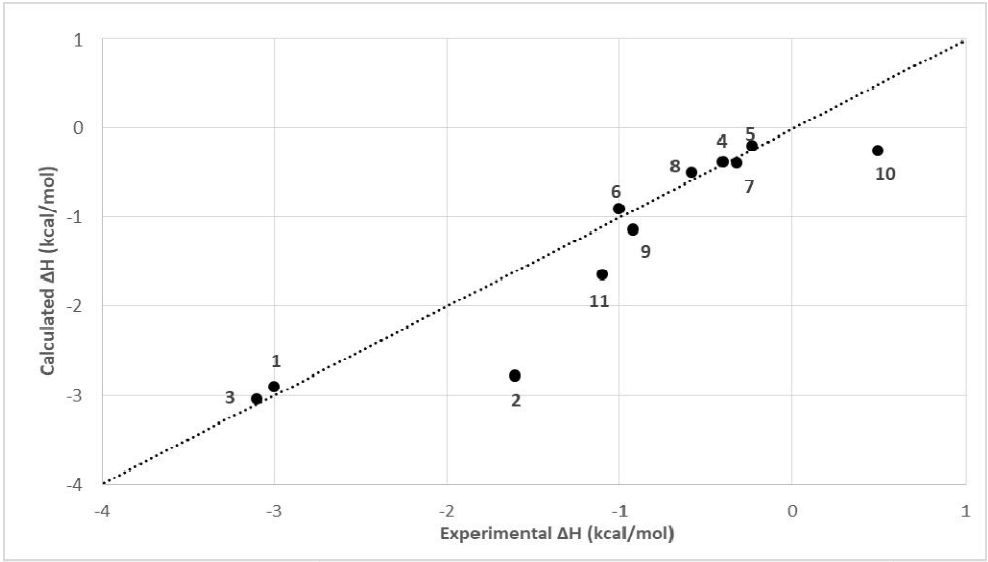

Fig. 5. Calculated vs experimental ΔH for tautomeric equilibrium of compounds 1-11 in $CDCl_3$

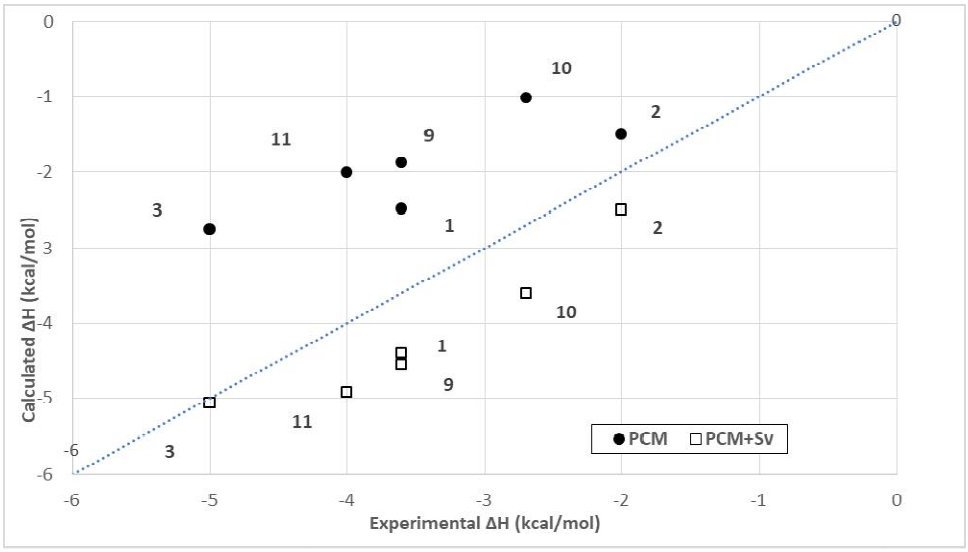

Fig. 6. Calculated vs experimental ΔH for tautomeric equilibrium of compounds 1-3 and 9-11 in DMSO-d_6

Internal hydrogen bonds: In order to correlate enol contents and thermodynamic functions (Δ*H* and Δ*S*) with the stability of the intramolecular hydrogen bonds, the dependence of δ of OH and NH hydrogens (δ_{OH} and δ_{NH}) with temperature was studied for compounds **1**-**3** and **9**-**11** in $CDCl_3$. Previous works have proved that Δ*δ*/Δ*T* values can be correlated with the stability of hydrogen bonds (the lower the value of Δ*δ*/Δ*T*, the greater the stability of the bond) [28]. The data are presented in Table 5.

This analysis could not be made for compounds **4**-**8**, since the signals corresponding to NH hydrogen are overlapped with the aromatic peaks, impeding a precise determination of their δ.

Table 5. Temperature dependence of δ_{OH} and δ_{NH} for compounds 1-3 and 9-11 in $CDCl_3$

Tautomeric form	Compound	Δ*δ*/Δ*T* (ppb/K)
	1 (R_1 = Ph / R_2 = CH_3)	−1.6 ± 0.1
	2 (R_1 = *p*-MeOPh / R_2 = CH_3)	−1.8 ± 0.2
	3 (R_1 = *p*-ClPh / R_2 = CH_3)	−1.2 ± 0.1
	9 (R_1 = H / R_2 = Ph)	−1.7 ± 0.2
	10 (R_1 = H / R_2 = *p*-MeOPh)	−1.5 ± 0.5
Z-enolamide	**11**(R_1 = H / R_2 = *p*-ClPh)	−1.15 ± 0.03
	1 (R_1 = Ph / R_2 = CH_3)	−6.80 ± 0.06
	2 (R_1 = *p*-MeOPh / R_2 = CH_3)	−6.5 ± 0.6
	3 (R_1 = *p*-ClPh / R_2 = CH_3)	−7.3 ± 0.8
	9 (R_1 = H / R_2 = Ph)	−5.80 ± 0.06
	10 (R_1 = H / R_2 = *p*-MeOPh)	−5.2 ± 0.8
	11(R_1 = H / R_2 = *p*-ClPh)	−6.0 ± 0.6
ketoamide		

The calculated Δ*δ*/Δ*T* values agree with the ones obtained in previous works for similar compounds (Δ*δ*/Δ*T* < 4 ppb/K for O─H···O and Δ*δ*/Δ*T* < 9 ppb/K for N─H···O) [28], corroborating that the hydrogen bonds are, indeed, intramolecular. Similar trends are obtained in DMSO-d_6.

Data from Table 5 are consistent with the previous assumptions regarding the effect of the internal hydrogen bonds on the stability of the tautomers. In other words, compounds showing lower values of $\Delta\delta_{OH}/\Delta T$ and higher values of $\Delta\delta_{NH}/\Delta T$ are also the ones that have higher enolic content and *vice versa*.

These assumptions about the strength of hydrogen bonds can be further corroborated by means of a method previously reported for diamines which compares the calculated OH and NH vibration frequencies of the molecules with and without internal hydrogen bonds [29]. Such frequencies are in each case lower for the conformer that presents hydrogen bond and higher for the one that does not. The difference between these two values is correlated to the energy of the hydrogen bond (the higher the difference in frequency, the higher the bond strength).

The values obtained in a previous work for these eleven β-ketoamides [24] show that electron acceptors (no matter their position) would reinforce the O─H···O=C bond in the *Z*-enolamide tautomer and weaken the C=O···H─N bond in the ketoamide tautomer, being the effect opposite in the case of donors placed at C2. Donors at C3 would make both hydrogen bonds stronger, but the effect would be more important in the ketoamide tautomer. These results support the assumptions stated above (Electronic effect section), remarking the importance of hydrogen bond as a crucial factor affecting equilibrium shift in this system.

4. CONCLUSIONS

Keto-enol tautomerism is observed in a series of β-ketoamides by means of NMR spectroscopy, being amide-imidol equilibrium not detectable. The equilibrium is strongly dependent on solvents, temperature and substituents. Intramolecular hydrogen bond formation seems to be a significant factor that stabilizes the different tautomeric forms.

In solution, these compounds exist mainly as ketoamide and *Z*-enolamide tautomers, both forming internal hydrogen bonds. The rest of the possible tautomers (ketoimidol, *E*-enolamide, *E*- and *Z*-enolimidol) show very low concentration (at least lower than the detection limit) or probably do not exist in neutral solution.

In all cases, the equilibrium is shifted to the *Z*-enolamide form by several factors:

1) Electron withdrawing substituents (e.g. *p*-chlorophenyl).
2) A temperature decrease, since the equilibria are exothermic (except for one compound).
3) Bulky groups at C2 position. This effect is less important when there are two phenyl groups at C2 and C3 positions, because of the steric hindrance.
4) The presence of hydrogen bond acceptor solvents (e.g. DMSO), but only when there are no bulky groups on C2. Otherwise, hydrogen bond acceptor solvents decrease the enol content.

All these factors increase the enolamide content apparently by stabilizing the *Z*-enolamide tautomers (strengthening the internal O─H···O=C hydrogen bond) and/or destabilizing the ketoamide tautomer (weakening the internal C=O···H─N hydrogen bond).

ACKNOWLEDGEMENTS

Financial support is highly acknowledged to Facultad de Ciencias Exactas-UNLP (Universidad Nacional de La Plata, Buenos Aires, Argentina), CONICET (Consejo Nacional de Investigaciones Científicas y Técnicas) and CIC BA (Comisión de Investigaciones Científicas de la Provincia de Buenos Aires).

COMPETING INTERESTS

Authors have declared that no competing interests exist.

REFERENCES

1. Bunting JW, Kanter JP. Acidity and tautomerism of β-Keto-Esters and amides in aqueous-solution. Journal of the American Chemical Society. 1993;115(25):11705-11715. Available:http://dx.doi.org/10.1021/ja00078a008

2. Yamasaki K, Kajimoto O. Solvent effect in super critical fluids: Keto-Enol equilibria of acetylacetone and ethyl acetoacetate. Chemical Physics Letters. 1990;172(3-4):271-274.
Available:http://dx.doi.org/10.1016/0009-2614(90)85401-W
3. Ruiz DL, Albesa AG, Ponzinibbio A, Allegretti PE, Schiavoni MM. Solvent effects on tautomerics equilibria in β-Ketonitriles: NMR and theoretical studies. Journal of Physical Organic Chemistry. 2010;23(10):985-994.
Available:http://dx.doi.org/10.1002/poc.1764
4. Hynes MJ, Clarke EM. Kinetics of enolisation of β-Ketoamides. Journal of the Chemical Society, Perkin Transactions 2. 1994;4:901-904.
5. Wengenroth H, Meier H. (E)-und (Z)-Enole von β-Ketocarbonsäureamiden. Chemische Berichte. 1990;123(6):1403-1409.
Available:http://dx.doi.org/10.1002/cber.19901230633
6. Naoum MM, Saad GR. Solvent effect on tautomeric equilibria and dipole moments of some alpha substituted benzoylacetanilides. Journal of Solution Chemistry. 1998;17(1):67-76.
Available:http://dx.doi.org/10.1007/BF00651854
7. Valters RE, Fülöp F, Korbonits D. Recent developments in ring-chain tautomerism. II. Intramolecular reversible addition reactions to the C=N, C=N, C=C, and C=C groups. Advances in Heterocyclic Chemistry. 1996;66:1.
Available:http://dx.doi.org/10.1016/S0065-2725(08)60304-9
8. Lázár L, Fülöp F. Recent developments in the ring-chain tautomerism of 1,3-heterocycles. European Journal of Organic Chemistry. 2003;2003(16):3025-3042.
9. Lázár L, Göblyös A, Evanics F, Bernáth G, Fülöp F. Ring-chain tautomerism of 2-Aryl-substituted imidazolidines. Tetrahedron. 1998;54(44):13639-13644.
Available:http://dx.doi.org/10.1016/S0040-4020(98)00840-0
10. Göblyös A, Lázár L, Evanics F, Fülöp F. Ring-chain tautomerism of 2-aryl-substituted imidazoli dines. Heterocycles. 1999;51(10):2431- 2438.
Available:http://dx.doi.org/10.3987/COM-99-8624
11. Zelenin KN, Alekseyev VV, Ukraintsev IV, Tselinsky IV. 2-substituted hexahydropyrimidines and their tautomerism. Organic Preparations and Procedures International. 1998;30(1):53-61.
Available:http://dx.doi.org/10.1080/00304949809355259
12. Göblyös A, Lázár L, Fülöp F. Ring-chain tautomerism of 2-aryl-substituted-hexahydropyrimidines and tetrahydroquinazolines. Tetrahedron. 2002;58(5):1011-1016.
Available:http://dx.doi.org/10.1016/S0040-4020(01)01196-6
13. Maloshitskaya O, Sinkkonen J, Ovcharenko VV, Zelenin KN, Pihlaja K. Chain-ring-chain tautomerism in 2-aryl-substituted hexahydropyrimidines and 1H-2,3- dihydroperimidines. Does it appear? Tetrahedron. 2004;60(32):6913-6921.
Available:http://dx.doi.org/10.1016/j.tet.2004.05.092
14. Sinkkonen J, Zelenin KN, Potapov AK, Lagoda IV, Alekseyev VV, Pihlaja K. Ring-chain tautomerism in 2-substituted 1,2,3,4-tetrahydroquinazolines A ^{1}H, ^{13}C and ^{15}N NMR study. Tetrahedron. 2003;59(11):1939-1950.
Available:http://dx.doi.org/10.1016/S0040-4020(03)00148-0
15. Claramunt RM, López C, Santa María MD, Sanz D, Elguero J. The use of NMR spectroscopy to study tautomerism. Progress in Nuclear Magnetic Resonance Spectroscopy. 2006;49(3-4): 169-206.
Available:http://dx.doi.org/10.1016/j.pnmrs.2006.07.001
16. Barros MT, Geraldes CFGC, Mavcock CD, Silva M. A proton and ^{13}C NMR study of keto-enol tautomerism of some β-ketoamides. Journal of Molecular Structure. 1986;142:345-349.
Available:http://dx.doi.org/10.1016/0022-2860(86)85150-X
17. Laurella S, González Sierra M, Furlong J, Allegretti P. Analysis of tautomerism in β-ketobuanamides by nuclear magnetic resonance: Substituent, temperature and solvent effects. Journal of Applied Solution Chemistry and Modeling. 2012;1:6-12.
18. Hauser CR, Eby CJ. Cyclization of β-ketonitriles or β-ketoamides with ketones by polyphosphoric acid to form substituted 2-pyridones. Journal of the American Chemical Society. 1957;79(3):728-731.
Available:https://doi.org/10.1021/ja01560a062

19. Laurella SL, González Sierra M, Furlong JJP, Allegretti PE. Substituent, temperature and solvent effects on the keto-enol equilibrium in β-ketoamides: A nuclear magnetic resonance study. Open Journal of Physical Chemistry. 2013;3:138-149.
Available:http://dx.doi.org/10.4236/ojpc.2013.34017
20. Parr RG, Yang W. Density-functional theory of atoms and molecules. Oxford University Press, New York; 1989.
21. Frisch MJ, Trucks GW, Schlegel HB, Scuseria GB, Robb MA, Cheeseman JR, et al. Gaussian 03, Revision B.03, Gaussian, Inc., Pittsburgh PA; 2003.
22. Becke D. Density-functional thermochemistry. III. The role of exact exchange. Journal of Chemical Physics. 1993;98:5648-5652.
Available:https://doi.org/10.1063/1.464913
23. Cancs MT, Mennucci B, Tomasi J. A new integral equation formalism for the polarizable continuum model: Theoretical background and applications to isotropic and anisotropic dielectrics. Journal of Chemical Physics. 1997;107:3032-3041.
Available:https://doi.org/10.1063/1.474659
24. Laurella SL, Latorre CV, Dietrich RC, Furlong JJP, Allegretti PE. Tautomeric equilibria analysis of β-ketoamides by mass spectrometry. Journal of Physical Organic Chemistry. 2012;25(12): 1365-1373.
25. Rappoport Z, Biali S. Stable simple enols. 9. solid state structures and conformations of several simple enols and their keto tautomers. Journal of the American Chemical Society. 1985;105: 1701-1709.
26. Miller AR. Sterically stabilized enols: A study employing the internal rotational barriers of the destabilized ketones. The Journal of Organic Chemistry. 1976;41(22):3599-3602.
Available:http://dx.doi.org/10.1021/jo00884a026
27. Starikov EB, Nordén B. Entropy-enthalpy compensation as a fundamental concept and analysis tool for systematical experimental data. Chemical Physics Letters. 2012;538:118-120.
Available:http://dx.doi.org/10.1016/j.cplett.2012.04.028
28. Lämmermann A, Szatmári I, Fülöp F, Kleinpeter E. Inter- or intramolecular N···H−O or N−H···O hydrogen bonding in 1,3-amino-*α*/β-naphthols: An experimental NMR and computational study. The Journal of Physical Chemistry A. 2009;113(21):6197-6205.
Available:http://dx.doi.org/10.1021/jp902731n
29. Gellman SH, Dado GP, Liang G, Adams GBR. Conformation-directing effects of a single intramolecular amide-amide hydrogen bond: Variable-temperature NMR and IR studies on a homologous diamide series. Journal of the American Chemical Society. 1991;113:1164-1173.
Available:https://doi.org/10.1021/ja00004a016

Biography of author(s)

Diego D. Colasurdo
CEDECOR (Centro de Estudio de Compuestos Orgánicos), Facultad de Ciencias Exactas, Universidad Nacional de La Plata (UNLP), Calle 115 y 47, (1900) La Plata, Argentina and CONICET (Consejo Nacional de Investigaciones Científicas y Técnicas), Argentina.

Research and Academic Experience: He works as professor assistant in Organic Chemistry. He is finishing his doctoral thesis. He has worked in many research projects. He has participated in several national and international congresses.

Research Area: Organic Chemistry.

Number of Published papers: 6.

Any other remarkable point(s): He has participated on the publication of two books.

Dr. Patricia E. Allegretti
CEDECOR (Centro de Estudio de Compuestos Orgánicos), Facultad de Ciencias Exactas, Universidad Nacional de La Plata (UNLP), Calle 115 y 47, (1900) La Plata, Argentina and CIC-BA (Comisión de Investigaciones Científicas de la Provincia de Buenos Aires), Argentina.

Research and Academic Experience: She works as Associate Professor in Organic Chemistry. Not only has she supervised many doctoral theses and degree works but also she has worked in several research projects. She has participated in several national and international congresses.

Research Area: Organic Chemistry.

Number of Published papers: 86.

Special Award (If any): She has an awarded work in cosmetic Chemistry.

Any other remarkable point(s): She heads the Organic Compounds Research Center (CEDECOR) in Facultad de Ciencias Exactas, from Universidad Nacional de La Plata.

Dr. Sergio L. Laurella
CEDECOR (Centro de Estudio de Compuestos Orgánicos), Facultad de Ciencias Exactas, Universidad Nacional de La Plata (UNLP), Calle 115 y 47, (1900) La Plata, Argentina and CIC-BA (Comisión de Investigaciones Científicas de la Provincia de Buenos Aires), Argentina.

Research and Academic Experience: He works as Associate Professor in Organic Chemistry. He has worked in many research projects. He has participated in several national and international congresses. He is leading two doctoral theses currently.

Research Area: Organic Chemistry.

Number of Published papers: 26.

Special Award (If any): He has been distinguished by Universidad Nacional de La Plata as prominent graduate.

Any other remarkable point(s): He has published three books. He worked in many transference jobs and he has been involved in some technological developments.

© Copyright (2020): Author(s). The licensee is the publisher (Book Publisher International).

DISCLAIMER
This chapter is an extended version of the article published by the same author(s) in the following journal.
Open Journal of Physical Chemistry, 3: 138-149, 2013.

Chapter 3
Print ISBN: 978-93-90206-41-4, eBook ISBN: 978-93-90206-42-1

Recent Observations on Preparation of Novel Chitosan-Starch Blends as a Multi-function Thickening Agent and Their Application in Textile Printing

E. S. Abdou[1], H. M. El-Hennawi[2] and K. A. Ahmed[2*]

DOI: 10.9734/bpi/crdc/v4

ABSTRACT

Chitosan, a naturally available biopolymer which is now increasingly used as a functional finish on textile substrates to impart antimicrobial characteristics and increase1 dye uptake of fabrics, was blended with different ratios of gelatinized starch. e chitosan was extracted and characterized by IR, H-NMR, and X-ray powder direction. These blends were tested as thickeners in textile screen printing using *Curcuma tinctoria* as natural dye. e rheological properties and the viscosity of the printing paste were measured. The effect of chitosan on the printing properties of different fabrics (natural, blends, and synthetic fabrics) was studied by measuring the color strength value (K/S) and related color parameters of the printed fabrics. e antimicrobial properties of printed fabrics were assessed. The results proved that the printed fabrics using these new thickeners showed increase in the color strength value (K/S) giving darker color which means that chitosan increased the dye uptake on fabrics. Fastness properties of the printed fabrics to washiftng, rubbing, perspiration, and light have also been improved. Thee treated fabrics were found to be antimicrobial also these blends used as a multi-functional thickener via adding of chitosan to gelatinous starch that it act as antibacterial agent, binder, and improve the pigment printing properties of different fabrics.

Keywords: p(x)-Laplacian equation; existence; uniqueness; numerical blow-up; variable exponents; difference method.

1. INTRODUCTION

Improving the environmental impact and unifying processes as a result of using one class of dyes in coloring fabrics made of blends of chemical and natural fibers is one of the main trends in the evolution of textile dyeing and printing technology. Recently, there has been a revival of interest in natural dyes throughout the world as some synthetic dyes are being banned due to their toxic, carcinogenic, and polluting nature. Natural dyes are used for food coloring, painting, and textile dyeing [1,2]. They have shown a greater interest in textile dyeing because they are more eco-friendly than synthetic. Recently, there has been a revival of interest in natural dyes throughout the world as some synthetic dyes are being banned due to their toxic, carcinogenic, and polluting nature. Most natural dyes need the use of chemicals, called mordant, to help promoting dye absorption and fixing and prevent bleeding and fading of the colors. Mordants form chemical bonds between the dye molecules and the proteins of the fabrics (wool is generally the best fabric colored with natural dyes). Natural dyes are used for food coloring, painting, and textile dyeing [1,2]. They have shown a greater interest in textile dyeing because they are more eco-friendly than synthetic dyes. Curcumin (1,7-bis(4-hydroxy-3-methoxy phenyl)-1,6-heptadione-3,5-dione) is a yellow pigment present in rhizome of *Curcuma longa* which is widely used in food industry [3]. Treatment of textiles with chitosan which is considered as multifunctional finish not only contributes to its antimicrobial properties but also results

[1]*Department of Chemistry, Faculty of Science and Humanities, Salman Bin Abdualaziz University, Saudi Arabia.*
[2]*Department of Chemistry of Dyeing, Printing and Auxiliaries, Textile Division, National Research Center, Cairo, Egypt.*
**Corresponding author: E-mail: kawther_zaher@yahoo.com, k.ali@qu.edu.sa;*

in enhancement of color strength thus generating much interest towards chitosan [4-6]. It is also used as an auxiliary in printing of textiles. It has been reported that the printed samples have comparable color fastness to that of commercial printed samples, but chitosan film on fabric surface is not desirable since it causes the problem of fabric stiffness (poor handling) [7,8]. Blending of starch with chitosan results in formation of edible coating with a good film forming and mechanical properties [9]; starch must be gelatinized first before blending with chitosan. Hence the aim of the present study is to investigate the combined effect of chitosan and gelatinized starch as thickening agent in screen printing technique using natural dye and to explore its antimicrobial properties.

2. BASIC SPACES AND THE MAIN RESULTS

2.1. Materials

2.1.1 Soluble starch was obtained from Fluka Chemical Company

2.1.2 *Curcuma tinctoria* was purchased from the local market

2.1.3 High viscosity sodium alginate from brown algae, manufactured by (Fluka Chemical Company), was used as a thickening agent

2.1.4 Fabric

Cotton: Mill desized,2 bleached, and mercerized cot-ton fabrics (130 g/m) produced by Misr/Helwan for Spinning and Weaving Company, Egypt.

Wool: Mill scoured wool fabric (100%) supplied by Misr Co. for Spinning and Weaving, Mehalla El-Kubra, Egypt.

Nylon: Nylon-6 fabric produced by El-Shourbagy Co. Cairo, Egypt.

Polyester: Polyester- (PE-) knitted fabric of 150 g/m^2, supplied by a private sector company which was treated with a◦ solution containing 1 g/L nonionic detergent at 7°C for 1/2 h, thoroughly washed, and air-dried at room temperature.

Blend fabrics: Different kinds of blended fabrics comprise viscose/polyester (80/20) and cotton/polyester (60/40) were also used.

2.2 Methods

2.2.1 Extraction of chitosan

Chitosan was extracted from-marine shrimp shells%. e exoskeletons of the shrimps were crushed and treated in the usual way with HCl, NaOH 1-2 M then with 40 NaOH to extract the chitosan [10]. Chitosan was characterized 1using the Fourier transform infrared (FTIR) spectroscopy, H-NMR% spectroscopy, and X-ray powder diffraction.

The degree of deacetylation (DDA) of chitosan deter-mined by potentiometric titration [11], and the molecular weight % was calculated using the value of intrinsic viscosity%11 [12]. 44 measured×10 by an Ubbelohde viscometer. The value of (DDA) and4 molecular weight of chitosan were 85 and gm/mol, respectively.

2.2.2 Characterization of prepared chitosan

The Fourier Transform Infrared (FTIR) Spectroscopy. The FTIR spectra were measured in KBr pellets−1 in the transmission mode in the range 4001–7000 cm using Perkin-Elmer 2000 spec-trophotometer1. *H-NMR Spectra.* Nuclear magnetic resonance H-NMR spectra were measured2 using JNMAl 300; Jeol spectrometer at 300 MHz in D O in which drops of DCl was added to enhance solubility. *X-Ray Diffraction.* X-ray diffraction analysis (XRD) was applied to detect the crystallinity of the extracted samples of chitin and their corresponding chitosan. A Scintag powder diffractometer was

used for this purpose between 2θ angles of 5° and 40°. Ni-filtered Cu K -radiation was used as the X-ray source. The relative crystallinity of the polymers was calculated by dividing the area of the crystalline peaks by the total area under the curve.

2.2.3 Gelatinization of starch solution in microwave

Starch was gelatinized first in microwave before blending with chitosan. Starch samples with predetermined starch concentrations, were prepared by using soluble starch and distilled water, and the samples were stirred gently just before heating them in the microwave oven in order %to ensure that the starch was fully suspended in the water. e starch ratio in the prepared samples was 3, 4, 5, and 6. Then starch samples (150 mL) were heated at full power in the microwave oven WP800 for 2 minutes.

2.2.4 Blend formation

Chitosan was blended % with all the prepared gelatinized starch with fixed ratio 1 of the starch samples.

2.2.5 Preparation of printing paste

The suitability of chitosan and gelatinized starch blends as thickening agents in screen printing technique was investigated using *Curcuma tinctoria* as natural dye. To achieve this goal, different printing paste using the new thickeners and another one with sodium alginate as thickening agent for the sake of comparison were prepared according to the recipe given in Table 1.

Sodium alginate was first soaked in small amount of water overnight at room temperature before preparing the printing paste. The natural color and urea were then added on the thickener suspension as in the recipe mention then the total weight of the whole paste was adjusted to one kilogram with the addition of the necessary amount of water. All the printed samples except the wool samples werefi fixed via thermofixation at 160°C for 5 min. The wool printed samples were fixed by steaming at 100°C for 10 min after fixation the printed samples were washed as follows.

1. Washiftng with cold running water.

2. Soaping (using 2 g/L nonionic detergent namely Espycon 1030) at 45 C for 15 minutes.

3. Rinsing with cold water.

At this end the printed fabrics were dried and assessed for color strength value (K/S) and over all fastness properties.

Table 1. Printing paste recipe

Thickening agent (Sod.alginate suspension or chitosan-starch blends)	500 g
Curcuma tinctoria	30 g
Urea	100 g
Water	370 g
	1000 g

2.2.6 Rheological properties

Rheological properties of chitosan/gelatinous-starch blends were studied using Brookfield Digital Rheometer, model HA DVIII Ultra (Brookfield engineering Laboratories INC.), with spindle no. SC4-21 [13]. The rheological parameters for starch chitosan blends were measured at room temperature.

2.2.7 Determination of color strength and related parameters

The color strength of the printed samples was evaluated by Hunter Lab Ultra scan PRO. at λmax. The color difference and relative color strength % between chitosan/starch printed samples and control samples were also obtained using the following relationships. Relative color strength (%) = (K/S of chitosan/starch blend)/(K/S of control sample) ×100:

$$\Delta E = \sqrt{(\Delta L)^2 + (\Delta a)^2 + (\Delta b)^2}$$

$$\text{where } \Delta L = L - L^*; \qquad \Delta a = a - a^*; \qquad \Delta b = b - b^*. \tag{1}$$

"L" describes lightness; "a" measures redness or greenness "b" measures yellowness or blueness; where L^*, a^*, and b^* are color parameters of control sample.

2.2.8 Determination of fastness properties

Thee treated samples were washed as per the conditions specified in the test.

AATCC test method [14]. The color fastness to rubbing, perspiration, and light was determined according to the AATCC test methods [15–17].

2.2.9 Antibacterial activity

The Antibacterial activity was assayed in the Microanalytical Centre of Cairo University using Kirby-Bauer disc diffusion method [18].

3. MAIN RESULTS

This paper aims to produce a multi-functional thickener via adding of chitosan to gelatinous starch that it act as antibacterial agent, binder, and improve the pigment printing properties of different fabrics. The used chitosan was extracted from Egyptian marine shrimp shell and characterized by IR, ^{1}H-NMRand X-ray powder diffraction. The blends were prepared by adding fixed ratios of Chitosan to all the gelatinized starch samples. Different fabrics (natural, blend and synthetic) were printed by screen printing technique. For the comparison another samples were printed using the traditional printing paste which contain commercial binder.

Generally, the data showed that the printed samples using starch /chitosan blends either in a ratio of 5% or 6% achieved improvement in the colour strength and related colour parameters are higher than those printed using the traditional pigment printing paste with good to excellent fastness properties.

3.1 Existence

FTIR Spectra. The FTIR spectra of chitosan represent a characteristic band at 3424 cm^{-1} which is attributed to –NH2 and –OH groups stretching vibration, the band for amide at 1654 cm^{-1}, and the aliphatic C–H stretching between 2921 and 2876 cm^{-1}, When starch and chitosan are mixed, physical blends versus chemical interactions are reflected by changes in characteristic spectra peaks In the typical spectrum of chitosan/starch composite film, the amino peak of chitosan shiftfted from 1578 to 1584 cm^{-1} with the addition of starch). This result indicated that interactions were present between the hydroxyl groups of starch and the amino groups of chitosan [19,20].

3.2 1H-NMR Method

The chemical shiftft of methyl protons in acetamide group to appear at 2.07 ppm in acidic deuterium oxide solutions while the methyl group of glacial acetic acid appears at 2.12 ppm (The Aldrich Library

of NMR Spectra). Therefore, the peak around 2.1 ppm can be safely assigned to the methyl protons in the acetamide group, and that around 2.2 ppm is due to the methyl group in acetic acid moiety. The chemical shift is affected by solvent type, concentration and temperature, and taking these into account, one can explain the difference between the chemical shift value reported by Shen et al. [21], and those reported here.

In the obtained spectra, the difference in chemical shift s between peaks at about 2.1 and 2.2 ppm is constant (about 0.15 ppm) within the experimental errors. The setting of TMS peak to be 0 ppm is sometimes slightly affected by operational and spectral variations, and for peaks with many "spikes" as in our case, the reproducibility might be lowered. Therefore, it can be safely stated that the chemical shift for amide methyl protons can be set to 2.06 ppm and that for acetic acid moiety to 2.21 ppm.

3.3 X-Ray Diffraction

X-ray diffraction (XRD) analysis was applied to detect the crystallinity of the isolated chitin and the obtained chitosan the structure of α-chitin has been determined [22] using X-ray diffraction analysis, based on the intensity data from deproteinized lobster tendon. Least-squares refinement shows that adjacent chains have alternating sense (i.e., are antiparallel). In addition, there is a statistical distribution of side chain orientation such that all the hydroxyl group form hydrogen bonds. The unit cell is orthochromic.

The chains form hydrogen bonded sheets linked by C=O···H- - -N bonds approximately parallel to the a-axis, and each chain has an O-3′- - -H···O.5 intramolecular hydrogen bond, similar to that in cellulose. The results indicate also that a statistical mixture of CH2OH orientations is present equivalent to half oxygen on each residue, each forming interand intramolecular hydrogen bonds. As a result, the structure contains two types of amide groups, which differ in their hydrogen bonding, and account for the splitting of the amide I band in the infrared spectrum. The inability of this chitin polymorph to swell on soaking in water is explained by the extensive intermolecular hydrogen bonding.

3.4 Rheological Properties

The rheological behavior of the printing paste plays one of the most important roles in the process of textile printing because it affects the amount of printing paste applied on the textile surface and consequently on the quality of the printed substrate. Hence, pastes of the aforementioned blends were prepared and the rheological properties of the pastes were monitored before and after storing of the pastes for 24 h. e results obtained are shown in Figs. 1 and 2.

The rheograms reveal that all the pastes under investigation display non-Newtonian pseudoplastic behavior since the ascending and descending rheograms are coincident. This reveals the homogeneity of the molecular structure of the pastes which are amenable to rebuild themselves and retain their original state immediately after removal of the acting force, thereby exhibiting pseudoplastic behavior.

Fig. 1 shows that, the location of the rheograms with respect to the rate of shear axis depends on the nature of the thickening agent used. As the concentration of starch increases the rheogram is located far from the rate of shear axis indicating an increase in the apparent viscosity.

Fig. 2 represents the rheograms of the aforementioned pastes a er storing for 24 h. It is clear from the rheograms that storing has practically no effect on the rheological characteristics of these pastes where each of these pastes remains exhibiting non-Newtonian pseudoplastic behavior after storing.

The apparent viscosity at various rate of shear of the aforementioned pastes was calculated from the values of rate of shear. The results obtained are given in Tables 2 and 3. It is clear that the storing for 24 h does not affect so much the appearing viscosity of the prepared pastes.

Table 2. Effect of starch concentration on the apparent viscosity at various rate of shear for freshly prepared pastes

Rate of shear (sec^{-1})	Apparent viscosity			
	3% starch	4% starch	5% starch	6% starch
9.3	190	250	430	820
18.6	180	240	415	760
27.9	173.3	236.7	406.7	730
37.2	166	230	395	700
46.5	161.7	226	386	672
55.8	160	223.3	378.3	651
65.1	155	220	368.6	634.3
74.4	153.3	217.5	361.2	616.2
83.7	152	214.4	354.4	601.1
93	152	212	347	587
93	152.2	210	349	587
83.7	152.5	212.2	348	600
74.4	152.9	215	352.5	617.5
65.7	155	217.1	358.6	634.3
55.8	155	220	365	655
46.5	156	222	370	660
27.9	157.5	225	380	710
37.2	158.7	230	390	750
18.6	160	235	400	795
9.3	163	240	410	870

Table 3. Effect of starch concentration on the apparent viscosity at various rate of shear for prepared pastes after storing 24 hours

Rate of shear (sec^{-1})	Apparent viscosity			
	3% starch	4% starch	5% starch	6% starch
9.3	150	260	500	1070
18.6	145	243	475	955
27.9	140	236.7	458.7	903.3
37.2	140	230	442.5	890
46.5	130	226	428	864
55.8	136.7	221.7	418	850
65.1	135.7	218.6	408.6	840
74.4	133.7	215	400	853
83.7	133.7	212.2	392.2	830.8
93	133	210	386	814
93	132.	210	385	802
83.7	132.2	212.2	391.1	822.2
74.4	132.5	215	398.7	825
65.1	132.9	217.1	407	788
55.8	133.3	221.7	416.7	765
46.7	136	224	426	750
27.9	137.5	230	137.5	787.5
37.2	136.7	233.3	453.3	833
18.6	140	240	470	905
9.3	150	250	500	1010

Table 4. The K/S, relative color strength % of *Curcuma tinctoria* printed samples

Thickener used	Kind of fabric used											
	Cotton		Cotton/polyester		Polyester		Viscose/polyester		Polyamide		Wool	
	K/S	% K/S	K/S	% K/S	K/S	% K/S	K/S	% K/S	K/S	% K/S	K/S	% K/S
Sod. alginate	3.88	100	1.91	100	0.98	100	4.24	100	1.44	100	2.01	100
3% starch	6.46	167	7.45	390	5.01	511	8.15	192	5.74	399	9	474
4% starch	9.61	248	11.42	598	5.04	514	7.92	187	7.04	488	8.12	404
5% starch	7.94	205	5.93	311	5.12	523	7.06	167	7.94	551	6.57	327
6% starch	5.81	150	3.48	182	4.97	201	6.97	164	6.32	439	5.66	282

Table 5. Color parameter and the color difference of printed Fabrics

Printed sample	L*	a*	b*	L	a	b	ΔL	Δa	Δb	ΔE	$C_{a^*b^*}$	C_{ab}
Wool	76.22	-1.85	47.68	63.53	9.72	55.63	12.69	11.57	7.95	50.83	47.7	56.4
Polyamide	67.42	-4.44	16.29	64.53	−5.56	57.30	2.96	1.12	41.01	41.13	16.8	17.7
Polyester	83.96	-7.36	15.39	74.03	−5.39	63.21	9.93	1.97	47.82	48.88	17.0	63.4
Cotton/polyester	77.81	-2.16	41.39	67.50	11.48	49.02	10.31	13.46	7.81	18.66	41.4	50.3
Cotton	85.15	-4.14	13.6	70.54	6.64	62.82	14.61	10.78	49.22	51.71	14.2	63.1
Viscose/polyester	80.91	-4.93	22.02	72.63	2.38	58.51	8.28	7.31	36.49	38.13	22.5	58.5

Table 6. Fastness properties of control and highest K/S samples and surface roughness of fabrics

Printing paste	Rubbing fastness		Washing fastness		Perspiration fastness				Light fastness	Roughness
					Acid		Alkaline			
	Dry	Wet	Alt.	St.	Alt.	St.	Alt	St.		
Cotton fabric (100%)										
Commercial paste	4-5	4	4	4	4	4-5	4	4	1	13.01
5% starch/chitosan	4-5	3	4	4	4	4-5	4	4	3	13.11
Cotton/polyester blend fabric (35/65)										
Commercial paste	4-5	4-5	4	4	4	4	4	4	1	16.78
6% starch/chitosan	4-5	4	4	4	4	4	4	4	3-4	12.17
Viscose/polyester (80/20)										
Commercial paste	4-5	4-5	4	4	4	4	4	4	1	15.64
5% starch/chitosan	4-5	4	4	4	4	4	4	4	3	15.65
Polyester										
Commercial paste	4-5	4-5	4	4	4	4	4	4	1	18.62
6% Starch/chitosan	4-5	4-5	4	4	4	4	4	4	3-4	18.73
Polyamide										
Commercial paste	4-5	3	3	3	3	3	3	3	1	24.67
	4-5	4	3	3	3	3	3	3	3-4	18.49
Wool										
Commercial paste	4	4	4	4	4	4	4	4	1	25.01
6% Starch/chitosan	4	3	4	4	4	4	4	4	3	25.00

Table7. Antibacterial activity of different printed fabrics

Sample	**Inhibition zone diameter (mm/mg sample)**			
	***Bacillus subtilis* (G+)**	***Esherichia coli* (G−)**	***Staphylococcus aureus* (G+)**	***Pseudomonas aeruginosa* gram (G−)**
Control	0.0	0.0	0.0	0.0
Cotton	14	14	15	14
Cotton/polyester	15	15	15	16
Viscose/polyester	15	16	15	16
wool	16	16	15	16

3.5 Color Strength and Related Parameters

Chitosan has been proved to increase the rate of dye uptake and dye exhaustion of wool fabrics in the case of acid, reactive dyes and natural dye as henna [5,23,24]. However, combination of starch with chitosan to be used as thickening agent in textile printing has not been investigated so far. Therefore it has been taken up in the present study with natural dye. Thickeners act as a vehicle for the dye and during the fixation the dye transferred into the fabric then the thickener is washed off completely from the fabric. K/S value is directly proportional to the amount of dye present in the material and it can be used to evaluate the efficiency of new thickeners. e K/S values and the relative color strength of *Curcuma tinctoria* printed samples are given in Table 4.

It is clear from Table 4, that the K/S and the relative color strength values of all the printed samples using starch/chitosan thickeners are higher than that of the standard samples. ese results further affm that chitosan increases% the amount of *Curcuma tinctoria* uptake. This holds true in all printed samples despite the nature of fabric used and the % of starch in the thickener.

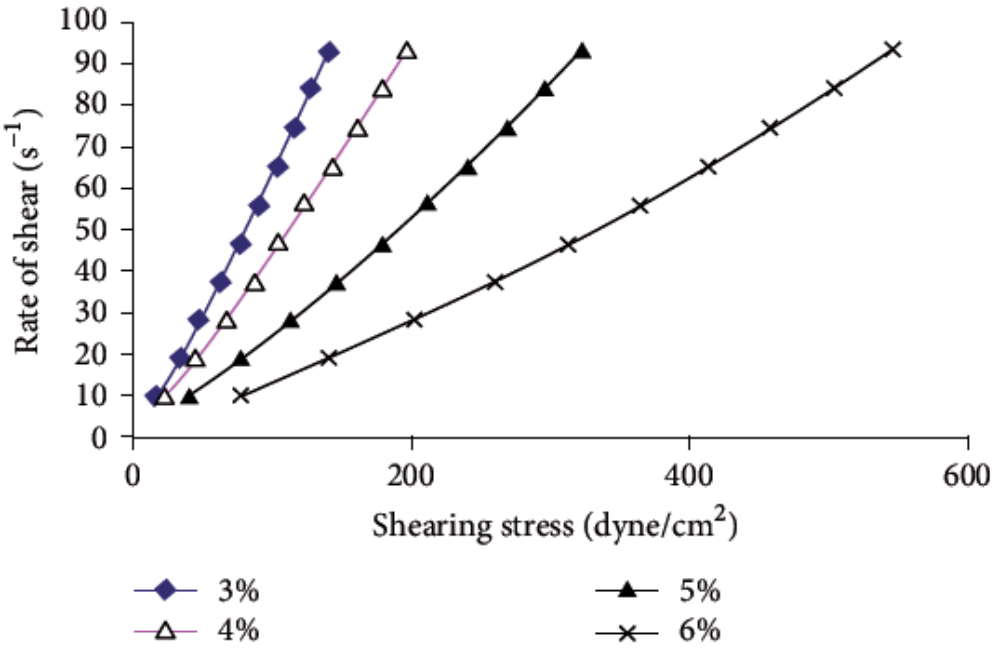

Fig. 1. Rheograms of different concentrations of fresh prepared starch/chitosan thickener

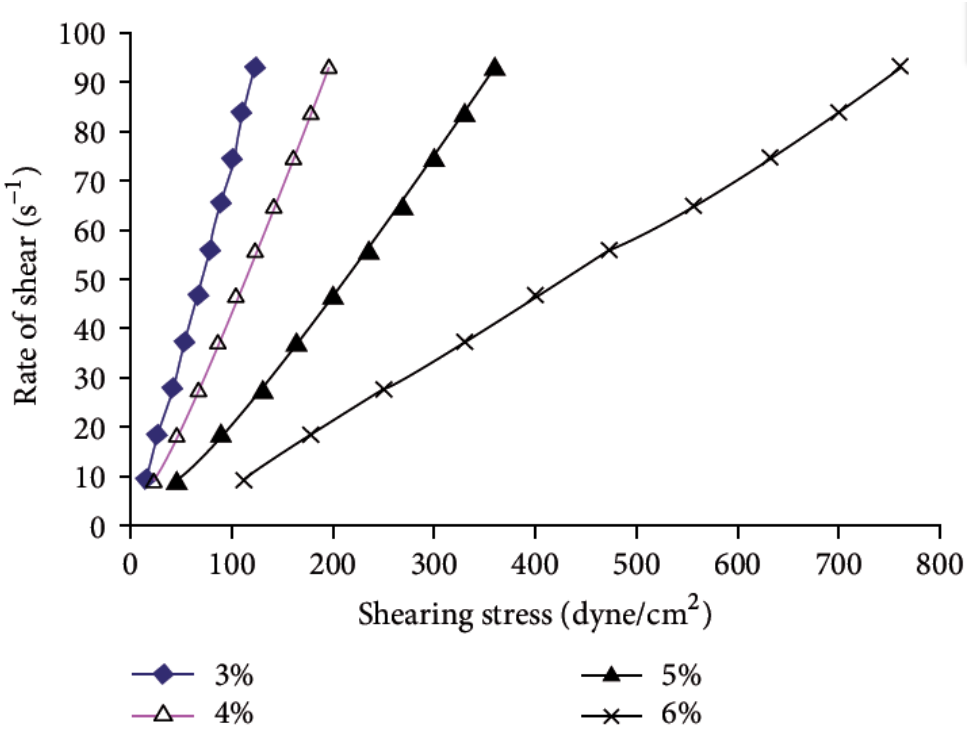

Fig. 2. Rheograms of different concentrations of starch/chitosan thickener after storing for 24 hours

It is known that all natural dye have low affinity to synthetic fabrics and this was one of its drawback especially with the increase in production of synthetic fabrics and their blends. e K/S values of the

printed synthetic fabrics and their blends reveal that the presence of this ratio of chitosan in the% new thickeners has overcome this prob-lem. Cotton/polyester% printed samples achieved the highest relative color 598, where the K/S increases from 1.91 to 11.42 using 4 starch/chitosan thickener. The K/S of others synthetic printed fabrics (polyester and polyamide) increase from 0.98 to 5.12 and from 1.44 to 7.94 with relative color strength 523 % and 551, respectively, using 5 % starch/chitosan thickener. For natural fabric as wool the highest K/S was achieved by using 3% starch/chitosan blend. These results refer that the highest K/S values have been achieved at different blends although the ratio of chitosan is constant, this may be due to the nature of the fabrics and the thickener viscosity.

To evaluate the color parameter and the color difference of printed fabrics with highest K/S value, CIE Lab system is used. Where *L* refers to lightness-darkness values from 100 to 0 representing white to black, values run from negative Δ (green) to positive (red) and values run from negative (blue) to positive (yellow), and the total color difference is given by ΔE.

It can be seen from Table 5 that the L values decrease in all the printed samples indicating that the sample becomes darker compared to that of the control sample. As seen from a and b values that the color hue changes to reddish yellow.

The color difference (ΔE) values are also given in Table 5 and it can be clearly seen that there is a significant color difference between the samples and the control samples though the dye concentration is constant.

The chroma is calculated as $(a^2 + b^2)^{1/2}$ as the chromaticity increases, a color becomes more intense; as it decreases a color become dull and this is clear from Table 5 that the chroma of sample (C_{ab}) increased.

3.6 Determination of Fastness Properties and Surface Rough-ness

It is clear from the data of Table 6 that with this new thickeners natural dye could print all kinds of fabrics under investigation with very good to excellent color fastness to rubbing, washing or perspiration. e notice of improvement is in the light fastness.

The surface properties of the antistatic-treated fabrics are very important because these fabrics are used mainly for garments in direct contact with human skin, that surface roughness has strong effect on the wearer comfort. Surface roughness results of cotton, polyester, polyamide, and blend fabrics are given in Table 6. The results showed the same or slight increase in the surface roughness of the using chitosan/starch blend compared with the standard.

3.7 Antimicrobial Activity of Treated Fabrics

Early research describing the antimicrobial potential of chitin, chitosan, and their derivatives dated from the 1980–1990s [25]. Generally, recent data in the literature has the tendency to characterize chitosan as bacteriostatic rather than bactericidal.

Table 7 shows that the printed fabrics using chitosan-starch blend exhibit antimicrobial characteristics compared with the control sample.

3.8 Uniqueness

Chitosan, which is a very useful nontoxic biopolymer, can be used as an effective antimicrobial finish and can also be used to increase the dye uptake of the fabrics. e new blends have definite rheological properties under varying shear stress during the entire printing process.

The addition of chitosan to gelatinous starch has twofold effects: nature dye has successfully printed all fabric with increase in the color strength and related parameters of the printed fabrics, and the other is that it produces antimicrobial fabrics. The fastness properties of these fabrics are good

against washing, light and perspiration. Thus, a nontoxic, ecofriendly, multifunctional finish has been developed for using natural dye in printing all fabrics.

4. CONCLUSION

Chitosan, which is a very useful nontoxic biopolymer, can be used as an effective antimicrobial finish and can also be used to increase the dye uptake of the fabrics. The new blends have definite rheological properties under varying shear stress during the entire printing process.

The addition of chitosan to gelatinous starch has twofold effects: Nature dye has successfully printed all fabric with increase in the color strength and related parameters of the printed fabrics, and the other is that it produces antimicrobial fabrics. The fastness properties of these fabrics are good against washing, light and perspiration. Thus, a nontoxic, ecofriendly, multifunctional finish has been developed for using natural dye in printing all fabrics.

The chitosan starch blends has been successfully formed and applied in textile pigment printing. Chitosan was extracted from Egyptian marine shrimp shell and characterized by IR, 1H-NMRand X-ray powder diffraction. Its blends were prepared by adding fixed ratios of chitosan to different gelatinized starch samples. The prints using starch /chitosan blends in a ratio of 5% or 6% achieved improvement in the colour strength and related colour parameters with good to excellent fastness properties. Roughness results show soft handle for all samples, except in commercial binder where the handle is harsh.

ACKNOWLEDGEMENTS

This work was supported by Dyeing, Printing and Auxiliaries Department, Textile Division, National Research centre.

COMPETING INTERESTS

Authors have declared that no competing interests exist.

REFERENCES

1. Nagia FA, EL-Mohamedy RSR. Dyeing of wool with natural anthraquinone dyes from Fusarium oxysporum. Dyes and Pigments. 2007;75(3):550–555.
2. Bechtold T, Mahmud-Ali A, Mussak R. Natural dyes for textile dyeing: A comparison of methods to assess the quality of Canadian golden rod plant material. Dyes and Pigments. 2007;75(2): 287–293,.
3. Sundrarajan M, Rukmani A, Rajiv Gandhi R, Vignesh-waran S. Eco friendly modification of cotton using enzyme and chitosan for enhanced dyeability of curcuma longa. Journal of Chemical and Pharmaceutical Research. 2012;4(3):1654–1660.
4. Bandyopadhyay BN, Sheth GN, Moni MM. Appli-cation of chitosan in dyeing and finishing. Bombay Textile Research Association Scan. 2001;31(1):5–12.
5. Lim SH, Hudson SM. Review of chitosan and its derivatives as antimicrobial agents and their uses as textile chemicals. Journal of Macromolecular Science. 2003;43(2):223–269.
6. Rajendran R, Radhai R, Balakumar C, Ahamed HAM, Vigneswaran C, Vaideki K. Synthesis and characterization of neem chitosan nanocomposites for development of antimicrobial cotton textiles. Journal of Engineered Fibers and Fabrics. 2012;7(1):136–141.
7. Tayel A, Moussa SH, El-Tras WF, Elguindy NM, Opwis K. Antimicrobial textile treated with chitosan from *Aspergillus niger* mycelial waste. International Journal of Biological Macromolecules. 2011;49(2):241–245.
8. Kittinaovarat S. Using chitosan for improving the dyeability of cotton fabrics with mangosteen rind dye. The Journal of Scientific Research Chulalongkorn University. 2004;29:155–164.

9. Srisuk S, Srikulkit K. Properties evaluation of some sodium nitrite chitosan-cotton fabric. Journal of Metals, Mate-rials and Minerals. 2008;18:41–45.
10. Mathew S, Abraham TE. Characterisation of ferulic acid incorporated starch-chitosan blend flims. Food Hydrocolloids. 2008;22(5):826–835.
11. Abdou ES, Nagy KSA, Elsabee MZ. Extraction and characterization of chitin and chitosan from local sources. Bioresource Technology. 2008;99(5):1359–1367.
12. Domard, Rinaudo M. Preparation and characterization of fully deacetylated chitosan. International Journal of Biologi-cal Macromolecules. 1983;5(1):49–52.
13. Ravindra R, Krovvidi KR, Khan AA. Solubility parameter of chitin and chitosan. Carbohydrate Polymers. 1998;36(2-3):121–127.
14. Bhandari PN, Singhal RS, Kale DD. Effect of succiny-lation on the rheological profile of starch pastes. Carbohydrate Polymers. 2002;47(4):365–371.
15. AATCC, Technical Manual, Method. 36 (1972), 68 (1993).
16. AATCC, Technical Manual, Method. 8, (1989), 68, 23(1993).
17. AATCC, Technical Manual, Method. 15, (1989), 68, 30 (1993).
18. AATCC, Technical Manual, Method. 16A, (1989), 68, 33 (1993).
19. National Committee for Clinical Laboratory Standards. Reference method for broth dilution antifungal susceptibility testing of filamentous fungi: Approved Standard M38-A. NCCLS. Wayne, Pa, USA; 2002.
20. Nunthanid J, Puttipipatkhachorn S, Yamamoto K, Peck GE. Physical properties and molecular behavior of chitosan flims. Drug Development and Industrial Pharmacy. 2001;27(2):143–157.
21. Shen XL, Wu JM, Chen Y, Zhao G. Antimicrobial and physical properties of sweet potato starch flims incorporated with potassium sorbate or chitosan. Food Hydrocolloids. 2010;24(4):285-290.
22. Lavertu M, Xia Z, Serreqi AN, et al. A validated 1H NMR method for the determination of the degree of deacetylation of chitosan. Journal of Pharmaceutical and Biomedical Analysis. 2003;32(6):1149–1158.
23. Stephen DR, Yulin X. Improving the dye ability of wool by treatment with chitosan. Journal of the Society of Dyers and Colorists. 1994;110:24–29.
24. Dev VRG, Venugopal J, Sudha S, Deepika G, Ramakrishna S. Dyeing and antimicrobial characteristics of chitosan treated wool fabrics with henna dye. Carbohydrate Polymers. 2009;75(4):646–650.
25. Hadwiger LA, Kendra DG, Fristensky BW, Wagoner W. Chitosan both activated genes in plants and inhibits RNA synthesis in fungi. in Chitin in Nature and Technology, Muzzarelli RAA, Jeuniaux C, Gooday GW, Eds., Plenum, New York, NY, USA; 1981.

Biography of author(s)

Dr. E. S. Abdou
Department of Chemistry, Faculty of Science and Humanities, Salman Bin Abdualaziz University, Saudi Arabia.

She obtained her Ph.D. degree in Physical Chemistry From Chemistry Department, Faculty of Science, Cairo University, Giza, Egypt. She is currently working as a Senior Researcher in Food Engineering and Packaging Department, food Technology Research Institute Agriculture Research Center, Giza, Egypt.

Dr. H. M. El-Hennawi
Department of Chemistry of Dyeing, Printing and Auxiliaries, Textile Division, National Research Center, Cairo, Egypt.

She is working as an associate professor in Dyeing Printing & Textile Auxiliaries Department, Textile Industries Division. Her main interest is textile coloration, decolourization and biotechnology application in textile.

Dr. K. A. Ahmed
Department of Chemistry of Dyeing, Printing and Auxiliaries, Textile Division, National Research Center, Cairo, Egypt.

She is working as an associate professor in Dyeing Printing & Textile Auxiliaries Department, Textile Industries Division. Her main interest is textile coloration, synthesis of dyes, organic compounds, and auxiliaries.

© Copyright (2020): Author(s). The licensee is the publisher (Book Publisher International).

DISCLAIMER
This chapter is an extended version of the article published by the same author(s) in the following journal.
Journal of Chemistry, 2013, 2013, Article ID 595810.

Chapter 4
Print ISBN: 978-93-90206-41-4, eBook ISBN: 978-93-90206-42-1

Research on Efficient One Pot Synthesis of TiO_2-induced Nanoparticles via Microwave Irradiation and Its Application in Cotton Dyeing with Some Acid Dyes

N. S. Elshemy[1*], S. A. Mahmoud[1], H. M. Mashaly[1] and K. Haggag[1]

DOI: 10.9734/bpi/crdc/v4

ABSTRACT

In the current approach, treatment and optimization of a non-traditional heating technique to assist a rapid method for one-pot synthesis of Titanium di-oxide nanoparticles (TiO_2NPs) within a few minutes was studied. The prepared TiO_2 NPs are submitted to innovative treatment using microwave irradiation. The effect of prepared TiO_2 NPs by using microwave irradiation as well as the conventional method of dyeing of cotton fabric with acid dye was studied. TiO_2 NPs were examined through transmission electron microscopy (TEM). The effects of TiO_2 NPs on the multifunctional properties of the cotton fibers including coloration, antibacterial, and anti UV were evaluated. The overall results point out that, the TiO_2 NPs are successfully prepared by using microwave heating by saving time and energy. The treated fabrics by prepared TiO_2 NPs exhibited excellent colorfastness as well as good antibacterial, and anti UV properties if compared to the untreated fabrics, in straightforward, the procedure adopted for fabricating these multifunctional fabrics is environmentally friendly beside time and energy-saving.

Keywords: Titanium di-oxide; nanoparticles; cotton treatment; microwave heating; antimicrobial; self-cleaning.

1. INTRODUCTION

Lately, there are increasing interest in photograph catalysis stimulation using semiconductor materials as photograph catalysts for the removal of ambient concentrations of inorganic and organic species from the aqueous phase or gas in cleaning up the environment, drinking water treatment, industrial and health applications. This is due to the ability of TiO_2 to oxidize organic and inorganic materials in air and water through redox processes [1].

TiO_2 NPs have many features when it converts to the nanoscale, like it may be increasing the surface area of some materials that may occur photocatalytic interactions. This photocatalytic activity may be attention in many applications, for example, air purification, self-cleaning, water purification, and the preparation of molecular hydrogen. However, the high ability of TiO_2 lie in self-cleaning which leads to the conversion of organic as well as biological molecules into the minimal molecular size so it becomes less harmful compounds. So, the search for different synthesis methods to produce TiO_2 motif is very useful to achieve maximum efficiency in applications of TiO_2 [2].

The polymer is antibacterial, non-toxic, biodegradable, and biocompatible. Researcher work has been done on the planning of chitosan/silver nanocomposites in the solid forms, such as fibers, powders, and films [3]. The use of chitosan covers of fields, for example, pharmaceutical and therapeutic applications, paper production, textile, wastewater treatment, biotechnology, cosmetics, sustenance preparation, and horticulture [4-11].

[1]Dyeing, Printing and Auxiliaries Department, National Research Centre, Tahrir St., Dokki, Giza, Cairo, Egypt.
**Corresponding author: E-mail: nanaelshemy@hotmail.com;*

Many researchers worked on the preparation of TiO_2 by several techniques [12-15] but there are fewer reports about the preparation of it via microwave irradiation to improve the multifunctional properties of different fabric surfaces. In addition, many researchers are interested in finding out novel technologies to achieve quality, time-saving, reduce water and energy consumption as well as eco-friendly processing [16-20]. When interacting materials have dielectric properties should be of these new technologies are known as “microwave technology” which could be used in different textile processes such as finishing, dyeing, printing, and wet processes while achieving the targets mentioned above [21-23]. One of the main advantages provided by microwave heating is homogenized, as the heating is uniformly distributed inhomogeneous manner and in all directions, while in the conventional heating technique, heating occurs from the outside to the inside of the heated system, which results in heterogeneity in the thermal distribution [24,25]. This leads to speed up healing when compared to the conventional way, so the microwave reduces power consumption and reduces operational time [26,27]. In addition, energy transfer at a molecular level can have some additional advantages, which known as “volumetric heating”.

Another advantage, microwave characteristics by used the “selective heating” of materials. The ability of the microwaves to interact with materials and transfer energy affects by molecular structure. When interact materials have dielectric properties, coupled with the higher loss material will selectively by microwaves [28,29]. This phenomenon of selective heating can be applied for a number of purposes. When classical heating is applied, considerable time and energy are consumed to heating up the interface by conduction through the substrates. While, when using microwaves, the joint interface can be heated in-situ by incorporating a higher loss material at interface [30]. In manifold stage materials, some stages may couple more easily with microwaves. Consequently, it may be possible to produce materials with new or individual microstructures by selectively heating a distinct stage. Microwaves can able to initiate chemical reactions through selective heating of reactants; so, new materials may be formed, which is not possible in classical processing [31-33].

Many researchers assume to investigate the ability to use microwaves for a wide range of materials, like ceramics, polymers, composites (ceramic and polymer matrix), powders, and minerals. Microwaves have also been investigated in a wide range of plasma processes (surface treatment, infiltration of chemical vapor, powder processing), chemical synthesis and processing, and waste treatment. Although, the great effort that has been spent in the development of the microwave process, there has been little industrial application till now, with most of the effort still in the laboratory stage. Some of the more important problems that have prevented industrial apply. The main problems have related to microwave processing, which puts the user cation of microwave processing are: i) equipment cost, ii) limited applicability, iii) variation in dielectric properties with temperature; and iv) the ingrained inefficiency of electric power.

The microwave-assisted route is one of the innovative methods and is a rapidly developing area of research. In contrast to conventional methods, microwave activity requires very short reaction time, consume less energy and it is able to produce small particles with narrow molecular size distribution and high purity that will lead to improvement of some physical, mechanical and chemical properties of these molecules.

Microwaves, like other radio waves, are a form of electromagnetic waves. Electromagnetic waves are the wavelike amplitude of electric and permanent magnetic fields. Electrical fields are what make electric charges attract or repel. Positive (e+) and/or negative (e-) electric charges produce electric fields which in convert act on other charges. In the same way, magnetic fields cause permanent magnetic forces [12]. These types of fields are vertical to one another and constantly oscillate between the maximum (e+) and maximum (e-) (pointing in the opposite way).

Currently, many microwave-based straightforward, quick, and energy-efficient routes have been created to prepare the nanostructured materials, including nanoparticles, nanowires, nanoplates, nanorods, etc. [34-38]. The purpose of this research was to develop a method suitable for prepared TiO_2 nanoparticles by using microwave heating within a couple of minutes was described. In comparison with routine heat preparation, microwave irradiation is a more efficient heating method due to its rapid heat and energy penetration, therefore decrease the reaction time as well as decrease

energy consumption. The effect of prepared TiO_2 by using microwave irradiation as well as the conventional method of dyeing of cotton fabric with acid dye was studied. The applicable of the prepared TiO_2 as antimicrobial and anti UV was also evaluated.

2. EXPERMINTAL

2.1 Materials

2.1.1 Substrate-cotton fabric

Scoured cotton fabrics 140 g/m^2 were supplied from Misr for Spinning and Weaving Company, Mahalla El- Kobra., Egypt. Cotton fabric was further treated with a solution containing 2 g/L nonionic detergent (Hostapal ® CV-Clariant), at 60°C for 30 minutes, then the fabrics were thoroughly rinsed with water and air dried at room temperature.

2.1.2 Chemicals and instrumentation

Chitosan (low molecular weight) (Aldrich), Titanium tetrachloride $TiCl_4$ (Fluka), acid dyes 1,2 which synthesized according to the published methods [39] and its structure shown in Fig. 1, Titanium dioxide TiO_2 nano particles were supplied from (Aldrich). All chemicals used in this study were of laboratory grade. UV spectra were recorded on a Perkin Elmer Lamb 15 UV/Vis spectrophotometer. Transmission electron microscope (TEM),

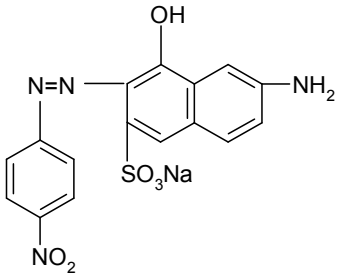

Acid dye 1

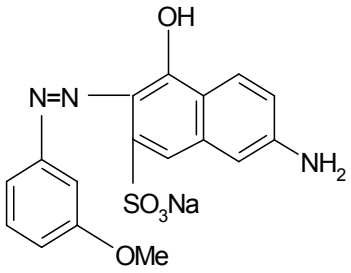

Acid dye 2

Fig. 1. Structure of acid dye according to the published

2.2 Preparation of TiO_2 Nano Particles

Synthesis of TiO_2 nano particle was done by Sol-Gel technique by following two different heating methods.

2.2.1 Conventional method

Titanium tetra chloride ($TiCl_4$) of 3.5 ml was added to 50 ml deionized water in ice bath and the process was done under fume hood followed by the addition of 35 ml of ethanol with vigorous stirring for 30 min at room temperature. Drops of ammonium hydroxide were added wisely into solution of the titanium tetra chloride ($TiCl_4$), ethanol and deionized water to neutralize it and precipitate was obtained. After stirring vigorously, the solution was made to settle for twelve hours. The obtained precipitate was washed with deionized water until the removals of chloride ion, centrifuged then filtrated. The precipitate was dried at 200°C to remove part of the absorbed water for 4 hours and finally amorphous TiO_2 was obtained. The obtained amorphous TiO_2 was calcinated at 400°C for four hours step by step. Finally, the powder TiO_2 nano material was obtained [40-43].

2.2.2 Microwave irradiation

The same procedures were repeated as mentioned above until the ppt. was obtained. Then the ppt. was dried via microwave for 8 min. and then calcinated amorphous TiO_2 in the microwave for 8 min. at 90 watt (total preparation time 16 min.). Instead of dried the ppt. at 200°C for 4 hours, then calcinated amorphous TiO_2 at 400°C for four hours (total preparation time 8 hours).

2.2.3 Treatment of cotton fabric with chitosan

Treated cotton fabric by different concentration of Chitosan (1, 1.5, 2% W.O.F) dissolve in distilled water and 2% acetic acid for 60 minutes at 60°C, squeezed, dried at ambient temperature then dyed with the tow acid dyes mentioned above [44].

2.2.4 Treatment of cotton fabric by TiO_2 nano particles [45]

Cotton fabrics were treated with different concentrations (0.5-2% W.O.F) of prepared TiO_2 nanoparticles by using microwave irradiation, conventional heating, and with commercial one via exhaustion method, for 20 min. at 80°C in the presence of a wetting agent in the dyeing machine. The liquor ratio of the exhaustion bath was 1:10. Then the treated Cotton fabrics were cured at 140°C for 10 min., washed at 60°C for 20 min. followed by drying at room temperature.

2.2.5 Dyeing of cotton fabric

The cotton fabrics was dyed using exhaustion dyeing processes [46] according to the following diagram.

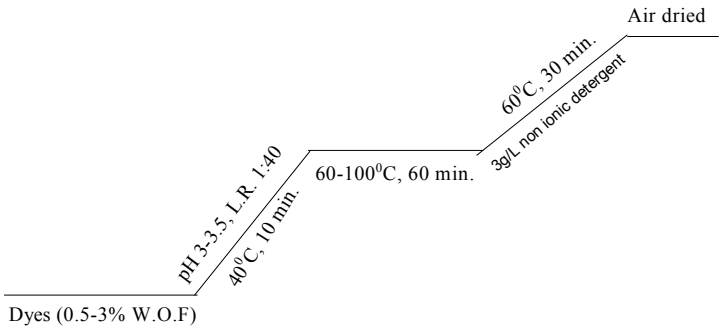

2.3 Color Measurements of Dyed Samples

2.3.1 Color strength

The colorimetric analysis of the dyed samples was performed using a Hunter Lab ultra-Scan® PRO spectrophotometer. The corresponding colour strength value (K/S) was assessed by applying the Kubelka Munk equation follows [47].

$$K/S = \frac{(1-R)^2}{2R} \quad (1)$$

Where,

R = decimal fraction of the reflection of the dyed fabric,
K = absorption coefficient, and S = scattering coefficient

2.4 Fastness Testing

The dyed samples were subjected to rubbing, washing, perspiration and light according to standard ISO methods, ISO 105-X12 (1987), ISO 105-co_4 (1989), ISO105-EO_4 (1989), ISO 105-BO_2 (1988) respectively.

2.5 Antimicrobial Activity

The standardized disc–agar diffusion method was followed to determine the activity of the synthesized compounds against the tested microorganism [48].

2.6 Antibacterial Assay

Antimicrobial activity was tested by the filter paper disc diffusion method [49]. SMA and Mueller Hinton agar (Difco) containing 100 ppm of 2,3,5-triphenyl tetrazolium chloride were used for the antibacterial assay. 2,3,5-triphenyl tetrazolium chloride was added to culture media to differentiate bacterial colonies and to clarify the inhibition zone (28). Each plate was inoculated with bacterial, Escherichia coli (G-), Staphylococcus aureus (G+) (0.1 ml) directly from the broth. All plates were incubated at 32°C for 4 days, after which the inhibition zones were measured and recorded in millimeters (mm). The scale of measurement was the following (disc diameter included):≥28 mm inhibition zone is strongly inhibitory ≤16 to 10 mm inhibition zone is moderately inhibitory; and ≤ 12 mm is no inhibitory [50-52]. Control plates were prepared by placing antibiotics to evaluate culture for antibiotic resistance patterns that might affect the sensitivity of the assay. The antibiotic used was penicillin 10 IU.

2.7 Self-clean Action

The self-cleaning action of TiO_2 treated cotton fabric was investigated by exposing the samples with adsorbed coffee stains to visible radiation. The measured quantity of a 6% coffee solution was introduced on the cotton fabric and was allowed to spread. One half of each stain on the fabric was exposed to sunlight for 12-48 h, while the other half was covered with a black paper to prevent its radiation from sunlight. The exposed part of the stain was compared with that of the covered part for self-cleaning action. Premier color scan SS 5100A Spectrophotometer was used to measure the photodegradation of coffee stain [53].

2.8 Photo-Induced Discoloration on Cotton Textile

This study aimed at the use of the stable and durable product of inorganic TiO_2 NPs with a focus on the photocatalytic properties of TiO_2 NPs as textile finishes. The influence of the surface coating on the photocatalytic degradation of acid dye I and II were studied since the photocatalytic activity of TiO_2 NPs in form of textile coating material was evaluated in a normal laboratory environment and after UV irradiation. The samples were irradiated by a UV lamp for 24 hr.

3. RESULTS AND DISCUSSION

3.1 Preparation of TiO_2 Nano Particles

Many researchers try to prepare TiO_2 NPs by using different techniques but the use of microwave irradiation as a heating source is scanty. Fig. 2 shows the TEM images of TiO_2 NPs prepared by two different heating methods (Traditional heating (2a) and microwave irradiation (2b)) and the commercial one (2c) for comparison. Fig. 2 (a) shows the effect of traditional heating method, TiO_2 powder appears aggregated and having elliptical shape and range of the particle size is between 9-16 nm, while when using microwave irradiation, the powder appears as a clear and having octahedral structure and the particle size is ranged between 8-11 (Fig. 2b). However, it has been noticed that the particle size of prepared TiO_2 by using microwave irradiation as a heating source is smaller than the commercial one (range of the particle size is between 9-18) (Fig. 2c) as well as the synthesized one by traditional heating. This may be attributed to microwave irradiation. The predominance of microwave

heating could emerge from that, the materials can absorb microwave energy specifically and inside and change over it into heat. This prompts points of interest, for example, quick, controlled, specific, and uniform heating in a short time.

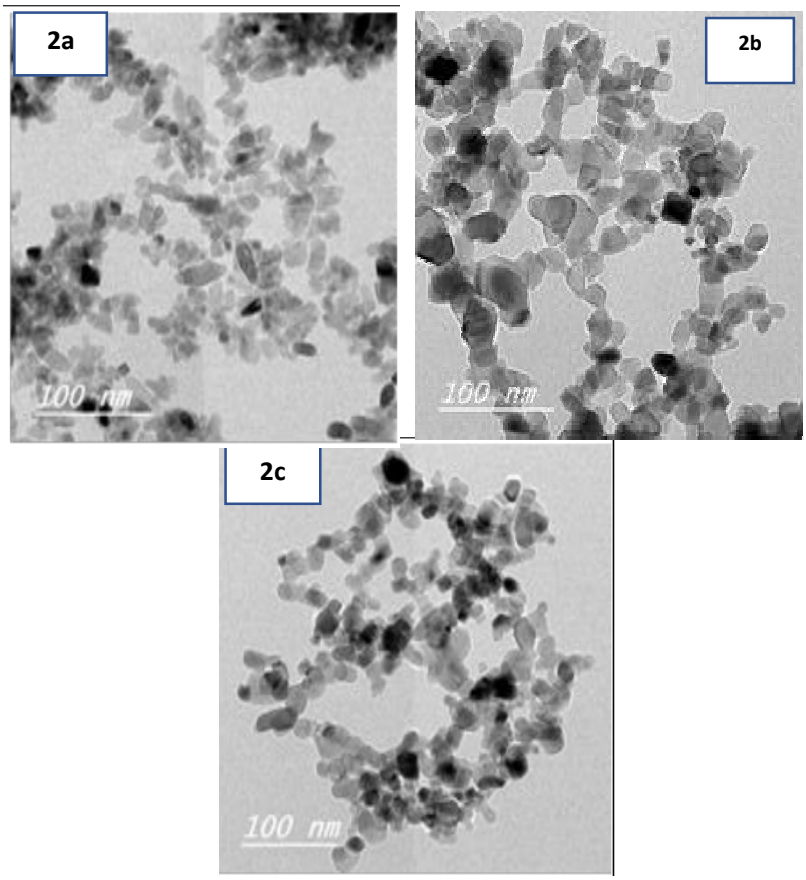

Fig. 2. Transmission electron microscopy (TEM) image of (a) commercial, (b) conventional, (c) Microwave irradiation TiO_2 nano particles

3.2 Treatment of Cotton Fabric with Chitosan

To optimize the chitosan concentration in the treatment conditions, cotton fabric was pretreated at different concentrations of chitosan (0.5-2% W.O.F.) for 60 min. at 60°C using thermal heating. The pretreated samples were then dyed by Acid dye 1, and Acid dye 2 using the conventional thermal dyeing method as described in the experimental section. The results are presented in Table 1.

The results clearly demonstrate that chitosan treatment enhances the color strength of both selective acid dyestuffs. As chitosan concentration increased, the average in color strength increased until 1.5%, irrespective of the type of dye. On the other hand, there is no significant increase in color strength when using higher chitosan concentration.

Table 1. Effect of chitosan concentration on the color strength of the dyed cotton fabrics

Dye	λ	K /S			
		0.5%	**1%**	**1.50%**	**2%**
acid dye1	540 nm	1.24	1.63	1.63	1.56
acid dye2	380 nm	3.24	3.94	4.1	3.71

Dyeing condition: 2% shade, pH: 3.5, L.R.1:40, at 100°C for 60 min

3.3 Treatment of Cotton Fabric by TiO_2 Nano Particles.

To determine the effect of treatment of cotton fabric by TiO_2 NPs on K/S values, cotton samples are pretreated before and after dyeing processes (2% shade, pH:3.5, L.R.1:40, at 100°C for 60min.) by different concentration of TiO_2 NPs (0.5-2% WOF) (Prepared by using microwave irradiation, conventional method as well as the commercial one). The samples were dyed by tow selective acid dyes, using the exhaustion dyeing method. The results are given in Figs. 3,4. From figures, It is clear that:

1) The K/S of dyed cotton increase by increasing TiO_2 concentration,
2) The high K/S value was obtained at 1.5% of TiO_2 when the fabric was treated before dyeing while the high value was obtained at 1% when fabric treated after dyeing, then there is no affected for increase TiO_2 treatment concentration
3) TiO_2 which prepared by using microwave irradiation processing can heat up in a very short time, and then achieve the effect of higher K/S value if compared to prepared by conventional heating.
4) The acid dye 1 give a high value of K/S in all cases than the acid dye 2. Accordingly, further studies of the pretreatment conditions were carried out at 1.5% for prepared TiO_2 NPs in microwave irradiation and 1% when using conventional methods. While when using commercial the highest K/S value was obtained at 2% concentration, Fig. 5. and then achieve the effect of higher K/S value if compared to prepared by conventional heating.

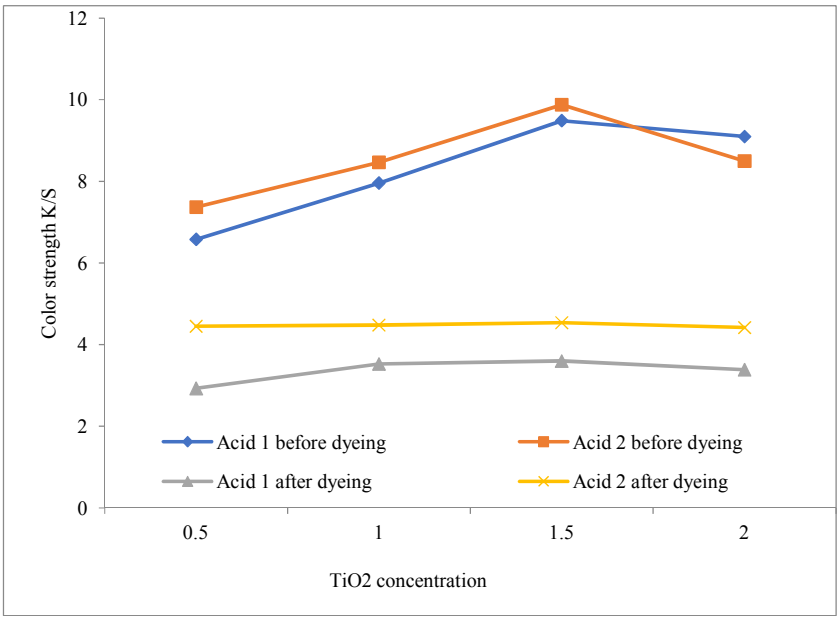

Fig. 3. Effect of TiO_2 concentration synthesis by using microwave irradiation on color strength of treated before and after dyeing of cotton fabric

3.4 Fastness Properties of NPs-treated Cotton Fabrics

The durability of colors on the treated before and after dyeing of cotton fabrics by TiO_2 NPs prepared by using microwave and conventional heating method as well as the commercial one was evaluated in term of fastness towards rubbing, washing, perspiration and to light fastness using the grayscale as shown in Table 2. As shown in Table 2, the fastness properties of treated cotton fabrics before dyeing are more resistant against rubbing, washing, and perspiration than those treated after dyeing, irrespective of mode and type of dye. Besides, the pretreated of cotton fabric by TiO_2 NPs which prepared by using microwave heating displayed higher colorfastness than those pretreated with the

same TiO_2 NPs prepared by thermal heating. It has also appeared that the fastness of pretreated cotton dyed samples with TiO_2 NPs by using microwave ranged from 4 to 5, while the prepared by conventional one ranged from 3 to 5.

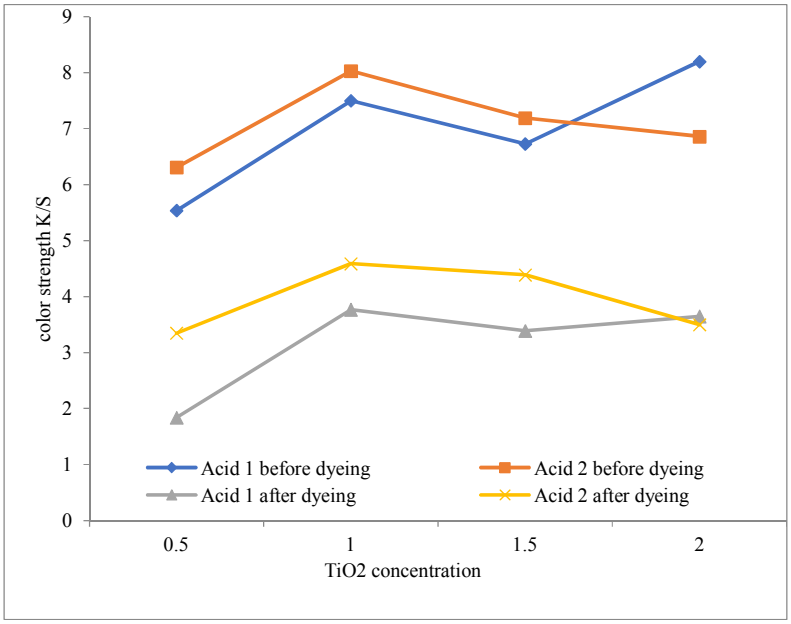

Fig. 4. Effect of TiO_2 concentration synthesis by using traditional heating on color strength of treated before and after dyeing of cotton fabric

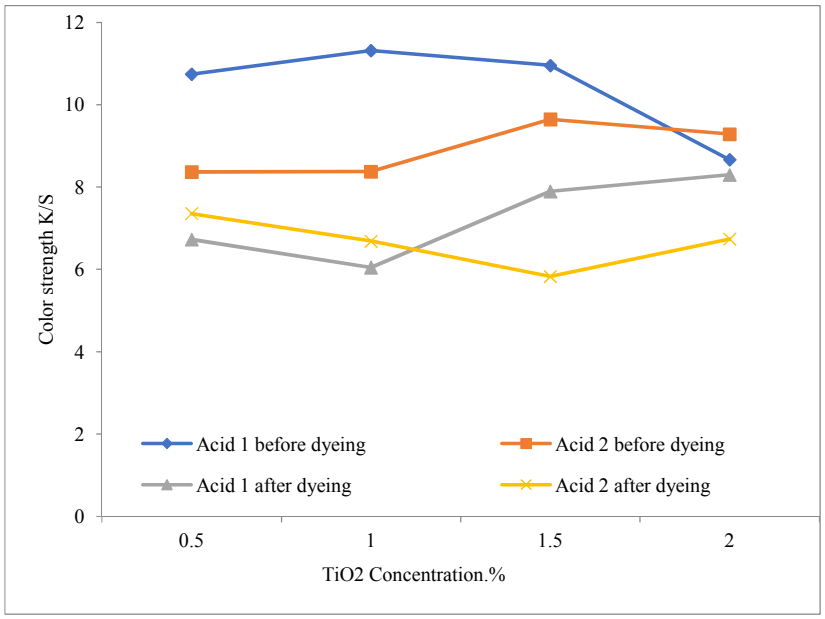

Fig. 5. Effect of commercial TiO_2 concentration on color strength of treated before and after dyeing of cotton fabric

The high color resistance of pretreated dyed samples by TiO_2 NPs prepared by microwave may be attributed to the increase of dye penetration and its interaction with fibers, where the fixation rate of the colors is accelerated, We can also notice that the light fastness is ranged from good to excellent in all cases.

Table 2. Fastness properties of the untreated andTiO_2NPs-treated dyed cotton fabrics

Prepared TiO_2	Washing fastness		Rubbing fastness		Perspiration fastness				Light fastness
					Acidic		Alkaline		
	Alt	Stain	Dry	Wet	Alt	Stain	Alt	Stain	
BD (M) Acid dye 1	4-5	4	4-5	4-5	4-5	4-5	4-5	4-5	6-7
AD (M) Acid dye 1	4-5	4	4-5	4-5	4-5	4	3-4	4	6-7
BD (T) Acid dye 1	3	3	4	3-4	3	3	2-3	2-3	5
AD (T) Acid dye 1	2-3	2-3	3	3	2-3	2-3	2	2	5
BD (C) Violet	4	4-5	4	4	4	4	4	4	6
AD (C) Acid dye 1	4	4	4	4	2-3	2-3	2-3	2-3	5-6
BD (M) Acid dye 2	4	4-5	4-5	4-5	4	4	4	4	6-7
AD (M) Acid dye 2	4	4	4-5	4-5	4	4	4	4	6
BD (T) Acid dye 2	2-3	2-3	3	3	2-3	2-3	2-3	2-3	5
AD (T) Acid dye 2	2	2	2-3	2-3	2	2	2	2	4-5
BD (C) Acid dye 2	4	4	4	4-5	4	4	3	3	6
AD (C) Acid dye 2	4	4	4	4	3-4	3-4	2-3	3	5-6

M = TiO_2 prepare by microwave, T = TiO_2 prepare by conventional method, C= TiO_2 commercial, BD= Before Dyeing, AD= After Dyeing;
Treatment condition: Dyeing condition: 2% shade, pH: 3.5, L.R.1:40, at 100°C for 60 min

3.5 Antibacterial Activity of NPs-treated Cotton Fabrics

The important characteristic of the material that is purposed for biomedical applications is the antibacterial property. TiO_2 atom and TiO_2 NPs are highly toxic to the microorganisms and they show strong antibacterial effects on the gram-positive and gram-negative bacteria. (E.coli) bacteria responsible for urinary tract and wound contaminations is a well-known test organism. (S. aureus) bacteria are harmful bacteria responsible for a lot of infections like toxic shock, fibrin coagulation, and endocarditic. Bacterial effects of unmodified and the NPs-modified cotton against both E. coli and S. aureus microorganisms were computed, Table 3. The photocatalytic effect of TiO_2 NPs, i.e. nano-metal oxides, is the basic reason for its antibacterial effect by the production of numbers of active oxygen species, e.g. superoxide anions, hydrogen peroxide, singlet oxygen, hydroxyl radicals that responsible for destroying of the bacterial cell. The treated cotton fabric by TiO_2 NPs exhibit an antibacterial effect on G+ve bacteria greater than on G −ve bacteria due to the existence of the external cell wall membrane in the G−ve bacteria thereby making as a bloke to the antibacterial effect.

In most cases, we noticed that the antibacterial activity of pre-treated fabric with TiO_2 NPs (before and after dyeing) that prepared by using microwave heating was greater than the prepared one by using traditional heating. Also, in most cases, the antibacterial activity of treated fabric against gram-positive bacteria was greater than the activity against gram-negative in both prepared TiO_2NPs. As shown in Table 3 antibacterial activity of undyed fabric shows higher antibacterial efficacy compared to dyed fabric.

3.6 Self-Cleaning of TiO_2 Nano Particles-Treated Cotton Fabrics

One of the susceptibilities of TiO_2 nanoparticles treated fibers is converting the absorbed light into the self-cleaning materials to decompose its stain. Table 4 shows the effect of C I RO 14 on untreated and TiO_2NPs treated cotton fabric after 24 h UV- illumination.

A partial change of the color affected by UV-light was observed for TiO_2 NPs striated cotton fabric. The treatment of cotton led to the development of thin-layer TiO_2 NPs that increases its hydrophilic properties. The high decay effect of TiO_2NPs has appeared on the treated cotton fabric.

The two types of surfaces that result from treating of cotton with TiO_2 NPs may explain its self-cleaning ability. Both hydrophilic and hydrophobic surfaces can remove the color from the cotton based on

different mechanisms. The idea of producing hydrophobic surfaces has been developed based on Lotus effect [30] (Stamate and Lazar, 2007). A hydrophobic surface stop the adsorption of dirt, preserves the surface of cotton clean in all the time. On the other hand, on hydrophilic surfaces water droplets are dispersion and subsequently a flood of water existing on the surface of cotton expels the pollutants [54].

Table 3. Antibacterial activity of TiO_2 NPs-treated cotton fabrics

Sample	Inhibition zone diameter (mm/ 1 cm Sample)	
	Staphylococcus aurous **(G^+)**	***Escherichia coli*** **(G^-)**
Comm. (control)	15	16
Microwave (control)	12	12
Traditional (control)	12	14
Before dyeing comm. acid (I)	16	17
Before dyeing comm. acid (2)	20	22
Before dyeing (T) acid (I)	26	26
Before dyeing (T) acid (2)	25	27
Before dyeing (m) acid (I)	22	21
Before dyeing (m) acid (2)	20	21
After dyeing comm. acid (I)	26	28
After dyeing comm. acid (2)	24	27
After dyeing (T) acid (I)	24	24
After dyeing (T) acid (2)	14	14
After dyeing (m) acid (I)	0.0	12
After dyeing (m) acid (2)	13	13

Dyeing condition: 2% shade, pH: 3.5, L.R.1:40, at 100°

Table 4. Self-cleaning % of cotton fabrics treated with different prepared TiO_2 NPs

Cotton samples treated	Dye removal %
Blank	-
Commercial TiO_2 treated cotton	85%
CH prepared TiO_2 treated cotton	80%
MV prepared TiO_2 treated cotton	80%

4. CONCLUSION

The multi-functionalization (coloration, antibacterial and photo catalytic properties) of TiO_2 NPs was successfully prepared by assisted microwave heating as a time, water and energy saving system. The result observed that the important two steps (dry and calcination step) was done at 8 min for dry as well as 8 min for calcination at 90 watts, instead of 4 hrs at 400ºC for drying and 2 hrs. at 600ºC for calcination. The transmission electron microscopy (TEM) proves the formation of TiO_2 in nanometer range. The effect of prepared TiO_2 NPs by using microwave irradiation as well as conventional heating on dyeing of cotton fabric with acid dye was studied as well as the commercial one. According to colorimetric data, the effects of TiO_2 NPs on the multifunctional properties of the cotton fibers coloration imparted bright colors with various shades. The treatment of cotton fabric by prepared TiO_2 NPs provides excellent antibacterial activity against *Escherichia coli (G-), and Staphylococcus aurous (G+)* antibacterial and anti UV. Treatment of cotton fibers by prepared TiO_2 NPs exhibited excellent color fastness to washing, rubbing and light fastness. It is worthy to say that it exhibited poor color fastness to respiration fastness.

COMPETING INTERESTS

Authors have declared that no competing interests exist.

REFERENCES

1. Kongsuebchart W, Praserthdam P, Panpranot J, Sirisuk A, Supphasrirongjaroen P, Satayaprasert C. Effect of crystallite size on the surface defect of nano-TiO_2 prepared via solvothermal synthesis. Journal of Crystal Growth. 2006;297:234-238.
2. Mitoraj D, Jaoczyk A, Strus M, Kisch H, Stochel G, Heczko PB, Macyk W. Visible light inactivation of bacteria and fungi by modified titanium dioxide. Photochemical & Photobiological Sciences. 2007;6:642-648.
3. Lan Y, Lu Y, Ren Z. Mini review on photocatalysis of titanium dioxide nanoparticles and their solar applications. Nano Energy. 2013;2(5):1031-1045.
4. Hu Z, Chan WL, Szeto YS. Nanocomposite of chitosan and silver oxide and its antibacterial property. Journal of Applied Polymer Science. 2008;108:52-56.
5. Muzzarelli RA, Zattoni A. Glutamate glucan and aminogluconate glucan, new chelating polyampholytes obtained from chitosan. International Journal of Biological Macromolecules. 1986;8:137-141.
6. Brine CJ, Sandford PA, Zikakis JP. Advances in chitin and chitosan. Elsevier Applied Science; 1992.
7. Domard Roberts GAF, Varum KM. Advances in that Chitin Science. 1997;II.
8. Ulanski P, Wojtasz-Pająk A, Rosiak JM, von Sonntag C, Peter MG, Muzzarelli RAA, Domard A. Advances in Chitin Science. University of Potsdam, Germany. 2000;4:429.
9. Sannan T, Kurita K, Ogura K, Iwakura Y. Studies on chitin: 7. IR spectroscopic determination of degree of deacetylation. Polymer. 1978;19:458-459.
10. Lim SH, Hudson SM. Review of chitosan and its derivatives as antimicrobial agents and their uses as textile chemicals. Journal of Macromolecular Science, Part C: Polymer Reviews. 2003;43:223-269.
11. Hudson SM, Smith C. Polysaccharides: Chitin and chitosan: Chemistry and technology of their use as structural materials. In Biopolymers from renewable resources. 1998;96-118.
12. Berkei M, Bettentrup H. Nanogate Coating Systems GmbH. Synthesis of Titanium Dioxide Nanoparticles. U.S. Patent Application 11/718, 133; 2009.
13. Peng T, Zhao D, Dai K, Shi W, Hirao K. Synthesis of titanium dioxide nanoparticles with mesoporous anatase wall and high photocatalytic activity. The Journal of Physical Chemistry B. 2005;109(11):4947-4952.
14. Sundrarajan M, Gowri S. Green synthesis of titanium dioxide nanoparticles by Nyctanthes arbor-tristis leaves extract. Chalcogenide Lett. 2011;8(8):447-451.
15. Jang HD, Kim SK. Controlled synthesis of titanium dioxide nanoparticles in a modified diffusion flame reactor. Materials Research Bulletin. 2001;36(3-4):627-637.
16. Shahid M, Mohammad F. Recent advancements in natural dye applications: A review. JOCP, 2013;53:310331.
17. Verma AK, Dash RR, Bhunia P. A review on chemical coagulation/ flocculation technologies for removal of colour from textile wastewaters. J. Environ. Manage. 2012;93:154-68.
18. Holme I. Innovative technologies for high performance textiles, COLOR TECHNOL. 2007;123: 59-73.
19. Clark JH, Luque R, Matharu AS. Green chemistry, biofuels, and biorefinery, Annu. Rev. Chem. Biomol. Eng. Published by: Annual Reviews. 2012;3:183-207.
20. Ram. Nidumolu, Coimbatore Prahalad K, Madhavan Rangaswami R. Why sustainability is now the key driver of innovation, HBR. 2009;87:56-64.
21. Ahmed NS, El-Shishtawy RM. The use of new technologies in coloration of textile fibers. J MATER SCI. 2010;45:1143-53.
22. Mohammad F. Emerging green technologies and environment friendly products for sustainable textiles. In Roadmap to Sustainable Textiles and Clothing. 2014;63-82.
23. Atav R. The use of new technologies in dyeing of proteinous fibers, INTECH Open Access Publisher; 2013.

24. Kitchen HJ, Vallance SR, Kennedy JL, TapiaRuiz N, Carassiti L, Harrison A, Whittaker AG, Drysdale TD, Kingman SW, Gregory DH. Modern microwave methods in solid-state inorganic materials chemistry: From fundamentals to manufacturing, Chem. Rev. 2013;14:1170-206.
25. Rosa R, Veronesi P, Leonelli C. A review on combustion synthesis intensification by means of microwave energy. Chem Eng Process. 2013;71:2-18.
26. Clark DE, Sutton WH. Microwave processing of materials. ANRMS. 1996;26:299-331.
27. Clark DE, Gac FD, Sutton WH. Microwaves: Theory and application in materials processing, ceramic transactions, 21, Westerville, J Am Ceram Soc. 1998;451-458.
28. Herrero MA, Kremsner JM, Kappe CO. Nonthermal microwave effects revisited: On the importance of internal temperature monitoring and agitation in microwave chemistry, Org. Chem. 2008;73:36-47.
29. Zhang C, Liao L, Gong S. Recent developments in microwave-assisted polymerization with a focus on ring-opening polymerization. Green Chem. 2007;9:303–14.
30. Mallakpour S, Rafiee Z. Application of microwave-assisted reactions in step-growth polymerization: A review. Iran Polymer J. 2008;17:907–35.
31. Hoogenboom R, Schubert US. Microwaveassisted polymer synthesis recent developments in a rapidly expanding field of research, Macromol Rapid Commun. 2007;28:368–86.
32. Xia J, Li H, Luo Z, Shi H, Wang K, Shu H, Yan Y. Microwave-assisted synthesis of flowerlike and leaf-like CuO nanostructures via room temperature ionic liquids, J Phys Chem Solids. 2009;70: 1461–4.
33. Morris RE. Ionic liquids and microwaves-making zeolites for emerging applications. Angew Chem Int Ed. 2008;47:442–4.
34. Li Q, Dunn ET, Grandmaison EW, Goosen MFA. Applications and properties of chitosan. Journal of Bioactive and Compatible Polymers. 1992;7:370-397.
35. Jou CJ. Degradation of pentachlorophenol with zero-valence iron coupled with microwave energy. Journal of Hazardous Materials. 2008;152:699-702.
36. Jou CJ. Degradation of pentachlorophenol with zero-valence iron coupled with microwave energy. Journal of Hazardous Materials. 2008;152:699-702.
37. Tsuji M, Hashimoto M, Nishizawa Y, Kubokawa M, Tsuji T. Microwave-assisted synthesis of metallic nanostructures in solution. Chemistry–A European Journal. 2005;11:440-452.
38. Tsuji M, Matsumoto K, Tsuji T, Kawazumi H. Rapid synthesis of gold nanostructures by a microwave–polyol method with the assistance of C n TAB (n= 10, 12, 14, 16) or C 16 PC. Materials Letters. 2005;59:3856-3860.
39. Li CC, Cai WP, Cao BQ, Sun FQ, Li Y, Kan CX, Zhang LD. Mass synthesis of large, single-crystal Au nanosheets based on a polyol process. Advanced Functional Materials. 2006; 16:83-90.
40. Youssef BM, Ahmed MHM, Arief MMH, Mashaly HM, Abdelghaffar RA, Mahmoud SA. Synthesis and application of functional (Anti-UV) Azo-dyes based on γ-acid on wool fabrics. Indian Journal of Science and Technology. 2014;7:1005-1013.
41. Hayle ST, Gonfa GG. Synthesis and characterization of titanium oxide nanomaterials using sol–gel method. Am. J. Nanosci. Nanotechnol. 2014;2(1):1-7.
42. Bessekhouad Y, Robert D, Weber JV. Preparation of TiO_2 nanoparticles by sol-gel route. International Journal of Photoenergy. 2003;5:153-158.
43. Shahruz N, Hossain MM. Synthesis and size-control of TiO_2 photocatalyst nanoparticles preparation using sol-gel method. World Appl. Sci. J. 2011;12:1981.
44. Vijayalakshmi R, Rajendran V. Synthesis and characterization of nano-TiO_2 via different methods. Arch App Sci Res. 2012;4:1183-1190.
45. Bhuiyan MR, Shaid A, Khan MA. Cationization of cotton fiber by chitosan and its dyeing with reactive dye without salt. Chemical and Materials Engineering. 2014;2:96-100.
46. Khalil E. Effect of titanium dioxide treatment on the properties of 100% cotton knitted fabric. American Journal of Engineering Research. 2014;3:87-90.
47. Williams S. Practical colour management. Optics & Laser Technology. 2006;38:399-404.
48. Venter JJ, Vannice MA. Applicability of “DRIFTS” for the characterization of carbon-supported metal catalysts and carbon surfaces. Carbon. 1988;26:889-902.
49. Meena MR, Sethi VIJAY. Antimicrobial activity of essential oils from spices. Journal of food science and technology. Mysore. 1994;31:68-70.
50. Harrigan WF, McCance ME. Laboratory methods in food and dairy microbiology-Rev; 1976.

51. Elgayyar M, Draughon FA, Golden DA, Mount JR. Antimicrobial activity of essential oils from plants against selected pathogenic and saprophytic microorganisms. Journal of Food Protection®. 2001;64:1019-1024.
52. Sivakumar A, Murugan R, Sundaresan K, Periyasamy S. UV protection and self-cleaning finish for cotton fabric using metal oxide nanoparticles. Indian Journal of Fibre and Textile Research. 2013;285-292.
53. Stamate M, Lazar G. Application of titanium dioxide photocatalysis to create self-cleaning materials. Modeling and Optimization in the Machines Building Field (MOCM). 2007;13:280-285.
54. Mashaly HM, Abdelghaffar RA, Kamel MM, Youssef BM. Dyeing of polyester fabric using nano disperse dyes and improving their light fastness using ZnO nano powder. Indian Journal of Science and Technology. 2014;7:960-967.

Biography of author(s)

Prof. N. S. Elshemy
Dyeing, Printing and Auxiliaries Department, National Research Centre, Tahrir St., Dokki, Giza, Cairo, Egypt.

She is a professor of Chemistry and Technology of dyeing and Dyes, Textile Research Division, National Research Center, has more international and local publications, supervises 7 Masters of Science, and 5 Ph.D. theses. She served as a Member of many scientific societies and she acted as a reviewer in many international and national journals. In addition, she acted as an organizes and conducts international and local training courses as well as national Conferences. Her research focuses on the microwave in textile dyeing and printing processes to save energy, water and time, nanotechnology, improving performance properties of colored textile (dyeing and printing), dye synthesis as well as a nanomaterial.

S. A. Mahmoud
Dyeing, Printing and Auxiliaries Department, National Research Centre, Tahrir St., Dokki, Giza, Cairo, Egypt.

She was born on 1979 in Egypt. Her education is as follows: Graduate from Faculty of science, Alazhar University, Chemistry Department, Chemistry Department in May 2002. Master degree: from Benha University, Organic Chemistry, And August 2008. Ph.D. degree: from Benha University, Organic Chemistry, 2013. She is working in National Research Center with a Position of researcher in Dyeing, Printing and Auxiliary Division - Textile Division.

Dr. H. M. Mashaly
Dyeing, Printing and Auxiliaries Department, National Research Centre, Tahrir St., Dokki, Giza, Cairo, Egypt.

He was born on December 23, 1969 in Mansoura, Egypt. Raised in Mansoura, he received the Bachelor of Science degree from faculty of Science, Mansoura University, the Master of Science degree from Zagazig University in 2000, and the Ph.D. degree from Ain Shams University in 2005, where he studied many courses in Dyeing technology. He worked as a Professor at Textile Research Division, National Research Centre since 1993. He is specialized in preparation and application of synthetic and natural dyes on cotton, wool and silk fabrics, which was the main subject of his Master and PhD thesis. He also supervised nine theses about dyeing with natural and basic dyes using Ultrasonic energy. The new technology of ultrasonic energy was used for extraction of natural dyes and dyeing of synthetic fabrics for developing good fast colors. This is an eco-friendly trend,

which has a good environmental impact on the society. He also worked in modification of different kinds of fabrics using wet (cationization, mordanting, finishing and dyeing) and plasma technique which consider as an environmentally friendly technique. He has about 59 papers published in international journals. In (2008), he worked as a visiting scholar at College of Textiles, North Carolina State University, USA for 9 months. He is a Professor. since 2015 in NRC , Egypt , most of his publications in highly ranked journals such as Carbohydrate polymers , dyes and pigments , coloration technology ,……..

Dr. K. Haggag
Dyeing, Printing and Auxiliaries Department, National Research Centre, Tahrir St., Dokki, Giza, Cairo, Egypt.

She has more than 104 international publications and 3 patents. She has also supervised 26 Masters of Science and PH.D theses. Furthermore she is decorated with a number of awards including; NRC Scientific encouraging Prize in Chemistry, Egypt in 1991, International Federation of Inventors Mediterranean competition for inventions protecting the environment. Italy in 1995, Prof. Dr. M. K. Tolba's Environmental Prize for: "The Best Applied Research to Protect Air, Water and/or Soil" (ARST) 1998 and NRC Scientific Appreciation Prize, Egypt 2012. In addition she was awarded a number of certifications including; Certificate of Appreciation from Syndicate of Chemistry for her contribution dissemination of culture and scientific information in 2007 and Certificate of scientific achievement at NRC for four consecutive years in 2009, 2010, 2011 and 2012. She acted as Principal Investigator (PI) and Co PI for the National and international research on a number of projects. She acted as a referee for international and national research papers, projects and theses. She organizes and conducts international training courses addition to Chairing and Co-chairing International and national Conferences& Exhibitions. She has conducted a number of presentations in the field of wet processing of textiles at the National Research Centre. Her research focuses on microwave in textile wet processes, nanotechnology in textile, improving performance properties of colored textiles, Eco-friendly dyeing and pigment printing , pollution prevention and cleaner production in textile.

© Copyright (2020): Author(s). The licensee is the publisher (Book Publisher International).

DISCLAIMER
This chapter is an extended version of the article published by the same author(s) in the following journal.
International Journal of Pharmaceutical Sciences Review and Research, 41(2): 41-47, 2016.

Chapter 5
Print ISBN: 978-93-90206-41-4, eBook ISBN: 978-93-90206-42-1

Cu^{II} Complexes with (2-benzylidenehydrazinyl)- 4-Phenylthiazole Ligands: An Experimental and Theoretical Study

Emanoel Hottes[1], Thiago Moreira Pereira[1], Arthur Eugen Kummerle[1], Amanda Porto Neves[1], Clarissa Oliveira da Silva[1] and Marcelo H. Herbst[1*]

DOI: 10.9734/bpi/crdc/v4

ABSTRACT

Cu^{II} complexes of (E)-2-(2-benzylidenehydrazinyl)-4-phenylthiazole, **L1**, (E)-2-(2-(4 chlorobenzylidene)hydrazinyl)-4-phenylthiazole, **L2**, and(E)-2-(2-(4- methoxybenzylidene)hydrazinyl)-4-phenylthiazole **L3** ligands were prepared and characterized by spectroscopic methods. The EPR spectroscopy indicates the formation of two complexation products for **L2** and **L3**, but of one major product for **L1**. The spectrum of CuL1 shows hyperfine parameters $A_{\parallel}$ = 122(±1) G and $g_{\parallel}$ = 2.40(±0.01); $A_{\perp}$ = 13(±2) G and $g_{\perp}$ = 2.08(±0.02). The spectra of both CuL2 and CuL3 show two different species, the most prominent one with the same hyperfine parameters measured for CuL1, and the second one with hyperfine parameters $A_{\parallel}$ = 109(±2) G and $g_{\parallel}$ = 2.36(±0.02); $A^{\perp}$ = 10(±2) G and $g^{\perp}$ = 2.06(±0.02). The EPR spectra of both species are typical of tetragonal-distorted environments around the Cu^{II} center. Semi-empirical calculations at the PM6 level of the ligands indicate the possibility of different conformers under the reactional conditions, suggesting that the different species measured in the EPR spectra should be cis/trans isomers. Semi-empirical calculations at the PM3 level of the complexes suggest that the reaction products should actually be a mixture of (preferentially) trans and cis N1-S structures. These results are corroborated by the FAR-IR and EPR spectra.

Keywords: Thiazole; Cu^{II} complexes; EPR; conformational analysis.

1. INTRODUCTION

Thiazole compounds are a large class of biological active molecules, presenting antibacterial and anti-inflammatory [1,2], anti-depressive [3], anti-tumor [4], anti-tuberculosis [5], anti-parasite [6] and anti-microbial [7] activities. Thiazoles are widely employed as intermediates in the fabrication of synthetic drugs, fungicides and dyes, and occur naturally as in vitamin B1 (tiamine). It is also the active principle of the Ritanovir (Novir®), used in the treatment of HIV, as well as anti-neoplasia drugs bleomicine and thiazofurine [8-9]. Some studies are promising in using (2-benzylidenehydrazinyl)-4-phenylthiazoles against Chagas disease as inhibitors of the biosynthesis of estherols of the cruzain enzyme [10]. The synthesis of (2-benzylidenehydrazinyl)-4-phenylthiazoles, as well as experimental and theoretical studies of this class of molecules are documented in the literature [11-13]. It has been also reported studies on the synthesis and applications of metal complexes bearing thiazole ligands, but there are scarce crystalline structures described, and the structures have been elucidated through spectroscopic analysis [14-21]. For instance, Sobiesiak *et al.* reported the crystalline structures of phenylthiazoles metal complexes that presented cytotoxic activity against leukemia and melanoma cells [18]. Herein, we present an experimental and theoretical (semi-empirical) investigation on the Cu^{II} complexes bearing (2-benzylidenehydrazinyl)-4- phenylthiazole ligands, aiming to contribute to the understanding about the structures of such complexes, as well as the scarcity of crystalline structures.

[1]Universidade Federal Rural do Rio de Janeiro, BR465 km 7 Seropédica, RJ, Brazil.
**Corresponding author: E-mail: herbst@ufrrj.br;*

2. METHODOLOGY

2.1 Synthesis of the (2-benzylidenehydrazinyl)-4-phenylthiazoles

The (E)-2-(2-benzylidenehydrazinyl)-4-phenylthiazole (**L1)**, (E)-2-(2-(4- chlorobenzylidene)hydrazinyl)-4-phenylthiazole (**L2)**, and (E)-2-(2-(4- methoxybenzylidene)hydrazinyl)-4-phenylthiazole(**L3)** molecules were prepared in two steps as described below and according to Scheme 1 [21].

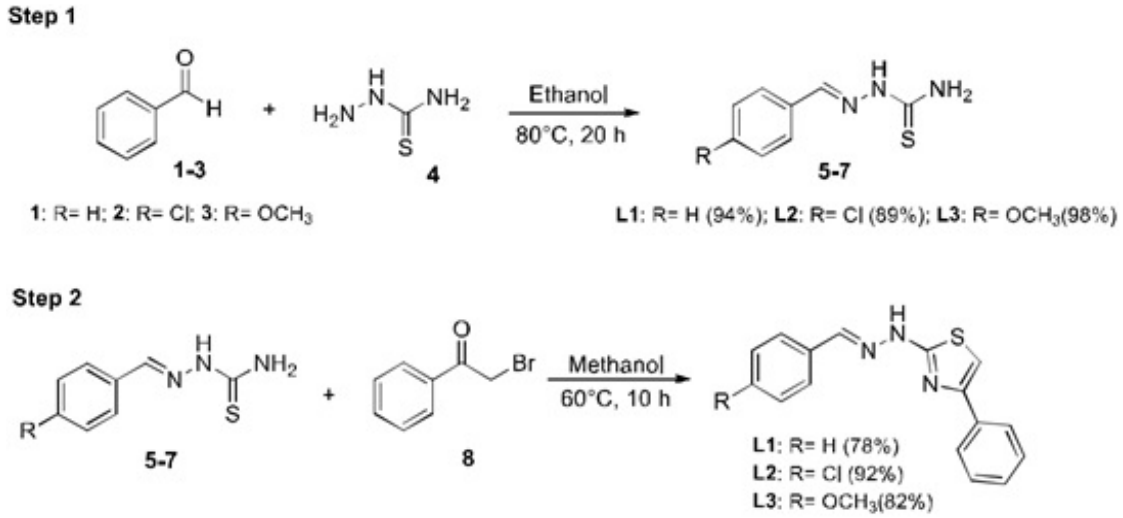

Sheme 1. Synthetic route to the phenylthiazoles L1-L3

All reagents and solvents were purchased from Vetec-Sigma-Aldrich, Brazil. In a round- bottom flask were added 200 mg of aldehyde **1-3** (1 equiv.), 1.2 equiv. of thiosemicarbazide **4**, 10 mL of ethanol and 2 drops of acetic acid. The solution was stirred under heating for about 20 h, cooled in ice bath to precipitate the thiosemicarbazone **5-7**, which was further washed twice with cold ethanol and with cold water and dried (89-98% of yield). In the second step, the respective thiose micarbazone **5-7** (200 mg) was dissolved in methanol at 60ºC, then an equimolar amount of 2-bromo-1-phenylethanone **8** was added dropwise. The solution was stirred under heating for about 10h. After that, the solvent was partially removed affording a precipitate that was filtered, washed with cold ethanol and dried. The **L1** And **L2** compounds were recrystallized from methanol, and the **L3** compound was recrystallized from acetonitrile with ~80% yield. They were characterized by ^{1}H NMR, FTIR, electronic spectroscopy and melting points ((±1°C) **L1=** 222°C; **L2=**226°C; **L3=**219°C), and agree with the literature [21]. Spectra are available upon request to the corresponding author.

2.2. Synthesis of the Cu^{II} phenylthiazole Complexes

In a round-bottom flask it were dissolved 0.20 mmol of the respective phenylthiazole **L1**-**L3** in 5 mL of ethanol at 70°C. To those solutions it was slowly added 2 mL of an ethanol solution of 0.11 mmol $CuCl_2.2H_2O$, affording dark green precipitates and a brownish supernatant. The mixture was kept under stirring for about 4h, cooled to room temperature under stirring and centrifuged. The supernatants tested negative for free chloride. The solids were sequentially washed with ethanol and hot ethanol three times and dried. They were characterized by FTIR, electronic spectroscopy and EPR. Attempts to determine the melting points of the complexes resulted in decomposition above ~155ºC. FTIR and electronic absorption spectra are available upon request to the corresponding author.

2.3 Equipment

The FTIR spectra were acquired in the solid state, in a Bruker Vertex 70 spectrometer equipped with an diamond ATR cell; the electronic absorption spectra were measured in quartz cuvettes, in DMF

solutions, in a Shimadzu UV-1800 spectrophotometer; the ^{1}H NMR spectra of the ligands were obtained in DMSO-d^6 solutions in a Bruker Avance III spectrometer, with a 11.4 T field at the Larmor frequency of 500 MHz for the H nucleus, using TMS as internal standard; the EPR spectra were measured in frozen solutions of DMF at 77K in a Bruker EMX-500 (Laboratório de EPR, UFPR, Brazil), operating in X-Band, using modulation amplitude of 5.0G, gain $4.5x10^3$ and modulation frequency of 100kHz. It was measured five scans for each sample. The computational calculations were done at the semi empirical PM6 level for the phenylthiazoles or at the PM3 level for the Cu^{II} complexes, using the Spartan 14 package.

3. RESULTS AND DISCUSSION

3.1 Spectroscopic Investigation

The electronic UV-vis absorption spectra of the Cu^{II} complexes CuL1, CuL2 and CuL3 present new bands in the visible region, as well as the typical intraligand $\pi-\pi^*$ transitions ($\varepsilon \sim 10^4$) at the 300-350 nm UV region. The visible absorption bands between 500 and 800 nm were assigned to ligand-field *d-d* transitions ($\varepsilon \sim 10^3$). After deconvolution it was possible to assign two maxima at 575 and 670 nm to the *d-d* transitions of CuL1 and CuL2, and at 568 and 661 to the *d-d* transitions of CuL3. Taking into account the d^9 electronic configuration for the Cu^{II} center, the transitions were attributed to $^2B_{1g} \rightarrow {}^2B_{2g}$ and $^2B_{1g} \rightarrow {}^2E_g$, that is, the Cu^{II} center is in a tetragonal distorted environment of ligands [17-19]. The EPR spectrum of CuL1 shows one major species, with hyperfine parameters $A_{\parallel} = 122(\pm1)$ G and $g_{||} = 2.40(\pm0.01)$; $A_{\perp} = 13(\pm2)$ G and $g_{\perp} = 2.08(\pm0.02)$.The g-values greater than 2 are characteristic of Cu^{II} systems with an unpaired electron in the atomic-like d_{x2-y2} orbital, and the $g_e < g_{\perp} < g_{\parallel}$ values mean axial symmetry [22], Fig. 1a.

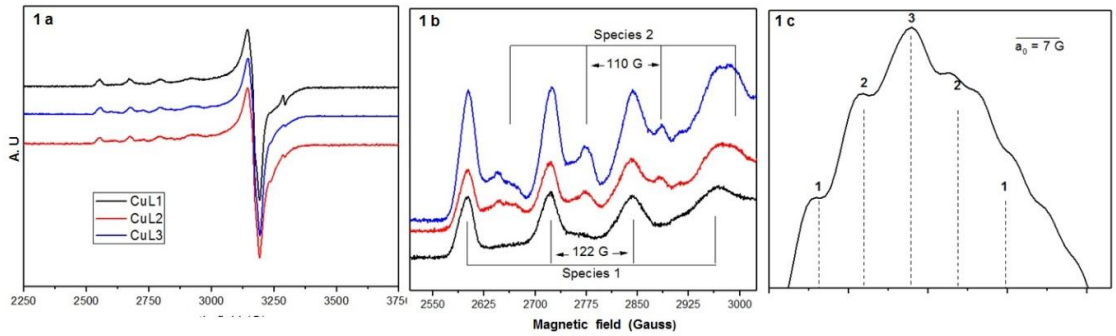

Fig. 1. (1a) Frozen DMF solution EPR spectra measured at 77K for the Cu^{II} complexes. (1b) Expanded parallel part and indication of the two species. (1c) Filtered and magnified fourth parallel line of CuL1 spectrum showing the pattern of superhyperfine lines due to the coupling of the Cu^{II} electron spin to the ^{14}N nuclear spin (I = 1)

On the other hand, the spectra of both CuL2 and CuL3 show two different species, the most prominent one with the same hyperfine parameters measured for CuL1, and the second one with hyperfine parameters $A_{\parallel} = 109(\pm2)$ G and $g_{||} = 2.36(\pm0.02)$; $A_{\perp} = 10(\pm2)$ G and $g_{\perp} = 2.06(\pm0.02)$, Fig. 1b. Such relatively low values of $A_{\parallel}$ hyperfine parameters for both species are indicative of a strong covalent interaction with the ligands, that is, the electron spin density is strongly delocalized onto the ligand-centered molecular orbitals. This is also shown in Fig. 1c, where the filtered magnified fourth parallel line of the EPR spectrum of CuL1 presents five superhyperfine lines ($a_{14N} = 7$ G), indicating that two magnetically equivalent nitrogen nuclei are bonded to the Cu^{II} center. It should be noted that the pattern consists of overlapping groups of lines which cannot be completely resolved, presumably due to the coupling to the two Cu^{II} isotopes. The spectra of the CuL2 and CuL3 compounds consists of two species, which prevent such observation. Finally, in the EPR spectra of the three Cu^{II} samples it was also observed a weak line at $g_{iso}=2.0036(\pm0.0001)$, typical of organic-centered radicals. This signal was not further investigated.

The mid-FTIR spectra of the complexes presented shifts of the azomethyne bands, from 1617 and 1595 cm^{-1}, 1623 and 1600 cm^{-1} and 1621 and 1600 cm^{-1} respectively for L1, L2 and L3, to 1600 and 1558 cm^{-1}, 1595 and 1572 cm^{-1} and 1603 and 1570 cm^{-1} for CuL1, CuL2 and CuL3, indicating coordination of the nitrogen atom of the C=N group [14-18]. The far-FTIR spectra of the complexes presented bands that corroborate the complexation through the nitrogen atom, at 509 cm^{-1} for the CuL1, and at 511 and 482 cm^{-1} for CuL2 ,and at 509 and 528 cm^{-1} for CuL3. In the Cu-S region it was observed a broad band with two maxima at 260 and 275 cm^{-1}, and in the Cu-Cl region the spectra presented a band at 240 cm^{-1}. It is interesting to note that the spectrum of CuL1 shows one unique band in the region of Cu-N, suggesting that only the trans N1-S isomer was formed. On the other hand, the spectra of CuL2 and CuL3 present two bands in the Cu-N region, suggesting that both trans N1-S and cis N1-S isomers are formed. In order to address this question, we have performed a theoretical investigation on the possible isomers [15-20].

3.2 Theoretical Investigation

Based on the EPR, UV-Vis and FTIR spectra of the Cu^{II} complexes, and also on the chemical evidence that indicated the absence of chloride ions in the reaction medium, a theoretical investigation on the possible structural isomers was carried out. Both the EPR and UV-Vis spectra indicate that the Cu^{II} complexes have tetragonal distorted geometries, and the FTIR indicate that the Cu^{II} centers are bonded to N, S and Cl atoms, so the search for the most stable isomers was restricted to octahedral geometries in which the chloro ligands are trans to each other. First, the different possible conformers of L1, L2 and L3 ligands were estimated, since the single bond present in the ligands allow them to bonding to the Cu^{II} center by the N_1 of the C=N moiety and either through the N_3 or by the S atom of the thiazole ring, as shown in Scheme 2.

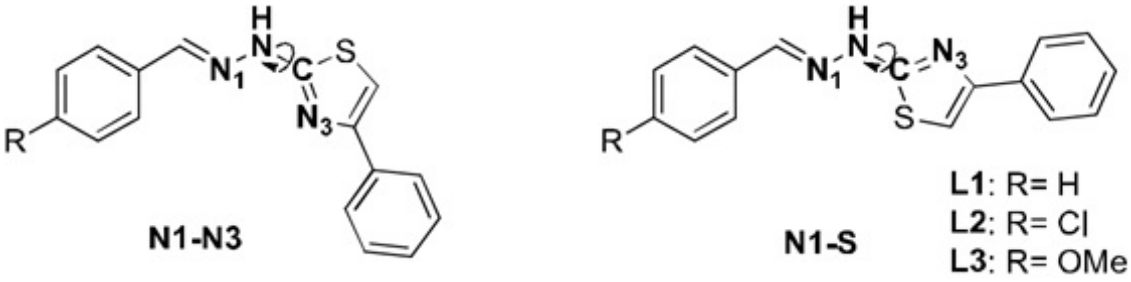

Scheme 2. The conformers of ligands L1, L2 and L3

The energies of the conformers (N1-N3, N1-S), as a function of the rotation angle, calculated at the PM6 level, are shown in Table 1 for L1-L3.

Table 1. Rotation angle [*] and conformer energy for phenylthiazoles L1-L3

	Energy of the conformers (kJ/mol)				
	180°	**100º**	**0**	**-100º**	**-180º**
Compounds					
L1	533,82	543,16	512,11	544,23	533,89
L2	491,15	500,04	470,14	500,80	491,25
L3	344,79	354,73	323,11	355,31	344,92

[*] 0° correspond to the N1-S, and 180º correspond to the N1-N3 conformers. The dihedral angle is formed by the N1-N2-C-N3 atoms, as shown in Scheme 2, ranging from 180° to -180°

As shown in Table 1, the lower-energy conformer for **L1-L3** is the N1-S one, suggesting that upon complexation the phenylthiazoles adopt preferentially this conformation. However, the energy barrier to the N1-N3 conformers is relatively low for the three phenylthiazoles, 21 kJ/mol. Such a low

barrier may lead, even under mild reactional conditions, to the simultaneous occurrence of the two most stable conformers. Fig. 2 shows the graphical correlation between torsion angle and conformer energy (exemplified for **L1**, as neither the profile nor the energy barrier was affected by the substituent in **L2** or **L3**).

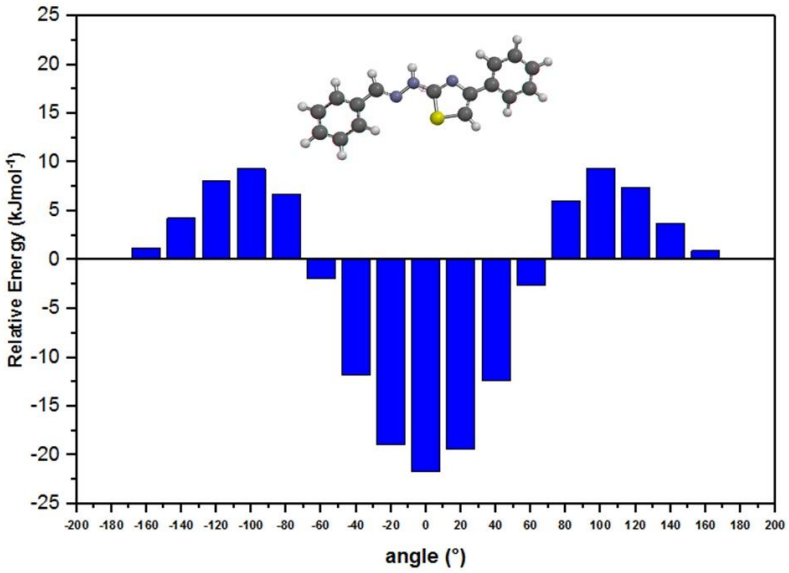

Fig. 2. Correlation profile between torsion angle and conformer energy for L1

Concerning the preferential N1-S conformation, it should be noted that, to the best of our knowledge there are crystalline structures of only three (2-benzylidenehydrazinyl)-4- phenylthiazoles, namely **L2** [23], and the compounds reported by [24] and [9], and they present the N1-S conformation in the solid state. This preferred N1-S conformation is probably due to a 1,4-N·S σ-hole intramolecular interaction as related for similar systems [25].

If the two conformers presented in Scheme 2 are considered, there will be three pairs of possible isomers for each complex, namely N1N3/N1N3 (cis) and N1N3/N3N1 (trans), N1N3/N1S (cis N1) and N1N3/SN1 (trans N1), and N1S/N1S (cis) and N1S/SN1 (trans), as illustrated in Fig. 3.

Table 2 presents the relative energy values of the proposed structural isomers of complexes $Cu(L1)_2(Cl)_2$, $Cu(L2)_2(Cl)_2$, $Cu(L3)_2(Cl)_2$. The energy values indicate that the trans isomers are more stable than the cis isomers, possibly due to the larger distance between the aromatic moieties in the trans structures, as shown in Fig. 3.

Considering the three different possibilities of bonding, the structures in which the phenylthiazole ligands are bonded either by N1 and S atoms have lower energies than their counterparts, as the aromatic groups are far apart in those structures. These data suggest that the reaction products should actually be a mixture of (preferentially) trans and cis N1-S structures. It should be also noted that the energy difference between the cis and trans N1-S isomers of CuL1 (23.5 kJ/mol), CuL2 (63.3kJ/mol) and CuL3 (52.1 kJ/mol) is not large.

Nevertheless, the discrepancies in the theoretical energy values between the CuL1 isomers and the CuL2 and CuL3 isomers should be attributed to the intrinsic limitations of the parametrized semi empirical methods. For instance, at the computational level of the calculations discussed here, the much higher energy values of the cis isomers of CuL2 and CuL3 in comparison with the CuL1 cis isomer should be due to the size of substituent groups in L2 and L3, which are absent in L1. Also, the calculations are made for the isolated systems (as if they were *in vacuo*), and do not consider the

interactions of the solute with the solvent molecules, which are certainly important in the formation of a given isomer.

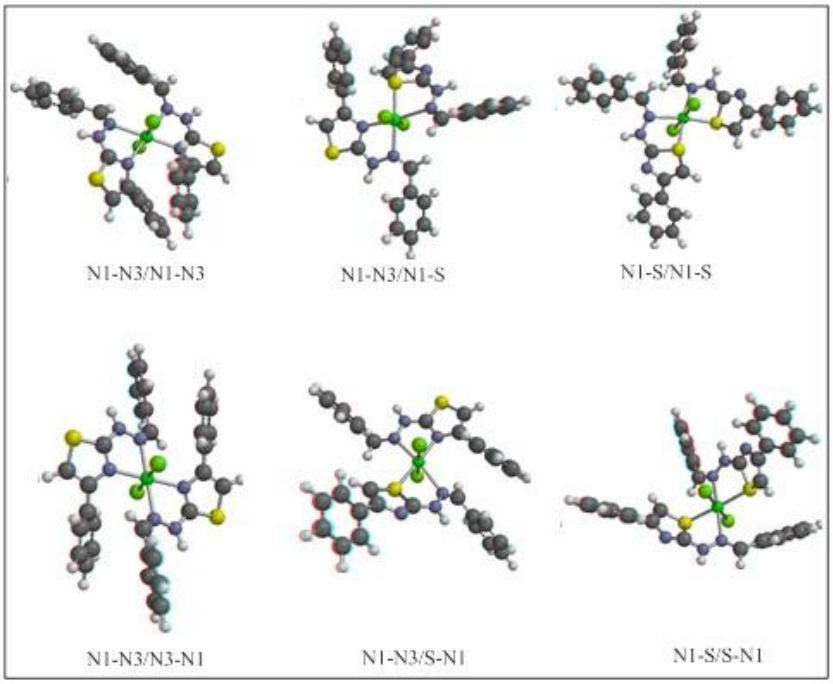

Fig. 3. The possible structural isomers of the Cu^{II} phenylthiazole complexes. Color code: Cl green; S yellow; N blue; C gray and H white

Table 2. Relative energies of the structural isomers of the Cu^{II} complexes at the PM3 level

Complex	cis (kJ/mol)			trans (kJ/mol)		
	N1-N3/N1-N3	**N1-N3/N1-S**	**N1-S/N1-S**	**N1-N3/N3-N1**	**N1-N3/S-N1**	**N1-S/S-N1**
$Cu(L1)_2(Cl)_2$	1123.26	466.00	**67.91**	368.81	417.00	**44.45**
$Cu(L2)_2(Cl)_2$	1193.75	580.37	**114.66**	406.02	478.63	**51.29**
$Cu(L3)_2(Cl)_2$	1145.57	508.71	**110.13**	410.58	461.32	**58.03**

4. CONCLUSION

Cu^{II} complexes of three (2-benzylidenehydrazinyl)-4-phenylthiazole ligands were prepared and characterized by spectroscopic methods. EPR spectroscopy indicate the formation of two complexation products for **L2**, and **L3**, but of one major product for **L1**. The spectrum of CuL1 shows hyperfine parameters $A_{\|}$ = 122(±1) G and $g_{\|}$ = 2.40(±0.01); $A_{\perp}$ = 13(±2) G and $g_{\perp}$ = 2.08(±0.02). The spectra of both CuL2 and CuL3 show two different species, the most prominent one with the same hyperfine parameters measured for CuL1, and the second one with hyperfine parameters $A_{\|}$ = 109(±2) G and $g_{\|}$ = 2.36(±0.02); $A_{\perp}$ = 10(±2) G and $g_{\perp}$ =2.06(±0.02). Such relatively low values of $A_{\|}$ hyperfine parameters for both species are indicative of a strong covalent interaction with the ligands, that is, the electron spin density is strongly delocalized onto the ligand-centered molecular orbitals. Semi-empirical calculations at the PM6 level of the ligands indicate the possibility of different conformers under the reactional conditions, suggesting that the different Cu^{II} complexes measured in the EPR spectra should be cis/trans isomers. Indeed, semi-empirical calculations at the PM3 level of the possible structures for the complexes suggest that the reaction products should actually be a mixture of (preferentially) trans and cis N1-S structures. This is corroborated by the EPR spectra of both species, typical of tetragonal-distorted environments around the Cu^{II} center, and by the superhyperfine lines observed in the EPR spectra of CuL1, that point to the formation of the trans

isomer, which is therefore the major product on CuL2 and CuL3. FAR-IR also shows that the trans isomers are preferentially formed.

ACKNOWLEDGEMENTS

Authors acknowledge FAPERJ for financial support. This study was financed in part by the Coordenação de Aperfeiçoamento de Pessoal de Nível Superior – Brasil (CAPES) – Finance Code 001. E.H. also thanks CNPq for a research grant. Authors thank to Prof. Dr. Ronny Rocha Ribeiro (UFPR) for measuring the EPR spectra, and to Prof. Dr. Ney Vernon Vugman for valuable suggestions.

COMPETING INTERESTS

Authors have declared that no competing interests exist.

REFERENCES

1. Siddiqui N, Arshad MF, Ahsan W, Alam S. Thiazoles: A Valuable Insight into the RecentAdvances and Biological Activities. Int. J. Pharm. Biol. Sci. 2009;1:136-143.
2. Holla BS, Malini KV, Rao BS, Sarojini BK, Kumari NS. Synthesis of some new 2,4- disubstituted thiazoles as possible antibacterial and anti-inflammatory agents. Eur. J. Med. Chem. 2003;38:313-318.
3. Harnett JJ, Roubert V, Dolo C, Charnet C, Spinnewyn B, Cornet S, et al. Phenolic thiazoles as novel orally-active neuroprotective agents. Bioorg. Med. Chem. Lett. 2004;14:157-160.
4. Hassan GS, El-Messery SM, Al-Omary FA, El-Subbagh HI. Substituted thiazoles VII. Synthesis and antitumor activity of certain 2-(substituted amino)-4-phenyl-1,3-thiazole analogs. Bioorg. Med. Chem. Lett. 2012;22:6318-6323.
5. Al-Omary FA, Hassan GS, El-Messery SM, El-Subbagh HI. Substituted thiazoles V. Synthesis and antitumor activity of novel thiazolo[2,3-b] quinazoline and pyrido[4,3-d]thiazolo[3,2-a]pyrimidine analogues. Eur. J. Med. Chem. 2012;47:65-72.
6. Andreani A, Granaiola M, Leoni A, Locatelli A, Morigi R, Rambaldi M. Synthesis and antitubercular activity of imidazo[2,1-b]thiazoles. Eur. J. Med. Chem. 2001;36:743-746.
7. Branowska D, Farahat AA, Kumar A, Wenzler T, Brun R, Liu Y, Wilson WD, Boykin DW. Synthesis and antiprotozoal activity of 2,5-bis[amidinoaryl]thiazoles. Bioorg. Med. Chem. Lett. 2010;18:3551-3558.
8. Fallah-Tafti A, Foroumadi A, Tiwari R, Shirazi AN, Hangauer DG, Bu Y, Akbarzadeh T, Parang K, Shafiee A Substituted thiazoles VI. Synthesis and antitumor activity of new 2- acetamido- and 2 or 3-propanamido-thiazole analogs. Eur. J. Med. Chem. 2012;54:615-625.
9. Cardoso MVO, Siqueira LRP, Silva EB, Costa LB, Hernandes MZ, Rabello MM, et al. 2- Pyridyl thiazoles as novel anti-Trypanosoma cruzi agents: Structural design, synthesis and pharmacological evaluation. Eur. J. Med. Chem. 2014;86:48-59.
10. Moreira DRM, Costa SPM, Hernandes MZ, Rabello MM, Filho GBO, Melo CML, et al. Structural Investigation of Anti-Trypanosoma cruzi 2-Iminothiazolidin-4-ones Allows the Identification of Agents with Efficacy in Infected Mice. J. Med. Chem. 2012;55(24):10918-10936.
11. Alam MS, Liu L, Lee YE, Lee DU. Synthesis, antibacterial activity and quantum-chemical studies of novel 2-arylidenehydrazinyl-4-arylthiazole analogues. Chem Pharm Bull. 2011;59(5):568-73.
12. Hassan AA, Mohamed NK, Aly AA, Tawfeek HN, Brase S, Nieger M. Synthesis and Crystallographic evaluation of diazenyl- and hydrazothiazoles. [5.5] sigmatropic rearrangement and formation of thiazolium bromide dihydrate derivatives. J. Mol. Struct. 2019;1176:346-356.
13. Grozav A, Găină LI, Pileczki V, Crisan O, Silaghi-Dumitrescu L, Therrien B, *et al*. The Synthesis and Antiproliferative Activities of New Arylidene-Hydrazinyl-Thiazole Derivatives. Int. J. Mol. Sci. 2014;15:22059-22072.
14. Alvarez MG, Gloria Alzuet G, Borras J, Agudo LC, Granda SG, Bernardo JMM. Strong protective action of Copper(II) N-substituted sulfonamide complexes against reactive oxygen species. J. Inorg. Biochem. 2004;98:189-198.

15. Chaviara AT, Cox PJ, Repana KH, Papi RM, Papazisis KT, Zambouli D, et al. Copper(II) Schiff base coordination compounds of dien with heterocyclic aldehydes and 2-amino-5- methyl-thiazole: synthesis, characterization, antiproliferative and antibacterial studies. Crystal structure of CudienOOCl2. J. Inorg. Biochem. 2004;98:1271-1283.
16. Chohan ZH, Kausar S. Synthesis, characterization and biological properties of tridentate nno, nns and nnn donor thiazole-derived furanyl,thiophenyl and pyrrolyl schiff bases and their Co(ll), Cu(ll),Ni(ll) and Zn(ll) metal chelates. Met Based Drugs. 2000;7(1);17-22.
17. Pontiki E, Litina DH, Chaviara AT. Evaluation of anti-inflammatory and antioxidant activities of Copper (II) Schiff mono-base and Copper(II) Schiff base coordination compounds of dien with heterocyclic aldehydes and 2-amino-5-methyl-thiazole. J. Enzyme Inhib. Med. Chem. 2008; 23(6):1011-1017.
18. Sobiesiak M, Muzioł T, Rozalski M, Krajewska U, Budziszd E. Co(II), Ni(II) and Cu(II) complexes with phenylthiazole and thiosemicarbazone-derived ligands: synthesis, structure and cytotoxic effects. New J.Chem. 2014;38:5349-5361.
19. Chohan ZH. Ni(ll), Cu(ll) and Zn(ll) metal chelates with some thiazole derived Schiff- bases: their synthesis, characterization and bactericidal properties. Met Based Drugs.1999;6(2);75-80.
20. Haddad R, Yousif E, Ahmed A. Synthesis and characterization of transition metal complexes of 4-Amino-5-pyridyl-4H-1,2,4-triazole-3-thio. . SpringerPlus. 2013;2:510-515.
21. Bolos CA, Chaviara AT, Mourelatos D, Iakovidou Z, Mioglou E, Chrysogelou E, Papageorgiou A. Synthesis, characterization, toxicity, cytogenetic and *in vivo* antitumor studies of 1,1-dithiolate Cu(II) complexes with di-, tri-, tetra- amines and 1,3-thiazoles. Structure-activity correlation. Bioorg Med Chem. 2009;17(8):3142-51.
22. Vugman NV, Herbst MH. Fundamentos e Aplicações da Ressonância Magnética Nuclear: Introdução à Ressonância Paramagnética Eletrônica de onda contínua. Aplicações ao estudo de complexos de metais de transição. AUREMN. N. 3, 2007. (in Portuguese)
23. Hottes, E. M.Sc. Dissertation. UFRRJ; 2016. (in Portuguese)
24. Shih MH, Su YS, Wu CL. Syntheses of aromatic substituted hydrazino-thiazole Derivatives to clarify structural characterization and antioxidant activity between 3-arylsydnonyl and aryl substituted hydrazino-thiazoles. Chem Pharm Bull . 2007;55(8):1126-35.
25. Pinheiro, PSM, Rodrigues, DA, Alves, MA, Tinoco, WL, Ferreira, GB, Sant'Anna, CMR Fraga, CAM. Theoretical and Experimental Characterization of 1,4-N·S σ-hole Intramolecular Interactions in Bioactive N-Acylhydrazone Derivatives. New J Chem. 2017;42:497-505.

Biography of author(s)

Emanoel Hottes
Universidade Federal Rural do Rio de Janeiro, BR465 km 7 Seropédica, RJ, Brazil.

Research and Academic Experience: The author is finishing his Ph.D thesis, and develops research in the areas of inorganic chemistry with an emphasis on the study of hybrid materials and also works on the development of analytical validation methods involving chromatography.

Research Area: Inorganic and Analytical Chemistry

Number of Published papers: 2

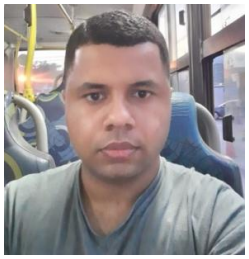

Thiago Moreira Pereira
Universidade Federal Rural do Rio de Janeiro, BR465 km 7 Seropédica, RJ, Brazil.

Research and Academic Experience: He is a Chemistry PhD student at University of Strasbourg and Rural Federal University of Rio de Janeiro under supervision of Dr. Martine Schmitt and Dr. Arthur Eugen Kümmerle. He obtained his master's degree in chemistry in 2018 at Federal Rural University of Rio de Janeiro on Kümmerle's group and the Licentiate and Bachelor's degree in Chemistry in 2016. Has experience on organic synthesis, mainly on the synthesis of heterocyclic with biological activity and fluorescent compounds and in the photophysical evaluation of luminescent molecules.

Research Area: Organic Synthesis and Medicinal Chemistry

Number of Published papers: 10

Special Award (If any): Best research in Biological Chemistry at Annual Meting of Brazilian Chemistry Society – 2014

Arthur Eugen Kummerle
Universidade Federal Rural do Rio de Janeiro, BR465 km 7 Seropédica, RJ, Brazil.

Research and Academic Experience: He has received his B. Pharmacy degree at the Federal University of Rio de Janeiro (Rio de Janeiro, Brazil) in 2003, and developed his graduate studies at the same University under supervision of Prof. Eliezer J. Barreiro, receiving his Ph. D. degree in Chemistry in 2009, and post-doctoral training at the Université de Strasbourg (France). Since 2010, he is a Professor of Organic Chemistry at the Organic Chemistry Department, Federal Rural University of Rio de Janeiro (UFRRJ), developing research in the fields of Pharmacy and Organic Chemistry, with emphasis on Medicinal Chemistry

and synthesis of new heterocycles as bioactive lead and theranostic compounds, using Microwave synthesis, cross-coupling reactions and multi-component reactions as main chemical tools. Currently he is a Tier 2 Researcher Grantee at CNPq (Brazilian National Council for Scientific and Technological Development), "Young Scientist of Our State" at FAPERJ (Rio de Janeiro State Research Foundation) and Director of the Division of Medicinal Chemistry of the Brazilian Chemical Society.

Research Area: Organic Synthesis and Medicinal Chemistry

Number of Published papers: 45

Special Award (If any): Young Scientist of Our State 2015 and 2018
Young Fluminense Researcher 2017

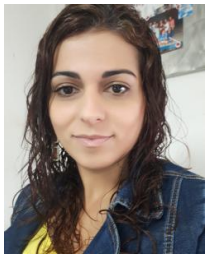

Amanda Porto Neves
Universidade Federal Rural do Rio de Janeiro, BR465 km 7 Seropédica, RJ, Brazil.

Research and Academic Experience: Research on the synthesis of metal complexes, especially Cu(II), Zn(II), Co(II/III), Ru(II) and Pt(II) for biological applications, fluorescence studies and interaction with DNA. Experience with synthesis, cytotoxic assays, DNA interaction / cleavage, and cell accumulation.

Research Area: Medicinal Inorganic Chemistry

Number of Published papers: 17

Clarissa Oliveira da Silva
Universidade Federal Rural do Rio de Janeiro, BR465 km 7 Seropédica, RJ, Brazil.

Research and Academic Experience: Studies on theoretical models for solvated systems and their properties; theoretical descriptions of mono and disaccharides; anomeric effect and theoretical prediction of specific rotation of monosaccharides in solution.

Research Area: Physical Chemistry – Quantum chemistry

Number of Published papers: 37

Any other remarkable point(s): The third bibliographic reference on Wikipedia for anomeric effect.

Marcelo H. Herbst
Universidade Federal Rural do Rio de Janeiro, BR465 km 7 Seropédica, RJ, Brazil.

Research and Academic Experience: BSc in Chemistry from the State University of Londrina (1995) and PhD in Chemistry from the State University of Campinas (2001) with emphasis on organometallic compounds of Pt-fullerene-60. Post-doc at the Laboratory of Magnetic Resonance Applications of the Institute of Physics of UFRJ between 2001 and 2005, under the supervision of Professor Ney Vernon Vugman. Associate Professor at the Federal Rural University of Rio de Janeiro (since 2006). He has publications in the areas of Inorganic Chemistry, Materials and Catalysis, and Chemistry Education, working mainly on the following topics: synthesis and characterization of coordination compounds containing Schiff base or organophosphorus ligands, materials derived from lamellar double hydroxides, electronic paramagnetic resonance (EPR), and didactics in science teaching. Co-author of the book Introduction to Continuous Wave Electronic Paramagnetic Resonance. Applications to the study of transition metal complexes (Auremn, 2007), and of four book chapters. Researcher of the Interinstitutional and Interdisciplinary Group of Studies in Epistemology (www.epistemologia.ufrj.br), with production in the area of science teaching. Coordinator of the Postgraduate Program in Chemistry of UFRRJ between 2015 and 2017.

Research Area: Inorganic Chemistry

Number of Published papers: 39

Special Award: Petrobras Inventor Award 2013

© Copyright (2020): Author(s). The licensee is the publisher (Book Publisher International).

Chapter 6
Print ISBN: 978-93-90206-41-4, eBook ISBN: 978-93-90206-42-1

Acetamide Derivatives of *N*-Methyl-4-Hydroxyaniliniumsulfate: Design, Synthesis, Spectral Characterization and *in silico* Study to Report them as Therapeutic Agents

Misbah Irshad[1,2*], Muhammad Athar Abbasi[2] and Aziz-Ur-Rehman[2]

DOI: 10.9734/bpi/crdc/v4

ABSTRACT

The compounds bearing sulfamoyl and acetamoyl groups have been found to show various biological activities. In the present research work, a series of *O*- and *N*-substituted derivatives were synthesized, starting with planetol (**1**). First *N*-methyl-4-hydroxyanilinium sulfate (**1**; planetol or metol) was treated with different aryl sulfonyl chlorides (**2a-j**) using aq. sodium carbonate solution as reaction medium to yield *N*-substituted derivatives, **3a-j**. The electrophile, *N*-(2,3-dihydro-1,4-benzodioxin-6-yl)-2-bromoacetamide (**5**) was prepared by the reaction of 2,3-dihydro-1,4-benzodioxin-6-amine (**4**) and 2-bromoacetylbromide in a weak basic aqueous medium. The target *O*-substituted molecules, **6a-j**, were synthesized by gearing up the electrophile, **5**, with the molecules, **3a-j**, in a polar aprotic solvent using LiH as activator. The proposed structures of all the synthesized molecules were corroborated by IR, ^{1}H-NMR and EIMS spectral data. The *in vitro* enzyme inhibition and antibacterial studies rendered the synthesized molecules as better cholinesterase inhibitors and moderately better antibacterial agents. To explore the binding modes of the synthesized compounds, all of them were computationally docked against the active sites of acetyl cholinesterase (AChE), butyryl cholinesterase (BChE) and lipoxygenase (LOX). The compounds showed significant interactions and good correlation with the experimental data.

Keywords: 2,3-Dihydro-1,4-benzodioxin-6-amine; antibacterial activity; enzyme inhibition; planetol.

1. INTRODUCTION

Sulfonamide was first identified as the red azo dye known as prontosil rubrum in 1935 by Domagk and his colleagues. Prontosil does not demonstrate any activity *in vitro*; however on hydrolysis *in vivo* it gives the active metabolite sulfanilamide. It can interrupt the synthesis of bacterial DNA and act as potent antimicrobial agent [1]. Sulfonamides show various pharmacological activities such as antidiabetic [2] antitumor activity by inhibition of numerous enzymes like carbonic anhydrase (CA) creatine phosphate enzyme (CP) and cyclooxygenase [3]. Additionally they have potential therapeutic applications in cancer chemotherapy, diuretics, hypoglycemia [4] and inhibit HIV reverse transcriptase [5]. Due to the structural similarity of sulfonamides to *p*-aminobenzoiacacid (PABA) (that is needed by bacteria for the synthesis of folic acid and its growth) they inhibit the conversion of PABA into folic acid by competing it in binding to the active site of dihydropteroate synthase (DHPS) enzyme. DHPS is involved in the folate synthesis with pABA to give the folate intermediate 7,8- dihydropteroate (DHF). Subsequently, DHF is transformed to tetrahydrofolic acid (THF) through the action of the dihydrofolatereductase (DHFR) enzyme. Inhibiting the action of either DHPS or DHFR enzymes would ultimately block the synthesis of purine and DNA [6].

[1]Department of Chemistry, Division of Science and Technology, University of Education, Township Campus, Lahore-54770, Pakistan.
[2]Department of Chemistry, Government College University, Lahore-54000, Pakistan.
**Corresponding author: E-mail: misbahirshad@ue.edu.pk;*

Compounds containing 1,4-benzodioxane moiety exhibited important pharmacological activities like antihepatotoxic [7], α-adrenergic blocking agent [8], anti-inflammatory and D_2 antagonist/5-HT1A partial agonistic activity [9]. 1,4-Benzodioxan-2-carboxylic acid has been used for the preparation of doxazosinmesylate which is an alphablocker used to treat high blood pressure and benign prostatichyperplasia. Doxazosinmesylate has been developed as an oral solid dosage form for benign prostatic hyperplasia (BPH) and antihypertensive activity [10]. The compounds containing dioxane rings are of interest for the introduction of a variety of substituents into common skeleton, novel transformations, and can provide new and generalroutes to a variety of organic molecules.

Cholinesterase (ChE) represents important class of enzymes which are responsible for catalyzing the hydrolysis of acetyl choline (ACh) into choline and acetic acid. Hydrolysis of ACh is an essential process for the establishment of the neurotransmission. Acetylcholinesterase (AChE) and butyrylcholinesterase (BChE) are two types of cholinesterase [11]. AChE and BChE share 65% amino acid sequence homology and have similar molecular forms and active sites despite being products of different genes on the human chromosomes [12]. AChE is known to be abundant in the muscle, brain, and erythrocyte membrane, whereas BChE hasa higher activity in liver, intestine, heart, kidney, and lung [13]. The symptomatic Alzheimer's disease (AD) treatment involves the use of cholinesterase inhibitors (ChEIs) such as Rivastigimine.ChEIs are the first-line drugs in the symptomatic treatment of AD, as by inhibiting cholinesterase they lead to an increased synaptic level of the neurotransmitter [14].

Lipoxygenase (LOX) are key enzymes in the biosynthesis of variety of bioregulatory compounds such as hydroxyeicosatetraenoic acids, leukotrienes, lipoxins and hepoxylines [15]. It has been found that these lipoxygenase products play a role in a variety of disorders such as bronchial asthma, inflammation [16] and tumor angiogenesis(the formation of new capillary vessels from pre-existing ones) [17]. LOXs are therefore potential target for the rational drug design and discovery based on the inhibition mechanism of inhibitors for the treatment of bronchial asthma, inflammation, cancer and autoimmune diseases.

The synthesis of various sulfonamides and acetamides, to inaugurate new less toxic and more efficient molecules, prompted us to take into account the synthesis of such molecules bearing both the moieties. The present work is the protraction of our successful efforts for the synthesis of potent bioactive sulfonamides, acetamides and heterocyclic compounds [18-21]. The series of synthesized molecules were found to be potentially more active against cholinesterase enzymes, moderate against Gram-bacterial strains and less against lipoxygenase enzyme.

2. EXPERIMENTAL

2.1 General

Melting points of the synthesized compounds were recorded on open capillary tube Griffin and George melting point apparatus and were uncorrected. Purity was checked out by thin layer chromatography (TLC) on pre-coated silica gel G-25-UV_{254} plates with different polarity solvent systems using ethyl acetate and *n*-hexane giving single spot. Identification of spots was carried out at 254 nm UV lamp, and by ceric sulphate reagent on heating. The IR spectra were recorded in KBr pellet method on a Jasco-320-A spectrophotometer with wave number in cm^{-1}. Nuclear magnetic resonance spectra were recorded in CD_3OD on a Bruker spectrometers operating at 300 MHz. Chemical shifts are given in ppm taking TMS as internal reference standard and coupling constant (*J*) in Hz. The abbreviations used in ^{1}H-NMR were s = singlet, d = doublet and dd = doublet of doublet. Mass spectra (EIMS) were recorded on a JMS-HX-110 spectrometer, with a data system. All the spectra were taken at 25°C (r. temp.). All the chemicals taken into account were purchased from Alfa Aesar, Sigma Aldrick and Merck through local suppliers. The solvents used in the discussed project were of analytical grade.

2.2 General Procedure for the Synthesis of N-substituted Derivatives of Planetol (3a-j)

N-methyl-4-hydroxyanilinium sulfate (**1**; 10.0 mmol) was dissolved in 25 mL distilled water in a 100 mL round bottom (RB) flask and basified to pH of 8-10 by 10% aqueous Na_2CO_3 solution. The aryl sulfonyl chlorides (**2a-j**; 10.0 mmol) were added to the reaction medium gradually in 5-10 minutes. The reaction mixture was stirred for 4-5 hours along with monitoring by TLC till the single spot. At the end of reaction, dil. HCl (2.0 mL) was added slowly along with vigorous hand shaking to adjust the pH to 3-5. The precipitates were generated after a stay of 5-10 min which were filtered, washed with distilled water and dried to afford the title solid compounds, **3a-j** in good yields. Recrystallization was progressed in methanol.

2.3 *N*-(4-hydroxyphenyl)-*N*-methylbenzenesulfonamide (3a)

Light brown amorphous solid; Yield: 92%; M.P.: 106°C; Molecular formula: $C_{13}H_{13}NO_3S$; Molecular weight: 263 $gmol^{-1}$; HR-MS: $[M]^+$ 263.3132 (Calcd. for $C_{13}H_{13}NO_3S$; 263.3361); IR (KBr, cm^{-1}) ν_{max}: 3365 (O-H stretching), 3061 (C-H stretching of aromatic ring), 2923 (-CH_2- stretching), 1623 (C=C stretching of aromatic ring), 1376 (-SO_2 stretching), 1154 (C-O-C stretching of ether); ^{1}H-NMR (CD_3OD, 300 MHz): δ (ppm) 7.64 (brd, J = 9.0 Hz, 2H, H-2' & H-6'), 7.62-7.51 (m, 3H, H-3' to H-5'), 6.84 (d, J = 8.7 Hz, 2H, H-2 & H-6), 6.67 (d, J = 8.7 Hz, 2H, H-3 & H-5), 3.11 (s, 3H, CH_3-1''), EIMS: *m/z* 263 $[M]^+$, 199 $[M\text{-}SO_2]^+$, 141 $[C_6H_5SO_2]^+$, 122 $[C_7H_8NO]^+$, 93 $[C_6H_5O]^+$, 77 $[C_6H_5]^+$, 51 $[C_4H_3]^+$.

2.4 *N*-(4-hydroxyphenyl)-*N*,4-dimethylbenzenesulfonamide (3b)

Light grey amorphous solid; Yield: 93%; M.P.: 125°C; Molecular formula: $C_{14}H_{15}NO_3S$; Molecular weight: 277 $gmol^{-1}$; HR-MS: $[M]^+$ 277.3403 (Calcd. for $C_{14}H_{15}NO_3S$; 277.3610); IR (KBr, cm^{-1}) ν_{max}: 3356 (O-H stretching), 3059 (C-H stretching of aromatic ring), 2937 (-CH_2- stretching), 1604 (C=C stretching of aromatic ring), 1378 (-SO_2 stretching), 1145 (C-O-C stretching of ether); ^{1}H-NMR (CD_3OD, 300 MHz): δ (ppm) 7.42 (d, J = 8.4 Hz, 2H, H-2' & H-6'), 7.34 (d, J = 8.1 Hz, H-3' & H-5'), 6.84 (d, J = 8.7 Hz, 2H, H-2 & H-6), 6.67 (d, J = 8.7 Hz, 2H, H-3 & H-5), 3.01 (s, 3H, CH_3-1''), 2.41 (s, 3H, CH_3-4'); EIMS: *m/z* 277 $[M]^+$, 213 $[M\text{-}SO_2]^+$, 155 $[CH_3C_6H_5SO_2]^+$, 122 $[C_7H_8NO]^+$, 93 $[C_6H_5O]^+$, 91 $[CH_3C_6H_5]^+$, 50 $[C_4H_2]^+$.

2.5 4-(*tert*-butyl)-*N*-(4-hydroxyphenyl)-*N*-methylbenzenesulfonamide (3c)

Blackish brown amorphous solid; Yield: 90%; M.P.: 76°C; Molecular formula: $C_{17}H_{21}NO_3S$; Molecular weight: 319 $gmol^{-1}$; HR-MS: $[M]^+$ 319.4207 (Calcd. for $C_{17}H_{21}NO_3S$; 319.4371); IR (KBr, cm^{-1}) ν_{max}: 3355 (O-H stretching), 3066 (C-H stretching of aromatic ring), 2913 (-CH_2- stretching), 1615 (C=C stretching of aromatic ring), 1390 (-SO_2 stretching), 1167 (C-O-C stretching of ether); ^{1}H-NMR (CD_3OD, 300 MHz): δ (ppm) 7.58 (d, J = 8.7 Hz, 2H, H-2' & H-6'), 7.47 (d, J = 8.4 Hz, H-3' & H-5'), 6.86 (d, J = 9.0 Hz, 2H, H-2 & H-6), 6.68 (d, J = 8.7 Hz, 2H, H-3 & H-5), 3.10 (s, 3H, CH_3-1''), 1.36 (s, 9H, $(CH_3)_3$C-4'); EIMS: *m/z* 319 $[M]^+$, 255 $[M\text{-}SO_2]^+$, 197 $[(CH_3)_3CC_6H_5SO_2]^+$, 133 $[(CH_3)_3CC_6H_5]^+$, 122 $[C_7H_8NO]^+$, 93 $[C_6H_5O]^+$, 50 $[C_4H_2]^+$.

2.6 *N*-(4-hydroxyphenyl)-*N*,2,4,6-tetramethylbenzenesulfonamide (3d)

Black amorphous solid; Yield: 84%; M.P.: 60°C; Molecular formula: $C_{16}H_{19}NO_3S$; Molecular weight: 305 $gmol^{-1}$; HR-MS: $[M]^+$ 305.3934 (Calcd. for $C_{16}H_{19}NO_3S$; 305.4106); IR (KBr, cm^{-1}) ν_{max}: 3364 (O-H stretching), 3069 (C-H stretching of aromatic ring), 2924 (-CH_2- stretching), 1604 (C=C stretching of aromatic ring), 1395 (-SO_2 stretching), 1159 (C-O-C stretching of ether); ^{1}H-NMR (CD_3OD, 300 MHz): δ (ppm) 6.95 (s, 2H, H-3' & H-5'), 6.92 (d, J = 8.7 Hz, 2H, H-2 & H-6), 6.65 (d, J = 9.0 Hz, 2H, H-3 & H-5), 3.19 (s, 3H, CH_3-1''), 2.38 (s, 6H, CH_3-2' & 6'), 2.27 (s, 3H, CH_3-4'); EIMS: *m/z* 305 $[M]^+$, 241 $[M\text{-}SO_2]^+$, 183 $[(CH_3)_3C_6H_5SO_2]^+$, 122 $[C_7H_8NO]^+$, 119 $[(CH_3)_3C_6H_5]^+$, 93 $[C_6H_5O]^+$.

2.7 4-(acetylamino)-*N*-(4-hydroxyphenyl)-*N*-methylbenzenesulfonamide (3e)

Grayish brown amorphous solid; Yield: 91%; M.P.: 152°C; Molecular formula: $C_{15}H_{16}N_2O_4S$; Molecular weight: 320 $gmol^{-1}$; HR-MS: $[M]^+$ 320.3654 (Calcd. for $C_{15}H_{16}N_2O_4S$; 320.3849); IR (KBr,

cm^{-1}) ν_{max}: 3369 (O-H stretching), 3073 (C-H stretching of aromatic ring), 2927 (-CH_2- stretching), 1613 (C=C stretching of aromatic ring), 1379 (-SO_2 stretching), 1153 (C-O-C stretching of ether); ^{1}H-NMR (CD_3OD, 300 MHz): δ (ppm) 7.72 (d, *J* = 8.7 Hz, 2H, H-3' & H-5'), 7.47 (d, *J* = 8.7 Hz, 2H, H-2' & H-6'), 6.86 (d, *J* = 8.7 Hz, 2H, H-2 & H-6), 6.68 (d, *J* = 9.0 Hz, 2H, H-3 & H-5), 3.10 (s, 3H, $\underline{CH_3}$CONH-4'), 2.14 (s, 3H, CH_3-1''); EIMS: *m/z* 320 $[M]^+$, 256 $[M\text{-}SO_2]^+$, 198 $[CH_3CONHC_6H_5SO_2]^+$, 134 $[CH_3CONHC_6H_5]^+$, 122 $[C_7H_8NO]^+$, 93 $[C_6H_5O]^+$, 50 $[C_4H_2]^+$.

2.8 4-bromo-*N*-(4-hydroxyphenyl)-*N*-methylbenzenesulfonamide (3f)

Dark brown amorphous solid; Yield: 90%; M.P.: 78°C; Molecular formula: $C_{13}H_{12}BrNO_3S$; Molecular weight: 341 $gmol^{-1}$; HR-MS: $[M]^+$ 341.2091 (Calcd. for $C_{13}H_{12}BrNO_3S$; 341.2235); IR (KBr, cm^{-1}) ν_{max}: 3354 (O-H stretching), 3051 (C-H stretching of aromatic ring), 2926 (-CH_2- stretching), 1608 (C=C stretching of aromatic ring), 1372 (-SO_2 stretching), 1147 (C-O-C stretching of ether); ^{1}H-NMR (CD_3OD, 300 MHz): δ (ppm) 7.71 (d, *J* = 8.7 Hz, 2H, H-2' & H-6'), 7.44 (d, *J* = 8.4 Hz, 2H, H-3' & H-5'), 6.87 (d, *J* = 9.0 Hz, 2H, H-2 & H-6), 6.69 (d, *J* = 9.0 Hz, 2H, H-3 & H-5), 3.12 (s, 3H, CH_3-1''); EIMS: *m/z* 343 $[M+2]^+$, 341 $[M]^+$, 277 $[M\text{-}SO_2]^+$, 219 $[BrC_6H_5SO_2]^+$, 155 $[BrC_6H_5]^+$, 122 $[C_7H_8NO]^+$, 93 $[C_6H_5O]^+$, 50 $[C_4H_2]^+$.

2.9 4-chloro-*N*-(4-hydroxyphenyl)-*N*-methylbenzenesulfonamide (3g)

Blackish grey amorphous solid; Yield: 94%; M.P.: 100°C; Molecular formula: $C_{13}H_{12}ClNO_3S$; Molecular weight: 297 $gmol^{-1}$; HR-MS: $[M]^+$ 297.3586 (Calcd. for $C_{13}H_{12}ClNO_3S$; 297.3739); IR (KBr, cm^{-1}) ν_{max}: 3351 (O-H stretching), 3070 (C-H stretching of aromatic ring), 2931 (-CH_2- stretching), 1607 (C=C stretching of aromatic ring), 1379 (-SO_2 stretching), 1178 (C-O-C stretching of ether); ^{1}H-NMR (CD_3OD, 300 MHz): δ (ppm) 7.53 (d, *J* = 8.1 Hz, 2H, H-2' & H-6'), 7.45 (d, *J* = 8.1 Hz, 2H, H-3' & H-5'), 6.87 (d, *J* = 8.4 Hz, 2H, H-2 & H-6), 6.69 (d, *J* = 8.7 Hz, 2H, H-3 & H-5), 3.12 (s, 3H, CH_3-1''); EIMS: *m/z* 299 $[M+2]^+$, 297 $[M]^+$, 233 $[M\text{-}SO_2]^+$, 175 $[ClC_6H_5SO_2]^+$, 122 $[C_7H_8NO]^+$, 111 $[ClC_6H_5]^+$, 93 $[C_6H_5O]^+$, 50 $[C_4H_2]^+$.

2.10 2,5-dichloro-*N*-(4-hydroxyphenyl)-*N*-methylbenzenesulfonamide (3h)

Blackish grey amorphous solid; Yield: 87%; M.P.: 76°C; Molecular formula: $C_{13}H_{11}Cl_2NO_3S$; Molecular weight: 331 $gmol^{-1}$; HR-MS: $[M]^+$ 331.2035 (Calcd. for $C_{13}H_{11}Cl_2NO_3S$; 331.2148); IR (KBr, cm^{-1}) ν_{max}: 3375 (O-H stretching), 3072 (C-H stretching of aromatic ring), 2937 (-CH_2- stretching), 1617 (C=C stretching of aromatic ring), 1379 (-SO_2 stretching), 1170 (C-O-C stretching of ether); ^{1}H-NMR (CD_3OD, 300 MHz): δ (ppm) 7.81 (s, 1H, H-6'), 7.71 (d, *J* = 8.4, 1H, H-3'), 7.58 (d, *J* = 8.4, 1H, H-4'), 6.87 (d, *J* = 8.7 Hz, 2H, H-2 & H-6), 6.69 (d, *J* = 9.0 Hz, 2H, H-3 & H-5), 3.12 (s, 3H, CH_3-1''); EIMS: *m/z* 335 $[M+4]^+$, 333 $[M+2]^+$, 331 $[M]^+$, 267 $[M\text{-}SO_2]^+$, 209 $[Cl_2C_6H_5SO_2]^+$, 145 $[Cl_2C_6H_5]^+$, 122 $[C_7H_8NO]^+$, 93 $[C_6H_5O]^+$.

2.11 3,5-dichloro-*N*-(4-hydroxyphenyl)-*N*-methylbenzenesulfonamide (3i)

Black amorphous solid; Yield: 89%; M.P.: 100°C; Molecular formula: $C_{13}H_{11}Cl_2NO_3S$; Molecular weight: 331 $gmol^{-1}$; HR-MS: $[M]^+$ 331.2035 (Calcd. for $C_{13}H_{11}Cl_2NO_3S$; 331.2148); IR (KBr, cm^{-1}) ν_{max}: 3353 (O-H stretching), 3059 (C-H stretching of aromatic ring), 2910 (-CH_2- stretching), 1612 (C=C stretching of aromatic ring), 1371 (-SO_2 stretching), 1161 (C-O-C stretching of ether); ^{1}H-NMR (CD_3OD, 300 MHz): δ (ppm) 9.80 (s, 1H, HO-4'), 7.62 (d, *J* = 2.4 Hz, 2H, H-2', H-6'), 7.54 (d, *J* = 2.1 Hz, 1H, H-4'), 6.98 (d, *J* = 8.7 Hz, 2H, H-2 & H-6), 6.70 (d, *J* = 8.7 Hz, 2H, H-3 & H-5), 2.72 (s, 3H, CH_3-1''); EIMS: *m/z* 335 $[M+4]^+$, 333 $[M+2]^+$, 331 $[M]^+$, 267 $[M\text{-}SO_2]^+$, 209 $[Cl_2C_6H_5SO_2]^+$, 145 $[Cl_2C_6H_5]^+$, 122 $[C_7H_8NO]^+$, 93 $[C_6H_5O]^+$.

2.12 *N*-(4-hydroxyphenyl)-*N*-methyl-2-naphthalenesulfonamide (3j)

Dark brown amorphous solid; Yield: 95%; M.P.: 72°C; Molecular formula: $C_{17}H_{15}NO_3S$; Molecular weight: 313 $gmol^{-1}$; HR-MS: $[M]^+$ 313.3725 (Calcd. for $C_{17}H_{15}NO_3S$; 313.3834); IR (KBr, cm^{-1}) ν_{max}: 3347 (O-H stretching), 3058 (C-H stretching of aromatic ring), 2927 (-CH_2- stretching), 1609 (C=C

stretching of aromatic ring), 1391 (-SO_2 stretching), 1164 (C-O-C stretching of ether); ^{1}H-NMR (CD_3OD, 300 MHz): δ (ppm) 8.14 (s, 1H, H-1'), 7.96-7.90 (m, 2H, H-4' & H-5'), 7.87 (d, *J* = 8.1 Hz, 1H, H-3'), 7.64 (dd, *J* = 8.1, 2.1 Hz, 1H, H-8'), 7.52-7.47 (m, 2H, H-6' & H-7'), 6.85 (d, *J* = 8.7 Hz, 2H, H-2 & H-6), 6.66 (d, *J* = 8.7 Hz, 2H, H-3 & H-5), 3.16 (s, 3H, CH_3-1''); EIMS: *m/z* 313 $[M]^+$, 249 $[M\text{-}SO_2]^+$, 191 $[C_{10}H_7SO_2]^+$, 127 $[C_{10}H_7]^+$, 122 $[C_7H_8NO]^+$, 93 $[C_6H_5O]^+$.

2.13 Procedure for the Synthesis of N-(2,3-dihydro-1,4-benzodioxin-6-yl)-2-bromoacetamide (5)

2,3-dihydro-1,4-benzodioxin-6-amine (**4**; 110.0 mmol) was suspended in 100 mL distilled water in a 250 mL iodine flask and 10% Na_2CO_3 solution was added to adjust the pH 8-10. The reaction mixture was hand shaked for 5-10 minutes and then 2-bromoacetylbromide (110.0 mmol) was poured drop wise along with vigorous shaking till the formation of solid precipitates. After complete addition, the iodine flask was kept on stirring for further 15-20 min. The solid precipitates were verified through TLC giving single spot and acidified up to pH of 3-5. The precipitates were filtered, washed with distilled water and dried to yield the electrophile, **5**. Purplish grey amorphous solid; Yield: 95%; M.P.: 56°C; Molecular formula: $C_{10}H_{10}BrNO_3$; Molecular weight: 271 gmol^{-1}; HR-MS: $[M]^+$ 271.0952 (Calcd. for $C_{10}H_{10}BrNO_3$; 271.1076); IR (KBr, cm^{-1}) ν_{max}: 3460 (N-H stretching), 3067 (C-H stretching of aromatic ring), 2919 (-CH_2- stretching), 1618 (C=C stretching of aromatic ring), 1157 (C-O-C stretching of ether); ^{1}H-NMR (CD_3OD, 300 MHz): δ (ppm) 10.20 (s, 1H, NH), 7.20 (d, *J* = 2.1 Hz, 1H, H-5), 6.95 (dd, *J* = 8.7, 2.1 Hz, 1H, H-7), 6.80 (d, *J* = 8.7 Hz, 1H, H-8), 4.19 (s, 4H, CH_2-2 & CH_2-3), 3.97 (s, 2H, CH_2-2'); EIMS: *m/z* 273 $[M+2]^+$, 271 $[M]^+$, 150 $[C_8H_8NO_2]^+$, 135 $[C_8H_7O_2]^+$, 122 $[C_6H_4NO_2]^+$, 121 $[C_2H_2BrO]^+$, 107 $[C_6H_3O_2]^+$, 66 $[C_4H_4N]^+$.

2.14 General Procedure for the Synthesis of O-substituted Derivatives (6a-j)

N-(4-hydroxyphenyl)-*N*-methylarylsulfonamides (**3a-j**; 10.0 mmol) were homogeneously dissolved in *N,N*-dimethylformamide (DMF; 10 mL) in a 100 mL RB flask and activated by the addition of lithium hydride (10.0 mmol). The mixture was stirred for 15-25 min and then the calculated equimolar amount of electrophile, *N*-(2,3-dihydro-1,4-benzodioxin-6-yl)-2-bromoacetamide (**5**) was added to reaction mixture and further stirred for 5-6 hours. The reaction progress was supervised *via* TLC till single spot. Aqueous Na_2CO_3 solution (30-40 mL) was added to the flask and hand shaked slowly. The target precipitated products were collected by filtration, washed with distilled water and dried.

2.15 2-{4-[methyl(phenylsulfonyl)amino]phenoxy}-*N*-(2,3-dihydro-1,4-benzodioxin-6-yl)acetamide (6a)

Light brown amorphous solid; Yield: 81%; M.P.: 157°C; Molecular formula: $C_{23}H_{22}N_2O_6S$; Molecular weight: 454 gmol^{-1}; HR-MS: $[M]^+$ 454.4975 (Calcd. for $C_{23}H_{22}N_2O_6S$; 454.5031); IR (KBr, cm^{-1}) ν_{max}: 3462 (N-H stretching), 3060 (C-H stretching of aromatic ring), 2921 (-CH_2- stretching), 1621 (C=C stretching of aromatic ring), 1381 (-SO_2 stretching), 1159 (C-O-C stretching of ether); ^{1}H-NMR (CD_3OD, 300 MHz): δ (ppm) 7.64 (dd, *J* = 7.8, 1.8 Hz, 2H, H-2' & H-6'), 7.51-7.41 (m, 3H, H-3' to H-5'), 7.17 (d, *J* = 2.4, 1H, H-5'''), 7.02 (dd, *J* = 8.4, 1.2 Hz, 1H, H-7'''), 6.99 (d, *J* = 7.5 Hz, 1H, H-8'''), 6.97 (d, *J* = 8.1 Hz, 2H, H-2 & H-6), 6.78 (d, *J* = 8.7 Hz, 2H, H-3 & H-5), 4.21 (s, 4H, CH_2-2''' & CH_2-3'''), 3.92 (s, 2H, CH_2-2''''), 3.14 (s, 3H, CH_3-1''); EIMS: *m/z* 454 $[M]^+$, 390 $[M\text{-}SO_2]^+$, 150 $[C_8H_8NO_2]^+$, 141 $[C_6H_5SO_2]^+$, 135 $[C_8H_7O_2]^+$, 122 $[C_6H_4NO_2]^+$, 122 $[C_7H_8NO]^+$, 107 $[C_6H_3O_2]^+$, 93 $[C_6H_5O]^+$, 77 $[C_6H_5]^+$, 66 $[C_4H_4N]^+$, 51 $[C_4H_3]^+$.

2.16 2-(4-{methyl[(4-methylphenyl)sulfonyl]amino}phenoxy)-*N*-(2,3-dihydro-1,4-benzodioxin-6-yl)acetamide (6b)

Light grey amorphous solid; Yield: 80%; M.P. 155°C; Molecular formula: $C_{24}H_{24}N_2O_6S$; Molecular weight: 468 gmol^{-1}; HR-MS: $[M]^+$ 468.5234 (Calcd. for $C_{24}H_{24}N_2O_6S$; 468.5364); IR (KBr, cm^{-1}) ν_{max}: 3464 (N-H stretching), 3073 (C-H stretching of aromatic ring), 2911 (-CH_2- stretching), 1610 (C=C stretching of aromatic ring), 1377 (-SO_2 stretching), 1149 (C-O-C stretching of ether); ^{1}H-NMR (CD_3OD, 300 MHz): δ (ppm) 7.45 (d, *J* = 8.1 Hz, 2H, H-2' & H-6'), 7.38 (d, *J* = 8.4 Hz, H-3' & H-5'),

7.19 (d, *J* = 2.4, 1H, H-5'''), 7.06 (dd, *J* = 8.1, 1.5 Hz, 1H, H-7'''), 6.89 (d, *J* = 8.1 Hz, 2H, H-2 & H-6), 6.72 (d, *J* = 7.5 Hz, 1H, H-8'''), 6.69 (d, *J* = 8.7 Hz, 2H, H-3 & H-5), 4.21 (s, 4H, CH_2-2''' & CH_2-3'''), 3.91 (s, 2H, CH_2-2''''), 3.09 (s, 3H, CH_3-1''), 2.42 (s, 3H, CH_3-4'); EIMS: *m/z* 468 $[M]^+$, 404 $[M\text{-}SO_2]^+$, 155 $[CH_3C_6H_5SO_2]^+$, 150 $[C_8H_8NO_2]^+$, 135 $[C_8H_7O_2]^+$, 122 $[C_6H_4NO_2]^+$, 122 $[C_7H_8NO]^+$, 107 $[C_6H_3O_2]^+$, 93 $[C_6H_5O]^+$, 91 $[CH_3C_6H_5]^+$, 66 $[C_4H_4N]^+$, 50 $[C_4H_2]^+$.

2.17 2-{4-[{[4-(*tert*-butyl)phenyl]sulfonyl}(methyl)amino]phenoxy}-*N*-(2,3-dihydro-1,4-benzodioxin-6-yl)acetamide (6c)

Light brown amorphous solid; Yield: 79%; M.P.: 71°C; Molecular formula: $C_{27}H_{30}N_2O_6S$; Molecular weight: 510 $gmol^{-1}$; HR-MS: $[M]^+$ 510.6034 (Calcd. for $C_{27}H_{30}N_2O_6S$; 510.6166); IR (KBr, cm^{-1}) ν_{max}: 3459 (N-H stretching), 3063 (C-H stretching of aromatic ring), 2921 (-CH_2- stretching), 1621 (C=C stretching of aromatic ring), 1390 (-SO_2 stretching), 1168 (C-O-C stretching of ether); ^{1}H-NMR (CD_3OD, 300 MHz): δ (ppm) 7.58 (d, *J* = 8.4 Hz, 2H, H-2' & H-6'), 7.47 (d, *J* = 8.4 Hz, H-3' & H-5'), 7.17 (d, *J* = 1.8, 1H, H-5'''), 6.95 (dd, *J* = 8.1, 1.5 Hz, 1H, H-7'''), 6.86 (d, *J* = 8.7 Hz, 2H, H-2 & H-6), 6.77 (d, *J* = 8.7 Hz, 1H, H-8'''), 6.68 (d, *J* = 8.7 Hz, 2H, H-3 & H-5), 4.21 (s, 4H, CH_2-2''' & CH_2-3'''), 3.91 (s, 2H, CH_2-2''''), 3.10 (s, 3H, CH_3-1''), 1.34 (s, 9H, $(CH_3)_3$C-4'); EIMS: *m/z* 510 $[M]^+$, 446 $[M\text{-}SO_2]^+$, 197 $[(CH_3)_3CC_6H_5SO_2]^+$, 150 $[C_8H_8NO_2]^+$, 135 $[C_8H_7O_2]^+$, 133 $[(CH_3)_3CC_6H_5]^+$, 122 $[C_6H_4NO_2]^+$, 122 $[C_7H_8NO]^+$, 107 $[C_6H_3O_2]^+$, 93 $[C_6H_5O]^+$, 66 $[C_4H_4N]^+$, 50 $[C_4H_2]^+$.

2.18 2-{4-[(mesitylsulfonyl)(methyl)amino]phenoxy}-*N*-(2,3-dihydro-1,4-benzodioxin-6-yl)acetamide (6d)

Black sticky solid; Yield: 81%; Molecular formula: $C_{26}H_{28}N_2O_6S$; Molecular weight: 496 $gmol^{-1}$; HR-MS: $[M]^+$ 496.5764 (Calcd. for $C_{26}H_{28}N_2O_6S$; 496.5824); IR (KBr, cm^{-1}) ν_{max}: 3468 (N-H stretching), 3062 (C-H stretching of aromatic ring), 2936 (-CH_2- stretching), 1625 (C=C stretching of aromatic ring), 1395 (-SO_2 stretching), 1162 (C-O-C stretching of ether); ^{1}H-NMR (CD_3OD, 300 MHz): δ (ppm) 7.11 (d, *J* = 2.4, 1H, H-5'''), 6.97 (s, 2H, H-3' & H-5'), 6.94 (dd, *J* = 8.4, 2.1 Hz, 1H, H-7'''), 6.87 (d, *J* = 8.4 Hz, 2H, H-2 & H-6), 6.76 (d, *J* = 8.1 Hz, 1H, H-8'''), 6.67 (d, *J* = 8.4 Hz, 2H, H-3 & H-5), 4.21 (s, 4H, CH_2-2''' & CH_2-3'''), 3.93 (s, 2H, CH_2-2''''), 2.99 (s, 3H, CH_3-1''); EIMS: *m/z* 496 $[M]^+$, 432 $[M\text{-}SO_2]^+$, 183 $[(CH_3)_3C_6H_5SO_2]^+$, 150 $[C_8H_8NO_2]^+$, 135 $[C_8H_7O_2]^+$, 122 $[C_6H_4NO_2]^+$, 122 $[C_7H_8NO]^+$, 119 $[(CH_3)_3C_6H_5]^+$, 107 $[C_6H_3O_2]^+$, 93 $[C_6H_5O]^+$, 66 $[C_4H_4N]^+$.

2.19 2-{4-[{[4-(acetylamino)phenyl]sulfonyl}(methyl)amino]phenoxy}-*N*-(2,3-dihydro-1,4-benzodioxin-6-yl)acetamide (6e)

Brownish grey amorphous solid; Yield: 85%; M.P.: 140°C; Molecular formula: $C_{25}H_{25}N_3O_7S$; Molecular weight: 511 $gmol^{-1}$; HR-MS: $[M]^+$ 511.5488 (Calcd. for $C_{25}H_{25}N_3O_7S$; 511.5574); IR (KBr, cm^{-1}) ν_{max}: 3467 (N-H stretching), 3034 (C-H stretching of aromatic ring), 2936 (-CH_2- stretching), 1602 (C=C stretching of aromatic ring), 1386 (-SO_2 stretching), 1162 (C-O-C stretching of ether); ^{1}H-NMR (CD_3OD, 300 MHz): δ (ppm) 7.72 (d, *J* = 8.7 Hz, 2H, H-3' & H-5'), 7.46 (d, *J* = 8.5 Hz, 2H, H-2' & H-6'), 7.18 (d, *J* = 2.4, 1H, H-5'''), 6.98 (dd, *J* = 8.4, 1.8 Hz, 1H, H-7'''), 6.87 (d, *J* = 8.7 Hz, 2H, H-2 & H-6), 6.77 (d, *J* = 8.1 Hz, 1H, H-8'''), 6.68 (d, *J* = 8.7 Hz, 2H, H-3 & H-5), 4.21 (s, 4H, CH_2-2''' & CH_2-3'''), 3.91 (s, 2H, CH_2-2''''), 3.11 (s, 3H, $\underline{CH_3}CONH$-4'), 2.98 (s, 3H, CH_3-1''); EIMS: *m/z* 511 $[M]^+$, 447 $[M\text{-}SO_2]^+$, 198 $[CH_3CONHC_6H_5SO_2]^+$, 150 $[C_8H_8NO_2]^+$, 135 $[C_8H_7O_2]^+$, 134 $[CH_3CONHC_6H_5]^+$, 122 $[C_6H_4NO_2]^+$, 122 $[C_7H_8NO]^+$, 107 $[C_6H_3O_2]^+$, 93 $[C_6H_5O]^+$, 66 $[C_4H_4N]^+$, 50 $[C_4H_2]^+$.

2.20 2-{4-[[(4-bromophenyl)sulfonyl](methyl)amino]phenoxy}-*N*-(2,3-dihydro-1,4-benzodioxin-6-yl)acetamide (6f)

Light grey amorphous solid; Yield: 81%; M.P.: 83°C; Molecular formula: $C_{23}H_{21}BrN_2O_6S$; Molecular weight: 532 $gmol^{-1}$; HR-MS: $[M]^+$ 532.3937 (Calcd. for $C_{23}H_{21}BrN_2O_6S$; 532.4032); IR (KBr, cm^{-1}) ν_{max}: 3446 (N-H stretching), 3072 (C-H stretching of aromatic ring), 2908 (-CH_2- stretching), 1606 (C=C stretching of aromatic ring), 1376 (-SO_2 stretching), 1177 (C-O-C stretching of ether); ^{1}H-NMR (CD_3OD, 300 MHz): δ (ppm) 7.76 (d, *J* = 8.7 Hz, 2H, H-2' & H-6'), 7.51 (d, *J* = 8.4 Hz, 2H, H-3' & H-5'), 7.15 (d, *J* = 2.1, 1H, H-5'''), 6.93 (dd, *J* = 8.4, 1.8 Hz, 1H, H-7'''), 6.87 (d, *J* = 8.7 Hz, 2H, H-2 & H-6),

6.77 (d, *J* = 8.1 Hz, 1H, H-8'''), 6.69 (d, *J* = 8.4 Hz, 2H, H-3 & H-5), 4.21 (s, 4H, CH_2-2''' & CH_2-3'''), 3.91 (s, 2H, CH_2-2''''), 2.98 (s, 3H, CH_3-1''); EIMS: *m/z* 534 $[M+2]^+$, 532 $[M]^+$, 468 $[M-SO_2]^+$, 219 $[BrC_6H_5SO_2]^+$, 155 $[BrC_6H_5]^+$, 150 $[C_8H_8NO_2]^+$, 135 $[C_8H_7O_2]^+$, 122 $[C_6H_4NO_2]^+$, 122 $[C_7H_8NO]^+$, 107 $[C_6H_3O_2]^+$, 93 $[C_6H_5O]^+$, 66 $[C_4H_4N]^+$, 50 $[C_4H_2]^+$.

2.21 2-{4-[[(4-chlorophenyl)sulfonyl](methyl)amino]phenoxy}-*N*-(2,3-dihydro-1,4-benzodioxin-6-yl)acetamide (6g)

Dark brown amorphous solid; Yield: 87%; M.P. 84°C; Molecular formula: $C_{23}H_{21}ClN_2O_6S$; Molecular weight: 488 $gmol^{-1}$; HR-MS: $[M]^+$ 488.5415 (Calcd. for $C_{23}H_{21}ClN_2O_6S$; 488.5516); IR (KBr, cm^{-1}) ν_{max}: 3447 (N-H stretching), 3072 (C-H stretching of aromatic ring), 2934 (-CH_2- stretching), 1606 (C=C stretching of aromatic ring), 1378 (-SO_2 stretching), 1161 (C-O-C stretching of ether); ^{1}H-NMR (CD_3OD, 300 MHz): δ (ppm) 7.74 (d, *J* = 8.4 Hz, 2H, H-2' & H-6'), 7.52 (d, *J* = 8.1 Hz, 2H, H-3' & H-5'), 7.12 (d, *J* = 2.1, 1H, H-5'''), 6.95 (dd, *J* = 8.4, 2.1 Hz, 1H, H-7'''), 6.88 (d, *J* = 8.7 Hz, 2H, H-2 & H-6), 6.79 (d, *J* = 8.4 Hz, 1H, H-8'''), 6.68 (d, *J* = 8.7 Hz, 2H, H-3 & H-5), 4.21 (s, 4H, CH_2-2''' & CH_2-3'''), 3.92 (s, 2H, CH_2-2''''), 2.98 (s, 3H, CH_3-1''); EIMS: *m/z* 490 $[M+2]^+$, 488 $[M]^+$, 424 $[M-SO_2]^+$, 175 $[ClC_6H_5SO_2]^+$, 150 $[C_8H_8NO_2]^+$, 135 $[C_8H_7O_2]^+$, 122 $[C_6H_4NO_2]^+$, 122 $[C_7H_8NO]^+$, 111 $[ClC_6H_5]^+$, 107 $[C_6H_3O_2]^+$, 93 $[C_6H_5O]^+$, 66 $[C_4H_4N]^+$, 50 $[C_4H_2]^+$.

2.22 2-{4-[[(2,5-dichlorophenyl)sulfonyl](methyl)amino]phenoxy}-*N*-(2,3-dihydro-1,4-benzodioxin-6-yl)acetamide (6h)

Black amorphous solid; Yield: 82%; M.P.: 146°C; Molecular formula: $C_{23}H_{20}Cl_2N_2O_6S$; Molecular weight: 522 $gmol^{-1}$; HR-MS: $[M]^+$ 522.3865 (Calcd. for $C_{23}H_{20}Cl_2N_2O_6S$; 522.3987); IR (KBr, cm^{-1}) ν_{max}: 3476 (N-H stretching), 3059 (C-H stretching of aromatic ring), 2937 (-CH_2- stretching), 1606 (C=C stretching of aromatic ring), 1393 (-SO_2 stretching), 1151 (C-O-C stretching of ether); ^{1}H-NMR (CD_3OD, 300 MHz): δ (ppm) 7.81 (s, 1H, H-6'), 7.71 (d, *J* = 8.4 Hz 1H, H-3'), 7.44 (d, *J* = 8.4 Hz 1H, H-4'), 7.17 (d, *J* = 2.4, 1H, H-5'''), 6.94 (dd, *J* = 8.4, 2.4 Hz, 1H, H-7'''), 6.87 (d, *J* = 8.7 Hz, 2H, H-2 & H-6), 6.77 (d, *J* = 8.7 Hz, 1H, H-8'''), 6.69 (d, *J* = 8.7 Hz, 2H, H-3 & H-5), 4.21 (s, 4H, CH_2-2''' & CH_2-3'''), 4.12 (s, 2H, CH_2-2''''), 3.10 (s, 3H, CH_3-1''); EIMS: *m/z* 526 $[M+4]^+$, 524 $[M+2]^+$, 522 $[M]^+$, 458 $[M-SO_2]^+$, 209 $[Cl_2C_6H_5SO_2]^+$, 150 $[C_8H_8NO_2]^+$, 145 $[Cl_2C_6H_5]^+$, 135 $[C_8H_7O_2]^+$, 122 $[C_6H_4NO_2]^+$, 122 $[C_7H_8NO]^+$, 107 $[C_6H_3O_2]^+$, 93 $[C_6H_5O]^+$, 66 $[C_4H_4N]^+$.

2.23 2-{4-[[(3,5-dichlorophenyl)sulfonyl](methyl)amino]phenoxy}-*N*-(2,3-dihydro-1,4-benzodioxin-6-yl)acetamide (6i)

Light brown amorphous solid; Yield: 86%; M.P.: 120°C; Molecular formula: $C_{23}H_{20}Cl_2N_2O_6S$; Molecular weight: 522 $gmol^{-1}$; HR-MS: $[M]^+$ 522.3865 (Calcd. for $C_{23}H_{20}Cl_2N_2O_6S$; 522.3987); IR (KBr, cm^{-1}) ν_{max}: 3476 (N-H stretching), 3072 (C-H stretching of aromatic ring), 2923 (-CH_2- stretching), 1614 (C=C stretching of aromatic ring), 1391 (-SO_2 stretching), 1160 (C-O-C stretching of ether); ^{1}H-NMR (CD_3OD, 300 MHz): δ (ppm) 7.27 (s, 2H, H-2', H-6'), 7.16 (s, 1H, H-4'), 7.01 (d, *J* = 2.1, 1H, H-5'''), 6.94 (dd, *J* = 8.4, 2.4 Hz, 1H, H-7'''), 6.80 (d, *J* = 8.1 Hz, 2H, H-2 & H-6), 6.70 (d, *J* = 8.1 Hz, 1H, H-8'''), 6.66 (d, *J* = 8.4 Hz, 2H, H-3 & H-5), 4.20 (s, 4H, CH_2-2''' & CH_2-3'''), 3.92 (s, 2H, CH_2-2''''), 2.98 (s, 3H, CH_3-1''); EIMS: *m/z* 526 $[M+4]^+$, 524 $[M+2]^+$, 522 $[M]^+$, 458 $[M-SO_2]^+$, 209 $[Cl_2C_6H_5SO_2]^+$, 150 $[C_8H_8NO_2]^+$, 145 $[Cl_2C_6H_5]^+$, 135 $[C_8H_7O_2]^+$, 122 $[C_6H_4NO_2]^+$, 122 $[C_7H_8NO]^+$, 107 $[C_6H_3O_2]^+$, 93 $[C_6H_5O]^+$, 66 $[C_4H_4N]^+$.

2.24 2-{4-[methyl(2-naphthylsulfonyl)amino]phenoxy}-*N*-(2,3-dihydro-1,4-benzodioxin-6-yl)acetamide (6j)

Light brown amorphous solid; Yield: 89%; M.P.: 90°C; Molecular formula: $C_{27}H_{24}N_2O_6S$; Molecular weight: 504 $gmol^{-1}$; HR-MS: $[M]^+$ 504.5552 (Calcd. for $C_{27}H_{24}N_2O_6S$; 504.5625); IR (KBr, cm^{-1}) ν_{max}: 3475 (N-H stretching), 3070 (C-H stretching of aromatic ring), 2937 (-CH_2- stretching), 1612 (C=C stretching of aromatic ring), 1376 (-SO_2- stretching), 1182 (C-O-C stretching of ether); ^{1}H-NMR (CD_3OD, 300 MHz): δ (ppm) 8.14 (s, 1H, H-1'), 7.99-7.93 (m, 2H, H-4' & H-5'), 7.67 (d, *J* = 8.1 Hz, 1H, H-3'), 7.59 (dd, *J* = 8.1, 2.1 Hz, 1H, H-8'), 7.49-7.42 (m, 2H, H-6' & H-7'), 7.17 (d, *J* = 2.4, 1H, H-5'''),

6.93 (dd, *J* = 8.7, 2.1 Hz, 1H, H-7'''), 6.85 (d, *J* = 8.7 Hz, 2H, H-2 & H-6), 6.78 (d, *J* = 8.4 Hz, 1H, H-8'''), 6.67 (d, *J* = 8.7 Hz, 2H, H-3 & H-5), 4.21 (s, 4H, CH_2-2''' & CH_2-3'''), 3.91 (s, 2H, CH_2-2''''), 3.16 (s, 3H, CH_3-1''); EIMS: *m/z* 504 $[M]^+$, 440 $[M\text{-}SO_2]^+$, 191 $[C_{10}H_7SO_2]^+$, 150 $[C_8H_8NO_2]^+$, 135 $[C_8H_7O_2]^+$, 127 $[C_{10}H_7]^+$, 122 $[C_6H_4NO_2]^+$, 122 $[C_7H_8NO]^+$, 107 $[C_6H_3O_2]^+$, 93 $[C_6H_5O]^+$, 66 $[C_4H_4N]^+$.

2.25 Cholinesterase Assays

The AChE & BChE inhibition activities were executed according to the reported method [22] with small modifications. A volume of 100 µL comprising 60 µL Na_2HPO_4 buffer with concentration of 50 mM (pH 7.7), 10 µL test compound (0.5 mM $well^{-1}$) and 10 µL (0.005 unit $well^{-1}$ for AChE & 0.5 unit $well^{-1}$ for BChE) enzyme was developed. This homogeneous mixture was pre-read at 405 nm followed by pre-incubation for 10 min at 37 ºC. The reaction was started by the addition of 10 µL of 0.5 mM $well^{-1}$ substrate (acetylthiocholine iodide for AChE & butyrylthiocholine chloride for BChE) and the addition of 10 µL DTNB (0.5 mM $well^{-1}$). After 15 min of incubation at 37°C absorbance was measured at 405 nm using 96-well plate reader Synergy HT, Biotek, USA. All experiments were carried out with their respective controls in triplicate. Eserine (0.5 mM $well^{-1}$) was used as a positive control. The percent inhibition was calculated by the following equation:

$$\text{Inhibition (\%)} = \frac{\text{Control} - \text{Test}}{\text{Control}} \times 100$$

where control is the activity without inhibitor and test is the activity in the presence of test compound. IC_{50} values were calculated using EZ–Fit Enzyme kinetics software (Perrella Scientific Inc. Amherst, USA). The IC_{50} values were the average of three independent experiments.

2.26 Lipoxygenase Assay

Lipoxygenase (LOX) activity was assayed according to the reported method of Baylac & Racine [23] with small modifications. Total volume of lipoxygenase assay mixture was 200 µL containing 150 µL Na_3PO_4 buffer (100 mM & pH 8.0), 10 µL test compound (0.5 mM $well^{-1}$) and 15 µL (600 units $well^{-1}$) enzyme. The contents were mixed, pre-read at 234 nm and pre-incubated for 10 minutes at 25°C. The reaction was initiated by addition of 25 µL substrate solution. The change in absorbance was observed after 6 min at 234 nm using 96-well plate reader Synergy HT, Biotek, USA. All reactions were performed in triplicates. The positive and negative controls were included in the assay. Baicalein (0.5 mM $well^{-1}$) was used as a positive control. The percentage inhibition (%) and IC_{50} values were calculated by the same method as described cholinesterase enzymes.

2.27 Antibacterial Assay

The antimicrobial activity was determined following the principle that increased absorbance of broth medium is directly related to log phase of growth and was performed in sterile 96-wells microplates under aseptic conditions [24-25]. Three gram-negative (*Escherichia coli, Pseudomonas aeruginosa* and *Salmonella typhi*) and two gram-positive bacteria (*Bacillus subtilis, Staphylococcus aureus*) were included in the study and were maintained on stock culture agar medium. The test samples (with suitable solvents and dilutions) 20 µg/well and 180 µL fresh bacterial culture (with suitable dilution by fresh nutrient broth) was poured into wells to make a volume of 200 µL. The initial absorbance of the culture was kept 0.12-0.19 at 540 nm. The absorbance was measured at 540 nm using microplate reader, before and after incubation at 37°C for 16-24 hours with lid on the microplate. The difference was related to bacterial growth. The percent inhibition was calculated using the formula:

$$\text{Inhibition (\%)} = \frac{X - Y}{X} \times 100$$

where, X is absorbance in control with bacterial culture and Y is absorbance in test sample. Results are mean of triplicate (n=3, ± sem). Ciprofloxacin was taken as reference standard. Minimum

inhibitory concentration (MIC) was measured with suitable dilutions (5-30 µg/ well) and results were calculated using EZ-Fit Perrella Scientific Inc. Amherst USA software.

2.28 Statistical Analysis

All the measurements were executed in triplicate and statistical analysis was performed by Microsoft Excel 2010. Results are presented as mean ± sem.

3. DOCKING STUDIES

To explore the binding modes of the synthesized compounds, all of them were computationally docked against the active sites of acetyl cholinesterase (AChE), butyryl cholinesterase (BChE) and lipoxygenase (LOX).

3.1 Computational Methodology

3.1.1 Protein preparation

From protein data bank, the AChE, BChE and LOX protein molecules were retrieved. Using MOE applications the 3D protonation of the protein molecule was carried out; after removing H_2O molecules. Energy minimization algorithm of MOE tool was used to minimize the energy of the protein molecules, in order to get more stable configuration. The following parameters were used for energy minimization; gradient: 0.05, force field: MMFF94X+solvation, chiral constraint: current geometry. Energy minimization was terminated when the root mean square gradient falls below the 0.05. The minimized structure was used as the template for docking.

3.1.2 Molecular docking

The binding mode of the ligands into the binding pocket of protein molecule was predicted by MOE-Dock implemented in MOE. After the completion of docking we analyze the best poses for hydrogen bonding/π-π interactions by using MOE applications [26].

4. RESULTS AND DISCUSSION

The sulfamoyl and acetamoyl functionalities have been successfully geared up through a series of benignant methods by the protocol sketched in Scheme 1 and R groups employed are provided in Table 1. All the procedures with reaction conditions are mentioned in experimental section. The synthesized molecules were evaluated for the anti-enzymatic and antibacterial activities and found to be valuable potent molecules as evident from their IC_{50} (Table 2) and MIC (Table 3) values respectively.

4.1 Chemistry

The presented research work is comprised of three major steps. First *N*-(4-hydroxyphenyl)-*N*-methylarylsulfonamides (**3a-j**) were synthesized by the reaction of *N*-methyl-4-hydroxyanilinium sulfate (**1**) and different aryl sulfonyl chlorides (**2a-j**) in a weak basic aqueous medium. The reaction was processed in basic media with pH of 8-10 to avoid the capturing of lone pair present at nitrogen by the acid produced which suppresses the nucleophilic character and also the rate of reaction. The products were separated after acidification to get rid of unreacted amine and also to enhance the yield but excess of it was obviated because of decrement in yield. The synthesized molecules, **3a-j**, were further treated with *N*-(2,3-dihydro-1,4-benzodioxin-6-yl)-2-bromoacetamide (**5**) to yield the final products, **6a-j**, in a weak basic aprotic polar medium. The products, **6a-j**, were collected after basifying the reaction mixture in order to remove unreacted **3a-j** molecules. The electrophile, **5**, was prepared by the vigorous reaction of 2,3-dihydro-1,4-benzodioxin-6-amine (**4**) with the 2-bromoacetylbromide in a basic medium and was also collected after acidification. The structures of all the synthesized compounds were confirmed through spectral analysis as depicted in experimental

section. The physical data for the final product **6a** is given in experimental section. The HR-MS provided a $[M]^+$ peak at 454.4975 (Calcd. for $C_{23}H_{22}N_2O_6S$; 454.5031). The molecular formula $C_{23}H_{22}N_2O_6S$ was also supported by molecular ion peak at *m/z* 454 in EIMS and the number of protons in its ^{1}H-NMR spectrum. The peaks of EIMS spectrum which well supported the molecule, were *m/z* 150, 141 and 121 for the cations of 2,3-dihydro-1,4-benzodioxin-6-amino group, phenylsulfonyl group and 4-(methylamino)phenoxy group respectively. The IR spectrum supported the structure by two characteristics absorption bands at 3462 cm^{-1} and 1381 cm^{-1} for N-H (stretching) of amide and S=O (stretching) of sulfonyl group, respectively. Benzenesulfonyl ring was confirmed by two signals in the aromatic region of ^{1}H-NMR spectrum appearing at *δ* 7.64 (dd, *J* = 7.8, 1.8 Hz, 2H, H-2' & H-6') and 7.51-7.41 (m, 3H, H-3' to H-5'). The benzodioxine ring was supported by four signals, three in aromatic region and one in aliphatic region, at *δ* 7.17 (d, *J* = 2.4, 1H, H-5'"), 7.02 (dd, *J* = 8.4, 1.2 Hz, 1H, H-7'"), 6.99 (d, *J* = 7.5 Hz, 1H, H-8'") and 4.21 (s, 4H, CH_2-2'" & CH_2-3'"). The two doublets resonating at *δ* 6.97 (d, *J* = 8.1 Hz, 2H, H-2 & H-6) and 6.78 (d, *J* = 8.7 Hz, 2H, H-3 & H-5) were assigned to the protons of 1,4-disubstituted phenyl ring. In the aliphatic region of the ^{1}H-NMR spectrum, the two singlets, appearing at *δ* 3.92 (s, 2H, CH_2-2"") and 3.14 (s, 3H, CH_3-1") in 2:3 ratio, indicated the presence of two methylene and three methyl protons in the molecule. The proposed structure of **6a** was corroborated and named, 2-{4-[methyl(phenylsulfonyl)amino]phenoxy}-*N*-(2,3-dihydro-1,4-benzodioxin-6-yl)acetamide. ^{1}H-NMR spectrum of compound **6g** is given in Fig. 1 for convenience.

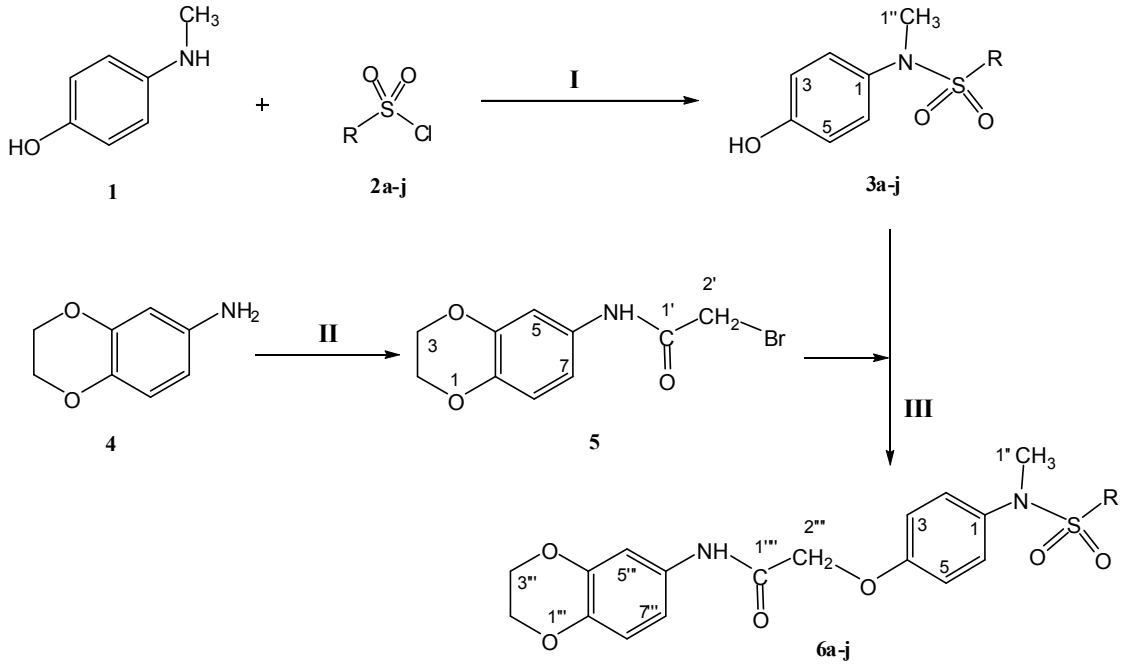

Scheme 1. Synthesis of *O*- and *N*-substituted derivatives of planetol. Reagents and conditions: (I) Na_2CO_3/H_2O, stirring for 4-5 hours, pH = 8-10 (II) Na_2CO_3/H_2O, stirring for 30 min, pH = 8-10 (III) LiH/DMF, stirring for 5-6 hours

The structures of *N*-(4-hydroxyphenyl)-*N*-methyl-substituted sulfonamides **(3a-i)** were further confirmed by EIMS fragmentation patterns**.** Compound **3a** gave molecular ion at *m/z* 263, **3b** at *m/z* 277, **3c** at *m/z* 319, **3d** at *m/z* 305, **3e** at *m/z* 320, **3f** at *m/z* 341, **3g** at *m/z* 297, **3h** at *m/z* 331 & **3i** at *m/z* 313 which was in accordance to their M.W. M^+ of all compounds losses $H^•$ to give M-$H^{+•}$ peak at one unit less *m/z* in comparison to their respective M.W.

Molecular ion losses $C_7H_8NO^•$ to form SO_2R^+ which appeared at *m/z* 141 for **3a**, **3b** at *m/z* 155, **3c** at *m/z* 197, **3d** at *m/z* 183, **3e** at *m/z* 198, **3f** at *m/z* 220, **3g** at *m/z* 175, **3h** at *m/z* 209 & **3i** at *m/z* 191; which further looses neutral molecule SO_2 to give R^+, whose detail already discussed earlier except for

3c & **3h.** For **3c** R^+ is phenyl cation having *tert*-butyl group on *para* position, it looses acetylene molecule (C_2H_2) to give $C_4H_2(CH_3)_3^+$ at *m/z* 107; similarly in case of **3h** $C_6H_3Cl_2^+$ at *m/z* 145 looses HCl to give $C_6H_2Cl^+$ at *m/z* 109.

Table 1. Different R groups employed for the synthesis of *O*- and *N*-substituted derivatives of planetol

Compd.	R	Compd.	R	Compd.	R
3a,6a		**3e,6e**	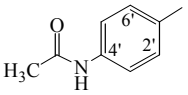	**3i,6i**	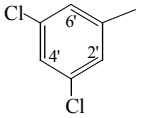
3b,6b	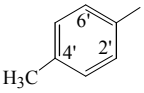	**3f.6f**	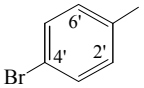	**3j,6j**	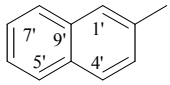
3c,6c	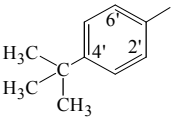	**3g,6g**	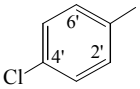		
3d,6d	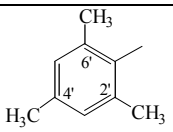	**3h,6h**	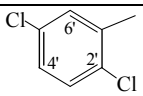		

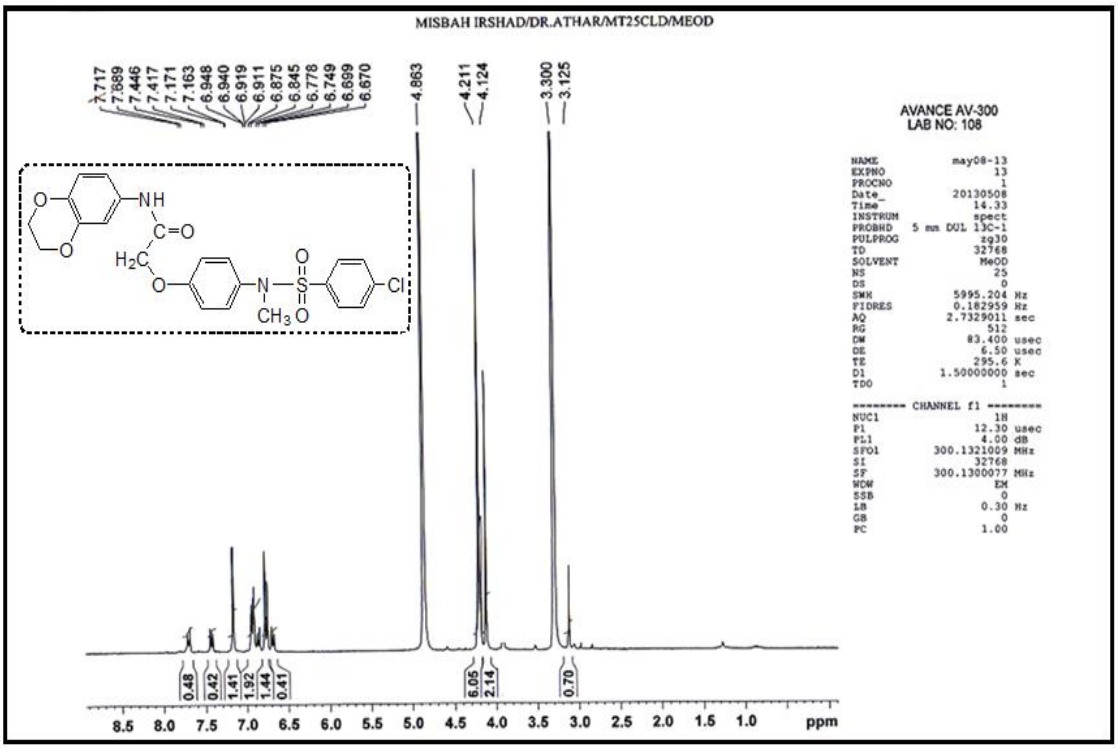

Fig. 1a. ^{1}H-NMR spectrum of compound 6g

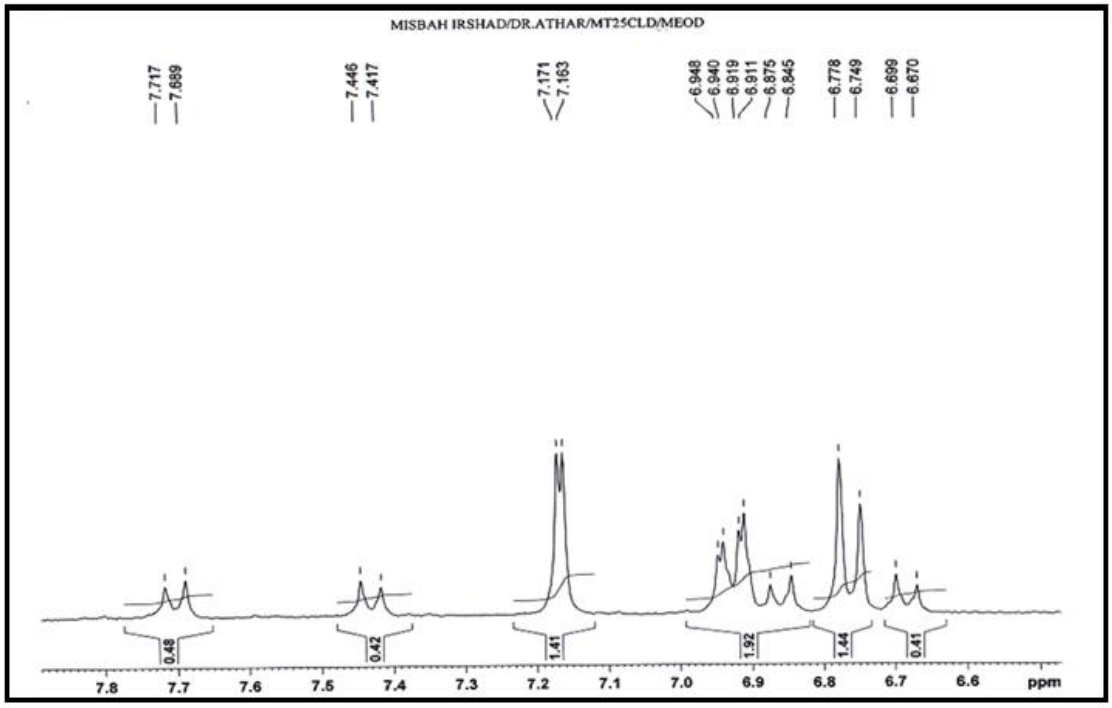

Fig. 1b. ^{1}H-NMR spectrum of compound 6g (aromatic region)

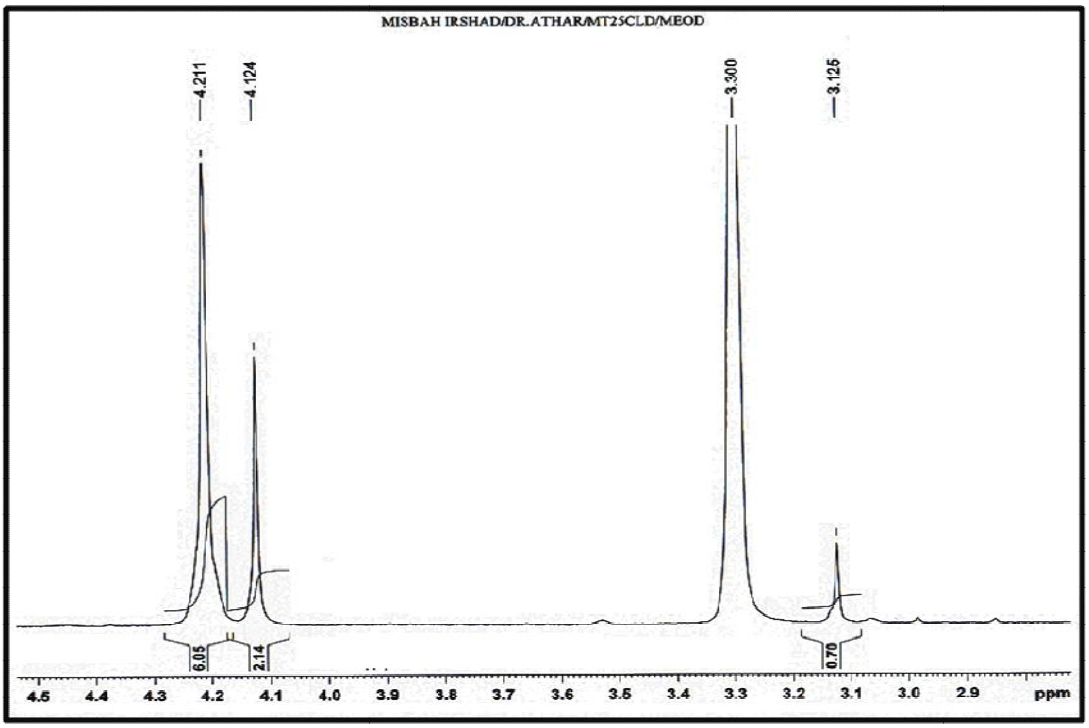

Fig. 1c. ^{1}H-NMR spectrum of compound 6g (aliphatic region)

Table 2. % age inhibition and IC_{50} values for enzyme inhibition activity of synthesized molecules

Compd.	AChE		BChE		LOX	
	Inhibition (%)	IC_{50} (µM)	Inhibition (%)	IC_{50} (µM)	Inhibition (%)	IC_{50} (µM)
3a	70.75±1.11	153.83±0.82	51.82±0.52	489.12±0.59	37.92±0.17	-
3b	93.49±1.22	21.62±0.53	88.88±0.96	170.10±0.62	37.71±0.16	-
3c	93.41±0.81	59.10±0.61	88.41±1.13	66.30±0.89	73.29±0.65	365.5±0.32
3d	89.92±0.91	135.22±0.69	81.18±0.89	187.54±0.74	44.79±0.45	>500
3e	79.88±0.86	135.62±0.32	79.53±0.97	208.33±0.72	66.46±0.12	308.1±0.75
3f	85.24±0.86	62.81±0.63	81.53±1.19	239.64±0.84	73.02±0.16	194.3±0.54
3g	93.53±1.21	90.52±0.82	90.82±0.93	140.21±0.47	93.71±0.82	174.7±0.35
3h	87.82±1.16	132.86±0.75	86.88±1.12	221.42±0.69	93.75±0.42	169.3±0.86
3i	87.54±1.12	75.61±0.78	80.41±0.87	223.41±0.56	46.77±0.12	>500
3j	94.92±0.91	93.13±0.62	85.18±0.92	48.11±0.59	96.25±1.45	306.8±0.95
5	82.58±0.96	270.81±0.73	84.53±0.89	338.81±0.43	14.90±0.25	
6a	83.69±0.98	231.34±0.45	60.65±1.11	447.42±0.58	47.81±0.38	>500
6b	35.56±0.53	>500	31.47±0.36	>500	89.48±0.11	335.6±0.21
6c	98.10±0.97	109.11±0.79	96.43±0.87	172.23±0.57	86.75±0.85	253.7±0.95
6d	96.15±1.12	161.83±0.81	83.76±0.87	302.31±0.78	33.54±0.65	-
6e	93.69±0.84	87.53±0.49	93.43±0.96	133.93±0.77	75.61±0.96	351.9±0.12
6f	81.94±1.25	183.11±0.89	86.10±0.98	62.10±0.52	79.80±0.38	323.8±0.45
6g	77.78±0.95	206.77±0.79	51.41±0.66	494.23±0.41	47.80±0.63	>500
6h	85.48±1.19	145.81±0.93	86.71±1.15	217.41±0.92	70.15±0.55	385.1±0.54
6i	91.35±1.16	46.10±0.54	87.82±0.79	45.62±0.61	72.07±0.12	225.9±0.75
6j	95.63±1.14	168.11±0.91	89.12±0.81	135.92±0.72	99.64±1.85	73.12±1.99
Control	**91.29±1.17[a]**	**0.04±0.0001[a]**	**82.82±1.09[a]**	**0.85±0.0001[a]**	**93.79±1.27[b]**	**22.4±1.3[b]**

Note: IC_{50} values (concentration at which there is 50% enzyme inhibition) of compounds were calculated using EZ–Fit Enzyme kinetics software (Perella Scientific Inc. Amherst, USA).

AChE = Acetyl cholinesterase; BChE = Butyryl cholinesterase; LOX = Lipoxygenase; a = Eserine; b = Baicalein

Table 3. % age inhibition and MIC values of antibacterial activity of synthesized molecules

Compound	*S. typhi (-)*		*E. coli (-)*		*P. aeroginosa (-)*		*B. subtilis (+)*		*S. aureus (+)*	
	% age inhibition	**MIC**	**% age inhibition**	**MIC**	**% age inhibition**	**MIC**	**% age inhibition**	**MIC**	**% age inhibition**	**MIC**
3a	68.07±1.13	11.03±2.00	71.16±0.18	11.66±3.22	56.63±2.50	16.96±5.00	47.67±3.40	-	47.64±2.21	-
3b	53.27±2.47	16.08±3.64	53.96±1.52	18.32±2.76	49.63±4.50	-	41.07±0.67	-	46.57±0.57	-
3c	69.67±1.53	10.64±3.55	64.82±1.40	13.56±3.89	48.31±4.31	-	44.60±1.67	-	52.29±4.14	18.44±4.64
3d	61.33±1.20	11.55±1.82	55.98±3.05	14.49±4.05	51.50±1.25	19.33±4.17	46.80±1.73	-	59.43±4.71	13.83±1.98
3e	63.47±1.33	11.82±2.76	53.05±2.93	16.62±4.17	60.00±0.38	17.30±5.00	35.07±0.40	-	47.36±0.36	-
3f	50.20±1.27	19.70±4.18	44.82±3.60	-	43.94±1.94	-	32.33±2.60	-	38.07±0.93	-
3g	49.33±2.93	-	29.57±4.23	-	44.06±0.06	-	24.73±1.80	-	40.93±2.93	-
3h	67.47±0.00	10.85±4.73	61.40±2.26	14.83±2.33	58.94±0.19	16.99±5.00	38.53±0.40	-	55.43±4.71	16.01±2.73
3i	55.47±0.67	13.31±5.00	44.21±2.26	-	42.56±0.06	-	48.93±3.73	-	47.93±0.64	-
3j	67.47±3.60	11.02±1.54	60.67±1.52	15.91±1.67	44.88±2.75	-	49.00±1.40	-	49.43±0.14	-
5	85.47±0.00	10.79±1.73	85.67±0.18	11.32±3.89	77.13±0.00	10.64±2.43	84.00±0.93	10.64±1.40	86.14±0.86	10.46±1.77
6a	54.40±3.47	11.98±2.09	44.76±4.98	-	48.00±1.00	-	30.73±0.33	-	37.50±3.93	-
6b	63.87±0.40	11.26±3.13	75.30±0.06	15.43±3.56	57.19±1.06	17.83±3.83	30.93±0.00	-	55.14±2.71	18.14±1.44
6c	67.73±0.13	10.24±2.52	69.33±1.40	10.69±3.72	54.06±1.44	16.58±3.33	61.87±4.27	12.87±1.28	59.14±0.57	14.80±2.31
6d	59.87±0.93	13.36±1.87	53.84±0.06	17.43±2.44	37.63±0.25	-	35.60±4.13	-	42.57±4.57	-
6e	58.40±1.33	14.76±3.73	43.96±3.43	-	57.31±1.81	17.41±5.00	41.73±4.27	-	56.93±2.36	17.52±2.00
6f	78.33±1.13	10.98±1.76	70.43±4.72	12.19±2.39	65.13±1.38	13.05±4.50	60.00±1.20	12.52±2.36	62.86±4.00	12.11±3.91
6g	66.93±0.40	11.94±3.00	64.15±1.34	10.82±1.06	58.13±0.63	18.47±4.08	42.53±1.87	-	51.00±1.57	17.44±3.27
6h	81.80±0.87	10.43±2.64	82.01±1.16	10.83±1.41	67.13±0.25	10.46±2.67	69.20±2.27	11.65±1.42	60.93±1.36	14.22±2.42
6i	57.27±0.73	14.52±4.07	53.60±0.30	18.36±3.88	50.69±2.56	19.68±1.42	36.13±1.07	-	52.93±4.64	15.07±1.08
6j	80.80±0.40	10.88±4.09	73.54±0.85	11.90±4.22	65.88±1.00	12.39±1.17	73.27±1.40	11.41±1.47	69.93±2.79	11.25±2.12
Ciprofloxacin	**91.65 ±1.04**	**9.22±1.36**	**90.98±1.43**	**8.79±2.00**	**90.46±1.99**	**8.93±2.42**	**89.90±0.79**	**9.43±1.87**	**92.04±1.44**	**9.04±1.50**

Note: Minimum inhibitory concentration (MIC) was measured with suitable dilutions (5-30 µg/ well) and results were calculated using EZ-Fit Perrella Scientific Inc. Amherst USA software

The characteristic fragment for **3a-i** appeared as base peak at *m/z* 122 for $C_6H_4OHNCH_3^+$ due to the loss of $SO_2R^\bullet$ from molecular ion. This cation ($C_6H_4OHNCH_3^+$) further looses H_2O to form $C_6H_3NCH_3^+$ at *m/z* 104. The EIMS patterns are illuminated in Figs. 2 and 3.

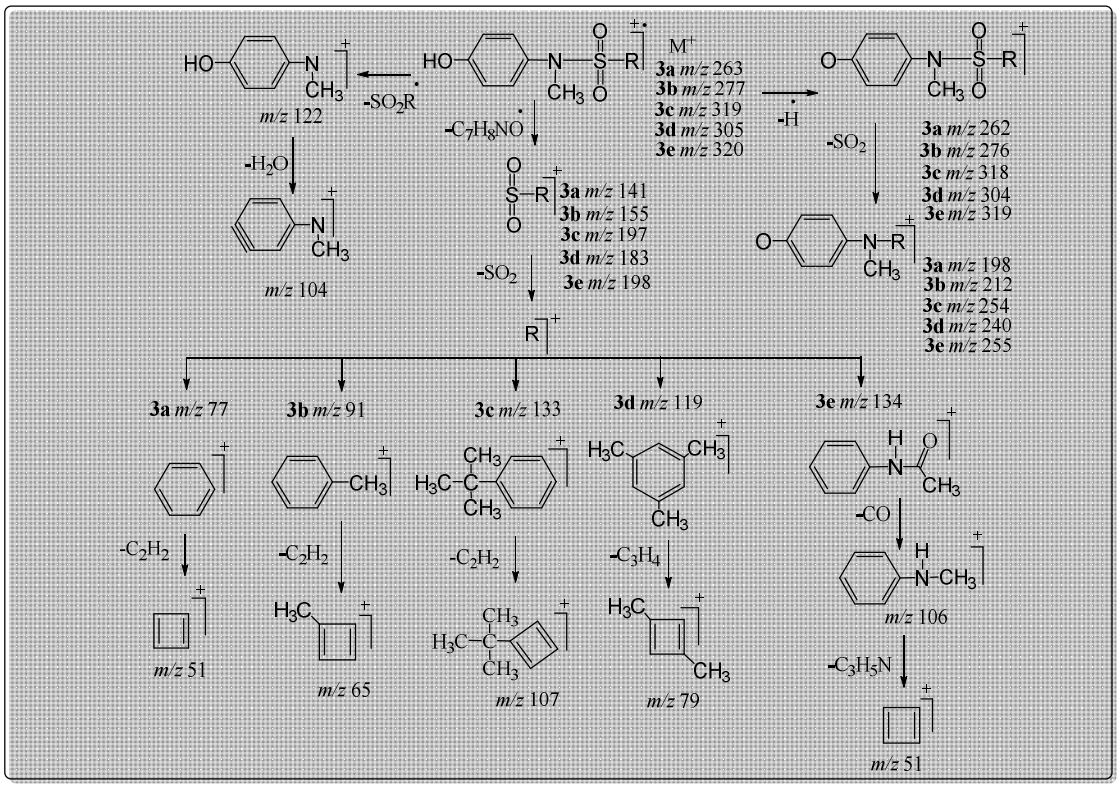

Fig. 2. Mass fragmentation pattern of *N*-(4-hydroxyphenyl)-*N*-methyl-substituted sulfonamides (3a-e)

The structures of 2-(4-(substituted-sulfonamido)phenoxy)-*N*-(2,3-dihydrobenzo [1,4]dioxin-6-yl)acetamides **(6a-i)** were further confirmed by EIMS fragmentation patterns**.** Compound **6a** gave molecular ion at *m/z* 454, **6b** at *m/z* 468, **6c** at *m/z* 510, **6d** at *m/z* 496, **6e** at *m/z* 511, **6f** at *m/z* 533, **6g** at *m/z* 488, **6h** at *m/z* 522 & **6i** at *m/z* 504 which was in accordance to their M.W.

Molecular ion of all compounds **6a-i** losses $C_8H_7SO_4R^\bullet$ to form $C_6H_4NCH_3OCH_2NHCO^+$ which appeared at *m/z* 178. Another fragment $C_6H_3C_2H_4O_2NHCO^+$ appeared at *m/z* 178 due to the loss of $C_8H_9SO_3R^\bullet$ from molecular ion; which further looses CO to give $C_6H_3C_2H_4O_2NH^+$ at *m/z* 150 and afterwards it give up C_2H_4 to form $C_6H_3O_2NH^+$ at *m/z* 122 and latter it form cation $C_6H_3NH^+$ at *m/z* 90 by losing oxygen. One more important fragment $C_6H_3C_2H_4O_2NHCOCH_2^+$ appeared at *m/z* 192 due to the loss of $C_7H_7NSO_3R^\bullet$ from M^+. A heavy M.W. fragment emerged at *m/z* 313 due to the formation of $C_{17}H_{17}N_2O_4^+$ after the loss of $SO_2R^\bullet$ from M^+, which on losing CO formed $C_{16}H_{17}N_2O_3^+$ at *m/z* 285. The related fragmentation pathways are provided in Figs. 4 and 5.

4.2 Enzyme Inhibition Activity

The results of screening against all the three enzymes are presented in Table 1 in the form of %age inhibition and IC_{50} values. The screening of synthesized molecules against acetyl cholinesterase enzyme showed that all the molecules exhibited promising inhibitory action and **3b** was the most prominent with the lowest IC_{50} value of 21.62±0.53 µM relative to the reference standard, eserine, with IC_{50} value of 0.04±0.0001 µM. Only **6b** molecule remained inactive as evident from IC_{50} value. Butyryl cholinesterase enzyme was also promisingly inhibited by all the molecules except **6b**. **6i** was

the most active against this enzyme by the IC_{50} value of 45.62±0.61 µM relative to reference standard, eserine, with IC_{50} value of 0.85±0.0001 µM. The most potent molecules against both the cholinesterase enzymes were **3e**, **3j** and **6i** with the structural features of *p*-substituted acetamoyl group, naphthyl group interacting at large area and dichloro substituted phenyl ring at both meta positions, respectively. Against lipoxygenase enzyme, some were inactive and most of them showed moderate inhibitory action. The most potent molecule against this enzyme was **6j** with IC_{50} value of 73.12±1.99 µM relative to baicalein with IC_{50} value of 22.4±1.3 µM.

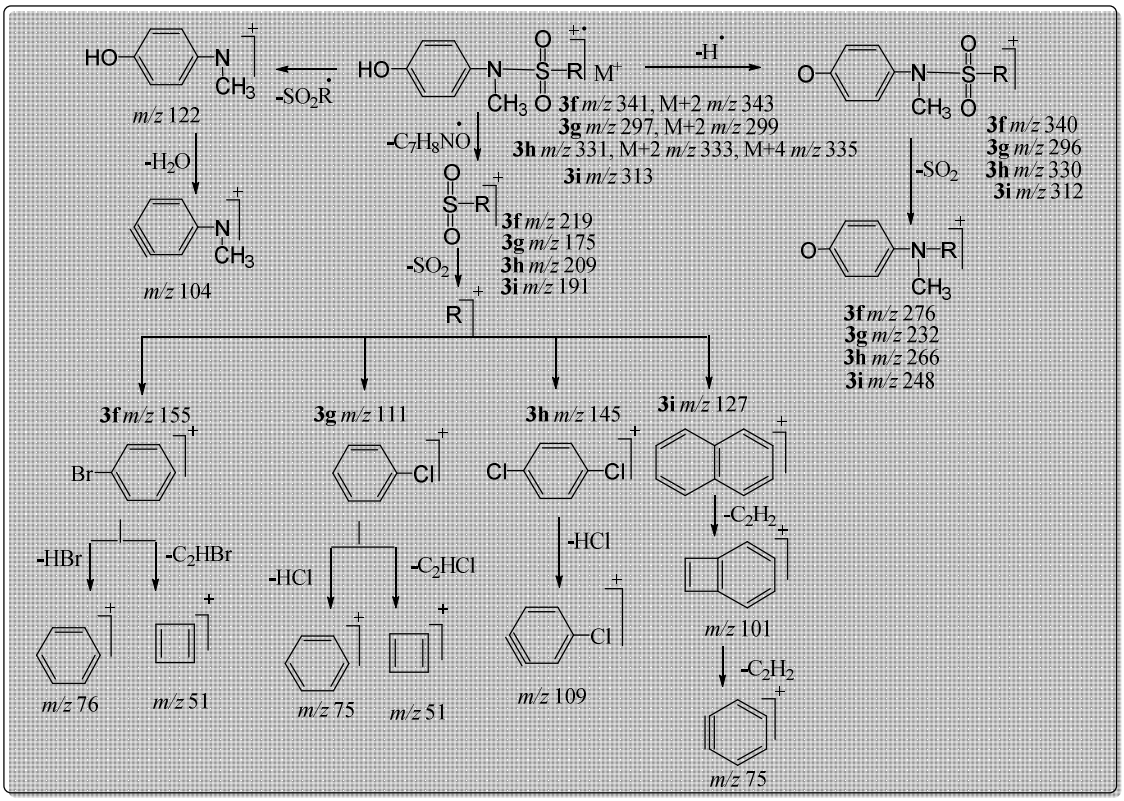

Fig. 3. Mass fragmentation pattern of N-(4-hydroxyphenyl)-N-methyl-substituted sulfonamides (3f-i)

4.3 Antibacterial Activity

All the synthesized molecules were screened against three Gram-negative and two Gram-positive bacterial strains and were found to be moderate inhibitors. The results are tabulated as %age inhibition and MIC values in Table 2. Most of the compounds showed activities against the both Gram-positive bacterial strains except a few. Almost all the compounds showed the same inhibition potential against *S. typhi* and *E. coli*, as that of the reference standard, ciprofloxacin used. *P. aeroginosa* and *S. aureus* were inhibited by the majority of the molecules with 50% inhibitory action as that of the reference used. The synthesized molecules, 5, 6f, 6h and 6j were active against all the bacterial strains with much low MIC values, credibly because of the presence of bromo group at 2nd carbon of acetyl group, bromo group at 4th position of phenyl group, two chloro groups at 2nd and 5th position of phenyl group and naphthyl group, respectively. The aromatic naphthyl rings are responsible for more interaction and the halogens in better positions are creditworthy for the antibacterial inhibition potential.

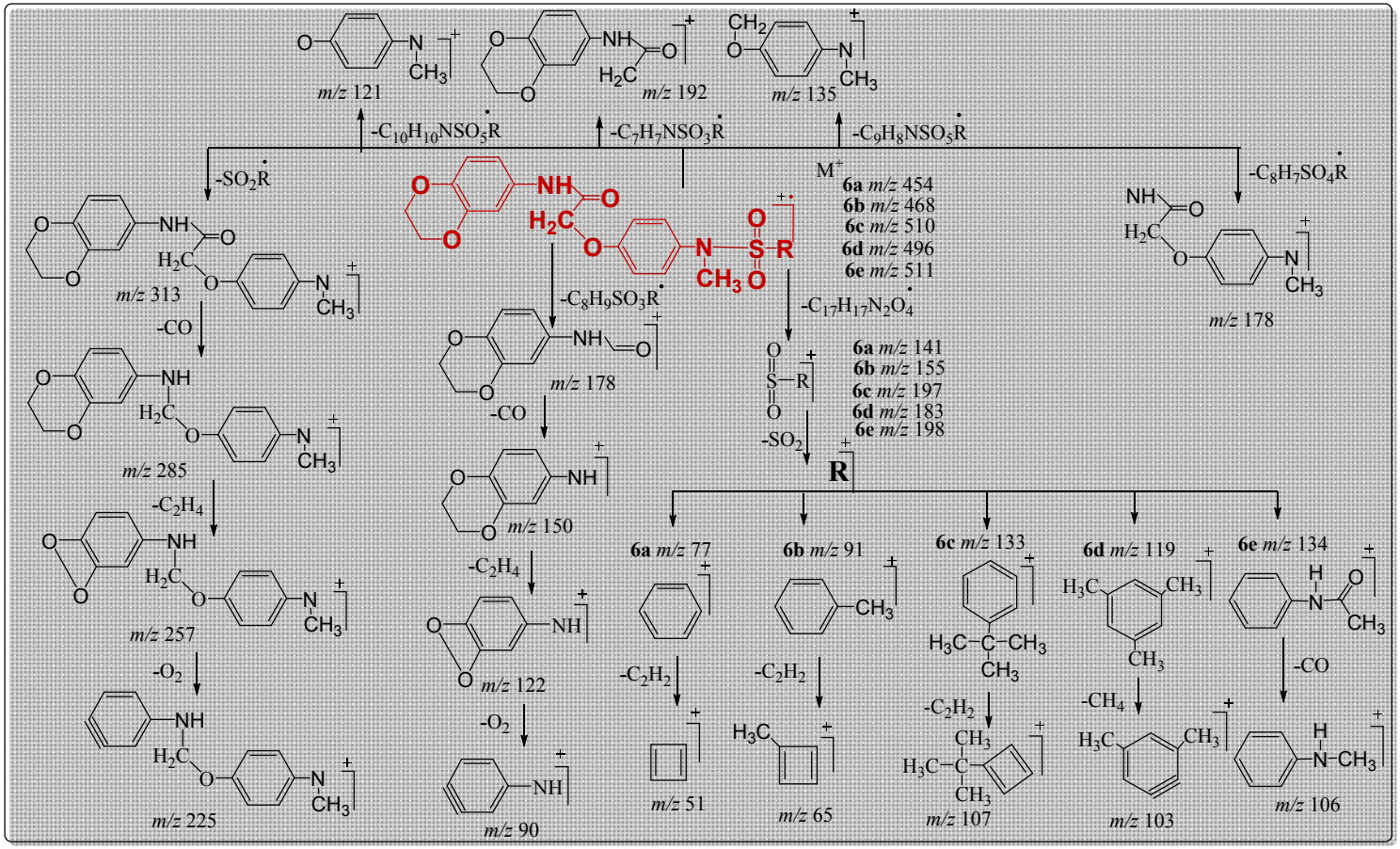

Fig. 4. Mass fragmentation pattern of 2-(4-(substituted-sulfonamido)phenoxy)-*N*-(2,3-dihydrobenzo[1,4]dioxin-6-yl)acetamides (6a-e)

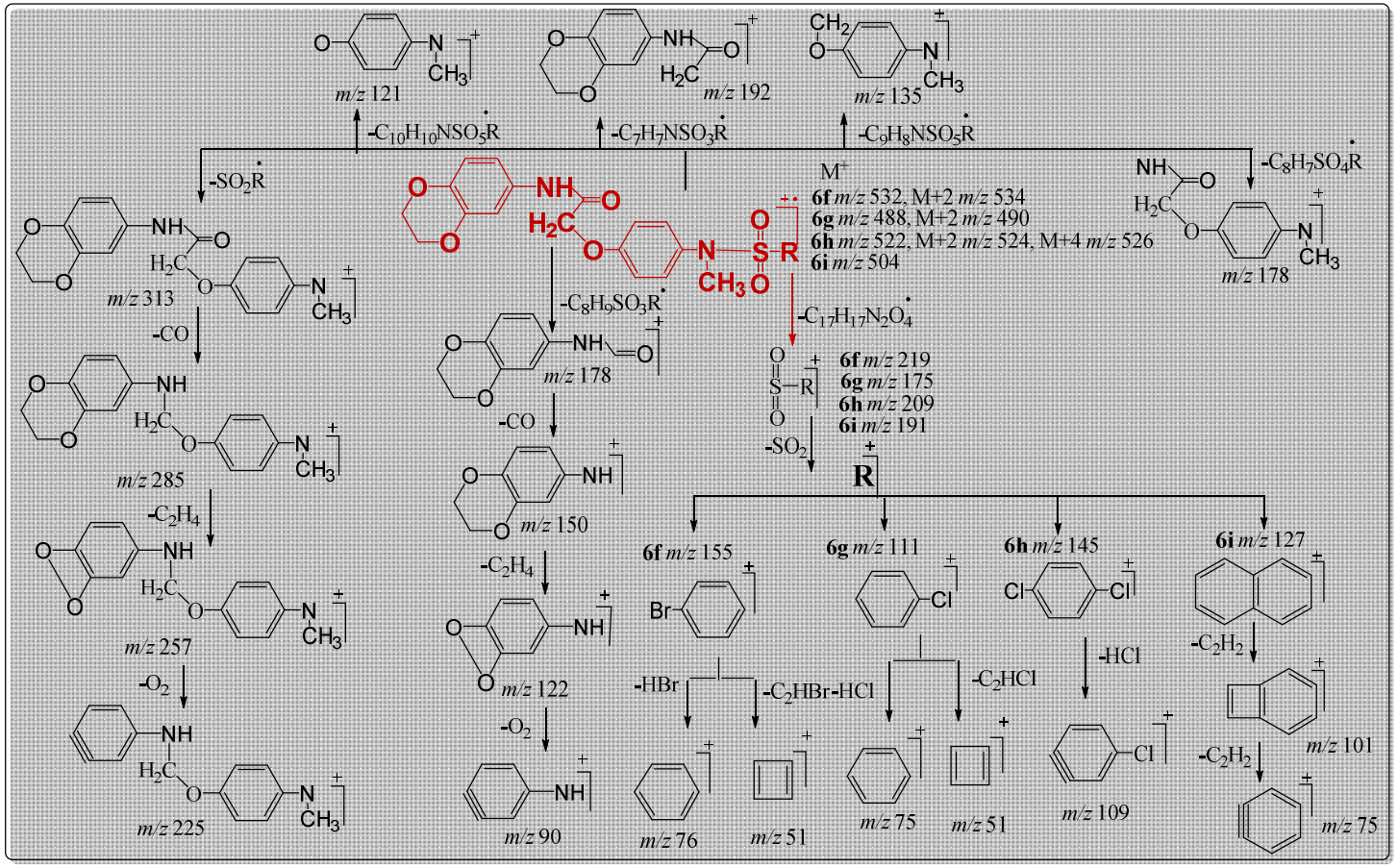

Fig. 5. Mass fragmentation pattern of 2-(4-(substituted-sulfonamido)phenoxy)-N-(2,3-dihydrobenzo[1,4]dioxin-6-yl)acetamides (6f-i)

4.4 Computational Analysis of Potent Compounds from 3a-i

One of the potent compound **3b** showed very decent interaction with the active site of the target protein AChE. A total of six interactions were observed with five residues of the active sites. Three residues (Tyr70, Trp84, Asn85) made interaction with the hydrogen, while one residue Asp72 linked to the oxygen atom of OH group of phenol ring respectively. However, Trp84 also interacted with the toluene moiety through arene-hydrogen bonding. Ser122 interacted with oxygen atom of sulfonamide group and make the interaction of compound stronger (Fig. 6). So, in this interaction analysis we observed that three different moieties of compound are contributing in the interaction between ligand and protein.

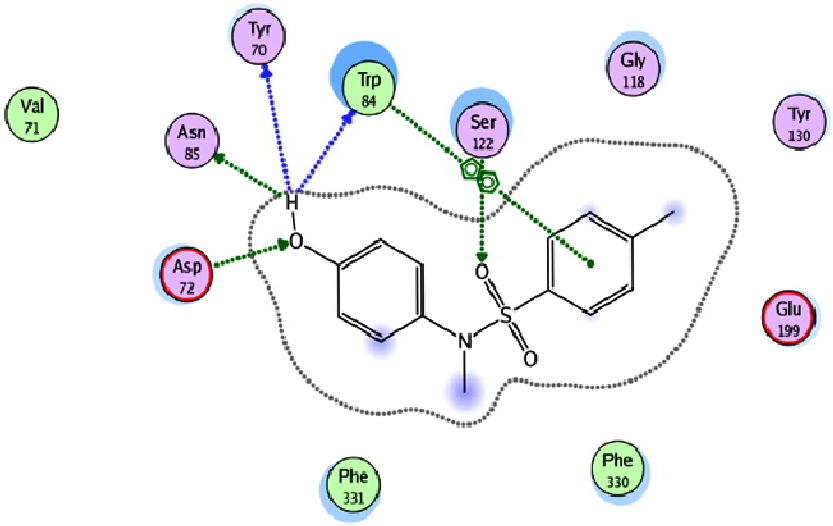

Fig. 6. The 2D interaction analysis of *N*-(4-hydroxyphenyl)-*N*,4-dimethyl benzenesulfonamide (3b) against AChE

The interaction analysis of compound **3c** in case of BChE revealed that two important moieties are contributing in the three interactions with two residues of cavity. Asn85 interacted with the oxygen atom of OH group of phenol moiety; whereas His126 interacted with the one oxygen atom of sulfonamide group directly as well as through water molecule (Fig. 7).

The importance of sulfonamide group is depicted from the interaction analysis of compound **3f**. Two amino acid residues Tyr121 and Ser122 from the binding cavity of AChE protein interacted directly with the oxygen of the sulfonamide group as shown in Fig. 8.

For compound **3i** three interactions were observed through two amino acids residues against BChE. Lys131 interacted with the oxygen of phenol group directly as well as through water molecule and Tyr61 interacted with the oxygen of sulfonamide group directly without intervening water molecule (Fig. 9). In both cases **(3c** & **3i)** experimentally determined potency of inhibitor strongly agreed with docking results.

4.5 Computational Analysis of Potent Compounds from 6a-i

The interaction analysis of compound **6c** showed that four amino acid residues from the active site of acetylcholinesterase protein contributed in the interaction between compound and protein. Four residues Tyr70, Tyr121, Phe330 and Gln74 interacted with molecule as shown in (Fig. 10). Tyr121 interacted with the oxygen of acyl group, while Phe330 and Tyr70 interacted through arene-hydrogen

bonding with the phenyl rings of 1,4-benzodioxane and phenoxy moieties respectively; whereas Gln74 interacted with one oxygen atom SO_2 group of sulfonamide moiety.

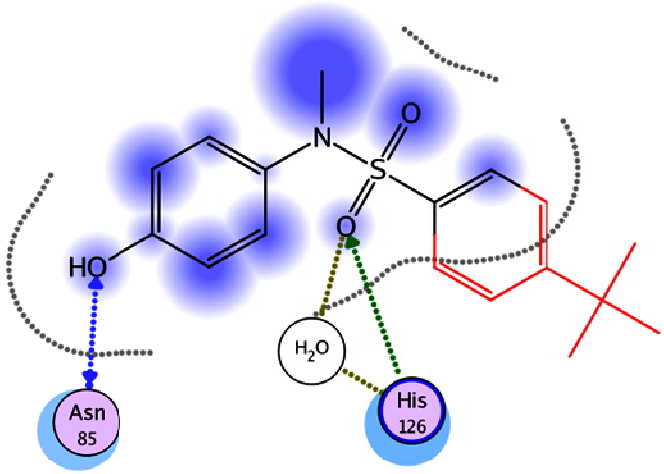

Fig. 7. The 2D interaction analysis of 4-(*tert*-butyl)-*N*-(4-hydroxyphenyl)-*N*-methylbenzenesulfonamide (3c) against BChE

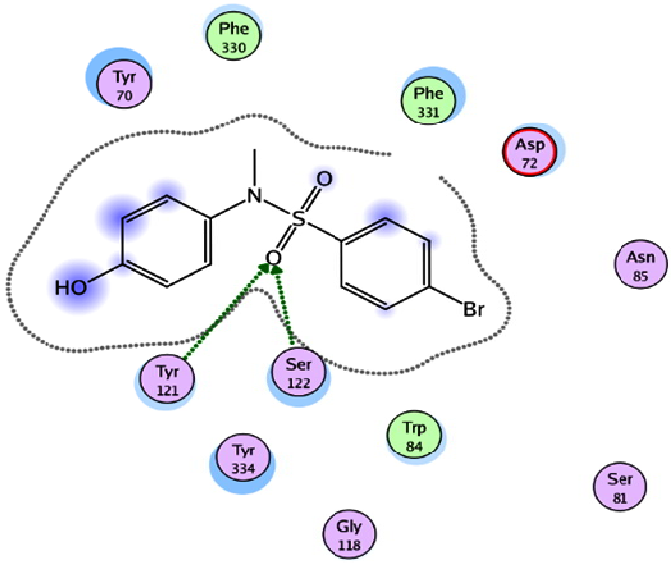

Fig. 8. 2D interaction analysis of 4-bromo-*N*-(4-hydroxyphenyl)-*N*-methylbenzenesulfonamide (3f) against AChE

The interaction analysis of compound **6f** showed that four amino acid residues from the active site of protein contributed in the six interactions between compound and protein. Three important water molecules were also involved in the interactions. Lys131 interacted with the ligand at three different points, directly with the SO_2 group of 4-bromobenzene sulfonamide, the one oxygen atom (at 1st position) of 1,4-benzodioxine moieties respectively and through arene-hydrogen with the phenyl ring of 1,4-benzodioxine ring. All the other three residues Tyr61, His126 and Asp129 interacted through water molecule as shown in (Fig. 11). His126 interacted through one water molecule with the oxygen

of acyl group and by another H_2O molecule to the one oxygen atom (at 4th position) of 1,4-dioxane ring; whereas Asp129 and Tyr61 interacted through two and one H_2O molecules respectively to the one oxygen atom (at 4th position) of 1,4-dioxane ring. Thus important interaction occurred through dioxane moiety. The compound proofed acceptable interactions and good inhibition as well.

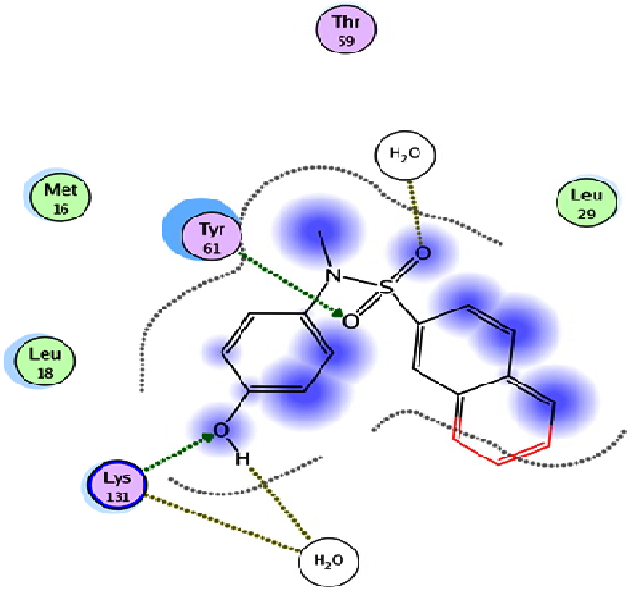

Fig. 9. The 2D interaction analysis of *N*-(4-hydroxyphenyl)-*N*-methyl-2-naphthalene sulfonamide (3i) against BChE

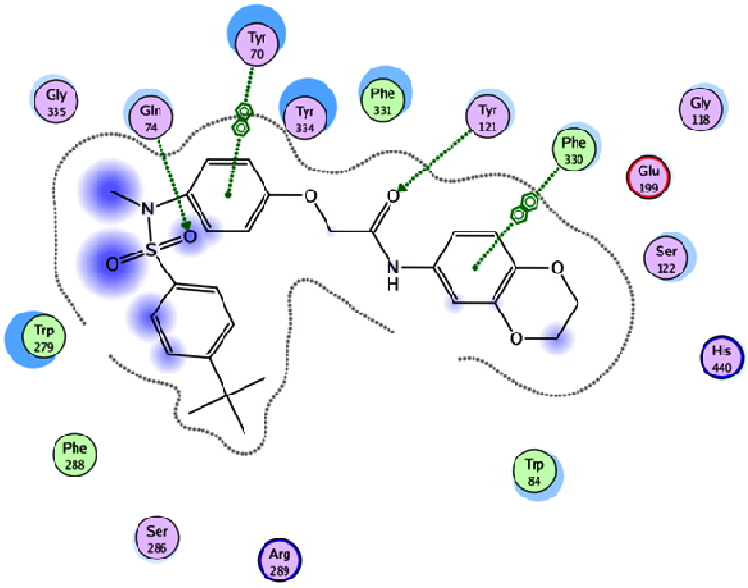

Fig. 10. 2D interaction of 2-(4-(4-*tert*-butyl-*N*-methylphenylsulfonamido)phenoxy)-*N*-(2,3-dihydrobenzo[1,4]dioxin-6-yl) acetamide (6c) against AChE

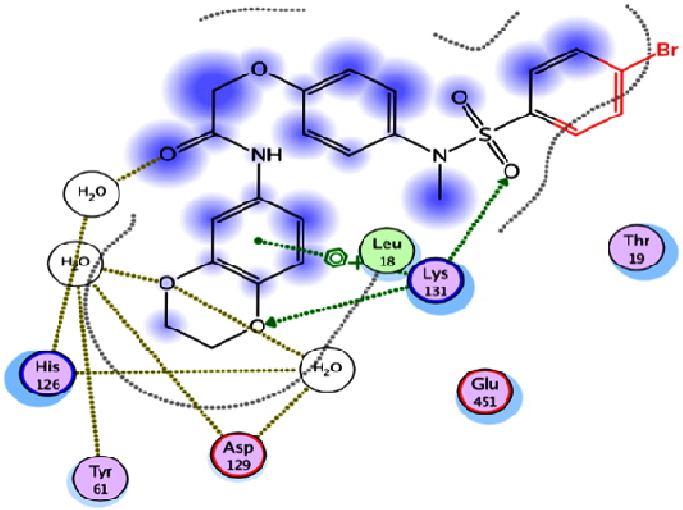

Fig. 11. The 2D interaction analysis of 2-(4-(4-bromo-*N*-methylphenylsulfonamido) phenoxy)-*N*-(2,3-dihydrobenzo[1,4]dioxin-6-yl)acetamide (6f) against BChE

The interaction analysis of compound **6i** in case of LOX revealed that two important moieties are contributing in the interactions. This reflected the importance of acetamido and sulfonamide groups. A total of six interactions were observed with five residues of the active sites. Val566 showed direct interaction with the oxygen of SO_2 group, whereas His518 and Gln716 interacted with oxygen atom adjacent to methylene group and to the hydrogen (NH) respectively of acetamido moiety. Carbonyl oxygen of acetamido moiety was linked by two residues i.e. His513 and Gln514. Sixth interaction was found from hydrogen (NH) to the His513 residue of LOX protein. The experimentally determined inhibition of a compound was well supported by the docking studies (Fig. 12).

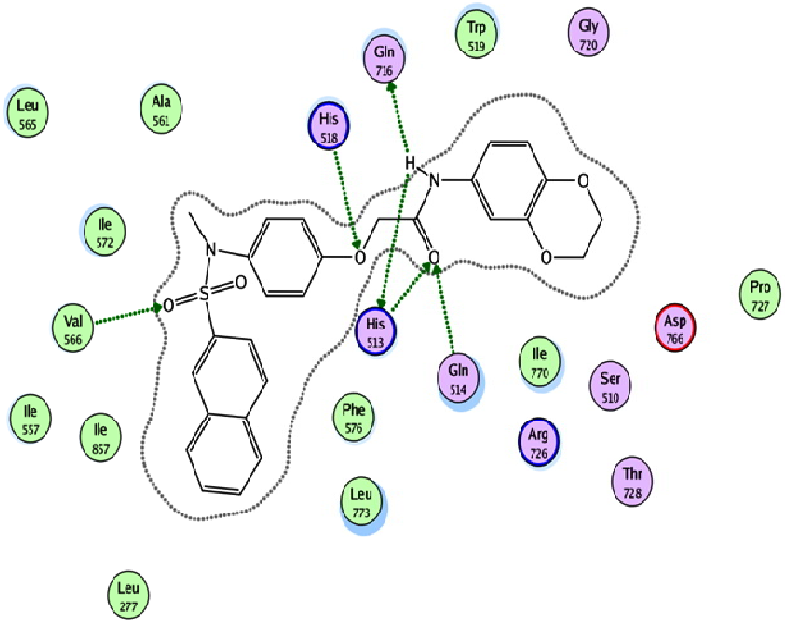

Fig. 12. 2D interaction analysis of *N*-(2,3-dihydrobenzo[1,4]dioxin-6-yl)-2-(4-(*N*-methylnaphthalene-2-sulfonamido)phenoxy)acetamide (6i) against LOX

5. CONCLUSION

All the compounds were synthesized in good yields by the depicted methods in experimental section. The proposed structures were corroborated by the spectroscopic analysis using IR, ^{1}H-NMR and EIMS techniques. All the synthesized compounds were evaluated for the enzyme inhibition and antibacterial activities. The IC_{50} values of these molecules rendered them better inhibitors of cholinesterase enzymes and moderately less inhibitors of lipoxygenase enzyme. The MIC values of taken into account molecules against the different bacterial strains, showed them potent against two of three Gram-negative bacterial strains and moderately good against two Gram-positive bacterial strains. All these biological results depicted the synthesized molecules as an important pathway for the pharmacological industries in drug designing.

ACKNOWLEDGEMENT

The authors are thankful to the Higher Education Commission of Pakistan for the financial support regarding this research work and the spectroscopic analysis.

COMPETING INTERESTS

Authors have declared that no competing interests exist.

REFERENCES

1. Thomas G. Medicinal Chemistry: An introduction. 2nd edition. John Wiley & Sons. 2007;54.
2. Riaz S, Khan IU, Bajda M, Ashraf M, Shaukat A, Rehman TU, Mutahir S, Hussain S, Mustafa G, Yar M. Pyridine sulfonamide as a small key organic molecule for the potential treatment of type-II diabetes mellitus and Alzheimer's disease: *In vitro* studies against yeast α-glucosidase, acetylcholinesterase and butyrylcholinesterase. Bioorg Chem. 2015;63:64−71.
3. Supuran CT, Casini A, Scozzafava A. Protease inhibitors of the sulfonamide type: Anticancer, anti-inflammatory and anti-viral agents. Med Res Rev. 2003;23:535-358.
4. Supuran CT, Innocenti A, Mastrolorenzo A, Scozzafava A. Antiviral sulfonamide derivatives. Mini-Rev Med Chem. 2004;4:189-200.
5. Zhao Z, Wolkenberg SE, Lu M, Munshi V, Moyer G, Feng M, Carella AV, Ecto LT, Gabryelski LJ, Lai MT, Prasad SG, Yan Y, McGaughey GB, Miller MD, Lindsley CW, Hartman GD, Vacca JP, Williams TM. Novel indole-3-sulfonamides as potent HIV non-nucleoside reverse transcriptase inhibitors (NNRTIs). Bioorg Med Chem Lett. 2008;18:554-559.
6. El-Sayed NS, El-Bendary ER, El-Ashry SM, El- Kerdawy MM. Synthesis and antitumor activity of new sulfonamide derivatives of thiadiazolo [3, 2-a] pyrimidines. Eur J Med Chem. 2011;46:3714-3720.
7. Ahmed B, Habibullah, Khan S. Synthesis and antihepatotoxic activity of 2-(substituted-phenyl)-5- (2,3-dihydro-1,4-benzodioxane-2-yl)-1,3,4-oxadiazole derivatives. J Enz Inhib Med Chem. 2011;26:216-221.
8. Chapleo CB, Myers PL, Butler CM, Doxey JC, Roach AG, Smith CFC. α-adrenoreceptor reagents. Synthesis of some 1,4-benzodioxans as selective presynaptic .alpha. 2-adrenoreceptor antagonists and potential antidepressants. J Med Chem. 1983;26:823-831.
9. Vazquez MT, Rosell G, Pujol MD. Synthesis and anti-inflammatory activity of rac-2-(2, 3-dihydro-1,4-benzodioxin) propionic acid and its R and S enantiomers. Eur J Med Chem. 1997;529-534.
10. Yasuda G, Hasegawa K, Kuji T, Ogawa N, Shimura G, Umemura S, Tochikubo O. Effects of doxazosin on ambulatory blood pressure and sympathetic nervous activity in hypertensive type 2 diabetic patients with overt nephropathy. Diabet Med. 2005;22:1394-1400.
11. Aksu K, Topal F, Gulcin I, Tumer F, Goksu S. Acetylcholinesterase inhibitory and antioxidant activities of novel symmetric sulfamides derived from phenethylamines. Arch Pharm (Weinheim). 2015;348:446-455.

12. Allderdice PW, Garner HAR, Galutira D, Lockridge O, Ladu BN, M cAlpine PJ. The cloned butyrylcholinesterase (BCHE) gene maps to a single chromosome site, 3q26. Genomics. 1991;11:452-454.
13. Dave KR, Syal AR, Katyare SS. Tissue cholinesterases. A comparative study of their kinetic properties. Z Naturforsch. 2000;55:100-108.
14. Oztaskın N, Cetinkaya Y, Taslimi P, Goksu S, Gulcin I. Antioxidant and acetylcholinesterase inhibition properties of novel bromophenol derivatives. Bioorg Chem. 2015;60:49-57.
15. Lands WEM. Mechanism of action of anti-inflammatory drugs. Adv Drug Res 1985;14:147–167.
16. Steinhilber D. 5-Lipoxygenase: A target for anti-inflammatory drug revisited. Curr Med Chem. 1999;6:71–86.
17. Nie D, Honn KV. Cyclooxygenase, lipoxygenase and tumor angiogenesis. Cell Mol Life Sci. 2002;59:799–807.
18. Aziz-ur-Rehman, Fatima A, Abbas N, Abbasi MA, Khan KM, Ashraf M, Ahmad I, Ejaz SA. Synthesis, characterization and biological screening of 5-substituted-1, 3, 4-oxadiazole-2yl-N-(2-methoxy-5-chlorophenyl)-2-sulfanyl acetamide. Pak J Pharm Sci. 2013;26:345-352.
19. Khalid H, Aziz-ur-Rehman MA. Abbasi and KM Khan. Int J Pharm Pharm Sci. 2012;4:443.
20. Aziz-ur-Rehman, Nafeesa K, Abbasi MA, Khalid H, Khan KM, Ashraf M, Ahmad I, Ejaz SA. Synthesis, spectral characterization and biological activity of S-subtituted derivatives of 5-(nitrophenyl)-1, 3, 4-oxadiazole-2-thiol. Asian J Pharm Hea Sci. 2012;2:370-376.
21. Aziz-ur-Rehman , Siddiqui SZ, Abbas N, Abbasi MA, Khan KM, Shahid M, Mahmood Y, Akhtar MN, Lajis NH. Synthesis, antibacterial screening and hemolytic activity of S-substituted derivatives of 5-benzyl-1, 3, 4-oxadiazole-2-thiol. Int J Pharm Pharm Sci. 2012;4:676-680.
22. Ellman GL, Courtney KD, Andres V, Featherstone RM. A new and rapid colorimetric determination of acetylcholinesterase activity. Biochem Pharmacol. 1961;7:88-95.
23. Baylac S, Racine P. Inhibition of 5-lipoxygenase by essential oils and other natural fragrant extracts. Int J Aromather. 2003;13:138-142.
24. Kaspady M, Narayanaswamy VK, Raju M, Rao GK. Synthesis, antibacterial activity of 2, 4-disubstituted oxazoles and thiazoles as bioisosteres. Lett Drug Des Discov. 2009;6:21-28.
25. Yang CR, Ying Z, Jacob MR, Khan SI, Zhang YJ, Li XC. Antifungal activity of C-27 steroidal saponins. Antimicrob Agents Ch. 2006;50:1710-1714.
26. Wadood A, Riaz M, Jamal SB, Shah M. Interactions of ketoamide inhibitors of HCV NS3/4A protease target: molecular docking studies. Mol Biol Rep. 2014;41:337-345.

Biography of author(s)

Dr. Misbah Irshad
Department of Chemistry, Division of Science and Technology, University of Education, Township Campus, Lahore-54770, Pakistan and Department of Chemistry, Government College University, Lahore-54000, Pakistan.

Research and Academic Experience: Since October 2015, serving as Assistant Professor at University of Education, Township Campus Lahore.
About 13 years of research experience

Research Area: Synthesis and structural analysis of organic molecules of pharmaceutical interests. Purification, characterization and structural modifications of various natural molecules to study their structure-activity relationship and in vitro assessment of relief by different samples to oxidative injury.

Number of Published papers: 23 published, 2 accepted

Special Award (If any): Five years scholarship under “Indigenous Ph.D. Fellowship Program” Awarded by Higher Education Commission of Pakistan for M.Phil leading to PhD program.

As Principal Investigator Completed 0.5 M project under SRGP of HEC (Project # 862) entitled "Synthesis, Characterization and Applications of Chalcone Based Chemosensors".

Any other remarkable point(s): Have supervised 24 BS/MSC/MS students.

Prof. Dr. Muhammad Athar Abbasi
Department of Chemistry, Government College University, Lahore-54000, Pakistan.

He has carried out postdoctoral research in Medicinal Chemistry at Kongju National University, South Korea. He secured his PhD degree from International Center of Chemical and Biological Sciences, HEJ Research Institute of Chemistry and also completed one year postdoctoral research at the same institute, soon after doctorate. He has published 290 research articles in reputed journals in the field of Organic and Medicinal Chemistry; with total citations: 1,635. He has supervised 11 PhD scholars and 53 MS/M.Phil. scholars. He has completed 05 funded research projects. He is author of six books. He is (seven times) recipient of Research Productivity Award conferred by Pakistan Council for Science and Technology, Ministry of Science and Technology, Islamabad, Pakistan. He is an Associate Editor of the "Organic and Medicinal Chemistry International Journal" and "Bioequivalence & Bioavailability International Journal". He is also an Editorial Board Member of "Journal of Single Molecule Research" and "Advances in Pharmacology and Pharmacy". His current research interest lies in the synthesis of organic poly-functional molecules to explore new therapeutic potentials.

© Copyright (2020): Author(s). The licensee is the publisher (Book Publisher International).

DISCLAIMER
This chapter is an extended version of the article published by the same author(s) in the following journal.
Asian Journal of Chemistry, 26(4): 1151-1160, 2014.

Chapter 7
Print ISBN: 978-93-90206-41-4, eBook ISBN: 978-93-90206-42-1

Critical Research on Enhancement of the Inhibitor Efficiency of 4-Phenyl-1,2-dithiol-3-thione on Corrosion of Mild Steel for 20% Sulphuric Acid

M. Dakmouche[1*], M. Saidi[1], M. Hadjadj[1], M. Yousfi[2] and Z. Rahmani[1]

DOI: 10.9734/bpi/crdc/v4

ABSTRACT

Substituted 4-phenyl-1,2-dithiol-3-thione (PDTT) synthesized and tested as inhibitors for the corrosion for mild steel in the presence of oxygen by potentiodynamic polarization and electrochemical impedance spectroscopy (EIS) technique in 20% H_2SO_4 at 25ºC. This organic compound inhibits the acidic corrosion even at low concentration. The results obtained show that this sulfur compound is good inhibitors and are in good agreement. Polarization curves indicate that 4-phenyl-1,2-dithiol-3-thione is a cathodic inhibitor and able to reduce the corrosion current, obtained from electrochemical impedance spectroscopy measurement, were analyzed to model the corrosion inhibition process through appropriate equivalent circuit model. The adsorption of 4-phenyl-1,2-dithiol-3-thione on the steel surface in 20% H_2SO_4 solution, obeys to Langmuir's isotherm with a very high negative value of the free energy of adsorption ΔG°_{ad}.

Keywords: Acid; corrosion; inhibition; dithiole thione; mild steel; electrochemical impedance spectroscopy; adsorption.

1. INTRODUCTION

Organ sulfur derivatives are exogenic compounds known as antioxidants in various therapeutic applications. Among these sulfur compounds, 1,2-dithiol-3-thiones (dithiolethiones) are extensively investigated owing to their chemo preventive effect in numerous condition, prevention of hepato-, nephro-, ten toxicity, neuroprotection, effect in inflammation, cerebral and cardiac, ischemia and cancer chemoprevention [1]. A number of derivatives of 3*H*-1,2-dithiol-3-thiones have been shown to induce phase II detoxification enzymes [2].

First quantitative structure-activity relationships (QSAR) between electrophone detoxication properties of 1,2-dithiol-3-thiones, for example the use of Hammet electronic parameters δ, shows that electronic effect of the substituent may play an important role in DNA-binding of ligands [3] and determine their water/*n*-octanol partition coefficient, log P. A very significant linear property was found with some disubstituted derivatives. It was found that the less lipophilicity dithiolethiones were the most active [4].

1,2-Dithiol-3-thiones are five-member cyclic sulfur-containing compounds with antioxidant chemotherapeutic and chemo protective activities these compound are used in different domain, such as, oltipraz a member of a class of dithiol thione is induced phase 2 enzyme response conserved in cells lacking mitochondrial DNA [5], then sulfarlem is widely used in human therapy for its choler tic, sialogogic properties and as cytoprotective agent in lung precancerous lesions prevention in smokers [6] and finally 3-methylthio-1,2-dithiolium cation was easily reduced in DMF at a mercury electrode [7].

[1]*Laboratoire de Valorisation et Promotion des Ressources Sahariennes, Université Kasdi Merbah de Ouargla, 30000 Ouargla, Algeria.*
[2]*Laboratoire des Sciences Fondamentales, Université de Laghouat, 03000 Laghouat, Algeria.*
**Corresponding author: E-mail: mdakmouche@gmail.com;*

Acid solutions are used for the removal of undesirable scale and rust in many industrial processes [8]. It is well known that sulphuric acid used for the removal of undesirable scale and rust in several industrial processes trigger corrosion of pure metals and alloys [9]. Aggressive acids predominantly sulphuric acid are widely used for industrial and some specific treatments (*e.g.* chemical cleaning pickling) of mild steel most especially when intended for hot-dip galvanizing. However, these acids are known to cause severe corrosion problems [10]. In order to minimize the loss of mild steel, the use of inhibitors is one of the most practical methods for protection against metallic corrosion, especially in acidic media. Many organic compounds containing polar functions such as oxygen, nitrogen, sulphur and phosphorus in their molecular structures have been used as corrosion inhibitor for metal [11-21]. While sulphur containing inhibitors exert their best efficiency in sulphuric acids [22-24] such as sulphoxides, sulphide and thioureas [25]. Inhibitors find application in pickling cleaning and acid decaling processes in general organic compounds such as, amines, acetylene alcohol, heterocyclic compounds *etc.*, have found use as inhibitors in industrial applications [26].

The primary step in the action of organic corrosion inhibitors in acid solutions is usually adsorption at the metal-solution interface. The adsorption requires the existence of attractive forces between the adsorb ate and the metal. Accor-ding to the type of forces, adsorption can be physisorption, chemisorptions or a combination of both. Physisorption is due to electrostatic attractive forces between inhibiting organic ions or dipoles and the electrically charged surface of the metal. Chemisorptions is due to interaction between unshared electron pairs or π-electron of the adsorb ate with the metal in order to form a coordinate type of bond. It may take place in presence of heteroatom (P, Se, S, N, O), with lone-pair electrons [27], functional groups, steric factors, aroma city, electron density at the donor atoms and (π) orbital character of donating electrons [28] and also on the electronic structure of the molecules [29,30]. According to this mechanism, a reduction of either the anodic or the cathodic reaction or both arises from the adsorption of inhibitor on the corresponding active sites. The electronic characteristic of the molecules (adsorb ate), the chemical composition of the solution, the nature of the metal surface, the temperature of the reaction and the electro-chemical potential at the metal-solution interface determine the degree of adsorption and hence the effectiveness of inhibitor [27].

The compound 4-phenyl-1,2-dithiol-3-thione (PDTT), is an example of a new class of corrosion inhibitors (Fig. 1). The aim and the objective of the present work is to investigate the efficiency of 4-phenyl-1,2-dithiol-3-thione as corrosion inhibitors of mild steel X52 in 20% sulphuric acid, in order to study the influence of a sulfur atom and aromaticity, in the part of the molecule.

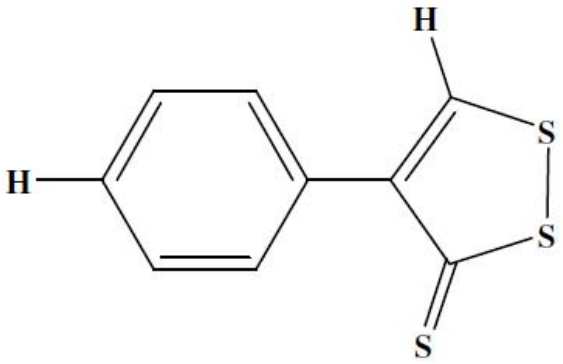

Fig. 1. Molecular structure of the 4-phenyl-1, 2-dithiol-3-thione (PDTT)

2. EXPERIMENTAL

The investigated 4-phenyl-1,2-dithiol-3-thione (PDTT) was synthesized in the laboratory according to described procedure [30] and was purified and analyzed by IR and measure point of fusion before used. The concentration range employed was 25×10^{-3} mM to 126×10^{-3} mM.

Corrosion tests have been carried out on electrodes of mild steel. Steel stips containing percentage composition of (in wt. %) C: 0.1038, Mn: 0.971, S: 0.0021 and remainder iron was used, as the working electrode for the electrochemical studies. The surface preparation of the specimens was carried out by grinding with emery paper grade 400 and 1200 they were dried at room temperature before use. The acid solution (20% H_2SO_4) was prepared by dilution of analytical grade 98% H_2SO_4 with distilled water.

Polarization curves were conducted at 25 ± 1ºC using an electrochemical measurement system controlled with Tacussel Radiometer PGP201 corrosion analysis. Electrochemical experiments were carried out in a glass cell with a capacity of 500 ml. A saturated calomel electrode (SCE) as a reference electrode. A platinum electrode was used as a counter. All potentials are reported *vs.* SCE.

For Tafel polarization technique and electrochemical impedance spectroscopy (EIS), the working electrode was in the form of a disc cut from mild steel under investigation and was embedded in a Teflon rod with an exposed area of 1.0 cm^2. A calomel electrode was placed close to the working electrode to minimize ohmic resistance. All test solution were aerated in the cell, the test solution was mixed with a magnetic. The anodic and cathodic polarization curves were recorded by a constant sweep rate of 0.5 mV s^{-1}.

Electrochemical impedance spectroscopy (EIS) was conducted in an electrochemical measurement system (Voltalab40) which comprises a PGZ301 potentiontat and Tacussel Frequency Response Analyzer.

A personal computer and Volta Master 4 software and posing a double glass cell equipped with a thermo stated cooling condenser. The solution volume was 500 ml. An ac sinusoid ± 10 mV was applied at the corrosion potentials (E_{corr}) over a frequency rang of 10^5 Hz-10^{-3} Hz with ten point par decade was employed. All tests were performed at 25 ± 1ºC Nyquist plots were obtained from these experiments.

3. RESULTS AND DISCUSSION

Polarization measurements have been carried out in order to gain knowledge concerning the kinetics of the anodic and cathodic reactions. Polarization curves of the mild steel in 20% H_2SO_4 solutions without and with addition of different concentrations of PDTT are shown in Fig. 2. The anodic and cathodic current-potential curves are extrapolated up to their intersection at a point where corrosion current density (i_{corr}) and corrosion potential (E_{corr}) are obtained [27]. Table 1 shows the electrochemical kinetic parameters (i_{corr}, E_{corr} and bc) obtained from Tafel plots for the steel electrode in 20 % H_2SO_4 solution without and with different concentration of the investigated (PDTT). The i_{corr} values were used to calculate the inhibition efficiency.

The inhibition efficiency, E (%) (listed in Table 1), is calculated by the following expression [31]:

$$E\ (\%) = \left[1 - \left(\frac{i_{corr}}{i^{o}_{corr}}\right)\right] \times 100 \qquad (1)$$

where i_{corr} and i^{o}_{corr} are the corrosion current densities in the presence and absence of the inhibitor in the solutions, respectively.

As was expected cathodic reactions of carbon steel electrode corrosion were inhibited with increase of the synthesized surfactant concentration. This result suggests that the addition of the synthesized inhibitors reduces anodic dissolution and also retards the hydrogen evolution reaction [22], the best inhibition efficiency was about 96.95% at concentration 126 × 10^{-3} mM. It can be seen that the corrosion rate decreased and inhibition efficiency (E%) increased by increasing inhibitor concentration, may result from the presence of a pair of electron on sulfur atoms which can absorb strongly on the metal surface [32] and also the presence of aroma city of the phenyl and the electron

density at this donor group in your oppositions a single pair of electrons on sulfur atoms. The shifting of E_{corr} indicates that the corrosion inhibitor is an cathodic inhibitor.

Table 1. Corrosion parameters obtained from electrochemical and impedance measurements for mild steel in 20 % H2SO4 containing various concentration of PDTT

	Conc. of PDTT (mM)	Tafel data					Impedance data		
		E_{corr} (mV *vs.* SCE)	i_{corr} (mA cm^{-2})	β_a (mV dec-1)	β_c (mV dec-1)	E %	R_{ct} (Ω cm^2)	C_{dl} (μF cm-2)	η (%)
Blank	0.000	- 433.5	1.6450	68.5	-73.3	–	1.690	2356.47	–
	0.025	- 457.0	0.8054	29.2	-40.9	51.04	1.448	1337.00	43.30
	0.050	-458.1	0.2620	31.0	-35.3	84.10	1.886	1176.00	50.10
	0.076	-451.9	0.1483	107.3	-99.6	91.03	16.000	391.32	83.39
	0.101	-447.2	0.1272	77.0	-95.6	92.27	24.540	259.56	88.98
	0.126	-438.8	0.0551	62.4	-90.3	96.65	48.740	51.62	97.81

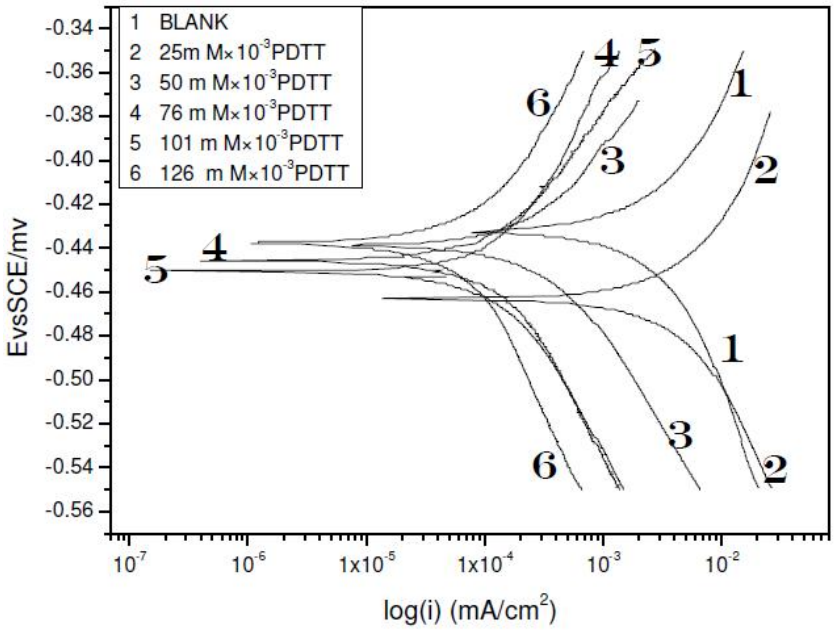

Fig. 2. Typical potentiodynamic polarization curves for mild steel in 20% H2SO4 containing different concentrations of PDTT at 25ºC

Impedance measurement of the mild steel electrode at its open circuit potential after 1 h of immersion in 20% H_2SO_4 solution with and without PDTT inhibitor were performed over the frequency range from 10^5 Hz to 10^{-3} Hz. Fig. 3 shows the obtained Nyquist plots of mild steel in 20% H_2SO_4 solution in absence and presence of different concentration of PDTT These curves show a typical set of Nyquist plots. It is clear from these plots that the impedance response of carbon steel has significantly changed after addition of the synthesized inhibitors in the corrosive media. This indicates that the impedance of an inhibited substrate increases with increasing concentration of inhibitor in 20% H_2SO_4.

The impedance parameters, solution resistance, charge transfer resistance Rct and double-layer capacitance (C_{dl}), are listed in Table 1. The Nyquist plots obtained in the real system represent a general behavior where the double layer on the interface of metal/ solution does not behave as a real capacitor. On the metal side electrons control the charge distribution whereas on the solution side it is controlled by ions. As ions are much larger than electrons, the equivalent ions to the charge on the metal will occupy quite a large volume on the solution side of the double layer [22] (Table 1).

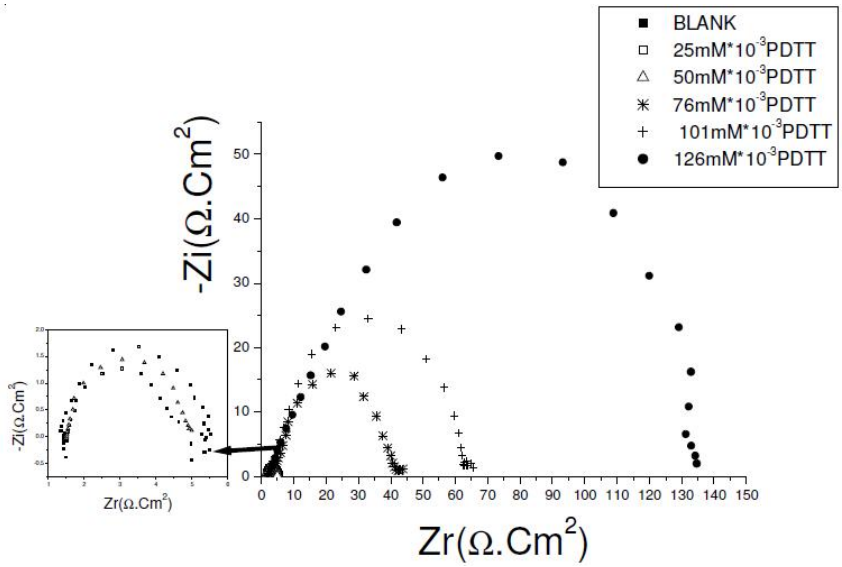

Fig. 3. Nyquiste plots of mild steel recorded in 20% H_2SO_4 containing different concentrations of PDTT at 25ºC

$$\eta = \frac{R_t^{-1} - R_{t(inh)}^{-1}}{R_t^{-1}} \times 100 \quad (2)$$

The double-layer capacitance (C_{dl}) was calculated from the following equations [23]:

$$f(-Z''_{max}) = \frac{1}{2\pi C_{dl} R_t} \quad (3)$$

where f(-Zimg) is the frequency at maximum imaginary component of the impedance and Rct are the charge transfer resistances.

Where Rt(inh) and Rt are the charge transfer resistance values with and without inhibitor for mild steel in acidic media respectively [26]. The impedance parameters derived from this investigation are given in Table 1.

As the PDTT concentration increased, Rt values increased, but C_{dl} values tended to decrease Table 1. The decrease in C_{dl} values was due to the adsorption of PDTT on the metal surface. The inhibition efficiency η reached 97.81% in 20% H_2SO_4 at 126 × 10^{-3} mM of inhibitor. The inhibition efficiency in 20% H_2SO_4 was lower. This was presumably caused by the lower surface coverage of the inhibitor on the mild steel surface in the 20% H_2SO_4 solution.

It is clear that charge transfer resistance Rct values were increased and the capacitance values C_{dl} decreased with increasing inhibitors concentration. Decrease in the capacitance, which can result from a decrease in local dielectric constant and/or an increase in the thickness of the electrical double layer, suggests that the inhibitor molecules.

Act by adsorption at the metal/solution interface [22]. The addition of the synthesized surfactants provides lower C_{dl} values, probably as a consequence of replacement of water molecules by the synthesized inhibitors at the electrode surface. The inhibitor molecules may also reduce the capacitance by increasing the double layer thickness according to the Helmholtz model [22].

The value of C_{dl} is always smaller in the presence of the inhibitor than in its absence, as a result of the effective adsorption of the synthesized inhibitors.

Results obtained from EIS measurements are in good agreement. The real part (Z') and imaginary part (Z") of the cell impedance were measured in ohms at various frequencies.

With that obtained from potentiodynamic polarization electrochemical impedance spectroscopy and polarization curves measurements were repeated several times and observed that they were highly reproducible.

Inhibition mechanism, the primary step in action of inhibition in acid solution is generally agreed to be adsorption on to the metal surface, which is usually oxide free in acid solution. The adsorption of inhibitor species (Inh) on the metal surface in aqueous solution should be considered a place exchanger reaction:

$$Inh_{aq} + xH_2O_{ads} \rightleftharpoons Inh_{ads} + xH_2O_{aq} \quad (4)$$

Where x the size ratio is the number of water molecules displaced by one molecule of organic inhibitor. When the equilibrium of the process described in eqn. 4 is reached, it is possible to obtain different expression of the adsorption isotherm plots and thus the degree of surface coverage θ = E %/100. Can be plotted as a function of the inhibitor under test [33].

It is well recognized that the first step in inhibition of metallic corrosion is the adsorption of organic inhibitor molecules at the metal/solution interface and that the adsorption depends on the molecule's chemical composition, the temperature and the electrochemical potential at the metal/solution interface. In fact, the solvent H_2O molecules could also adsorb at metal/solution interface so the adsorption of organic inhibitor molecules from the aqueous solution can be regarded as a quasi-substitution process between the organic compounds in the aqueous phase [$Org_{(aq)}$] and water molecules at the electrode surface [$H_2O_{(ads)}$] [34].

$$Org_{(aq)} + xH_2O_{ads} \rightleftharpoons Org_{(ads)} + xH_2O_{(aq)} \quad (5)$$

where x is the size ratio, *i.e.*, the number of water molecules replaced by one organic inhibitor. Basic information on the interaction between the inhibitor and the mild steel surface. It is well recognized that organic inhibitor molecules set up their inhibition action *via* the adsorption of the inhibitor molecules onto the metal/solution interface. The adsorption process is affected by the chemical structures of the inhibitors, the nature and charged surface of the metal and the distribution of charge over the whole inhibitor molecule. In general, owing to the complex nature of adsorption and inhibition of a given inhibitor, it is not possible for single adsorption mode between inhibitor and metal surface. Organic inhibitor molecules may be adsorbed on the metal surface in one or more of the following ways: (a) Electrostatic interaction between the charged molecules and the charged metal; (b) Interaction of unshared electron pairs in the molecule with the metal and (c) Interaction of π-electrons with the metal.

The inhibition efficiency afforded by 4-phenyl-1,2-dithiol-3-thione may be attributed to the presence of electron rich sulfur and aromatic rings [34].

Langmuir isotherm for monolayer chemisorptions is given by the following equation [35]:

$$C_{inb}/\theta = 1/K_{ads} + C_{inb} \quad (6)$$

where K_{ads} is the equilibrium constant of the adsorption/desorption process. The plots of C_{inb}/θ. C_{inh} yield straight line with nearly unit slope showing that the adsorption of PDTT can be fitted to Langmuir adsorption as presented in Fig. 4. Adsorption equilibrium constant (K_{ads}) and free energy of adsorption (ΔG^{o}_{ad}) were calculated using the relationships [35]:

$$K_{ads} = 1/C_{inb} \times [\theta/(1-\theta)] \quad (7)$$

$$\Delta G^{o}_{ad} = 2.3RT \log (55.5\ K_{ads}) \quad (8)$$

The value of 55.5 is the molar concentration of water in solution the values of adsorption equilibrium constant (K_{ads}) and free energy of adsorption (ΔG^{o}_{ad}).

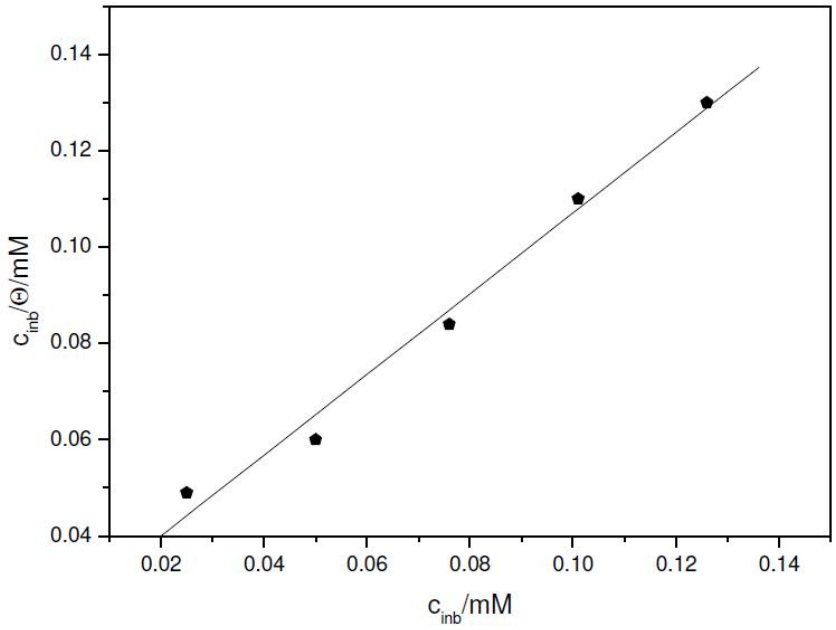

Fig. 4. Langmuir's isotherm plots for the adsorption of PDTT and on the surface of mild steel in 20 % H_2SO_4

The negative values of ΔG^{o}_{ad} indicate spontaneity of the adsorption process and stability of the adsorbed layer on the metal surface. Literature reveals that with regard to energetic of the adsorption process: Two types of adsorption process had been established, physisorption (electrostatic interaction between the charged molecules and charge metal) in which the ΔG^{o}_{ad}, is up to -20 kJ mol^{-1} and chemisorptions (charge sharing or transfer from the inhibitor (adsorb ate) molecules to the metal surface to form co-ordinate bond) where the ΔG^{o}_{ad} is more negative than -40 kJ mol-1.

The calculated standard free energy of adsorption ΔG^{o}_{ad} in the case of PDTT is -37.38 kJ mol^{-1} therefore, lower than -20 KJ mol^{-1}. This indicates that the adsorption mechanism is neither typical physisorption nor typical chemisorptions, but it is complex mixed type that is the adsorption of the investigated 4-phenyl-1,2-dithiol-3-thione (PDTT) on the mild steel surface in 20% H_2SO_4 involves both physisorption and chemisorptions but chemisorptions is predominant mode of adsorption [34].

4. CONCLUSION

The studied 4-phenyl-1, 2-dithiol-3-thione (PDTT) cation shows remarkable inhibition properties for the corrosion of mild steel in 20% H_2SO_4 at 25ºC and the inhibition efficiency increases with increasing of the PDTT concentration. The inhibitor efficiencies determined by weight loss, Tafel polarization and EIS methods are in reasonable agreement. Based on the polarization results, the investigated (PDTT) can be classified as cathodic inhibitor. The EIS spectra are well described by a relatively simple structural model having only one time constant. The calculated structural parameters show increase of the obtained R_{ct} values and decrease of the capacitance, C_{dl}, with PDTT concentration increase. It is suggested to attribute this to the increase of the thickness of the

adsorption layer a steel surface. The adsorption model obeys to the Langmuir adsorption isotherm and the negative value of the Gibbs free energy of adsorption (ΔG^{o}_{ad}) indicates that the adsorption of the PDTT is a spontaneous process. High negative value suggests that the inhibitive effect of 4-phenyl-1, 2-dithiol-3-thione (PDTT) is due to the formation of a chemisorbed film on the metallic surface and can be used as an excellent corrosion inhibitor for steel in acidic medium at room temperature.

COMPETING INTERESTS

Authors have declared that no competing interests exist.

REFERENCES

1. Hadjadj M, Dadamoussa B, Abasq ML, Saidi M, Burgot JL, Darchen A. Radical scavenger properties of some 1, 2-dithiol compounds against electropolymerization of aniline. Asian J. Chem. 2010;22:501.
2. Munday R, Zhang Y, Ch. M. Munday, Li J. Structure-activity relationships in the induction of phase II enzymes by derivatives of 3H-1,2-dithiole-3-thione in rats. Chem.-Biol. Interact. 2006;160:115.
3. Abasq ML, Saidi M, Burgot JL, Darchen A. Substituent effects of 1, 2-dithiole groups on the electrochemical oxidation of some ferrocenyl-1, 2-dithiole compounds, J. Organomet. Chem. 2009;694:36.
4. Burgot G, Bona M, CHristen MO, Burgot JL. Correlations between n-Octanol/Water partition coefficients and RP-HPLC capacity factors of 1,2-dithiole-3-thiones and 1,2-Dithiol-3-ones. Int. J. Pharmaceut. 1996;129:295.
5. Chua Y, Zhang D, Boelsterli U, Moore Ph. Oltipraz-induced phase 2 enzyme response conserved in cells lacking mitochondrial DNA, Biochem. Biophys. Res. Commun. 2005;337:375.
6. Pouzaud F, Christen MO, Warnet JM, Rat P. Anethole dithiolethione: An antioxidant agent against tenotoxicity induced by fluoroquinolones, Pathol. Biol. 2004;52:308.
7. Abasq M, Burgot J, Darchen A, Saidi M. Electrochemical behaviour of some 3-methylthio-1, 2-dithiolium cations in dimethylformamide solution, Electrochim. Acta. 2005;50:2219.
8. Khaled KF. An electrochemical study for corrosion inhibition of iron by some organic phosphonium chloride derivatives in acid media Appl. Surf. Sci. 2004;230:307.
9. Raja PB, Sethuraman MG. Inhibitive effect of black pepper extract on the sulphuric acid corrosion of mild steel**,** Mater. Lett. 2008;62:2977.
10. Umoren SA, Solomon MM, Udosoro II, Udoh AP. Synergistic and antagonistic effects between halide ions and carboxymethyl cellulose for the corrosion inhibition of mild steel in sulphuric acid solution Cellulose. 2010;17:635.
11. Obot IB. Synergistic effect of nizoral and iodide ions on the corrosion inhibition of mild steel in sulphuric acid solution. Portugal. Electrochim. Acta. 2009;27:539.
12. Monika, Siddique WA. Inhibiting effect of tetra-n-butylammonium iodide on the corrosion of mild steel in acidic medium, Portugal. Electrochim. Acta. 2007;25:443.
13. Larbi L, Benali O, Harek Y. Corrosion inhibition of copper in 1 M HNO3 solution by N-Phenyl oxalic dihydrazide and oxalic N-Phenylhydrazide N'-Phenylthiosemicarbazide, Portugal. Electrochim. Acta. 2006;24:337.
14. Tuken T, Yazici B, Erbil M. The effect of nicotinamide on iron corrosion in chloride. Solutions Turk. J. Chem. 2002;26:735.
15. Valek L, Martinez S. Copper corrosion inhibition by *Azadirachta indica* leaves extract in 0.5 M sulphuric acid, Mater. Lett. 2007;61:148.
16. Sherif EM, Park SM. Effects of 1,5-naphthalenediol on aluminum corrosion as a corrosion inhibitor in 0.50 M NaCl. J. Electrochem. Soc. 2005;152:B205.
17. Al-Mayouf AM, Al-Suhybani AA, Al-Ameery AK. Corrosion inhibition of 304SS in sulfuric acid solutions by 2-methyl benzoazole derivatives, Desalination. 1998;116:26.
18. Bekkouch K, Aouniti A, Hammouti B, Kertit S. Inhibition de la corrosion d'acier au carbone en milieu H3PO4 2M par des composés organiques de type "triazine". Journal de Chimie Physique et de Physico-Chimie Biologique. 1999;96:838.

19. Benchekroun K, Dalard F, Rameau JJ, El. Ghazali A. Inhibition de la corrosion du fer dans HCL 1 M. Partie II. Etude des propriétés inhibitrices du 2-aminothiophénol et du 2-aminophényl disulfure, par spectroscopie d'impédance, New J. Chem. 2002;26:946.
20. Tantawy N. Evaluation of new cationic surfactant as corrosion inhibitor for carbon steel in a metal working fluid, The Annals Of University Dunarea De Jos. 2005;112.
21. Da Silva AB, D'Elila E. Carbon steel corrosion inhibition in hydrochloric acid solution using a reduced Schiff base of ethylenediamine J.A. da cunha Ponciano Gomes, Corros. Sci. 2010; 52:788.
22. Hegaz MA. A novel Schiff base-based cationic gemini surfactants: Synthesis and effect on corrosion inhibition of carbon steel in hydrochloric acid solution. Corros. Sci. 2009;51:2610-2613.
23. Larbi L, Benali O, Harek Y. Corrosion inhibition of cold rolled steel in 1 M $HClO_4$ solutions by N-naphtyl N′-phenylthiourea, Mater. Lett. 2007;61:3288,3287.
24. Quraishi MA, Rawat J. Development and testing of an improved pickling inhibitor formulation for hot 20% sulfuric acid , Mater. Performance. 2001;42:40.
25. Jeyprabha C, Sathiyanarayanan S, Venkatachari G. Corrosion inhibition of pure iron in 0.5M H_2SO_4 solutions by ethanolamines, Appl. Surf. Sci. 2001;108:246.
26. Bentiss F, Traisnel M, Lagrenée M. Inhibitor effects of triazole derivatives on corrosion of mild steel in acidic media Br, Corros. J. 2000;35:315.
27. Bentiss F, Jama C, Mernari B, El Attari H, El Kadi L, Lebrini M, Traisnel M, Lagrenée M. Corrosion control of mild steel using 3,5-bis(4-methoxyphenyl)-4-amino-1,2,4-triazole in normal hydrochloric acid medium ,Corros. Sci. 2009;51:1628,1629,1630.
28. Kadiri C, Mokhtar S, Benbertal D, Ameur K. J. Saudi Chem. Soc. 2006;10:549.
29. Bentiss F, Traisnel M, Lagrenée M. Influence of 2,5-bis(4-dimethylaminophenyl)-1,3,4-thiadiazole on corrosion inhibition of mild steel in acidic media. J. Appl. Electrochem. 2001;31: 41.
30. Fields EK. Synthesis of 4-Aryl-1,2-dithiole-3-thiones by Reaction of Cumenes with Sulfur. J. Am. Chem. Soc. 1955;77:4255.
31. Morad MS, Sarhan AAO. Application of some ferrocene derivatives in the field of corrosion inhibition ,Corros. Sci. 2008;50:744.
32. Saidi M. Thèse de Docteur d'Etat de l'Université de Rennes. 1988;1:239.
33. Noor EA. Temperature effects on the corrosion inhibition of mild steel in acidic solutions by aqueous extract of fenugreek leaves. Int. J. Electrochem. Sci. 2007;2:1002.
34. Ahamad I, Prasad R, Quraishi MA. Inhibition of mild steel corrosion in acid solution by Pheniramine drug: Experimental and theoretical study. Corros. Sci. 2010;52:1474,1479,1480.
35. Singh AK, Quraishi MA. Inhibitive effect of diethylcarbamazine on the corrosion of mild steel in hydrochloric acid. Corros. Sci. 2010;52:1531.

Biography of author(s)

M. Dakmouche
Laboratoire de Valorisation et Promotion des Ressources Sahariennes, Université Kasdi Merbah de Ouargla, 30000 Ouargla, Algeria.

Research and Academic Experience: I am a doctor in university

Research Area: Algeria

Number of Published papers: 15 Publications

© Copyright (2020): Author(s). The licensee is the publisher (Book Publisher International).

DISCLAIMER
This chapter is an extended version of the article published by the same author(s) in the following journal.
Asian Journal of Chemistry, 24(11): 4887-4891, 2012.

Chapter 8
Print ISBN: 978-93-90206-41-4, eBook ISBN: 978-93-90206-42-1

The Use of Spectrophotometric and Thermodynamic Methods for the Determination of Glibenclamide

Nwanisobi Gloria[1*] and Ukoha Pius[2]

DOI: 10.9734/bpi/crdc/v4

ABSTRACT

A spectrophotometric and thermodynamic method is described for the assay of glibenclamide. The method involves a charge transfer complexation reaction between glibenclamide with 2,3-Dichloro-5,6-Dicyano-1,4-benzoquinone (DDQ) to form very intense coloured charge transfer complex having a stoichiometric ratio of 1:1. The resultant coloured product was analyzed at 474 nm under the optimized experimental conditions. Over the concentration range of 20-100 µg/ml, Beer - Lambert's law was obeyed. The apparent molar absorptivity was calculated and found to be 0.99×10^3 $L.mol^{-1}cm^{-1}$. The corresponding Sandell's sensitivity, Limits of detection and quantification were reported. Also, the thermodynamic parameters were determined. The proposed method was applied successfully to the determination of glibenclamide in pure and commercial forms with good average recovery of 98.24%. Statistical comparison was done using student t-test and f-test at 95% confidence level.

Keywords: Glibenclamide; spectrophotometry; thermodynamics; charge transfer; DDQ.

1. INTRODUCTION

1.1 Charge Transfer Complex

The term charge transfer denotes a certain type of complex which results from interaction of an electron acceptor and an electron donor with the formation of weak bonds [1]. Charge Transfer (CT) complexes have been widely studied [2-7]. 2,3-Dichloro-5,6-Dicyano-p-benzoquinone (DDQ) is an oxidizing [8], dehydrating agent in synthetic organic chemistry as well as it is known for its interaction with drugs having donor sites in their structures and form ion - pair charge transfer complexes which offers a basis for quantification of drugs [9]. DDQ as π-electron acceptor often form highly coloured CT complexes with various donors which provides the possibility of determination of drugs by spectrophotometric methods [10].

1.2 Glibenclamide

Glibenclamide chemically known as 5-chloro-n-[2-[4[(cyclohexylamino)carbonyl]-amino]sulphonyl] phenyl]-ethyl]-2-methoxy benzamide [11] is a second generation sulphonyl ureas antidiabetic drug used for the treatment of class II diabetes mellitus [12]. The literature survey shows that spectrophotometric methods have been employed for the determination of glibenclamide based on derivatization technique or coupling with another reagent [13,14], High pressure liquid chromatography methods are the most commonly used for the determination of glibenclamide. Fluorescence detection [15], Mass spectrometry [16], Thin layer chromatography [17], Voltametric method [18], Spectrofluorimetric method [19] have all been reported.

[1]Department of Pure and Industrial Chemistry, Faculty of Physical Sciences, Nnamdi Azikiwe University, Awka, Nigeria.
[2]Department of Pure and Industrial Chemistry, Faculty of Physical Sciences, University of Nigeria, Nsukka, Nigeria.
**Corresponding author: E-mail: glochinwa4real@yahoo.com, gc.nwanisobi@unizik.edu.ng;*

1.3 Justification of Study

In the developing country like Nigeria. Drugs are easily adultrated because of the greed of man and crave for wealth. Fake and substandard drugs are usually common and sold commercially at the local markets. This has led to loss of lives. There is need to develop a simple and cost effective method for easy assay of drugs this will invariably reduce the mortality rate and save lives.

1.4 Problem of Study

Some of the methods reported are time consuming, costly and lacks sensitivity. Spectrophotometric technique have been reported to be the most preferred methods for routine analytical work due to their simplicity and reasonable sensitivity with significant economic advantages [20].

1.5 Aim and Objectives

The aim of this work is to determine a method for the assay of glibenclamide that is fast, simple, sensitive and cost effective. The objectives of this research work are to:

(i). Establish the extent of CT complex formation between Glibenclamide and DDQ
(ii). Determine the optimum conditions that favours the CT complexes with respect to time, temperature and pH.
(iii). Apply the spectrophotometric method in the determination of Glibenclamide
(iv). Calculate the average recoveries of Glibenclamide in pure and commercial forms
(v). Validate the proposed method using International Conference on Harmonization Guideline [21]
(vi). Calculate the thermodynamic parameters

2. MATERIALS AND METHODS

2.1 Instrument

All spectrophotometric measurements were carried out using a UV-1800 Schimadzu and 752W UV-Visible grating spectrophotometer with a silica glass cell of 1 cm thickness.

2.2 Chemicals and Reagents

All chemicals used were of analytical grade and were used as such. Pure glibenclamide and tablet (5 mg) were supplied by Juhel Pharmaceuticals Nig. Ltd., Nigeria. 2,3-dichloro-5,6-dicyano-1,4-benzoquinone (98% purity) was supplied by Sigma- Aldrich Chemie, Germany.

2.3 Determination of optimum conditions for the formation of glibenclamide - DDQ complex

3 ml solution of DDQ (0.001 g/ml) was made in methanol and the wavelength of maximum absorption was determined. 3 ml of glibenclamide (0.001 g/ml) was made in methanol and the wavelength of absorption was determined. A colour was developed by mixing 2 ml of DDQ (0.001 g/ml) solution in methanol with 2 ml of glibenclamide (0.001 g/ml) solution in methanol and the wavelength of maximum absorption for the resultant solution was determined. Another mixture with a 1:1 ratio of DDQ and glibenclamide were prepared and absorbencies were measured at different time and temperatures against a blank. Between pH 1-13, the effect of pH on the formation of glibenclamide-v DDQ complex was investigated. In addition, different concentrations of the complex were prepared and their absorbance measured at the detected optimum conditions against the blank prepared above.

2.4 Proposed General Procedure

Transfer serial volumes of 0.036 ml to 0.4 ml in 0.04 step of the standard glibenclamide (0.001 g/ml) solution equivalent to 9.0 µg/ml-100 µg/ml into different test tubes. Add 0.2 ml each of buffer 2 into the set up with 2 ml of methanol. Add equal volumes of DDQ (0.001 g/ml) solution in methanol according to the stoichiometry of the drug and reagent. Mix the content and allow standing for 35 min at 40°C before analysis at 474 nm against a methanol blank.

2.5 Determination of Association Constant, Molar Absorptivity, Free Gibbs Energy and Benesi- Hildebrand plot of Glibenclamide-DDQ Complex

A constant volume of 0.4 ml of glibenclamide (1.0×10^{-3} M) was transferred into five different test-tubes and made up to 4 ml according to calculation. Varied volumes of (0.4, 0.6, 0.8, 1.0 and 1.2 ml) of 1.0×10^{-2} M of DDQ solution were added into the set-up containing the drug each to represent at least 10 fold in excess of the acceptor. The content was thoroughly mixed and left to stand for 35 min before their absorbance were determined at 474 nm against a methanol blank at room temperature. Further analysis of the reaction mixtures were done by subjecting them to temperatures of 40°C, 50°C and 60°C using a thermo stated water bath.

2.6 Assay Determination of Glibenclamide - DDQ Complex

Two glibenclamide tablets were grounded on a mortar. An amount equivalent to 0.01 g was dissolved with some methanol, stirred to extract the active ingredient. It was filtered with Whatman no. 1 filter paper and later made up to 10 ml to give 0.001 g/ml theoretical concentration. Serial volumes similar to the one prepared for the above procedure were transferred to different test tubes and treated similarly before analysis at 474 nm against a methanol blank.

3. RESULTS AND DISCUSSION

3.1 Absorption Spectra

A 2,3-dichloro-5-6-dicyano-1,4-benzoquinone solution in methanol displayed an absorption peak at 350 nm (Fig. 1).

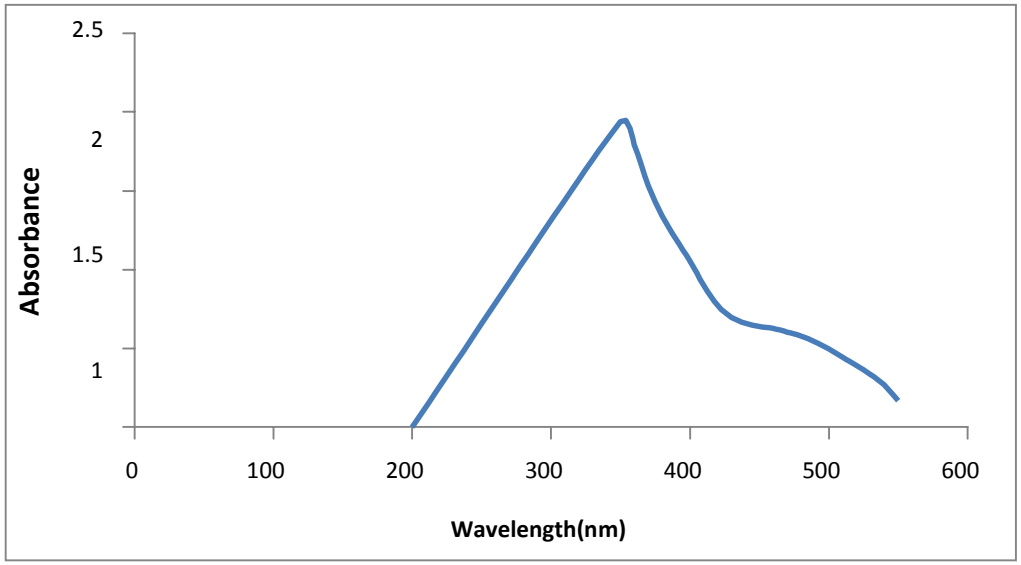

Fig. 1. Absorption spectra of DDQ

Glibenclamide showed absorption peaks at 229 nm and 299 nm (Fig. 2).

Similarly, mixing the solutions of glibenclamide in methanol to a solution of DDQ in methanol forms a reddish brown colouration and causes a bathochromic shift in the absorption maxima to 474 nm (Fig. 3).

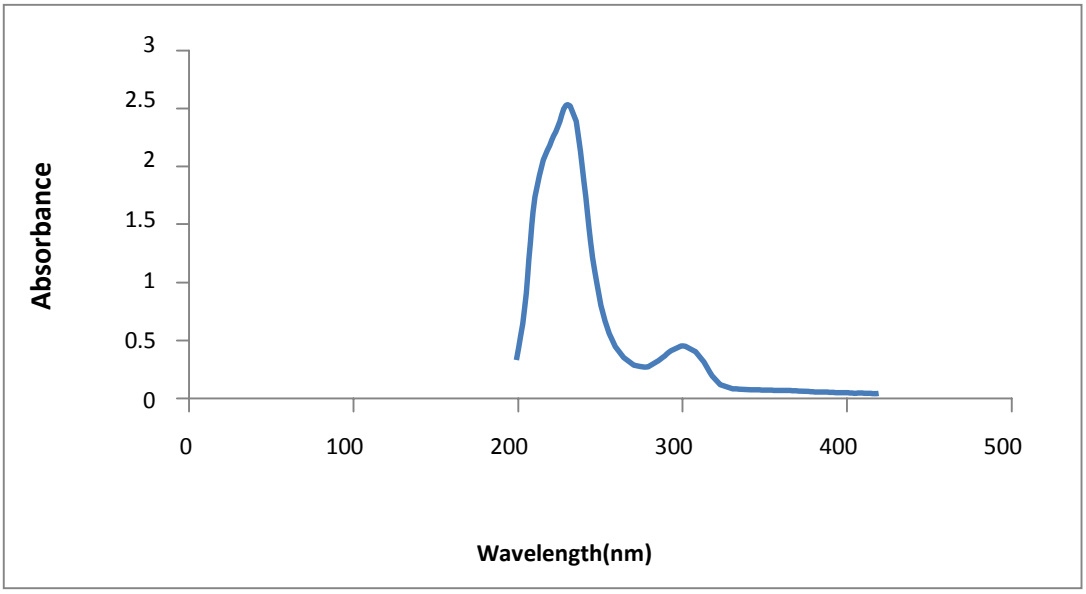

Fig. 2. Absorption spectra of glibenclamide

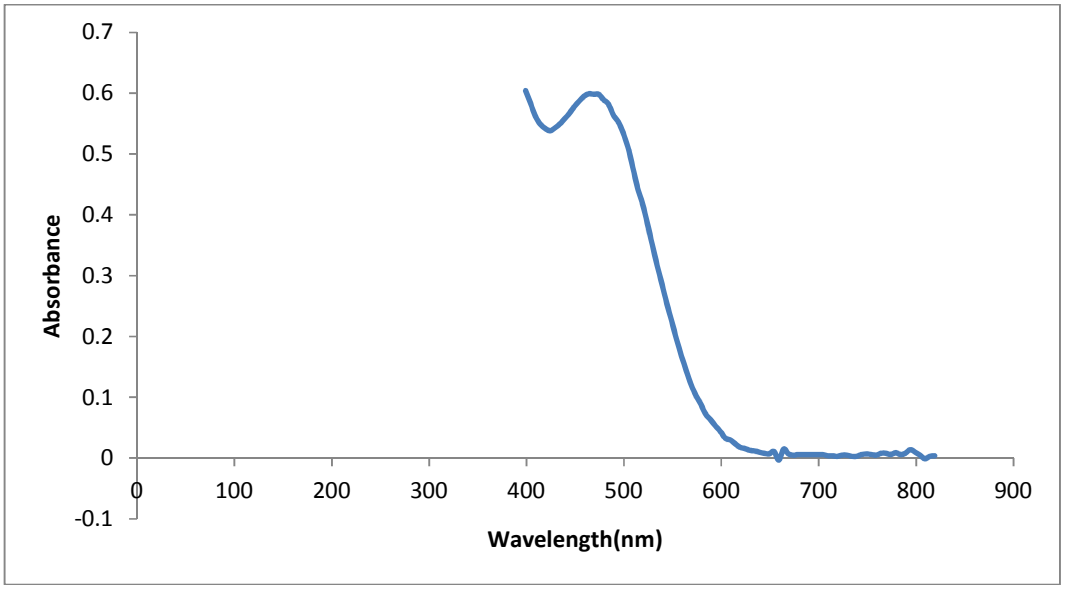

Fig. 3. Absorption spectra of glibenclamide - DDQ complex

3.2 Stoichiometry of Glibenclamide -DDQ complex

The mole ratio method [22] was used to establish the composition of the complex. Result indicates a 1:1 complex formation between glibenclamide and DDQ at 474 nm (Fig. 4). Similarly, mixing the solutions of glibenclamide in methanol to a solution of DDQ in methanol causes a bathochromic shift in the absorption maxima to 474 nm (Fig. 4). A reddish brown colouration was observed upon the

complex formation. Earlier reports had suggested charge transfer complex formation as reason for such new absorption peaks [23]. In addition, charge transfer complex forming reactions occurs when л- acceptors reacts with basic nitrogenous compounds, acting as n-donors. An absorption peak was similarly observed at 418 nm in a reported work involving glibenclamide and bromocresol purple [24]. In addition, this ratio may be attributed to the fact that only one amino group present in the drug is responsible for the product formation.

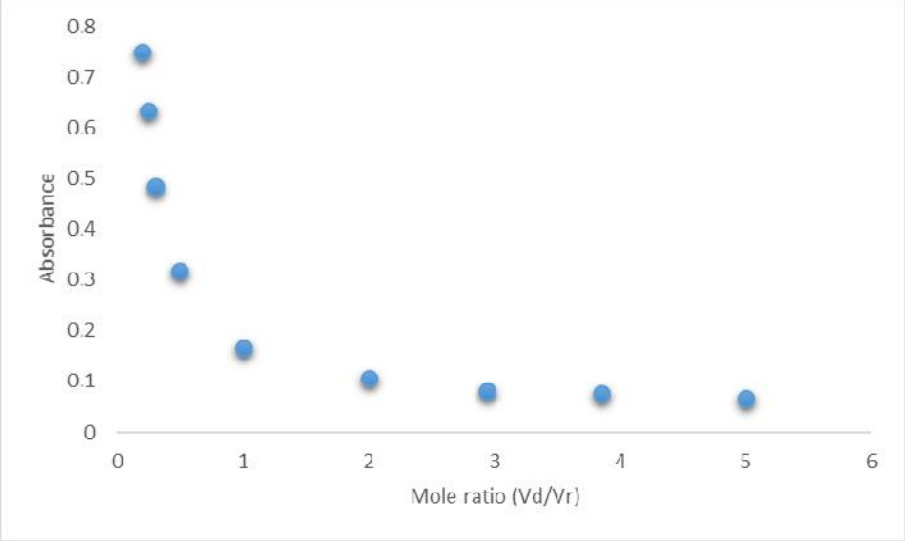

Fig. 4. Mole ratio of the drug (Vd/Vr) (Where Vd and Vr are the volumes of added Glibenclamide and DDQ respectively)

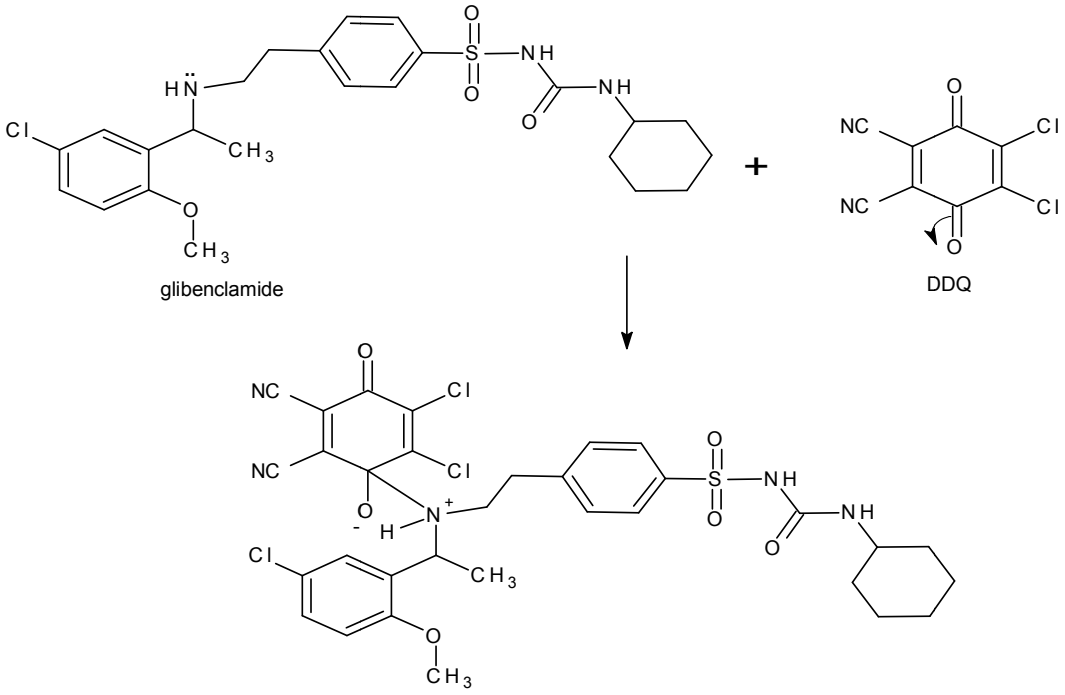

Scheme 1. Interaction of glibenclamide with DDQ to form the charge transfer complex

3.3 Effect of Charge Transfer Complexation for the Determination of Glibenclamide in Different Solvents

Glibenclamide was dissolved in different solvents by mixing solutions of glibenclamide in ethanol, chloromethane and ethylacetate with DDQ in methanol respectively (Fig. 5, Fig. 6 and Fig. 7). These showed peaks at 469 nm, 479 nm, 499 nm respectively. Comparing the wavelength of absorption of the complexes formed by glibenclamide and DDQ in different solvents shows that glibenclamide in ethylacetate had a greater shift which could be due to the polarity of the solvent. Glibenclamide in ethylacetate is considered to be the ideal solvent for the colour reaction as it offers solvent capacity and gave the highest yield of the radical as indicated by high molar absorptivity values.The dissociation of the donor - acceptor complex has been reported to promote the ionizing power of the polar solvent, ethylacetate as a result of its high dielectric constant [25], however glibenclamide in methanol - DDQ in methanol solvent was chosen due to its availability and low cost.

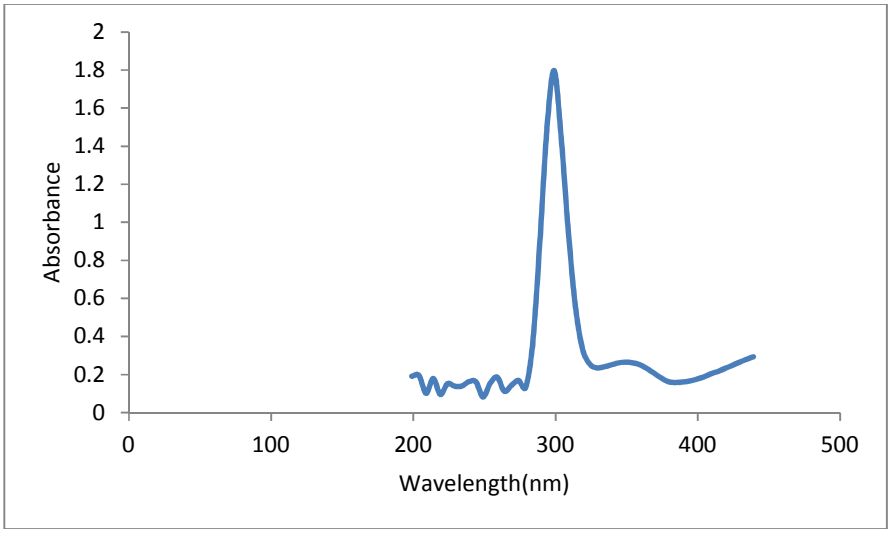

Fig. 5. Absorption spectra of glibenclamide in ethanol - DDQ in methanol complex

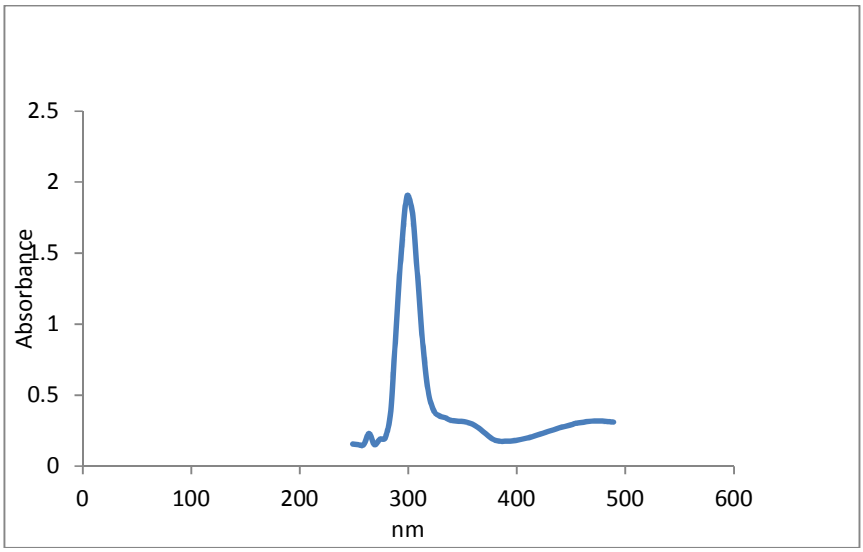

Fig. 6. Absorption spectrum of glibenclamide in chloromethane-DDQ complex in methanol

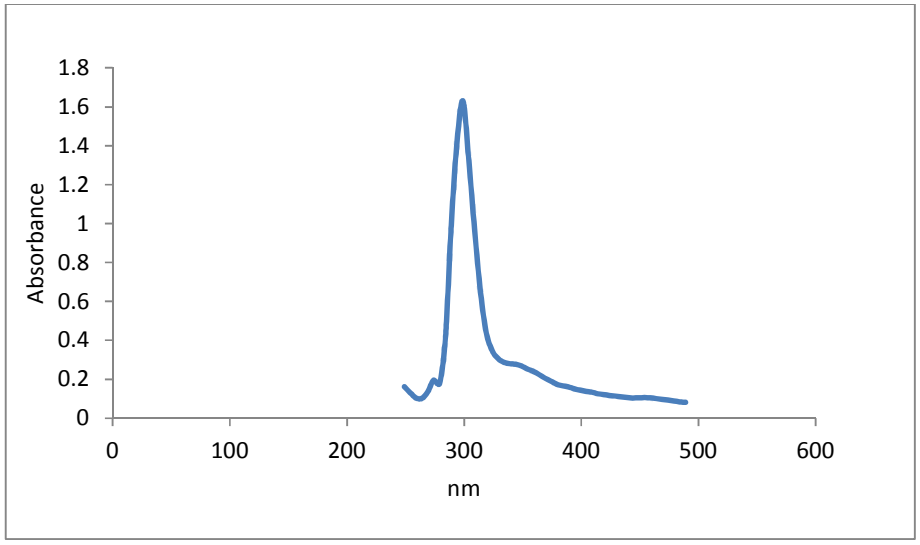

Fig. 7. Absorption spectrum of glibenclamide in ethylacetate – DDQ complex in methanol

3.4 Effects of Time on Glibenclamide - DDQ Complex

The absorbances of complex were slightly stable for 30 min as was obtained by the plot of the absorbance against time (Fig. 8). The optimum reaction time required for complete colour formation monitored at room temperature was at 35 min.

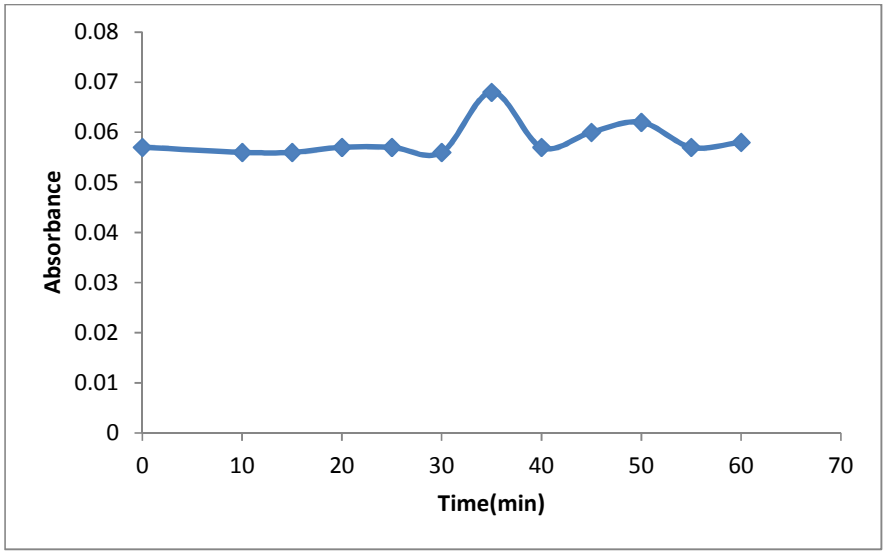

Fig. 8. Time of complex formation of glibenclamide complex

3.5 Effect of Temperature on the Formation of Glibenclamide - DDQ Complex

The plot of absorbance versus temperature for the glibenclamide - DDQ complex (Fig. 9) shows its maximum peak at 40°C, the effect of temperature on the formation and stability of the complex is easily seen from the result. Most reactions are faster when the operating temperature is increased. Increase in temperature has been equated to the increase in the collision of the reacting particles and

hence the rate of the reaction. The reaction was exothermic which reveals a great disorder, the combined changes in the enthalpy and entropy will lead to a large decrease in free energy, making the reaction spontaneous.

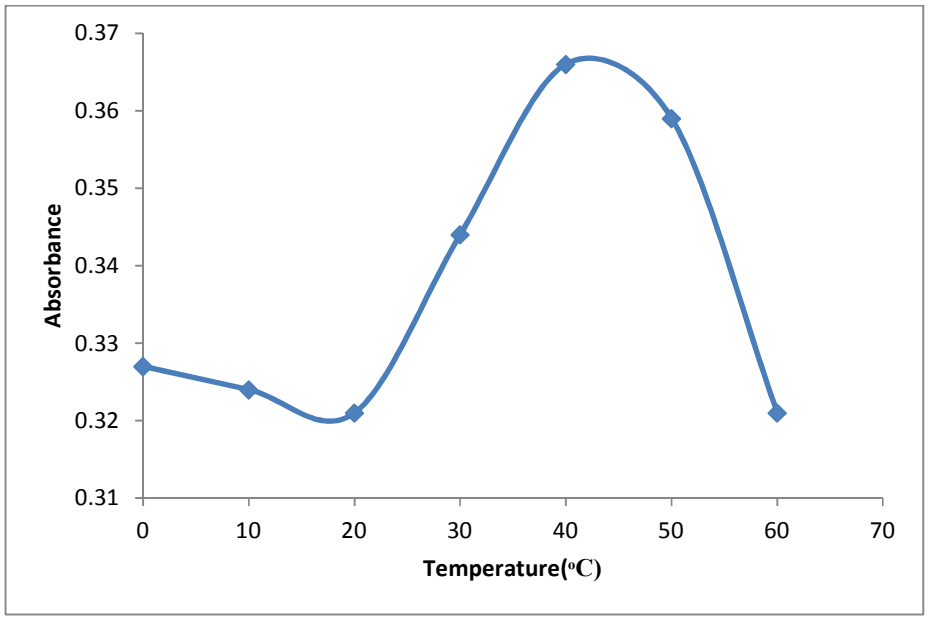

Fig. 9. Effect of temperature on formation of Glibenclamide-DDQ complex

3.6 Effect of pH Medium on Formation of the Glibenclamide -DDQ Complex

Between pH 1-13, the effect of pH on the formation of glibenclamide - DDQ complex was investigated It is evident that the maximum is shown to be at pH 2 (Fig. 10), this indicates that the best medium for the formation of this complex is buffer 2. This is similar to the result gotten from a reported work involving Ampicillin and Cloxacillin which had its peak at pH 2 and was stable till pH 8 [26].

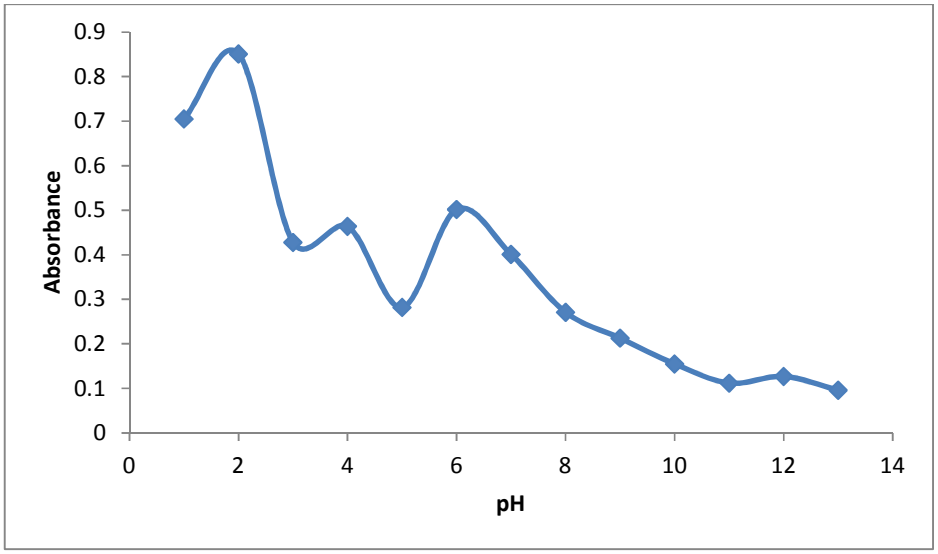

Fig. 10. Effect of pH on formation of glibenclamide -DDQ complex

3.7 Thermodynamic Studies

Based on a 1:1 complex, the thermodynamic parameters were calculated. The association constant of glibenclamide complex was calculated from a single mathematical model:

$$A + B = AB \quad (1)$$

And by application of Ross and labels equation [27] which is modification of Benesi-Hildebrand equation [28].

$$\frac{[A][D]}{[A]+[D]}\frac{1}{A_{\lambda}^{AD}} = \frac{1}{K_{\varepsilon\lambda}}\left(\frac{1}{[A]+[D]}\right) + \frac{1}{\varepsilon_{\lambda}} \quad (2)$$

Where [A] and [D] are the molar concentrations of the acceptor and donor respectively, A_{λ}^{AD} and ε_{λ} are the absorbance and the molar absorptivity of the complex at the specified λ_{max} and K is the association constant of the charge transfer complex. The value of ε_{λ} and K were obtained graphically (Fig. 11) from the slope and intercept of a plot of $\frac{[A][D]}{[A]+[D]}$ against $\frac{1}{[A]+[D]}$.

To minimize error, the slopes and intercepts were determined by the method of least squares fit (Fig. 12).

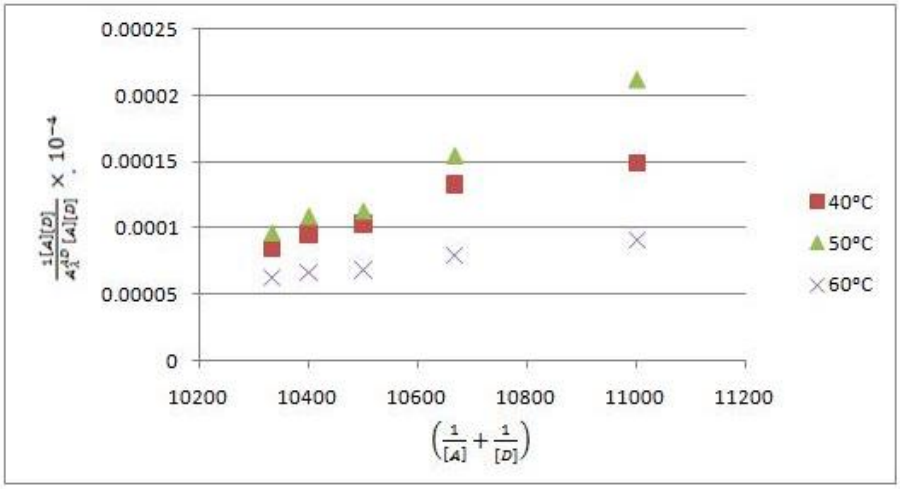

Fig. 11. Benesi plot at different temperatures for the formation of glibenclamide-DDQ complex

The thermodynamic parameters were calculated and results are presented in Table 1. The association constants were found to decrease with increase in temperatures from 40°C to 60°C but at 30°C, the omplex formed was not stable at lower temperatures. Decrease in association constant with increase in temperatures was seen in an earlier preliminary study [29]. A negative free energy change and positive entropy change are indicative of a spontaneous reaction [30] as seen in Table 1. The interaction between glibenclamide - DDQ complexes occured spontaneously as shown by a negative ΔH^{O} reveals the spontaneity of the reaction. The value of ΔH^{O} and the high values of association constant is a pointer that the complexes formed were relatively stable.

3.8 Validity of Beers law

The least square fits of absorbance versus concentration for the glibenclamide - DDQ complex at 474 nm is presented in (Fig. 13). Result follows a linear equation according to equation (3).

$$A_{474nm} = 0.002[D] + 0.008 \quad (3)$$

Where [D] is the concentration of glibenclamide in µg/ml. R^2 has the value of 0.991. This indicates that between the concentration ranges of 20µg/ml - 100µg/ml, Beer-Lambert's law was obeyed. This ensures the possibility of determining the drug within this range of concentration.

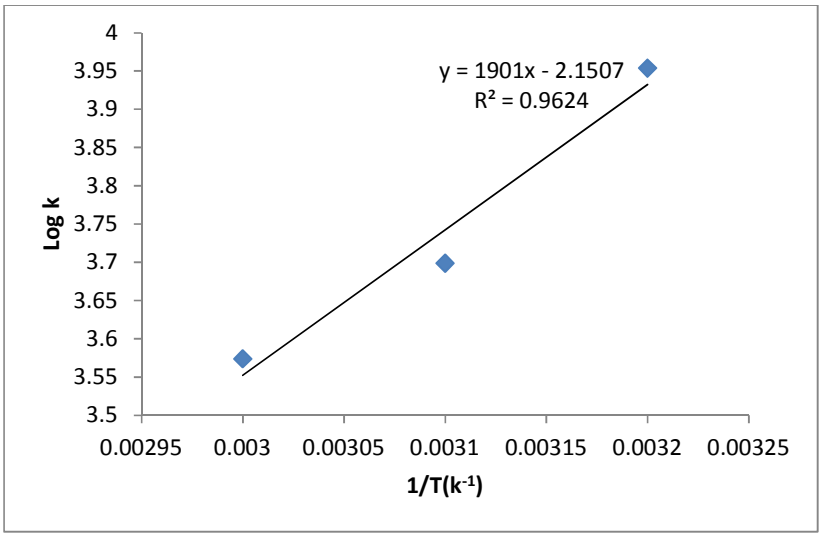

Fig. 12. Log k plot of glibenclamide - DDQ complex

Table 1. Association constant, molar absorptivity, free energy, enthalpy and entropy changes for the formation of the glibenclamide-DDQ complex

K(M^{-1})	ε ($Lmol^{-1}$ cm^{-1})	Log k	T (k)	1/T(k^{-1})	ΔG° (J/mol)	ΔS° (J/mol)
9000	1111.1	3.9542	313	0.0032	-23.70	40.58
5000	1000	3.6990	323	0.0031	-22.88	55.88
3750	3333.3	3.5740	333	0.0030	-22.79	55.95

$\Delta^{\circ}H$ = *36.40kJmol*$^{-1}$

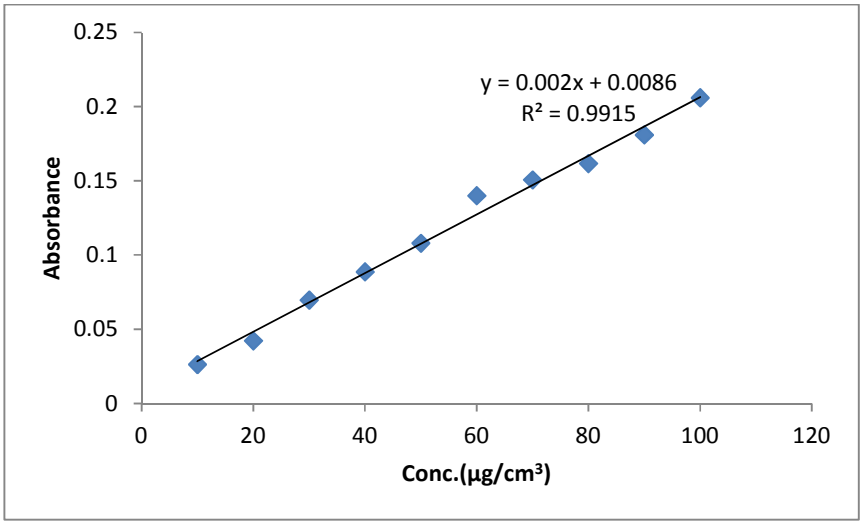

Fig. 13. Beer's plot for the formation of glibenclamide - DDQ complex

This is different from a reported work involving glibenclamide with linearity ranging between 5 -30 µg/cm^3 [31]. The limit of detection and quantification were calculated and found to be 3.47 and 10.5 with Sandell sensitivity of 0.95 and molar absorptivity of 0.99 x 10^3 mol^{-1}cm^{-1}.

3.9 Recovery studies on the formation of glibenclamide-DDQ complex

Table 2 reveals that the percentage recovery of glibenclamide was found to be 98.24% ± 0.011. The relative standard deviation in Table 3 indicates the precision and reliability of the proposed method with a t-test value of 0.71 and f-test value of 0.95 at 95% confidence level which does not differ variably from an earlier report [32].

Table 2. Application of the proposed method for the assay of glibenclamide

Conc. (µg/ml)	Extrapolated Conc. (µg/ml)	[a] Recovery (%)	R.S.D (%)	F -test	T -test
20	19.22	96.14	0.07	0.97	0.71
40	40.72	101.8	0.03		
60	52.57	87.62	0.02		
80	84.77	105.96	0.01		
100	99.68	99.68	0.005		

[a]*Average of five independent analyses*

4. CONCLUSION

The proposed spectrophotometric method for the determination of glibenclamide is simple, rapid, accurate and economical as compared to all the methods used previously. The proposed method has been validated and successfully applied for the determination of glibenclamide with good accuracy of 98.24% ± 0.011. Hence the proposed method is good for the quantitative analysis of glibenclamide.

ACKNOWLEDGEMENT

We are thankful to Juhel pharmaceutical, Nigeria for supplying us with the pure form of the drug.

COMPETING INTERESTS

Authors have declared that no competing interests exist.

REFERENCES

1. Hassib HB, Issa YM. Conductimetric studies of charge transfer complexes of some benzylidine aniline schiff bases with substituted rho-benzoquinones. Egyptian Journal of Chemistry. 1996; 39(4):329-338..
2. Kudige N, Kanakapura B. Acta Poloniae Pharmaceutica. 2012;69:213-223.
3. Chigozie C. Ezeanokete, Kenneth Gerald Ngwoke, Festus Basden C. Okoye, Patience O. Osadebe spectrophotometric determination of ampicillin andcloxacillin in pure and fixed dosage forms through charge transfer complexation. Eur. Chem. Bull., 2013;2(12):1009-1012.
4. Hala H, Eldaroti S, Gadir M, Refat S, Abdel M, Adam A. Int. J. Electrochem. Sci. 2013;8:5774-5800.
5. Frag EY, Mohamed GG, Farag AB, Yussof EB. Utility of π and σ-acceptor reagents for the spectrophotometric determination of cefotaxime sodium antibacterial drug via charge transfer complex formation. Insight Pharmaceutical Sciences. 2011;1(4):47-54.
6. Ramzin I, El-bagary E, Elkady F, Bassam M. Int. J. Biomed. Sci. 2012;3:204.
7. Farha O. J. Baghdad Sci. 2013;10:497-1081.
8. Braude E, Linstead R, Wooldridge K. J. Am. Chem. Soc. 1957;3070-3074.
9. Vmsi K, Gowri S. E-J. Chem. 2008;5:493-498.

10. Khaled E. Spectrophotometric determination of terfenadine in pharmaceutical preparations by charge-transfer reactions. Talanta. 2008;75(5):1167-1174..
11. Cicy E, Prasanth VG, Amita R. Int. J. ChemTech Res. 2012;4:356-360.
12. Adul BM, Swathimutyam P, Padmana A, Bha R, Nalini S, Prakash V. J. Pharm. Biomed. Sci. 2011;8:2230-7885.
13. Nalwaya N. The India Pharmacist. 2008;7:114-118.
14. Martins I, Nery C, Planeti G, Viana J, Vianna C. Braz. J. Pharm. Sci. 2007;43:63-70.
15. Khatri J, Abed O, Abraham B. J. Pharm. Pharm. Sci. 2001;4:201-206.
16. Smgh R, Chang S, Taylor L. Rapid Commun. Mass Spectrum. 1996;10:1019-1026.
17. Kumasaka K, Kojima T, Honda H, Doi K. Screening and quantitative analysis for sulfonylureatype oral antidiabetic agents in adulterated health food using thin-layer chromatography and high-performance liquid chromatography. Journal of Health Science. 2005; 51:453–460.
18. Radi A. J. Anal. Bioanal. Chem. 2004;378:822-826.
19. Karim D, Hassan A. J. Baghdad Sci. 2012;9:296-301.
20. Raza A. Spectrophotometric determination of tranexamic acid in commercial dosage forms. Anal Lett 2006; 39:2217-2226..
21. International conferences on Harmonization of Technical Requirements for Human Use London; 2005.
22. Bauer H, Christian G, Oreilly J. Instrumental Analysis, Allyn and Bacon, Inc. Boston. 1978;178-179.
23. Attama AA, Nnamani PO, Adikwu MU, Akidi FO. Spectrophotometric determination of haloperidol by charge transfer interaction with chloranilic acid S.T.P. Pharma Science. 2008; 13(6):419-421.
24. Parameswarao K, Satynarayana MV, Naga Raju, Ramana GV, Fekria MA. Use of charge transfer complex formation for the spectrophotometric determination of nortrityline, IL Farmaco. 2000;55:659-664.
25. Ramzia IE, Ehab FE, Bassam MA. Spectrophotometric methods based on charge transfer complexation reactions for the determination of saxaliptin in bulk and pharmaceutical preparation, Int. J. Biomed Sci. 2012;8(3):204-204.
26. Ezeanokete CC, Ngwoke GK, Basden Festus, Okoye C, Osadebe PO. Spectrophotometric determination of ampicillin and cloxacillin in pure and fixed dosage forms through charge transfer complexation. Eur. Chem. Bull. 2013;2(12):1009-1012.
27. Ross SD, Labes MM. Molecular compounds. VIII. Evidence for the existence of 2: 1 and 1: 2-complexes in chloroform solutions of 1, 3, 5-trinitrobenzene and N, N-dimethylaniline. Journal of the American Chemical Society. 1957;79(1):76-80.
28. Shehadeh M, Hajar T, Deeb M. Jordan J. Chem. 2007;2(2):145-153.
29. Al Obeidi FA, Boorazan HN. J. Pharm. Sci. 1976;65:982-985.
30. Martin AN, Swarbrick J, Cammarata A. Physical pharmacy. 3rd ed. Lea and Febiger, Philadelphia. 1983;108.
31. Cicy E, Prasanth VG, Amita R. Int. J. ChemTech Res. 2012;4:356-360.
32. Sawant R, Ahmed R, Ramdin S, Darade S.Int. Res. J. Pharm. 2012;3: 12-16.

Biography of author(s)

Nwanisobi Gloria
Department of Pure and Industrial Chemistry, Faculty of Physical Sciences, Nnamdi Azikiwe University, Awka, Nigeria.

Research and Academic Experience: Ph.D (Analytical Chemistry), M.Sc. (Analytical Chemistry), B.Sc. (Industrial Chemistry) Analytical Chemistry with special interest in drug assay.

Research Area: Drug Assay and Enviromental Chemistry

Number of Published papers: 15

Any other remarkable point(s): Institute of Chartered Chemist of Nigeria (Member)

Ukoha Pius
Department of Pure and Industrial Chemistry, Faculty of Physical Sciences, University of Nigeria, Nsukka, Nigeria.

Research and Academic Experience: Ph.D (Physical Inorganic Chemistry). MSc(Inorganic-Analytical Chemistry). Coordinator Coordination Chemistry and Inorganic Pharmaceuticals Research Group

Research Area: Coordination Chemistry, Reaction Mechanisms, Materials and Methods for Securing the Environment, Developing New Analytically Techniques.

Number of Published papers: 115 Journal Articles, 15 Proceedings, 4 Books, 6 Monographs

Special Award (If any): Federal Ministry of Science and Technology Award of Excellence (2010).

Any other remarkable point(s): Dean, Faculty of Physical Sciences (2014-2016)
Member National Steering Committee on Leather Policy in Nigeria. Management Committee Member, Federal College of Chemical and Leather Technology, Zaria (1998-2004).Head, Department of Pure and Industrial Chemistry.

© Copyright (2020): Author(s). The licensee is the publisher (Book Publisher International).

Chapter 9
Print ISBN: 978-93-90206-41-4, eBook ISBN: 978-93-90206-42-1

Studies on the Characterisation, Phytochemical and Functional Groups Assay of a Tropical Timber (*Bombax brevicuspe*) Stem

I. P. Udeozo[1*], C. M. Ejikeme[2], A. N. Eboatu[3] and H. I. Kelle[4]

DOI: 10.9734/bpi/crdc/v4

ABSTRACT

The elucidation of *Bombax brevicuspe* wood was analysed for thermal and physico-chemical techniques. The results obtained were as follows: afterglow time 253.67 sec, flame duration 113.33 sec, flame propagation rate $20.3x10^{-2}cm.s^{-1}$, ignition time 2.33 sec, thermal conductivity $51.34x10^{2}$Umoh/cm, electrical conductivity $5.3x10^{-3}Sm^{-1}$, ash content 3.4%, moisture content 29.97%, oven dry density $22.3x10^{-2}$ g.cm^{-3}, water imbibitions (at different time intervals: 30 mins 46.6%, 5hrs 87.6% and 24 hrs 148.9%), etc, Thin Layer Chromatographic (TLC) analysis gave Retardation factor (Rf) value of 0.62 in the chloroform-methanol extract. The phytochemical screening showed the presence of all the tested secondary metabolites except steroids which indicated its therapeutic ability. The Fourier Transform Infrared (FTIR) and Ultraviolet (UV) spectra suggested that the active compound might be 1,2,3-trisubstituted aromatic compound with C=O, O-H and C=N groups attached. The chemical components analysis showed the presence of cellulose 43%, hemicelluloses 20%, lignin 29% and other constituents in their right proportion. From the results, *Bombax brevicuspe* wood could be used for various construction purposes and it also poses some medicinal ability due to the presence of secondary metabolites.

Keywords: Bombax brevicuspe; tropical timber; thermal characteristics; phytochemical and functional groups.

1. INTRODUCTION

Wood is one of the most important natural and endlessly renewable sources of energy which has a major future role as an environmentally cost-effective alternative to burning fossils fuel. Wood energy is gradually penetrating the new energy markets of industrialized countries as a clean and locally available source of energy [1]. The major role of wood is not only the provision of energy but also the provision of energy-sufficient material for our buildings and many other products. In addition, developing wood cells represents one of the most important sinks for excess atmospheric carbon (iv) oxide, thereby reducing one of the major contributors to global warming [2]. Timber for construction is one of the many forest products used around the world [3].

It is the fifth most important product of the world trade. Vast quantities of wood are logged by foresters to provide fuel, fibres (for pulp, paper products and boards) and sawn timbers as commodities [2]. The size of a tree varies with the climate, the depth and type of soil in which it grows [4]. Environmental factors with a direct impact on plant performance (e.g., temperature and nutrients) should be preferred to indirect factors (e.g., elevation and geology), because direct factors are ecologically more comprehensible and have a larger spatial applicability [5,6]. The complex chemical make-up of wood (cellulose, hemicelluloses, lignin and pectins) also makes it an ideal raw material for

[1]*Department of Chemistry, Enugu State University of Science and Technology, Enugu State, Nigeria.*
[2]*Department of Chemical Science, Godfrey Okoye University, Enugu, Enugu State, Nigeria.*
[3]*Department of Pure and Industrial Chemistry, Nnamdi Azikiwe University, Awka, Anambra State, Nigeria.*
[4]*Chemistry Unit, National Open University of Nigeria, Victoria Island, Lagos, Nigeria.*
**Corresponding author: E-mail: ifyjideudeozo@yahoo.com;*

"ligno-chemical" industry. That could replace the petrochemical industry in providing not only plastic and all kinds of chemical products but also food and textile products [2]. The quality of timber depends on its heat resistance, density, moisture content, and susceptibility to insect attacks, workability, grains, colour, porosity and capacity to take polish and vanish [7]. In Nigeria, over 4600 plant species and 350 timbers have been identified [7,8]

Bombax brevicuspe is a plant that belongs to the *Bombacaceae* family with its common names as silk cotton tree, simal red cotton tree, *bombax* in Chinese also known as mumian meaning tree cotton. It is a tall tree of rainforest, 120 ft high with straight bole and small butresses, deciduous, white petals fragrant and fores as habitat. In Nigeria, its Igbo name is akpudele, awori in yoruba and kurya in Hausa [9,10]. Bombacaceae, the bombax or kapok family of flowering trees and shrubs, in the mallow order (Malvales), comprising 27 genera [11]. *Bombax* is a genus of mainly tropical trees in a mallow family, they are native to Western Africa, Indian subcontinent, South East Asia, as well as sub-tropical regions of East Asia and Northern Australia, distinguished from the genus *Ceiba* which has white flower [9]. There is dearth of information on the wood of *Bombax brevicuspe,* as a result, some thermal and variable properties, chemical constituents, phytochemical and functional group assay of the wood were investigated.

2. EXPERIMENTAL

2.1 Sample Collection and Identification

Bombax brevicuspe timber used for this work was collected from timber shed at Ikom in Ikom Local Government Area of Cross River State, the southern part of Nigeria. It was identified by timber dealer, forest officer and confirmed by literature [12].

2.2 Sample Preparation

The timbers were dried in an oven at 105°C for 24 hours before the experiments. Some samples were cut in a saw mill into two different shapes and sizes; splints of dimensions 30 x 1.5 x 0.5 cm and cubes of dimensions 2.5 x 2.5 x 2.5 cm. Some were ground into powder and then stored in a covered plastic container for analysis.

3. METHODS

3.1 Solubility Analysis

The sample solubility was determined by placing 1 g of the sample powder into nine different 250 cm^3 Kjeldahl flasks. 20 cm^3 of different solvents which include cold water, hot water, 1.0M dilute tetraoxosulphate (IV) acid, 1.0M dilute hydrochloric acid, concentrated tetraoxosulphate (IV) acid, concentrated hydrochloric acid, 1% sodium hydroxide, ether and ethanol was added separately to each flask. The mixture was allowed to stand for two hours and later boiled gently in a fume cupboard for one hour, to determine their solubility properties.

3.2 The Thermal and Physical Characteristics

Three oven dry splints of the sample were separately used for the determination of afterglow time, flame duration, flame propagation rate and ignition time. Three 2.5 cm cubes of the sample were separately used for the determination of oven dry density, moisture content, water imbibitions and electrical conductivity while the sample dust was used for the determination of ash content, thermal conductivity, elemental contents, specific gravity, charring temperature and destructive distillation of the wood sample. All were variously deterrmined using American Society for testing and material (ASTM) methods [13,14,15]. At the end of the each analysis, the average obtained values from the three samples were recorded as results.

3.3 The Microelement Composition

In determination of trace metal elements, the method used was atomic absorption spectrophotometer (AAS) model PG 990 manufactured by PG instrument Ltd U.S.A.

3.4 The Phytochemical Compounds

The following secondary metabolites: Resins, steroids, terpenoids, tanins, alkaloids, saponin, flavonoids, glycosides, phlobatannins, carbohydrate and protein were qualitatively and quantitatively determined using the sample dust by the various methods outlined by Harbone [16].

In determining the hydrogen ion concentration (PH), the method outlined by Amadi et al. [17] was used. It was done using electrical PH meter PHS-25 made by Life Care England.

3.5 The Chemical Constituents

Lignins, hemicellulose, cellulose, crude fibre, crude protein, carbohydrate, phenol and destructive distillation of the wood products were quantitatively determined using the sample dust by the various methods outlined by Goering, Vansoest, Oakley and Marzieh [18,19,20].

3.6 The Functional Group Analysis

The TLC, Fourier Transform Infrared and Ultraviolet Spectroscopic methods were used for the determination of functional group present in the sample using the sample chloroform-methanol extracts.

4. RESULTS AND DISCUSSION

4.1 Results

The results obtained are as presented in Tables 1-7.

Table 1. Solubility property of *Bombax brevicuspe*

Solvents	Results
Hot and cold water	Insoluble
1.0M Dilute H_2SO_4	Slightly Soluble
Concentrated H_2SO_4	Slightly Soluble
Concentrated H_2SO_4 + heat	Soluble
1.0M Dilute HCl	Insoluble
Concentrated HCl	Insoluble
Concentrated HCl + heat	Slightly Soluble
1% NaOH	Insoluble
Ethanol	Insoluble
Diethyl ether	Insoluble

4.2 Discussion

Table 1, indicated that *Bombax brevicuspe* wood powder was insoluble in hot and cold water, ethanol, sodium hydroxide, diethyl ether, dilute HCl and concentrated HCl. Slight solubility was detected with heated concentrated HCl, diluted H_2SO_4 and concentrated H_2SO_4. The sample only dissolved in a high temperatured concentrated H_2SO_4. This is in-line with Petterson (2007) who stated that woods are highly resistance and non degradedable by chemicals, though the chemicals can extract some extraneous materials from the wood. The solubilty result showed that *Bombax brevicuspe* wood could only dissolve in hot concentrated H_2SO_4 acids.

Table 2, showed that *Bombax brevicuspe* wood had low afterglow time of 253.67 sec (less than five minutes) which made it less hazardous in fire situations because it wouldn't glow long enough for rekindle to take place. Its flame duration, flame propagation rate and ignition time values indicated that it can moderately sustain combustion. Water imbibitions values at 30 mins 46.6%, 5 hrs 87.6% and 24 hrs 148% intervals showed the capacity of *Bombax brevicuspe* timber to absorb water over a period of time [21]. The oven dry density which is the best single criterion of strength and ash content

values are in line with the ascertain of Desch and Dinwoodie [22] which stated that denser and small ash content timbers are suitable in their use as a source of carbondioxide for internal combustion engine. The ash content value of 3.4% also indicated the presence of some essential mineral elements which is evident in Table 3. The result also showed a high moisture content value of 33.3% which is in-line with Arntzen [23] who stated that, the fiber saturation point usually varies between 21 and 28%. Wood gains and losses moisture as change occurs in the temperature and humidity of the surrounding air. Decrease in moisture content of a wood affects the weight dimensions and strength of the wood and as well affects both the physical and mechanical properties of wood, depending on whether the moisture content is above or below the fiber saturation point. The sample also showed good specific gravity which is a measure of their density and strength. According to Panshin and Dezeeuw [24], increase in specific gravity increases strength properties because internal stresses are distributed among more molecular material. As a result, wood with high specific gravity has high wood strength and high physical and mechanical properties. While those with low specific gravity will have low wood strength and their physical and mechanical properties will be affected too [24]. David et al. [15] explained that specific gravity of wood is based on oven dry weight of the wood and also reflect the presence of gums, resins and extravites which contribute little to mechanical properties.

Table 2. Thermal and physical characteristics of *Bombax brevicuspe*

Parameters	Units	Results
Afterglow time	Sec	253.67
Flame duration	Sec	113.33
Flame propagation rate	$cm.s^{-1}$	20.3×10^{-2}
Ignition time	Sec	2.33
Over dry density	$g.cm^{-3}$	22.3×10^{-2}
Ash content	%	3.4
Thermal conductivity	Umoh/cm	51.34×10^{2}
Electrical conductivity	Sm^{-1}	5.3×10^{-3}
Moisture content	%	29.97
30 mins water imbibitions	%	46.6
5 hrs Water imbibitions	%	87.6
24 hrs water imbibitions	%	148.9
Specific gravity		0.23
Porosity index	%	1.25
PH		6.0
Charring temperature	°C	81 - 92
Wood charcoal	(g)	2.5
Colour		Sandy brown

Table 3. Micro elemental composition % of *Bombax brevicuspe*

Zinc	0.05
Lead	0.08
Cadmium	0.003
Copper	0.01
Sodium	1.07
Calcium	Nil
Magnesium	0.07
Potassium	0.08
Arsenic	0.02
Mercury	0.01

Wood, a thermally degradable and combustible material has its charring as a primary factor that determines the load-carrying capacity of wood in high temperature environment. *Bombax brevicuspe* with high charring temperature of 81-92°C has high ability of load-carrying capacity in high

temperatured environment. The porosity index result indicated the presence of pore spaces in the wood. Pore spaces are filled with either water or air. Smaller pores tend to be filled with water are referred to as capillary porosity while large pores are typically filled with air and are referred to as non-capillary porosity. The porosity index and water imbibition at different intervals results give good estimate of the sample particle compactness and absorptivity [24]. The results showed that *Bombax brevicuspe* is a hardwood that could be very good for construction and other purposes.

Atomic Absorption Spectrophotometric analysis (Table 3) showed the presence of copper, magnesium and potassium which are involved in body enzymatic activities. Potassium also is necessary for proper functioning of the heart, kidney and muscles. Sodium helps in P^H balance of body fluids while zinc is essential for the activity of DNA polymerases, nucleic acid metabolism and cell division [25,26,27,28], arsenic, lead, mercury and cadmium were also present while calcium was absent.

Table 4. Phytochemical composition of *Bombax brevicuspe*

Class of phytochemical compound	Inference
Alkaloids	++
Flavonoids	++
Resins	+
Saponin	+++
Steroids	-
Terpenoids	++
Tannin	++
Carbohydrate	++
Protein	+
Glycoside	+

Key +++ *- highly present*
++ *- moderately present*
+ *- slightly present*
- *- absent*

Table 5. Results of quantitative chemical constituents of *Bombax brevicuspe*

Chemical constituents	Units	Results
Lignins	%	29.0
Hemicellulose	%	20.0
Cellulose	%	43.0
Crude fibre	%	6.2
Crude protein	%	1.55
Carbohydrate	Mg/g	1.62
Phenol	Mg/g	4.46
Tannin	Mg/100g	920
Alkaloids	%	5.6
Flavonoids	%	8.0
Saponins	%	10.2
Oxalate	g/100g	2.92
Total acidity	g/100cm^3	0.33
Cyanogenic glycoside	Mg/100g	356
Lipid	%	6.8
Pyroligneous acid	cm^3	1.75
Wood tar	cm^3	0.2
Wood gas	cm^3	840

Table 6. Thin layer chromatographic characteristics of the extract

Sample	Number of spot	Rf value
Chloroform-methanol extract	1	0.62

Table 7. Fourier Transformed Infrared and Ultraviolet Spectra for *Bombax brevicuspe* Chloroform – methanol extract

Wave number (cm^{-1})	Suspected chromophores
3410.26	O-H stretch for alcohol, phenol and carboxylic acid.
2958.90	C-H stretch for alkanes and aromatics.
2842.20	C-H stretch for alkanes
2511,40	C=N stretch for nitriles
1651.12	C=O stretch for ketones, acid amides and esters.
1408.08	C=C stretch for alkenes and aromatics
1108.14	C-O stretch for alcohols, carboxylic acids and esters
1020.38	C-H deformation bonds for alkyl groups.
λ_{max} 366.50 and 744.50	Indicating highly conjugated trisubstituted aromatic compound

The phytochemical screening result (Table 4) showed the presence of alkaloids, flavonoids, resins, saponin, terpernoids, tannin, protein, glycosides, carbohydrate and absence of steroid. The medicinal values of medicinal plants lie on these phytocompounds and as such produce definite physiological actions in human body. The alkaloids content showed that it can be used as antimycotics and also in the treatment of stomach pains [20]. It has been reported that Flavonoids exhibit an anti-inflammatory, anti-allergic effects, analgesic and anti-oxidant properties [19]. Saponin has been found to be anti carcinogenic, cholesterol reducer and anti-inflammatory substance. Resins are valued for their chemical properties and associated uses as the product of varnishes, adhesives and food glazing agents. Protein indicated high nutritional value of the extract, therefore can help in physical, mental growth and development [18] Tanins are also reported to exhibit anti-inflammatory, gastritics control, irritating bowel disorders and antimicrobial power which heals wounds and stop bleeding [29]. Terpenoids are associated with anti-cancer and also play a role in traditional and alternative medicine such as aromatherapy, antibacterial and other pharmaceutical functions. Resins are valued for their chemical properties and associated uses as the product of varnishes, adhesives and food glazing agents. The high carbohydrate content of the sample extract showed that it is a good source of energy. Protein indicated high nutritional value of the extract, therefore can help in physical, mental growth and development [30]. The high protein and carbohydrate contents indicate its potency in animal feed formulation.

From the results obtained from Quantitative Chemical Constituents of *Bombax brevicuspe* (Table 5) the sample contained 22% of lignin, 40% of cellulose, 28% of hemicelluloses, etc which help to confirm that the sample is a hard wood. Lignin contributes 20-25% of hardwood. It is largely responsible for the strength, rigidity of plant and shields carbohydrate polymers from microbial and enzymatic attack. Cellulose, a major chemical component of wood fibre wall, contributes 40-50% of hardwoods dry weight. Hemicellulose is a group of carbohydrate biopolymers that exist in close association with cellulose in the plant cell wall but it is less complex and easily hydrolysable [22,31,23,32]. The destructive distillation of *Bombax brevicuspe* gave rise to four products in the following compositions; wood charcoal (2.5 g), pyroligneous acid (1.75 cm^3), wood tar (0.2 cm^3) and wood gas (840 cm^3). As wood reaches elevated temperatures, the different chemical components undergo the thermal degradation that affects the performance of wood [33]. Crude fiber indicates the level of indigestible component of food. Low crude fiber content shows that the sample has high nutritional value [34]. There depicts low oxalate content (2.92 g/1009) in the analyzed sample. Foods high in oxalate causes inflammation, pain and burning, irritation of tissue and mucous membranes and contribute to the formation of calcium oxalate kidney stones [35]. The high lipid content of 6.80% in *Bombax brevicuspe* wood proves energy storage capacity in the structural component of the sample's cell membrane [36,37,38].

The thin layer chromatography of the extract (Table 6) showed one component with R_f value of 0.62 when chloroform-methanol extract was spotted. The TLC result confirmed its high purity and presence of some components shown in the FTIR and UV results explained below.

The FTIR and UV results of the analysed sample chloroform methanol extract (Table 7) revealed strong absorption at 3410 cm^{-1}, which indicated the presence of alcohols, carboxylic acids and phenols. The absorption at 2958 cm^{-1}, 2511 cm^{-1} and 1651 cm^{-1} showed the presence of alkanes, nitriles, amides and esters. The presence of C=C, C-O and C-H for carbon bond in alkenes and aromatics, keto attached to benzene ring and deformation bonds for alkyl groups were shown by absorption at 1408 cm^{-1}, 1108 cm^{-1} and 1020 cm^{-1} respectively. This suggested that the active compound might be 1,2,3-trisubstituted aromatic compound with C=O, O-H and C=N groups attached.

5. CONCLUSION

It was observed from the results of the various analyses that the wood from *Bombax brevicuspe's* stem could be useful in animal feed formulation, serve as a good material for various construction works, contained some bioactive compounds and be used in the cure and management of various diseases. Moreover, the complex chemical makeup of the timber showed the presence of cellulose, hemicelluloses, lignin and other components in the right proportion which confirmed the efficacy of *Bombax brevicuspe* stem as a tropical timber.

COMPETING INTERESTS

Authors have declared that no competing interests exist.

REFERENCES

1. Trossero MA. Wood energy: The way ahead. Unasylva. 2002;53(4):3-12.
2. Christophe Plomion, Gregoire Leprovost, Alexia Stokes. Wood formation in trees. An Article in plant physiology; 2002.
   Available:https://www.researchgate.net/publication/11613890
3. Ramage MH, Burridge H, Busse-Wicher M, Fereday G, Reynolds T, Shah DU, Allwood J. The wood from the trees: The use of timber in construction. Renewable and Sustainable Energy Reviews. 2017;68:333-359.
4. Ike PO. Analysis of flame characteristics of castor oil and some other inorganic flame retardants, a paper presented at the International Conference of the Chemical Society of Nigeria (CSN), Merit House Maitama, Abuja, Nigeria; 2007.
5. Guisan A, Zimmermann NE. Predictive habitat distribution models in ecology. Ecological Modelling. 2000;135:147–186.
6. Walthert L, Meier ES. Tree species distribution in temperate forests is more influenced by soil than by climate. Ecology and Evolution. 2017;7(22):9473-9484.
7. Eboatu AN, Altine AM. Studies on the thermal characteristics of some tropical wood. Nigerian Journal of Renewable Energy. 1991;2(1):49-53.
8. Akindele SO, LeMay VM. Development of tree volume equations for common timber species in the tropical rain forest area of Nigeria. Journal of forest Ecology and Management. 2006;226:41-48.
9. Arbonnier M. Trees, Shrubs and Lianas of West Africa dry zones. Grad, Magrat Publishers. 2004;1:574.
10. Udeozo IP, Eboatu AN, Arinze RU, Okoye HN. Some fire characteristics of fifty-two Nigerian Timbers. Anachem Journal. 2011;5(1):920-927.
11. Encyclopaedia Britannica Bombacaceae.
    Available:https://www.britannica.com/plant/Bombacaceae
12. Keay RWJ, Onochie CFA, Stanfield DP. Nigeria trees. Department of Forest Research Publishers Ibadan. 1964;1:38-265.
13. American Society for Testing and Materials. Standard test methods for five tests of building construction and materials. Designation E119-98. West Conshohocken, PA: ASTM; 1998b.

14. American Society for Testing and Materials. Direct moisture content measurement of wood and wood-based materials. Designation D4442-99. West Conshohocken, PA: ASTM; 1999a.
15. David WG, Jerrold EW, David EK. Wood handbook- wood as an engineering material. Gen. Tech. Rep.FSL-GTR-113. Madison, W.I.: U.S. Department of Agricultural, Forest Service, Forest Products from Forest Product Laboratory. 1999;463:2-26.
16. Harbon JB. Phytechemical method 3rd edition. Thomson Science 2-6 Boundary Row London, UK. 1998;1-290.
17. Amadi BA, Agomuo EN, Ibegbulam CO. Research methods in biochemistry. Supreme Publishers, Owerri. 2004;90-115.
18. Goering HD, Vansoest PJ. Forage fibre analysis. Washington DC: US Dept of Agricultural Research Services. 1975;23.
19. Oakley ET. Determination of Cellulose index of tobacco. Chemical Society. 1984;32:1192-1194.
20. Marzieh MN, Marjan MN. Utilization of sugar beat pulp as a substrate for the fungal production of cellulose and bioethanol. African Journal of Microbiology Research. 2010;4(23):2556-2561.
21. Udeozo IP, Eboatu AN, Kelle IH, Ejukwa EE. Thermal characteristics, photo-chemical and functional groups assessment of *Garcinian kola* as a tropical timber. IOSR Journal of Applied Chemistry. 2014;7(10):73-75.
22. Desch HE, Dinwoodie JM. Timber, its struture, properties and utilization. Macmillian Press Ltd., London, 6th Edition. 1981;155–208.
23. Arntzen CJ. Wood properties encyclopedia of agricultural sciences. FI: Academic Press, Orlando. 1994;549-561.
24. Panshin AJ, Dezeeuw P. Textbook of wood technology. McGraw-Hill, New York. 1964;1:187.
25. Maret W, Sandstead HH. Zinc requirement and the risks and benefits of zinc supplements. J Trace Elem Med Bio. 2006;20:3-18.
26. Hodgkin AL, Huxley AF. Currents carried by sodium and potassium. 1952;116(4):449-472.
27. Tahir MA, Chaudary M, Rasool MR, Naeen TM, Chughtai IR, Dhami MSI. Quality of drinking water samples of Sialkot and Gujranwala. Proceedings of Tenth National Chemistry Conference. 1999;62-69.
28. Konrad M, Weber S. Recent advances in molecular genetics of hereditary magnesium-losing disorders. Journal of American Society, Nephrol. 2003;14:249-260.
29. Gills LS. Ethnomedical uses of plants in Nigeria. UNIBEN Press, Benin City. 1992;36-42.
30. Akpuaka MU. Essential of natural products chemistry. Mason Publishers, Inc. Enugu Nigeria. 2009;34-65.
31. Petterson RC. The chemical composition of wood: The chemistry of solid wood. Advances in Chemistry Series 207, Washington, DC. 2007;712-718.
32. Desch HE, Dinwoodie JM. Timber, its structure, properties, conversion and use. Macmillan Press Ltd., London, 7th Edition. 1996;306.
33. White RH, Dietenberger MA. Wood productions: Thermal degradation and fire. Encyclopedia of Material Science and Technology. E/Science Ltd., Washington, DC. 2001;9712-9716.
34. AOAC. Official methods of analysis. 15th Ed. Washington DC. U.S.A. Association of Official Analytical Chemists; 1990.
35. Fatoki OD, Ekwenchi MM. The determination of oxalate contents of some nigerian vegetables. Nigerian Journal of Nutrition Science. 1998;2:7-11.
36. Fahy E, Subramaniam S, Murphy R, Nishijima M, Raetz C, Shimizu T, Spener F, Van Meer G, Wakelam M, Dennis EA. Update of the lipid maps, “Comprehensive Classification System for Lipids”. Journal of Lipid Research. 2009;50:59-514.
37. Udeozo IP, Ejikeme CM, Eboatu AN, Arinze RU. The efficacy of *Pycnanthus Angolensis* timber*:* An assay of its properties, chemical constituent and functional group analysis. Global Journal of Biotechnology and Biochemistry. 2015;10(3):121-125.
38. Udeozo Ifeoma P, Eboatu Augustine N, Umedum Ngozi L, Aneke Martin U. Thermal characteristics and pharmaceutical constituents of *Anogeissus leiocarpus* as a tropical timber. World Engineering & Applied Sciences Journal. 2014;5(3):13-16.

Biography of author(s)

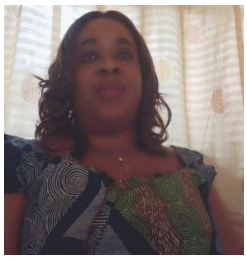

Dr. I. P. Udeozo
Department of Chemistry, Enugu State University of Science and Technology, Enugu State, Nigeria.

She graduated from Nnamdi Azikiwe University Awka, Anambra State, Nigeria with BSc, M.Sc. (in Pure and Industrial Chemistry) and PhD (in Environmental Chemistry). She is a lecturer in the Department of Industrial Chemistry, Enugu State University of Science and Technology (ESUT). Her research area is majorly in Environmental/Analytical chemistry. She has contributed to the science world majorly on chemistry of wood/timber, some plant and waste water analysis. She is a member of professional bodies: Chemical Society of Nigeria (MCSN), Institute of Chattered Chemists of Nigeria (MICCON) and Women in Chemistry (Nigeria). She has attended several conferences, presented papers and has published widely in scientific journals both locally and internationally. She is also a reviewer to many international journals.

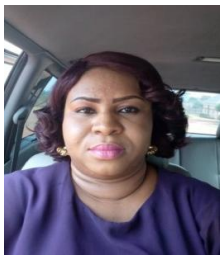

Dr. C. M. Ejikeme
Department of Chemical Science, Godfrey Okoye University, Enugu, Enugu State, Nigeria.

She obtained a Bachelor of Science (B.Sc.) in Industrial Chemistry at Ebonyi State University, Abakaliki, Ebonyi State in 2005. She holds a Master of Science (M.Sc.) and Doctor of philosophy (Ph.D) in Environmental Chemistry from Nnamdi Azikiwe University (NAU) Awka Anambra state in 2009 and 2012 respectively. She moved further to obtain a Post Graduate Diploma in Education from the Institute Of Ecumenical Education, Thinker's Corner, Enugu State in 2012. She joined the Chemical Science Department of Godfrey Okoye University (GOU), Ugwuomu – Nike, Enugu State in 2010 where she rose to the rank of Lecturer 1 in 2015. She also lectured at Institute of Ecumenical Education, Thinkers Corner Enugu under the Chemistry Education Department. Her teaching activity at GOU spans across undergraduate lectures in environmental, analytical and inorganic chemistry. She has made fifteen (15) scholarly publications in area of polymer and environmental chemistry.

Prof. A. N. Eboatu
Department of Pure and Industrial Chemistry, Nnamdi Azikiwe University, Awka, Anambra State, Nigeria.

Research and Academic Experience: Professor of Chemistry for twenty four (24) years.

Research Area: Environmental / Polymer Chemistry.

Number of Published papers: Numerous books and articles in reputable journals.

Special Award: Fellowships of the following: Royal Society of Nigeria (FRSC), Chemical Society of Nigeria (FCSN), Solar Energy Society of Nigeria (FSESN), Nigerian Institute of Science and Technology (FNIST), Institute of Chartered Chemist of Nigeria (FICCON), International Biographical Association (FIBA).

Any other remarkable point(s): He has supervised to completion 41 PhD and 27 MSc.

H. I. Kelle
Chemistry Unit, National Open University of Nigeria, Victoria Island, Lagos, Nigeria.

She holds a PhD in Environmental Chemistry from Nnamdi Azikiwe University, Nigeria. She is a lecturer with the Department of Pure and Applied Science, Faculty of Sciences, National Open University of Nigeria. She has written several scholarly articles in referred journals, conference proceedings and book chapters in academic books which address environmental issues. Her major contribution to the science world is on oil spill clean-up using natural sorbents and chemistry of woods.

© Copyright (2020): Author(s). The licensee is the publisher (Book Publisher International).

DISCLAIMER
This chapter is an extended version of the article published by the same author(s) in the following journal.
American Chemical Science Journal, 15(3): 1-8, 2016.

Reviewers' Information
(1) G. Meerabai, Rayalaseema University, Kurnool, India.
(2) Rahim Foroughbakhch, University of Nuevo Leon, Mexico.

Chapter 10
Print ISBN: 978-93-90206-41-4, eBook ISBN: 978-93-90206-42-1

Studies on the Characterisation of Poly blend-Nanofilms of Cellulose Acetate and Poly Styrene

S. Srilalitha[1*] and K. N. Jayaveera[2]

DOI: 10.9734/bpi/crdc/v4

ABSTRACT

Nanotechnology has potential to create many new materials and devices with wide range of applications in medicine, electronics and energy production etc. Blending technique is applied for production of new polymeric materials. As Cellulose acetate is cellulosic, non-toxic, non-allergic biocompatible, biodegradable, hydrophilic, soft, smooth, transparent, highly flexible, good chemical resistant, thermoplastic moulding material, it is used in industrial, biochemical and biomedical applications. In the present investigation, SEM and mechanical analysis of Cellulose acetate and Polystyrene nano films have been studied in accordance with the change in composition of polymer over a wide range of concentrations and temperatures. Super plasticity has been observed at low temperatures and at higher strain rates in nano crystalline materials. Mechanical properties of Cellulose acetate and Polystyrene nano films have been studied. Phase morphology of nano membranes have been studied by SEM. SEM studies were also performed to estimate pore size distribution of the support polymer. Nano structured ceramics readily interact with bone cells and have been applied as implant materials. The present investigation indicates the compatibility of Polymer blends may be studied by SEM and Mechanical analysis. It is clear that there is a distinct phase separation in the membranes at compositions of 50:50 of Poly styrene-Cellulose acetate. Poly styrene-Cellulose acetate blends show maximum values of stress and tensile strength at higher concentration of cellulose acetate.

Keywords: Polymeric materials; blending technique; cellulose acetate; polystyrene; SEM analysis; phase morphology.

1. INTRODUCTION

In recent years, nanotechnology has become one of the most important and exciting forefront fields in Physics, Chemistry, Biology, Engineering and Technology. Nanotechnology is the design, characterization, product and application of structures, devices and systems by controlling shape and size at the nanometer scale. Nanotechnology is commonly considered to deal with particles in the size range < 100 nm, and with the nanomaterials manufactured using nanoparticles [1]. Nanotechnology is the study of phenomenon and manipulation of materials at atomic, molecular and macromolecular scales, where properties differ significantly from those at a larger scale.

Characterisation of nanomaterial and nanostructures has been largely based on surface analysis technology and conventional characterisation methods developed for bulk material Fabrication of nanomaterials has been done by different physical, chemical, and mechanical methods that used temperature, pressure, and phase transformation to create nanostructures that have greatly enhanced devices, due to their revolutionized electronic, magnetic, opto electrical, and sensing capabilities [2,3]. Producers of polymeric materials have strong economic incentives to solve technical problems and upgrade their products by working with existing materials Polymer blending technique has been considered a convenient and best route for modification of properties for the development of new

[1]ACE Engineering College, Ankushapur, Hyderabad-501 301, India.
[2]Jawaharlal Nehru Technological University, Anantapur-515 001, India.
**Corresponding author: E-mail: ssrilalitha@yahoo.com;*

polymeric materials with a wide range of properties as blending is less expensive method and its relative freedom from the patent coverage and enforcement compared to the synthesis of new homo polymers and co-polymers [4-7]. The improvement of the physical and mechanical properties of the blend mainly depends on the extent of adhesion at the interphase and how fine the dispersion is of one phase into other [4,5,8-10].

The polymer blends are physical mixtures of structurally different polymers which interact with secondary forces with no covalent bonding and have assumed a very important status scientifically and technologically. Polymer blends are physical mixtures of structurally different polymers or copolymers which interact with secondary forces with no covalent bonding [11] such as hydrogen bonding, dipole-dipole forces, and charge-transfer complexes for homo polymer mixtures [12-15]. The polymer blends offer property, cost and processing advantages in their applications. Compatibility of polymers has been one of the important areas in the field of polymer science and technology [4,5,16-18]. Many experimental and theoretical methods [5,7] have been used to investigate the polymer-polymer miscibility and the interaction between the polymers [19-22].

In the present studies the scanning electron microscopic and mechanical analysis of Cellulose acetate (CA) and poly styrene (PS) nanofilms have been studied in accordance with the change in composition of polymer over a wide range of concentrations and temperatures.

2. EXPERIMENTAL

The grades of polymers used in the present investigation were Poly Styrene (PS) (BDH, England) and Cellulose Acetate (CA) (Aldrich, USA). The molecular weights are 1.0×10^5 and 1.6×10^5. The solvent 1,4-dioxane used was of BDH origin and of AR grade.

2.1 General Procedure

Poly blending: Poly (styrene) and Cellulose acetate blends with compositions of 0/100, 12.5/87.5, 25/75, 37.5/62.5, 50/50, 62.5/37.5, 75/25, 87.5/12.5 and 100/0 were prepared.

2.2 Detection Method

2.2.1 Film casting

Solutions of polymer blends of different compositions were used for casting of films of the desired thickness on a clean glass plate. The solvent was evaporated at room temperature for ten hours and then the plate was kept under vacuum at 60ºC for complete removal of the solvent. The thickness of the dry membranes was measured with a micrometer (Mituotoyu, No. 2109-10, Japan with an accuracy of ± 1 μm) and flakes of the films were used in the experiments.

2.2.2 Scanning Electron Microscopy (SEM)

The SEM studies of the films were carried out using Scanning Electron Microscope (Model Hitachi S-520).

2.2.3 Mechanical studies

Mechanical studies were performed by Instron (Model AGS-10KNG, Shimadzu, Japan).

3. RESULTS AND DISCUSSION

3.1 Scanning Electron Microscopy

Phase morphology characterization for the Poly(styrene)-Cellulose acetate blend systems of compositions Poly(styrene)/Cellulose acetate 0/100, 12.5/87.5, 25/75, 37.5/62.5, 50/50, 62.5/37.5, 75/25, 87.5/12.5 and 100/0, respectively has been done by SEM microscopic analysis.

From micrograph (Fig. 1) it is clear that Cellulose acetate rich phase shows homogeneity as it is completely miscible. With increase in the percentage composition of Polystyrene in the blend system formation of voids in the Cellulose acetate matrix starts by the addition of hard, rigid and crystalline Poly styrene as in Figs. 2 and 3. The heterogeneity of Polystyrene/ Cellulose acetate 50/50 is clearly seen by the microscopic observation which may be due to the formation of Polystyrene domains (Fig. 4). The increase in the weight percentage of Polystyrene causes "optical heterogeneity" as the formation of Polystyrene domains starts aggregating which is shown in the photomicrographs (Fig. 5). At the high composition range of Polystyrene *i.e.*, in Polystyrene/Cellulose acetate 100/0 blend homogeneity appears due to the presence of uniformly distributed highly transparent pure Polystyrene matrix transmission about 90% of visible light with high refractive index of 1.59 (Fig. 6).

From the microscopic examination of Polystyrene-Cellulose acetate blend system of various compositions it is evident that the cast films are found to be transparent and slightly yellowish. The transparency of the films at higher concentrations shows compatible nature of the system while the yellow colour at lower concentrations indicates the specific interactions between the constituent polymers. The yellow colour of films intensifies with concentration of cellulose acetate. The heterogeneity indicating the two phase morphology confirms that the Polystyrene-Cellulose acetate blend system is incompatible at all concentrations. SEM study found to be useful in the compatibility analysis of the polymer blend [23,24].

Fig. 1. SEM micrographs of Polystyrene-Cellulose acetate blends of various compositions Polystyrene/Cellulose acetate 0/100

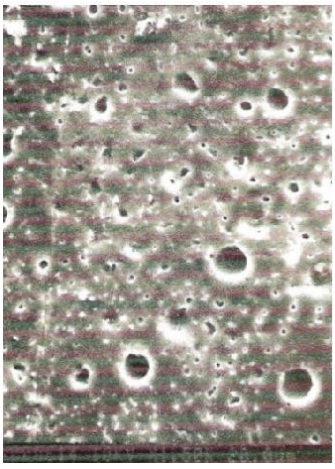

Fig. 2. SEM micrographs of Polystyrene-Cellulose acetate blends of various compositions Polystyrene/Cellulose acetate 12.5/100

Fig. 3. SEM micrographs of Polystyrene-Cellulose acetate blends of various compositions Polystyrene/Cellulose acetate 37.5/62.5

Fig. 4. SEM micrographs of Polystyrene-Cellulose acetate blends of various compositions Polystyrene/Cellulose acetate 50/50

Fig. 5. SEM micrographs of Polystyrene-Cellulose acetate blends of various compositions Polystyrene/Cellulose acetate 87.5/12.5

Fig. 6. SEM micrographs of Polystyrene-Cellulose acetate blends of various compositions Polystyrene/Cellulose acetate 100/0

3.2 Mechanical Studies

The various mechanical properties studied on a series of films of Poly blends of Polystyrene-Cellulose acetate system at various compositions are tabulated (Table 1).

It is observed from the table that Polystyrene/Cellulose acetate blends show higher values of strain and the percentage of elongation when the percentage composition of Poly blend Polystyrene/Cellulose acetate is 25/75. It shows maximum values of stress and tensile strength at higher concentrations of Cellulose acetate *i.e.*, 12.5/87.5 Polystyrene/Cellulose acetate. This may be due to the following reason. In thermoplastic Polystyrene, the intermolecular forces and the barriers to rotation about C-C bonds are greater than in the rubbers or elastomeric polymers. These increased forces may rise because of bottom molecular packing and a high degree of crystallinity by the presence of side chains and increased steric forces. In Cellulosic plastic, Cellulose acetate hydrogen bond forces contribute to the intermolecular cohesion.

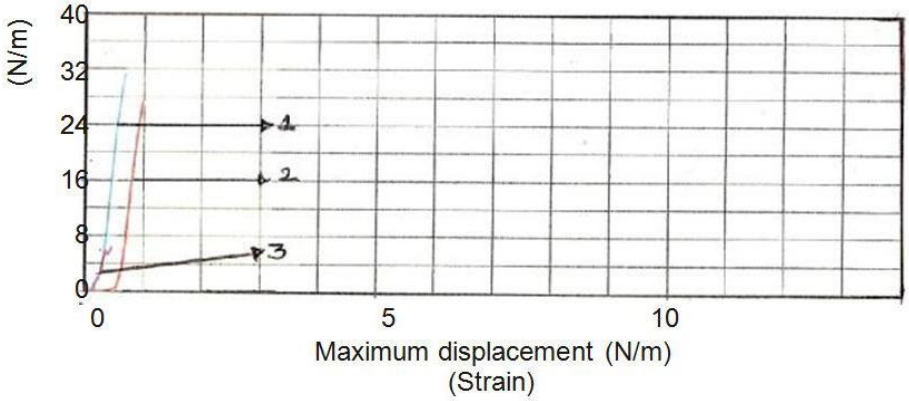

Fig. 7. Stress-Strain relationship of Polystyrene-Cellulose acetate blends of various compositions

The stress-strain curve of Polystyrene-Cellulose acetate blends of different compositions (Fig. 7) confirms that the Poly blend with maximum percentage composition of Cellulose acetate is highly amorphous, soft and tough. With increase in percentage composition of Polystyrene, the strength of the film decreases and becomes hard and brittle as Polystyrene is susceptible to photo oxidative

degradation which results in brittleness. So Poly blends with compositions Polystyrene/ Cellulose acetate 12.5/87.5 and 25/75 are hard and brittle whereas 37.5/62.5 is of hard and strong. In Polystyrene there is little yielding and fracture occurs at low strains. Polystyrene is namely considered brittle polymer at room temperature because it fractures in a tensile test run at normal speed after an elongation of only 1.5 % or so and has low impact strength. However, if similar tests are tested at temperature above 100ºC, they show ductile behaviour and have high impact strength and high extensibility.

Table 1. Mechanical studies of films of PS-CA blends of different compositions

Composition of PS-CA blends	Max-load (Stress) (N)	Max. Disp. (strain) (mm)	Tensile strength (N/mm^2)	Max-strain (%)	Break-load (N)	Break-disp (mm)	Break-stress 2 (N/mm)	Percentage of elongation (N/mm^2)
(1)12.5/87.5	31.2625	0.68400	6.56775	6.84000	30.8500	0.67600	6.48109	6.76000
(2)25/75	27.3125	0.99200	5.75000	9.92000	26.9375	0.98400	5.67105	9.84000
(3)37.5/62.5	6.3125	0.45900	2.86932	4.59000	6.31250	0.45900	2.86932	4.59000
Mean	21.6291	0.71167	5.06236	7.11667	21.3666	0.70633	5.00715	7.06333

4. CONCLUSION

The present investigation indicates the compatibility of Polymer blends may be studied by SEM and Mechanical analysis. It is clear that there is a distinct phase separation in the films at compositions of 50:50 of Polystyrene-Cellulose acetate. Polystyrene-Cellulose acetate blends show maximum values of stress and tensile strength at higher concentration of Cellulose acetate. The stress-strain curve of Polystyrene-Cellulose acetate blends of different compositions (Fig. 7), confirm that the Polymer blend with maximum percentage composition of Cellulose acetate is highly amorphous, soft and tough. Cellulose acetate films are flexible, highly glossy and good elongation at break. With increase in percentage composition of Polystyrene, strength of the film decreases becomes hard and brittle as Polystyrene is susceptible to photo oxidative degradation which results in brittleness. Super plasticity has been observed at low temperature and at high strain rates in non-crystalline materials. Bio sensitive nano-particles have been used to tagging of DNA and DNA chips. Nano-structured ceramics readily interact with bone cells and have been applied as implant materials.

ACKNOWLEDGEMENTS

The authors are grateful to Dr. P. Sita Devi, Dr. D.H.L. Prasad and Dr. V. Mohan Rao, Indian Institute of Chemical Technology, Hyderabad, India for providing research facilities.

COMPETING INTERESTS

Authors have declared that no competing interests exist.

REFERENCES

1. Ruth Lyddy. Nanotechnology. In: Information resources in toxicology (Fourth Edition). Academic Press. Pages. 2009;321-328
2. Li FJ, Zhang S, Lee JW, Guo J, White TJ, Li B, Zhao D. Orientation of silicon nanowires grown from nickel-coated silicon wafers. J. Cryst. Growth. 2014;404:26–33.
3. Ossai CI, Raghavan N. Nanostructure and nanomaterial characterization, growth mechanisms, and applications. Nanotechnology Reviews. 2018;7(2):209-231.
4. Utracki LA, Polymer alloys and blends, thermodynamics and rheology. Hansar Munich; 1989.
5. Olabisi O, Robeson LM, Shaw MT, In Polymer-polymer miscibility. Academic, New York; 1978.
6. Koning C, Buin MV, Pagroulle C, Jerome R. Polym. Sci. 1998;23:707.
7. Osamu K, Masahiro K, Ikeda Bassan Co., Japan, Patent 06,207, 037; Chem Abstr. 1995;122:135442d (1995).

8. Paul DR, in ed.: Newman S, In Polymer blends, Academic Press, New York. 1978;1(1).
9. Sathe SN, Rao GSS, Rao KV, Devi S. J. Appl. Polm. Sci. 1996;61:107.
10. Patel CA, Brahmbhatt BR, Sarawade BD, Devi S. J. Appl. Polym. Sci. 1996;81:1731(2001).
11. Krause S, Paul DR, Newman S, (Eds.), Polymer Blends. New York: Academic Press; 1979; 1.
12. Varnell DF, Coleman MM, FTIR studies of polymer blends: V. Further observations on polyester-poly (vinyl chloride) blends. Polymer. 1981;22:1324.
13. Varnell DF, Runt JP, Coleman MM. FTIR and thermal analysis studies of blends of poly(ε-caprolactone) with homo- and copolymers of Poly(vinylidene chloride). Polymer. 1983;24:37.
14. Woo EM, Barlow JW, Paul DR, Phase behavior of blends of aliphatic polyesters with a vinylidene chloride/vinyl chloride copolymer. Journal of Applied Polymer Science. 1986;32:3889.
15. Reddy VNM, Rao KK, Subha MCS, Rao KM, Rao KC. Miscibility behavior of pectin-poly (vinylalcohol) blends in water at 35° C. Indian Journal of Advances in Chemical Science. 2015;3(2):178-184.
16. Coleman MM, Graf JF, Painiter PC, Specific interaction and miscibility of polymer blends, Technomic Publishing. Lancaster. PA; 1991.
17. Amello C, De Rosa C, Gueffa G, Peffacone V, Coltadin P, Ajroldi G. Polymer. 1995;36:967.
18. Feng JY, Chan CM. Polymer. 1997;38:6371
19. Singh YP, Singh RP. Eur. Polym. J. 1984;20:201.
20. Sidkey MA, Abd Ei Fatta AM, Abd El All NS. J. Appl. Polym. Sci. 1992;46:581.
21. Paladhi R, Singh RP. J. Appl. Polym. Sci. 1994;51:1559.
22. Srilalitha S, Jayaveera KN, Madhvendhra SS. Characterisation and physico-chemical studies of membranes of Cellulose acetate and Poly(vinyl chloride). 58th Annual convention and International Seminar on Technolological Developments in the Fields of Oils, Fats and Allied Products, November. 2003;22-23.
23. Liang BR, White JL, Spruiell JE, Goswami BC. J. Appl. Sci. 1983;8:2011.
24. Hong SD, Burns CHJ. J. Appl. Polym. Sci. 1995;15:1971.

Biography of author(s)

Dr. S. Srilalitha
Professor of Chemistry & Head of R&D
Department of Humanities & Sciences
ACE Engineering College, Ankushapur, Hyderabad-501 301, India and Jawaharlal Nehru Technological University, Anantapur-515 001, India.

Research and Academic Experience: Academic Experience: 20 years

Research Experience: 13 years

Administrative Experience; Worked as Principal, Head of the Department of Chemistry & Head of the Department of Humanities & Sciences in various Institutions

Research Area: Nano Polymer Composites, Synthesis & Characterisation of Nano Films of Polymer Blends, Physico-Chemical properties of Polymers, Polymer Blends & Biosensors

Number of Published papers: 27

Special Award (If any):

- **Selected for PERFICIO AWARD for Research & Innovation of the year 2020** organised by **DHS** Foundation Collaboration with Campbell University, USA and awarded on 12th July 2020
- **Selected for Best Researcher Award** (9th Science and Technology Awards – 2020) organised by EET CRS Research Wing for Excellence in Professional Education & Industry and awarded on 7th June 2020
- **Selected for Best Faculty Award** (8th Academic Brilliance Awards – 2020) organized by Education Expo. and awarded on Women's Day, 8th March 2020

© Copyright (2020): Author(s). The licensee is the publisher (Book Publisher International).

DISCLAIMER
This chapter is an extended version of the article published by the same author(s) in the following journal.
Asian Journal of Chemistry, 25(Supplementary Issue), 2013.

Chapter 11
Print ISBN: 978-93-90206-41-4, eBook ISBN: 978-93-90206-42-1

Investigation on *in vitro* Evaluation of Antioxidant and Anti-inflammatory Properties of Methanol and Dichloromethane Extracts of the Leaf of *Globimetula oreophila*

Esther O. Faboro[1*], Idowu J. Olawuni[2], Bolajoko A. Akinpelu[2], Oluokun O. Oyedapo[2], Ezekiel O. Iwalewa[3] and Craig A. Obafemi[4]

DOI: 10.9734/bpi/crdc/v4

ABSTRACT

Aims: The study was designed to investigate the antioxidant and membrane stabilizing potentials of the leaf of *Globimetula oreophila,* with a view to providing scientific support for the acclaimed ethnomedicinal or traditional uses of the plant.
Methodology: The study involved collection, identification, drying, pulverizing, extraction and fractionation of extracts of the dried leaves of *G. oreophila*. Anti-inflammatory and antioxidant activities of the extracts and fractions were evaluated using red blood cell membrane stabilization technique, while assays (2,2-diphenyl-1-picrylhydrazyl hydrate, nitric oxide, total antioxidant capacity and ferric reducing antioxidant power).
Results: The results revealed that the extracts and the fractions of *G. oreophila* exhibited potent antioxidant activities. Fraction 1 of the methanol extract exhibited the highest antioxidant activity with IC_{50} of 45.83 ± 0.13 µg/ml while fraction 7 of the same extract was the most potent in stabilizing stressed red blood cells having 100±0.00% membrane stability. The activities of both the fractions and the extracts of *G. oreophila* compared favourably with the standard antioxidant and anti-inflammatory drugs. Moreover, the activities of the fractions and extracts are concentration dependent.
Conclusion: The study revealed that the extracts and fractions of *G. oreophila* possess and exhibit anti-inflammatory and antioxidant activities which were concentration dependent and compared favourably with those of nonsteroidal anti-inflammatory drugs. On the basis of these results, it could be inferred that the extracts and the fractions of *G. oreophila* contain principles that were capable of stabilizing bovine red blood cell membrane exposed to heat and hypotonic-induced lyses and could, therefore, serve as a scientific proof for the use of these plant extracts by the local traditional health practitioners in the management and treatment of inflammatory related diseases.

Keywords: Antioxidant; membrane stabilization; anti-inflammatory; red blood cells; G. oreophila.

1. INTRODUCTION

Medicinal plants have been demonstrated to be the valuable treasures which nature has bestowed on mankind for food and medicine. In the scientific community, the diverse medicinal values of these plants have aroused the interests of researchers across various disciplines all over the world. The plant *G. oreophila* (Loranthaceae family) has the potential of providing lead and new drugs that could be employed to combat the menace of cardiovascular diseases such as cancer, heart attack, hypertension, diabetes and infectious diseases [1,2]. It is acclaimed by the traditional health

[1]*Department of Chemistry, Bowen University, Iwo, Nigeria.*
[2]*Department of Biochemistry, Obafemi Awolowo University, Ile Ife, Nigeria.*
[3]*Department of Pharmacology and Therapeutics, University of Ibadan, Ibadan, Nigeria.*
[4]*Department of Chemistry, Obafemi Awolowo University, Ile Ife, Nigeria.*
**Corresponding author: E-mail: ofaboro@yahoo.com;*

practitioners in Nigeria that the extracts of this plant are employed in the prevention, treatment and management of cardiovascular related diseases and ailments.

Distinctively, the constituents of most European and Asian mistletoes are proteins, viscotoxins, lectins and carbohydrates. Mistletoes have been reportedly used for the treatment of cancer, hypertension, diabetes, arthritis, heart problems, insomnia, infertility and pneumonia [3-10]. The low molecular weight compounds including flavonoids and phenylpropanoids of varying structural types which contribute to the antioxidative properties of various *Loranthaceae* extracts have been examined. Many reports of the presence of lower molar mass compounds like alkaloids, flavonoids, tannins and other plant constituents in the African *Loranthaceae* have not been substantiated by isolation and proper identification [11]. The tea prepared from Loranthaceae is believed to cure bone fracture and body pains [12]. Faboro et al., 2016 [13] carried out a phytochemical profile of dichloromethane and methanol extracts as their TMS and FAME derivatives using GC-MS on *G. oreophila*. There were thirty-four (34) compounds detected which have not been reported in any other mistletoe species. They are cis-dihydro-3,4-bis[TMS2]-2(3H)-furanone, dodecanol, octadecenol, nonacosane, pentacosanol, hexatriacontane, octacosanol, triacontanol, dotriacontanol, cis-dihydro-3,4-bis[(trimethylsilyl)oxy]-2(3H)-furanone, butanedioic acid, glyceric acid, fumaric acid, 3,4-dihyroxybutanoic acid, malic acid, tetrahydroxy butane, 2,3,4trihydroxybutanoic acid, tartaric acid, arabitol, ribofuranose, isocitric acid, inositol, hexo-pyranose, inosose, methyl dimethoxy-hydroxybenzoate, 3,5,11,15 tetramethyl-2-hexadecen-1-ol, pentadecanoic acid, cis and trans phytol, eicosanoic acid, hexatriacontane, tricosanoic acid, pentacosanoic acid, nonacosane and hexacosanoic acid. These phytoconstituents were distributed among the following classes of organic compounds: ketones, monoarylphenolics, sugars, dicarboxylic acids, sugar acids, alcohols, cyclic compounds, hydroxycarboxylic acids, sugar alcohols, steroids and fatty acids. It was the first time this type of studies would be carried out on *G. oreophila*. Although pharmacological tests have been carried out on *G. braunii* [14,15,16] which is closely related to *G. oreophila*, such tests have not been carried out on *G. oreophila*.

The present study is aimed at evaluating the antioxidant and membrane stabilizing activities of the extracts and fractions of the leaves of *G. oreophila*, to establish the scientific evidence for the use of the plant as an anti-inflammatory agent as acclaimed by the traditional healers. In addition, there is a dearth of scientific information on the biological and chemical activities of the extract, fraction and bioactivity of the plant from the science community so this study could serve as a baseline for further study on the plant.

2. MATERIALS AND METHODS

2.1 Materials

The main material used in this study is the fresh leaves of *G. oreophila* which was sourced locally. Others include appropriate chemicals purchased from recognised chemical companies.

2.2 Collection and Identification of Plant Material

Fresh leaves of *G. oreophila* were collected from Iwo, Osun State, Nigeria. Iwo is located on latitude 7.6292°N and longitude 4.1872°E. The leaves were identified and authenticated by Mr. Gabriel Ibhanesebhor (a Taxonomist, the man in charge of the Herbarium), Department of Botany, Obafemi Awolowo University, Ile-Ife, Nigeria, and a voucher specimen was deposited at IFE Herbarium (ID no. 17089).

2.3 Reagents and Chemicals

All the reagents and chemicals used were of analytical grades and were purchased from various sources. Dichloromethane, methanol, ethyl acetate, 2,2-diphenyl-1-picrylhydrazyl hydrate, sodium nitroprusside, sulfanilamide, phosphoric acid, 2,4,6-tri-(2-pyridyl)-1,3,5-triazine, sodium phosphate, ammonium molybdate, N-1-naphthylethylenediamine dichloride, ferric chloride from Sigma-Aldrich

Chemical Company. Potassium iodide, sulphuric acid, trisodium citrate, ascorbic acid and trisodium citrate were purchased from British Drug House (BDH). All solutions, buffers and reagents were prepared using glass distilled water. Diclofenac (standard anti-inflammatory drug) was purchased from the Pharmacy Shop at the main Campus of Obafemi Awolowo University, Ile-Ife, Nigeria.

2.4 Methods

2.4.1 Preparation of plant materials and extraction

Collected fresh leaves of *G. oreophila* were rinsed with clean water, drained, air-dried for 2-3 weeks in shade and pulverized into the powdered form using a domestic blender. The powdered plant material was packed into an air-tight plastic container until extraction.

Powdered plant material (500 g) was extracted using dichloromethane (3L) and methanol separately overnight in a large Soxhlet apparatus. The extracts were concentrated under reduced pressure to afford dichloromethane and methanol respectively. Both extracts were weighed and kept in the desiccator until used for biochemical analyses. The weight and percentage yields of DCM extract was 19.4 g which represented 3.88% of the starting material. The weight of MeOH extract was 18.2 g which represented 3.64% of the starting plant material.

The extracts were fractionated on Silica gel 60 (40-60 mesh size) column using gradient solvent mixtures petroleum ether/ethyl acetate. Typically, each extract (1 g) was loaded onto the packed Silica gel 60 column and washed with petroleum ether. The elution was conducted sequentially with petroleum ether/ethyl acetate, 1:1v/v; 3:7v/v; ethyl acetate (100%); ethyl acetate/methanol (1:1v/v); and methanol (100%). Fractions (15 ml) were collected at a flow rate of 1 ml/min. A total of 78 fractions were collected for DCM extract and 65 fractions for methanol extract. Various fractions were chromatographed on pre-coated silica gel F254 plates. The plates were air dried, stained with specific staining reagent, p-anisaldehyde stain and heated at 105°C for spot development. The Rf values were calculated and the fractions were pooled together based on their Rf values as follows: F1 (fraction 1), F2 (fractions 2 and 3), F3 (fractions 4 and 5), F4 (fractions 6-12), F5 (fractions 13-48), F6 (fractions 49-57), F7 (fractions 58-63), F8 (fraction 64), F9 (fractions 65-67) and F10 (fractions 68-78) giving ten (10) fractions for DCM and were labelled as GDF1-F10 respectively. Similarly, the fractions for MeOH were pooled together as follows: F1 (fractions 1-4), F2 (fractions 5-10), F3 (fractions 11-28), F4 (fractions 29-36), F5 (fractions 37-49), F6 (fractions 50-52), F7 (fractions 53-57) and F8 (fractions 57-65) giving eight (8) fractions for MeOH extract were labelled as GMF1-F8 respectively.

2.5 Biochemical Analyses

2.5.1 Evaluation of antioxidant potentials of extracts and fractions of *G. oreophila*

The antioxidant potential of the extracts and the fractions *G. oreophila* were evaluated using four different antioxidant assays: (2, 2-diphenyl-1-picrylhydrazyl hydrate) DPPH assay; nitric oxide, NO assay; total antioxidant capacity, TAC assay and ferric reducing antioxidant power, FRAP assays.

2.5.1.1 Assay of DPPH – radical scavenging activity

The DPPH radical scavenging ability of the extracts and the fractions were determined using the stable radical DPPH (2, 2-diphenyl-1-picrylhydrazyl hydrate) and the concentration that inhibits 50% the DPPH free radical was estimated according to the procedure of Blois, 1958 [17] as slightly modified (Brand-Williams, [18]. Typically, to 1 ml of different concentrations (0.0, 0.3125, 0.625, 1.25, 2.5, 5, 10 µg/ml) of the extract and standard in various test tubes were added 0.3mM DPPH (1 ml) in methanol. The reaction mixture was mixed and incubated in the dark for 30 min., after which the absorbance was read at 517 nm against the blank. The standard drug ascorbic acid (AA) 1 µg/ml was employed and treated as the test extracts.

The percentage DPPH inhibition was calculated as:

$$\% \text{ Inhibition} = \frac{A_{\text{blank}} - A_{\text{sample}}}{A_{\text{blank}}} \times 100$$

where A_{blank} is the absorbance of the control reaction (containing all reagents except the test compound), and A_{sample} is the absorbance of the test compound. The concentration of the sample that caused 50% inhibition (IC_{50}) was extrapolated from the graph inhibition percentage against extract concentration.

2.5.1.2 Assay of nitric oxide (NO) radical scavenging activity

The inhibition of nitric oxide radical activity of the extract was carried out according to the earlier method [Green 19] as modified Marcocci [20]. Nitric oxide, generated from sodium nitroprusside in aqueous solution at physiological pH, interacts with oxygen to produce nitrite ions which were measured by Griess reaction.

The reaction mixture, consisted of 0.1 ml of different concentrations of the tested extracts/fractions (0.3125, 0.625, 1.25, 2.5, 5, 10 µg/ml) and 0.9 ml of sodium nitroprusside (2.5 mM) in phosphate buffered- saline was incubated under illumination for 2½ hr.This was followed by the addition of 1% (w/v) sulphanilamide in 5% (v/v) phosphoric acid (0.5 ml) incubated further in the dark for 10 min., and 0.5 ml 0.1% (w/v), N-1-naphthyl ethylenediamine dihydrochloride (0.5 ml) was added. The absorbance of the chromophore formed was measured at 546 nm against the reagent blank. The percentage inhibition of nitric oxide radical scavenging was calculated as expressed above in DPPH radical scavenging assay [21,22].

2.5.1.3 Evaluation of Total Antioxidant Capacity (TAC)

The evaluation of TAC of extracts/fractions was based on the reduction of Molybdenum (VI) to Molybdenum (V) by the extract and the subsequent formation of a green phosphate/Molybdenum (V) complex at an acidic pH as earlier reported [Prieto 23]. To 0.1 ml of the extract/fraction or standard solution of ascorbic acid (0, 20, 40, 60, 80, 100 µg/ml) was added 1ml of the reagent solution (0.6 M sulphuric acid, 28 mM sodium phosphate and 4 mM ammonium molybdate). The reaction mixture was incubated in a water bath at 95°C for 2½ hr and allowed to cool to room temperature and the absorbance was measured at 695 nm against reagent blank. The antioxidant activities of the extracts were expressed as an ascorbic acid equivalent.

2.5.1.4 Evaluation of Ferric Reducing Antioxidant Power (FRAP)

The evaluation of ferric reducing antioxidant power (FRAP) of the extracts/fractions was carried out as reported [24] with slight modification. The extract/fraction (50 µl) and standard (50 µl) (20, 40, 60, 80, 100 µg/ml) was added to 1 ml of FRAP reagent. The absorbance measurement was read at 593 nm exactly 10 minutes after mixing against reagent blank that contained distilled water. The reducing power was expressed as ascorbic acid (mg/g AAE).

2.6 Evaluation of Anti-inflammatory Properties

The evaluation of anti-inflammatory activity of the extracts and the fractions of the leaf of *G. oreophila* was based on red blood cell membrane stabilizing activity that was exposed to both heat, and hypotonic induced lyses as previously described [Oyedapo et al., 25]. The extracts and fractions with high antioxidant activities were selected for the membrane stability assay.

2.6.1 Preparation of bovine erythrocytes

Bovine erythrocyte was prepared according to the procedure reported by Oyedapo and Famurewa, [26]. A fresh blood sample was collected into an anticoagulant bottle containing trisodium citrate (3.8% w/v) and mixed thoroughly to prevent lysing. The blood was poured into clean centrifuge tubes

and centrifuged at 3000 rpm for 10 min. The supernatant was carefully removed with sterilized Pasteur pipette. The packed RBC (erythrocytes) was re-suspended in fresh isosaline, mixed gently and centrifuged at 3000 rpm for 10 min. The process was repeated five more times until a clear supernatant was obtained. Then, 2% (v/v) erythrocyte suspension was prepared by diluting 2 ml of packed red blood cells to 100 ml with normal saline.

2.6.2 Assay of red blood cell membrane stabilizing activity

The membrane stabilizing the activity of the extracts and fractions of *G. oreophila* was assayed according to a modified procedure [Oyedapo et al., 25]. Varying concentrations 0 - 300 µg/mL of the extracts, fractions and the standard drug were prepared. The assay mixture consisted of 1.0 ml hyposaline (0.42% w/v NaCl), 0.5 ml of 0.1 M sodium phosphate buffer, pH 7.2 (0.5 ml), varying volumes of drug sample and isosaline (0.85% w/v NaCl) to make the mixture up to 2.5 ml and followed by the addition of 2% (v/v) bovine erythrocyte suspension (0.5 ml). The drug control was pipetted as above but without 2% (v/v) erythrocyte suspension while the blood control contained all the reagents, extracts and fractions. Diclofenac (1 mg/ml) was used as the standard drug. The reaction mixtures were incubated at 56°C for 30 min on a water bath, cooled to room temperature under running water and followed by centrifugation at 3000 rpm on Gallenkamp UK Bench Centrifuge for 10 min. at room temperature. The absorbance of the released hemoglobin was read at 560 nm.

The percentage membrane stability was estimated using the expression:

$$100 - \frac{\text{(Abs of Test Drug - Abs of Drug Control)}}{\text{Abs of Blood Control}} \times 100$$

The blood control represents 100% lyses or zero percent stability.

2.7 Statistical Analysis

Each value represented the mean ± SEM of three consistent readings. Significance difference was analyzed using Student's t-test with $p<0.05$ as statistically significant.

3. RESULTS AND DISCUSSION

The study reported the antioxidant and anti-inflammatory potentials of the leaf extracts of *G. oreophila* with a view to providing scientific support for the use of the plant on the prevention, treatment and management of oxidant and inflammatory disorders. The weight and percentage yields of DCM extract was 19.4 g which represented 3.88% of the starting material. The weight of MeOH extract was 18.2 g which represented 3.64% of the starting plant material.

3.1 Biochemical Analyses

Four different antioxidant assays were carried out on the extracts and fractions of *G. oreophila* for the biochemical analyses.

3.2 Antioxidant Assays

3.2.1 Assay of DPPH – radical scavenging activity of DCM extracts and fractions

Table 1 is the summary of antioxidant activities of DCM extract and fractions of *G. oreophila.* It was observed that the extracts and the fractions exhibited potent and appreciable antioxidant activities. These were demonstrated in their ability to react with the stable free radical, thus the odd electrons of DPPH radical gave a strong absorption band at 517 nm in the visible spectroscopy (deep violet colour). As the electron became paired off in the presence of a free radical scavenger, the absorption vanishes and the resulting decolourised product is stoichiometric with the number of electrons taken up. The ability was also demonstrated in their percentage inhibition which is concentration dependent.

At the highest concentration, the DCM extract (GODE) has a percentage inhibition of 51. 97% with an IC_{50} value of 910 µg/ml. In a similar way the percentage inhibition of the fractions showed a dose dependent trend with fraction 8 (GDF8) having the highest percentage of 71.92% and an IC_{50} value of 490 µg/ml. The IC_{50} of fractions GDF1, GDF2, GDF3, GDF4, GDF5 and GDF9 were not determined because the values were well over 1000µg/ml which cannot be determined by extrapolation.

The MeOH extract and its fractions were subjected to the same assay. The percentage inhibition of the extract is 75.42% and the IC_{50} value of 140 µg/ml. All the fractions exhibited appreciable percentage inhibition with the exception of fraction 1 (GMF1) that shows negligible percentage inhibition and with no IC_{50} value Table 2. The observation might be due to the fact that plant constituents respond differently to different assays [27]. On the other hand fraction 7 (GMF7) has the highest antioxidant activity having 79.42% and 140 µg/ml as percentage inhibition and IC_{50} value respectively.

3.2.2 Assay of nitric oxide (NO) radical scavenging activity of DCM extracts and fractions

The antioxidant content of medicinal plants may play a vital role in the defence against diseases [28]. Another assay used to evaluate the free radical scavenging potential is NO. The percentage inhibition obtained for DCM extract (GODE) was 59. 00% with an IC_{50} of 250 µg/ml. All the fractions exhibited antioxidant activities with fractions 1 and 2 (GDF1 and GDF2) that showed an extremely low percentage inhibition of 5.7% and 10.75% respectively with no IC_{50} values Table 3. Again fraction 8 has the highest percentage inhibition of 65.20% and IC_{50} of 420 µg/ml.

Similarly, the MeOH extract and its fraction showed a dose-dependent activity with fraction 8 (GMF8) having 90.07% and IC_{50} 440 µg/ml respectively. Fraction 1 (GMF1) showed the highest antioxidant activity based on the IC_{50} of 45 µg/ml. Fraction 7 also showed an appreciable activity of 72.08% percentage inhibition and IC_{50} 250 µg/ml respectively Table 4.

It is a known fact that plant phenolic compounds, also called polyphenols, are a large and diverse class of compounds with one or more aromatic rings bearing hydroxyl substituent(s) and have an antioxidant potential due to their possibility to act as radical scavengers or free radical terminators. Antioxidant activity is significantly correlated with phenolic and flavonoid contents of plant materials [29]. These findings are in agreement with the phytoconstituents obtained by the GC-MS analysis of the extracts where phenolic compounds were detected [13].

The MeOH extract (GOME) and fractions (GMF) in the DPPH and the NO assays showed more reasonable antioxidant activities when compared to the DCM extract and its fractions. We could make this statement, because in our previous studies of GC-MS analysis on this plant the MeOH extract contained more polyhydroxyl compounds than the DCM extract [13]. It is also a known fact that polyhydroxyl compounds such as flavonoids are good antioxidants. Table 5 is the antioxidant activities of the standard used, ascorbic acid.

3.2.3 Evaluation of total antioxidant capacity (TAC) of DCM extracts and fractions

The concept of total antioxidant capacity (TAC), which originated from chemistry and then was applied to biology and medicine, and further to nutrition and epidemiology [30] was also used to assess the antioxidant activities the extracts and fractions as shown in Tables 6 and 7. The extract and the fractions possess some antioxidant activities. Fractions 4 and 8 (GDF4 and GDF8) with 4.55 and 5.11 mgAAE/g showed the highest antioxidant activities when compared to the standard. In the manner, the extract and its fractions were subjected to the same TAC evaluation. In this evaluation, it was only the fraction 2 GMF2 that showed an appreciable activity with 5.84 mgAAE/g when compared with the standard Table 7. The numerous available TAC assays correlate poorly with each other because various antioxidants react differently in each assay [26]. For example, the results of some assays include a substantial contribution from protein thiols, which do not react at all in other methods. Therefore, to interpret the results it is essential that one understands fully the relative contribution of the individual antioxidants to the methodology being used. Again, the total antioxidant capacity of a solution will depend on the nature of the oxidative abuse. TAC assays measure antioxidant capacity only in the defined conditions of the particular technique used.

Table 1. Antioxidant activities in DPPH test of DCM extract and the Fractions of *G. oreophila*

Conc (µg/ml)	Percentage inhibition							
	GO1	**GDF1**	**GDF2**	**GDF3**	**GDF4**	**GDF5**	**GDF8**	**GDF9**
1000	51.97 ± 1.57	11.63 ± 1.23	10.07 ± 0.72	26.14 ± 0.69	35.96 ± 0.98	38.52 ± 1.42	71.92 ± 1.19	36.52 ± 2.70
500	40.21 ± 1.49	8.01 ± 1.03	10.01 ± 0.74	25.08 ± 0.70	25.39 ± 0.77	34.77 ± 1.27	67.54 ± 1.32	26.77 ± 0.88
250	26.70 ± 2.03	7.44 ± 0.88	8.26 ± 0.22	15.76 ± 0.66	16.26 ± 0.80	22.89 ± 0.41	42.71 ± 0.95	16.20 ± 0.45
125	24.95 ± 1.70	5.82 ± 0.66	6.13 ± 0.33	11.44 ± 1.13	15.95 ± 0.50	15.95 ± 0.30	27.64 ± 0.45	7.38 ± 0.38
62.5	22.89 ± 1.68	4.88 ± 0.94	4.88 ± 0.50	7.44 ± 0.38	11.01 ± 0.88	12.82 ± 0.51	19.14 ± 0.57	6.50 ± 0.74
31.25	22.51 ± 1.88	4.19 ± 0.78	3.38 ± 0.32	8.26 ± 0.68	9.82 ± 0.74	12.13 ± 0.16	9.82 ± 0.29	3.56 ± 0.91
IC_{50} (µg/ml)	910 ± 50	NA	NA	NA	NA	NA	490 ± 10	NA

GO1: DCM Extract; GDF1, 2, 3, 4, 5, 8, 9 DCM Fractions.
Each value represented Mean ± SEM of n=3 reading. Value of p≤0.05 was taken as statistically significant.

Table 2. Antioxidant activities in DPPH test of MeOH extract and the fractions of *G. oreophila*

Conc (µg/ml)	Percentage inhibition				
	GO2	**GMF1**	**GMF2**	**GMF7**	**GMF8**
1000	75.42 ± 0.11	3.69 ± 0.27	70.98 ± 0.72	79.42 ± 0.72	76.92 ± 0.94
500	70.61 ± 1.09		63.85 ± 2.33	78.49 ± 0.41	75.42 ± 2.50
250	64.92 ± 1.89		42.09 ± 2.06	75.86 ± 0.91	71.92 ± 2.27
125	54.47 ± 1.66		27.33 ± 2.31	49.41 ± 3.87	60.48 ± 4.42
62.5	44.97 ± 0.35		12.01 ± 1.21	31.96 ± 1.97	47.53 ± 1.55
31.25	38.09 ± 2.95		2.94 ± 1.44	15.45 ± 2.35	28.33 ± 3.80
IC_{50} (µg/ml)	91.10 ± 10	NA	358.16 ± 10	140 ± 10	110 ± 30

GO2: MeOH Extract; GMF1, 2, 7, 8; MeOH Fractions
Each value represented Mean ± SEM of n=3 reading. Value of p≤0.05 was taken as statistically significant.

Table 3. Antioxidant activities in NO test of DCM extract and the fractions of *G. oreophila*

Conc (µg/ml)	Percentage inhibition							
	GO1	**GDF1**	**GDF2**	**GDF3**	**GDF4**	**GDF5**	**GDF8**	**GDF9**
1000	59.00 ± 2.16	5.74 ± 016	10.75 ± 0.23	49.07 ± 0.91	22.91 ± 1.13	41.62 ± 0.26	65.20 ± 0.11	47.67 ± 0.29
500	55.12 ± 0.88			48.35 ± 1.21	18.05 ± 0.08	22.91 ± 0.18	54.03 ± 0.69	35.57 ± 0.00
250	49.53 ± 2.41			41.37 ± 0.29	12.87 ± 1.50	15.93 ± 0.15	43.43 ± 0.37	26.27 ± 0.66
125	35.83 ± 0.77			34.49 ± 2.74	10.50 ± 1.72	10.65 ± 0.58	14.01 ± 0.66	23.37 ± 0.37
62.5	29.01 ± 0.11			16.91 ± 2.60	8.17 ± 0.80	4.86 ± 0.26	6.05 ± 0.33	13.60 ± 0.33
31.25	18.30 ± 1.54			9.41 ± 2.41	0.46 ±0.26	3.52 ± 0.95	2.69 ± 0.07	9.31 ± 0.22
IC_{50} (µg/ml)	250 ± 20	NA	NA	NA	NA	NA	420 ± 10	NA

GO1: DCM Extract; GDF1, 2, 3, 4, 5, 8, 9 DCM Fractions.
Each value represented Mean ± SEM of n=3 reading. Value of p≤0.05 was taken as statistically significant.

Table 4. Antioxidant activities in NO test of MeOH extract and the fractions of *G. oreophila*

Conc (µg/ml)	Percentage Inhibition				
	GO2	**GMF1**	**GMF2**	**GMF7**	**GMF8**
1000	65.77 ± 0.15	85.09 ± 2.45	30.56 ± 0.26	72.08 ± 1.24	90.07 ± 0.15
500	53.36 ± 1.17	75.13 ± 0.69	25.08 ± 1.13	64.89 ± 3.77	67.63 ± 2.71
250	28.90 ± 0.34	68.98 ± 0.15	13.44 ± 0.29	51.24 ± 0.04	39.14 ± 0.13
125	24.25 ± 1.65	60.91 ± 3.22	9.72 ± 0.29	48.14 ± 1.50	19.18 ± 0.11
62.5	17.32 ± 0.26	55.53 ± 1.54	7.55 ± 0.29	39.25 ± 0.11	8.89 ± 0.77
31.25	4.60 ± 1.43	43.43 ± 0.00	6.20 ± 0.22	26.16 ± 0.22	7.81 ± 0.48
IC_{50} (µg/ml)	472.12 ± 10	45.83 ± 0.13	NA	250 ± 20	440 ± 30

GO2: MeOH Extract; GMF1, 2, 7, 8; MeOH Fractions.
Each value represented Mean ± SEM of n=3 reading. Value of p≤0.05 was taken as statistically significant.

Table 5. Antioxidant activities of the standard, ascorbic acid

Conc (µg/ml)	DPPH		Nitric oxide
	Percentage inhibition	Conc (µg/ml)	Percentage inhibition
10	40.05 ± 1.89	125	86.86± 2.50
5	25.65 ± 1.67	62.5	52.86 ± 2.63
2.5	12.00 ± 1.62	31.25	34.98± 1.14
1.25	10.01 ± 0.95	15.625	16.61± 0.75
0.625	9.39 ± 0.91	7.8125	8.065± 0.58
0.3125	6.20 ± 0.25		
IC_{50} (µg/ml)	> 10	IC_{50} (µg/ml)	56.26 ± 0.22

Each value represented Mean ± SEM of n=3 reading. Value of p≤0.05 was taken as statistically significant.

Table 6. TAC and FRAP assays of DCM extract and the fractions of *G. oreophila*

Assays	Extracts and fractions								
	Rutin (Std)	GO1	GDF1	GDF2	GDF3	GDF4	GDF5	GDF8	GDF9
TAC (mg AAE/g)	8.34 ±0. 01	3.73 ± 0.15	0.43 ±0.11	3.07 ± 0.18	1.57 ± 0.14	4.55 ± 0.06	3.00 ± 0.44	5.11 ± 0.13	1.75 ± 0.09
FRAP (mg AAE/g)	826.56 ± 0.29	622 ± 11.6	70.7 ± 1.45	404 ± 4.90	603 ± 8.29	438 ± 18.9	640 ± 20.9	752 ± 7.40	394 ± 14.4

Table 7. TAC and FRAP assays of MeOH extract and the fractions of *G. oreophila*

Assays	Extract and fractions					
	Rutin (Std)	GO2	GMF1	GMF2	GMF7	GMF8
TAC(mg AAE/g)	8.34 ±0.01	1.04 ± 0.09	1.97 ± 0.24	5.84 ± 0.05	1.59 ± 0.09	0.04 ± 0.01
FRAP(mg AAE/g)	826.56 ± 0.29	672 ± 16.2	346 ± 4.01	599 ± 24.7	549 ± 7.31	447 ± 7.89

3.2.4 Evaluation of ferric reducing antioxidant power (FRAP) of DCM extracts and fractions

Possibly damaging reactive oxygen species (ROS) are produced as a consequence of normal aerobic metabolism These ‘‘free radicals’’ are usually removed or inactivated in vivo by a squad of antioxidants Individual members of the antioxidant defence team are deployed to prevent generation of ROS, to destroy potential oxidants, and to scavenge ROS. In this perspective, antioxidant power may be referred to analogously as reducing ability [31]. With this in mind, a method using reductants in a redox-linked colorimetric method employing an easily reduced oxidant in stoichiometric excess could offer a simple way of assessing this ability hence the use of FRAP to assess the reducing power of the extracts and the fractions in this study. The DCM extract (GODE) and fractions 3, 5 and 8 (GDF1, GDF3 and GDF8) showed appreciable antioxidant activities with 622, 603 and 752 mgAAE/g when compared with the standard of 826 mgAAE/g Table 6. Likewise the extract, (GME) exhibited potent antioxidant activity with 673 mgAAE/g compared to the standard. Fractions 2 and 7 showed reasonable activities in Table 7. This is in agreement to the observation of Young, [32]. This investigation is similar to the research of other investigators who worked on similar species such as *Globimetula braunii* [33,34], *Globimetula cupulata* [35].

3.3 Membrane Stabilization Profiles of *G. oreophila* Extracts and Fractions

Membrane stabilization is regarded as a possible mechanism of action of the anti-inflammatory activity of certain medicinal plants [36,37]. This is confirmed by several investigations that herbal preparation and their mixtures were capable of stabilizing the red blood cell membrane and exerting anti-inflammatory activity [38,39].

Erythrocytes have been used as a model system by numerous researchers for the study of the interaction of drugs with membranes [40,41,42]. When the RBC is subjected to hypotonic stress the release of hemoglobin (Hb) from RBC is prevented by anti-inflammatory agents because of membrane stabilization. So, the stabilization of RBC membrane by drugs against hypotonicity induced haemolysis serves as a useful in vitro method for assessing the anti-inflammatory activity of various compounds [43].

GO1DE, GDF8, GO2ME, GMF1, GMF2, GMF7 and GMF8 were selected for stability assays based on their antioxidant potency as depicted in Tables 1-4. Moreover, Fig. 1a - g depicts the profiles of the membrane stabilizing potentials of (DCM and MeOH) and their various fractions of bovine red blood cells exposed to both heat and hypotonic induced lyses. It was observed that all the extracts and fractions exhibited appreciable and significant membrane stabilizing activities. The extracts and fractions exhibited mixtures of the monophasic and biphasic mode of protection which are concentration dependent and compared favourably with that of standard (diclofenac) a non-steroidal anti-inflammatory drug (NSAD), Fig. 2. Also, the percentage membrane stability exhibited by the extracts and fractions ranged from 2.28 ± 0.01% (minimum) and 72.97 ± 0.12% (maximum), while the minimum and maximum membrane stabilizing activities of the standard drug was 3.45 ± 0.00% and 89.06 ± 0.01%. The findings of this study agreed with previous studies on the membrane stabilizing potentials of extracts and fractions of plants from various sources [44,45,46,47]

3.3.1 Membrane stabilizing profile of the standard drug (Diclofenac)

Diclofenac, the standard drug used has a membrane stability profile as shown in Fig. 2. The mode of response is biphasic in all the concentrations tested and has a minimum of 3.45± 0.00% and a maximum of 89.06 ± 0.01% membrane stability.

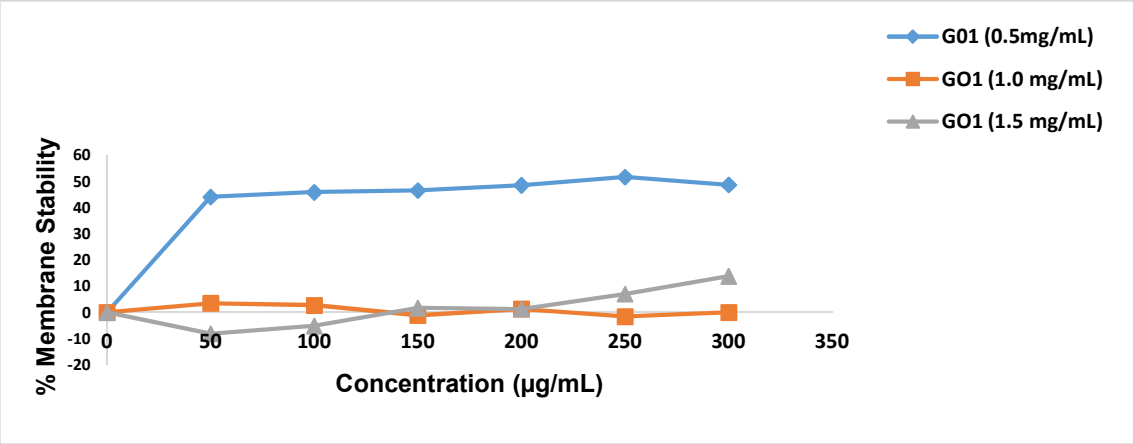

Fig. 1a. Membrane stabilizing profiles of DCM extract of *G. oreophila* on bovine erythrocytes exposed to both heat and hypotonic induced lyses
Each value represented the mean ± SEM of 3 readings

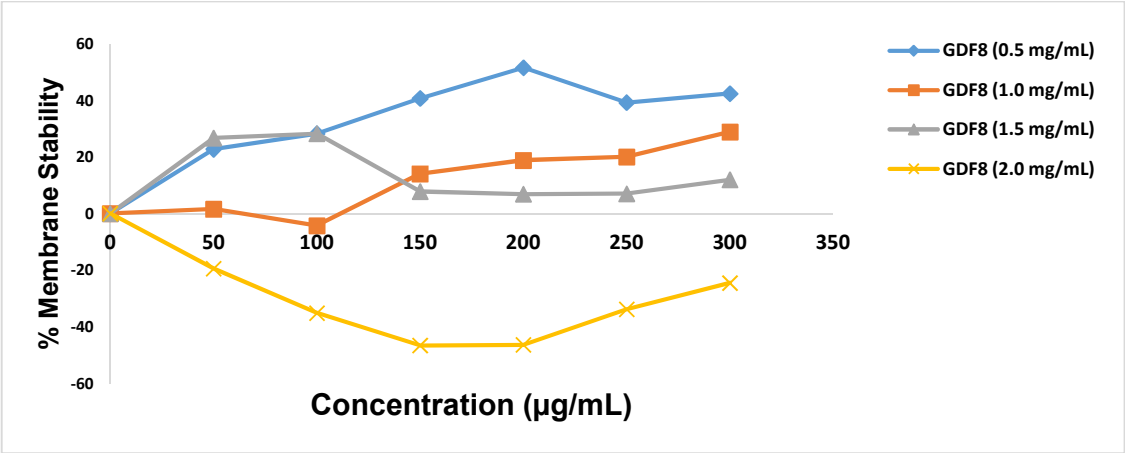

Fig. 1b. Membrane stabilizing profiles of fraction 8 (GDF8), DCM extract of *G. oreophila* on bovine erythrocytes exposed to both heat and hypotonic induced lyses
Each value represented the mean ± SEM of 3 readings

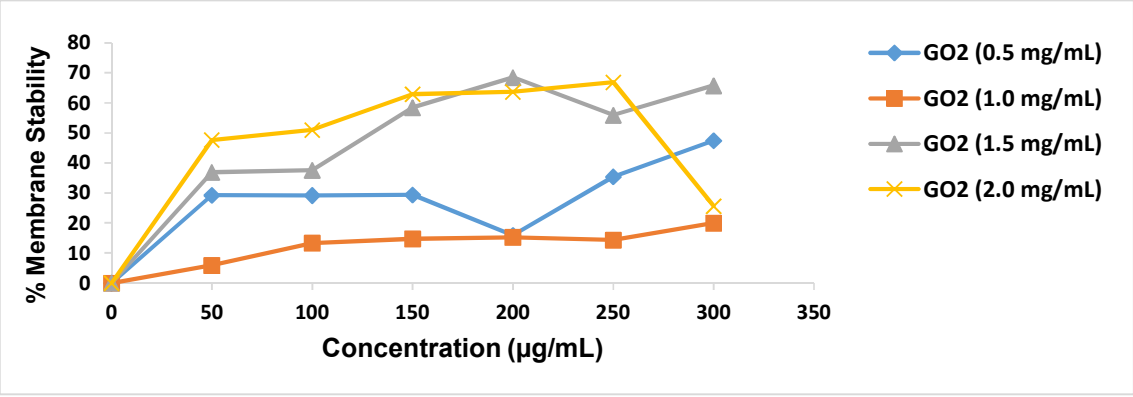

Fig. 1c. Membrane stabilizing profiles of MeOH extract of *G. oreophila* on bovine erythrocytes exposed to both heat and hypotonic induced lyses
Each value represented the mean ± SEM of 3 readings

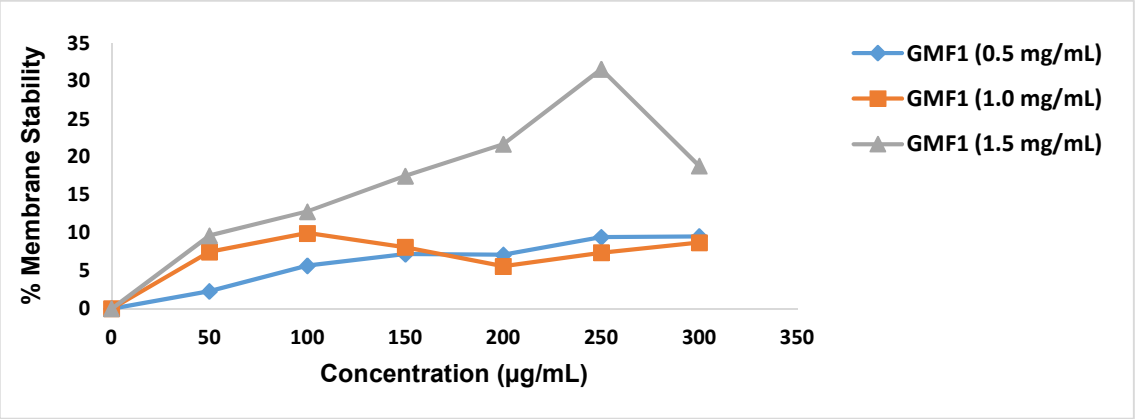

Fig. 1d. Membrane stabilizing profiles of fraction 1 (GMF1), MeOH extract of *G. oreophila* on bovine erythrocytes exposed to both heat and hypotonic induced lyses
Each value represented the mean ± SEM of 3 readings

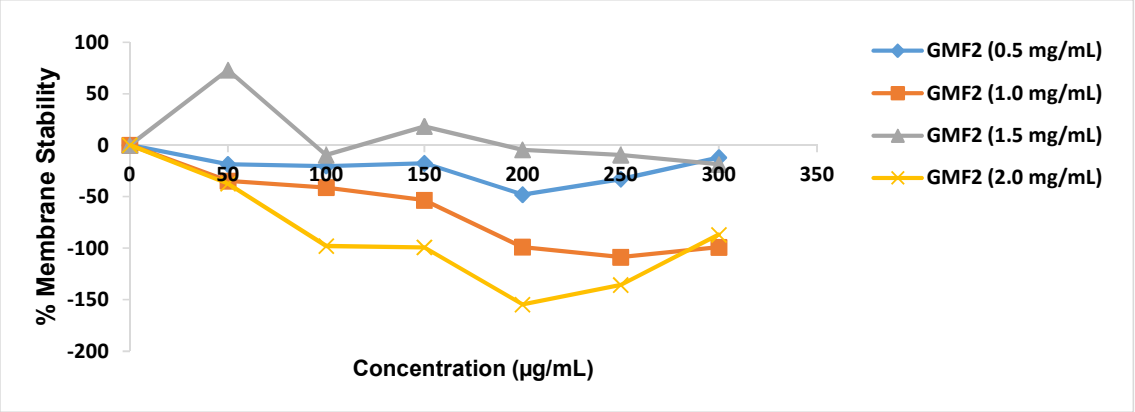

Fig. 1e. Membrane stabilizing profiles of fraction 2 (GMF2), MeOH extract of *G. oreophila* on bovine erythrocytes exposed to both heat and hypotonic induced lyses
Each value represented the mean ± SEM of 3 readings

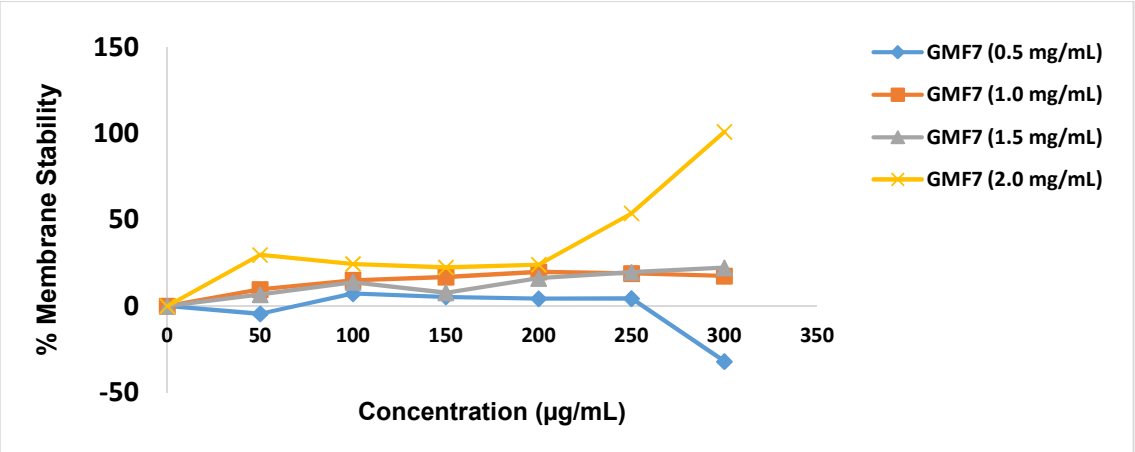

Fig. 1f. Membrane stabilizing profiles of fraction 7 (GMF7), MeOH extract of *G. oreophila* on bovine erythrocytes exposed to both heat and hypotonic induced lyses
Each value represented the mean ± SEM of 3 readings

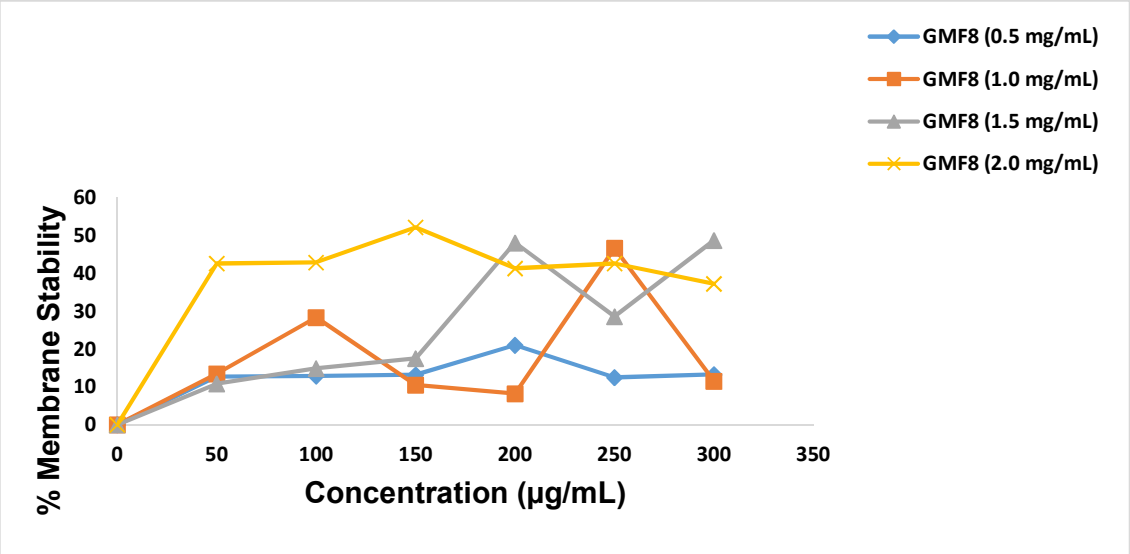

Fig. 1g. Membrane stabilizing profiles of fraction 8 (GMF8), MeOH extract of *G. oreophila* on bovine erythrocytes exposed to both heat and hypotonic induced lyses
Each value represented the mean ± SEM of 3 readings

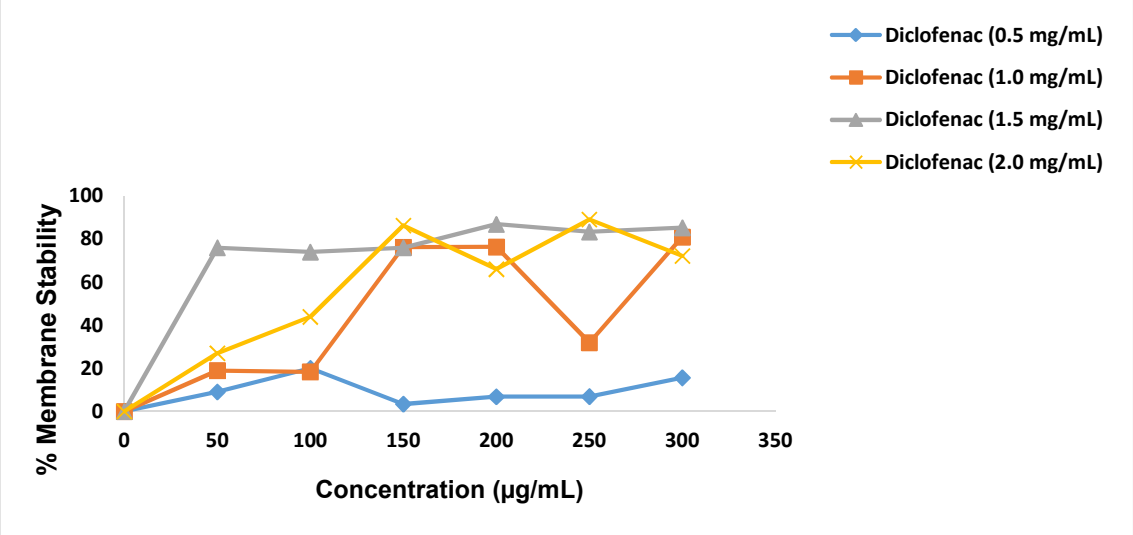

Fig. 2. Membrane stabilizing profiles of Diclofenac on bovine erythrocytes exposed to both heat and hypotonic induced lyses
Each value represented the mean ± SEM of 3 readings

4. CONCLUSION

The present study indicates that the extracts and fractions of *G. oreophila* have strong free radical scavenging activity and reducing power. This anti-oxidative effectiveness of the extracts and the fractions was evidenced in all the methods used for the antioxidant assays through their percentage inhibition and their IC_{50} values.

The study also showed that all the seven samples assayed, MeOH extract (GOME) and the fractions of *G. oreophila,* protected the stressed bovine erythrocyte membrane at some of the concentrations

used and compare favourably with Diclofenac (standard drug). It was also noted that MeOH extract of *G. oreophila* fraction 7 (GMF7), protected the erythrocyte membrane more effectively than the standard drug. Although, fraction GMF7 exhibited 100% mode of protection at 2.0 mg/mL but was not better in its activity at different concentrations when compared with the standard drug (diclofenac, Fig. 2). On the basis of these results, it could be inferred that the extracts and the fractions of *G. oreophila* contain principles that were capable of stabilizing bovine red blood cell membrane exposed to heat and hypotonic-induced lyses and could, therefore, serve as a scientific proof for the use of these plant extracts by the local traditional health practitioners in the management and treatment of inflammatory related diseases.

COMPETING INTERESTS

Authors have declared that no competing interests exist.

REFERENCES

1. Oluwole O, Osungunna MO, Abimbola Y, Phytochemical and antimicrobial screening of *Globimetula oreophila* (Oliv) van Tiegh and *Phragmanthera capitate* (Spreng) Balle. International Journal of Green Pharmacy. 2013;7:127–130.
2. Faboro Esther O, Wichitnithad Wisut, Fadare Olatomide A, Akinpelu David A, Obafemi Craig A. Antibacterial, Antioxidant activities and phytochemical screening of aqueous methanol extracts of eight Nigerian medicinal and aromatic plants. Journal of Pharmacy Research. 2016;10(7): 523-532.
3. Adodo A. Nature power: A Christian approach to herbal medicine. Lagos: Generation Press Limited. 2006;103-10.
4. Osadebe PO, Ukwueze SE. A comparative study of the phytochemical and antimicrobial properties of the Eastern
5. Nigerian species of African Mistletoe (*Loranthus micranthus*) sourced from different host areas trees. J Biol Res Biotechnol. 2004;2:18-23.
6. Osadebe PO, Okide GB, Akabogu IC. Study on anti-diabetic activities of crude methanolic extracts of *Loranthus micranthus* (Linn.) sourced from five different host trees. J Ethnopharmacol 2004; 95:133-8.
7. Uzochukwu IC, Osadebe PO. Comparative evaluation of antidiabetic activities of Flavonoids extract and crude methanol extract of *Loranthus micranthus* parasitic on Kola acuminate. J Pharmaceut Appl Sci 2007;4:2-7.
8. Obatomi DK, Bikomo EO, Temple VJ. Anti-diabetic properties of the African mistletoe in streptozotocin-induced diabetic rats. J Ethnopharmacol 1994;43:13-7.
9. Jadhav N, Patil CR, Chaudhari KB, Wagh JP, Surana SJ, Jadhav RB. Diuretic and natriuretic activity of two mistletoe species in rats. Pharmacognosy Res 2010;2:50-7.
10. Osadebe PO, Omeje EO. Comparative acute toxicities and immunomodulatory potentials of five Eastern Nigeria mistletoes. J Ethnopharmacol 2009;126:287-93.
11. Adesina SK, Illoh HC, Johnny II, Jacobs IE. African Mistletoes (Loranthaceac), ethnopharmacology, chemistry and medicinal values: An update. Afr. J. Tradit. Complement. Altern. Med. 2013;10(4):161-70.
12. Matsushima K, Nemoto K, Nakashima N, Dema D, Thapa L, Watanabe A, Maegawa F, Baba T, Matsushita G. Report of investigation for wild edible plants and their traditional knowledge in Bhutan. J. Fac. Agric. Shinshu Univ. 2006;42:37–46.
13. Faboro EO, Wei L, Liang S, McDonald AG. Obafemi CA. Characterization of dichloromethane and methanol extracts from the leaves of a medicinal plant*: Globimetula oreophila*. Industrial Crop and Products. 2016;83:391-399.
14. Le O, Zam NWORU. Oxytocic properties of the aqueous extract of *Globimetula braunni* (Loranthaceae). Pak J Pharm Sci. 2008;21:356-60.
15. Adediwura FJ, Temitope O, Oluwakemi A. Phytochemical and laxative studies of *Globimetula braunii* (Engle) van Tiegh growing on *Cola acuminata* (Schott & Endl). Afr. J. Tradit. Complement. Altern. Med. 2008;5:419.

16. Okpuzor J, Ogbunugafor H, Kareem GK. Antioxidative properties of ethyl acetate fraction of *Globimetula braunii* in normal albino rats. J BiolSci. 2009;9:470-75.
17. Blois MS. Antioxidant determinations by the use of a stable free radical. Nature 1958;29:1199-1200.
18. Brand-Williams W, Cuvelier ME, Berset C. Use of free radical method to evaluate antioxidant activity. Lebensm Wiss Technology. 1995;28:25-30.
19. Green LC, Wagner DA. Glogowski J, Skipper PL, Wishnok JS, Tannenbaum SR. Analysis of nitrate, nitrite and nitrate in biological fluids. Analytical Biochemistry 1982;126:131–138.
20. Marcocci L, Maguire JJ, Droy-Lefaix MT, Packer L. The nitric oxide-scavenging properties of *Ginkgo biloba* extract EGb 761. Biochem Biophys Res Commun. 1994;15:748–755.
21. Huang D, Ou B, Prior RL. The chemistry behind antioxidant capacity assays. Journal of Agricultural and Food Chemistry. 2005;53:1841-1856.
22. Gordon MH. The mechanism of antioxidant action in vitro. In food antioxidants, Hudson BJF (ed.). Elsevier: London. 1990;1-18.
23. Prieto P, Pineda M, Aguilar M. Spectrophometric quantitation of antioxidant capacity through the formation of phosphomolybdenum complex: Specific application to the determination of Vitamin E. Analytical Biochemistry. 1999;269:337-341.
24. Benzie IFF, Strain JJ. Ferric reducing antioxidant power assay: Direct measure of total antioxidant activity of biological fluids and modified version for simultaneous measurement of total antioxidant power and ascorbic acid concentration. Methods Enzymology. 1999;299:15–27.
25. Oyedapo OO, Akinpelu BA, Akinwunmi KF, Adeyinka MO, Sipeolu FO. Red blood cell membrane stabilizing potentials of extracts of *Lantana camara* and its fractions. International Journal of Plant Physiology and Biochemistry. 2010;2(4):46-51.
26. Oyedapo OO, Famurewa AJ. Antiprotease and membrane stabilizing activities of extracts of *Fagara Zanthoxyloides Olax subscorpioides* and *Tetrapleura tetraptera.* International Journal of Pharmacognosy. 1995;33:65-69.
27. Cao G, Prior RL. Comparison of different analytical methods for assessing total antioxidant capacity of human serum. Clinical Chemistry. 1998;44:1309–15.
28. Akinmoladun AC, Ibukun EO, Afor E, Akinrinlola BL, Onibon TR, Akinboboye AO, Obuotor EM, Farombi EO. Chemical constituents and antioxidant activity of *Alstonia boonei.* African Journal of Biotechnology. 2007;6:1197-1201.
29. Zhang R, Zeng Q, Deng Y, Zhang M, Wei Z, Zhang Y, Tang X. Phenolic profiles and antioxidant activity of litchi pulp of different cultivars cultivated in Southern China. Food Chemistry. 2013;136:1169–1176.
30. Sies H. Total antioxidant capacity: Appraisal of a concept. Journal of Nutrition 2007;137:1493–1495.
31. Iris FF, Benzie JJ. Strain. The ferric reducing ability of plasma (FRAP) as a Measure of antioxidant power: The FRAP assay. Analytical Biochemistry. 1996;239:70–76.
32. Young IS. Measurement of total antioxidant capacity. Journal of Clinical Pathology. 2001;54:339.
33. Okpuzor J, Ogbunugafor H, Kareem GK. Antioxidative properties of ethyl acetate fraction of *Globimetula braunii* in normal Albino rats. Journal of Biological Sciences. 2009;9(5):470-475.
34. Ja'afar MK, Jamil S, Basar N. Antioxidant activity of leaf extracts of *Globimetula braunii* (Engler) van tiegh parasitizing on *Piliostigma thonningii* and *Parkia biglobos*a Jurnal Teknologi (Sciences & Engineering). 2017;79:5,43–47
35. Cao G, Prior RL. Comparison of different analytical methods for assessing total antioxidant capacity of human serum. Clinical Chemistry. 1998;44:1309–15.
36. Sadique J, Al-Rqobah NA, Bughaith MF, El-Gindy AR. The bioactivity of certain medicinal plants on the stabilization of RBC membrane system. Fitoterapia LX. 1989;525-532.
37. Shinde UA, Phadke AS, Nair AM, Mungantiwar AA, Dikshit VJ, Saraf VO. Membrane stabilizing activity–a possible mechanism of action for the anti-inflammatory activity of *Cedrus deodara* wood oil. Fitoterapia. 1999;70:251-257.

38. Oyedapo OO, Akindele VR, Okunfolami KO. Effects of the extracts of *Olax subscorpioides* and *Aspilia africana* on bovine red blood cells. Phytotherapy Research. 1997;11:305-306.
39. Akinpelu BA, Makinde AM, Isa MO, Taiwo OP, Ojelabi OM, Oyedapo OO. *In vitro* evaluation of membrane stabilizing potential of selected bryophyte species. European Journal of Medicinal Plants. 2015;6(3):181-190.
40. Sessa G, Weisman G. Effect of components of the polyene antibiotic, Fillipin on phospholipids spherules (liposomes) and erythrocytes. Journal of Biological Chemistry. 1968;243:4364-4371.
41. Litman G, Litman RT, Hennry CJ. Analysis of lipophilic carcinogen-membrane interaction using model human erythrocytes membrane system. Cancer Research. 1976;36:438-444.
42. Horie T, Sugiyama V, Awazu S, Hanano M. The correlation between drug binding to the human erythrocyte and its hemolytic activity. Journal of Pharmacology. 1979;4:116-122.
43. Nambi RA, Sukumar D, Sethuraman V, Suluchana N, Sadique J. Satellite symposium on traditional medicine as Asian congress of pharmacology. Tamil University Thanjavur. 1985;140.
44. Sadique J, Al-Rqobah NA, Bughaith MF, El-Gindy AR. The bioactivity of certain medicinal plants on the stabilization of RBC membrane system. *Fitoterapia* LX. 1989;525-532.
45. Oyedapo OO, Famurewa AJ. Antiprotease and membrane stabilizing activities of extracts of *Fagara Zanthoxyloides Olax subscorpioides and Tetrapleura tetraptera.* Int. J. Pharmacogn. 1995;33:65-69.
46. Oyedapo OO, Akinpelu BA, Orefuwa SO. Anti-inflammatory effects of *Theobroma cacao*, L. root extract. J. Tropical Med. Plants (Malaysia). 2004;592:161-166
47. Oyedapo OO, Akinpelu BA, Akinwunmi KF, Adeyinka MO, Sipeolu FO. Red blood cell membrane stabilizing potentials of extracts of *Lantana camara* and its fractions. International Juornal of Plant Physiology and Biochemistry. 2010;2(4):46-51.

Biography of author(s)

Dr. Esther O. Faboro
Department of Chemistry, Bowen University, Iwo, Nigeria.

She obtained her Bachelor of Technology degree in Industrial Chemistry from Abubakar Tafawa Balewa University Bauchi, Nigeria in 1991. She had her Master of Science degree in Organic Chemistry from University of Ibadan, Nigeria in 2001. Upon graduation, she worked with Osun State Ministry of Education as Education Officer between 2001 and 2007. She joined Bowen University, Iwo, Nigeria as an Assistant Lecturer in 2007. She had her M. Phil. and Ph.D in Chemistry from Obafemi Awolowo University, Ile Ife, Nigeria in 2012 and 2016 respectively. She is presently a Lecturer at Bowen University. She has published many articles in both Local and International Journals and she is a reviewer to some International Journals; amongst them are European Journal of Medicinal Plants and Biotechnology Journal International. Her areas of interest include Spectroscopic Characterization of Natural Products, Phytomedicine, Pharmacological Studies and Traditional Medicine. She is a Fellow of the Chemical Society of Nigeria, Member, American Chemical Society and Institute of Chartered Chemists of Nigeria. She is the Chairman of Chemical Society of Nigeria, Osun State Chapter. In 2014, she was a recipient of Osun State Special Bursary Award granted to enable her carry out part of her research work in USA. She has been privileged to travel as a Visiting Scholar to West Virginia University, Morgantown, WV, USA in 2010 and to University of Idaho, Moscow, ID, USA in 2014. She has made presentations at both Local and International Conferences.

Mr. Idowu J. Olawuni
Department of Biochemistry, Obafemi Awolowo University, Ile Ife, Nigeria.

He is a Lecturer II in the Department of Biochemistry and Molecular Biology, Obafemi Awolowo University, Ile-Ife. He obtained a Bachelor of Science (B.Sc. Honours) Degree in Biochemistry from the Obafemi Awolowo University, Ile-Ife, Nigeria, in 2008. He also obtained a Master Degree (M.Sc.) in Biochemistry from the same university in 2014. Presently, he is on the verge of completing his Ph.D. degree in Biochemistry from Obafemi Awolowo University, Ile-Ife, Nigeria. His research work is in the area of Neurochemistry/Natural Product Research, geared towards exploiting compounds from natural products as potential inhibitors of enzymes relevant to Alzheimer's disease pathology, especially cholinesterase and beta secretase enzymes in order to enhance the cognitive function of individuals suffering from neurodegenerative disorders such as Alzheimer's disease (AD). He is an expert in computational biology, using various softwares to carry out computational studies such as molecular docking, molecular simulation, ADMET study, etc. His research work has established the anticholinesterase, antioxidant, as well as cognitive enhancing properties of essential oil from two Nigerian spices namely: *P. nigrum* and *M. myristica*. He is a beneficiary of Federal Government Needs Assessment for Academic Staff Training and Development (AST&D) in 2014/2015 Academic Session. He is a member of Nigerian Society of Biochemistry and Molecular Biology as well as a member of International Society for Neurochemistry. He has published up to 20 papers in reputable journals and has participated in various scientific conferences and workshops.

Dr. Bolajoko A. Akinpelu
Department of Biochemistry, Obafemi Awolowo University, Ile Ife, Nigeria.

She is an Associate Professor in the Department of Biochemistry and Molecular Biology, Obafemi Awolowo University, Ile- Ife. Her research work is focused in the area of natural product Biochemistry and toxicology particularly evaluating the biochemical basis on the ethnomedicinal uses of plants with the view to ascertain their possible mechanism of action. Through her research, she has contributed to available information on potential and safety on some plants and vegetables as well as certain bryophytes in the treatment of anti-inflammatory and oxidative stress related diseases. She is a recipient of Carnegie Sponsored Fellowship Award to University of Kwazulu-Natal, Durban, South Africa (May-Aug. 2008) and principal investigator of Tetfund and NRF award on research project titled: "Risk assessment of some commonly used pesticides on the West African honeybee *Apis mellifera adansonii* L. in Nigeria" (2018). She has published over 35 papers in reputed journals and has participated in reputable scientific conferences. She has also served as a reviewer for local and international scientific journals among which are Ife Journal of Science, Nigerian Journal of Natural Product and Medicine as well as Academic Journals. She is a member of Nigeria Society of Biochemistry and Molecular Biology, West African Network of Natural Products Research Scientists, West African Society of Pharmacology and Organization for Women in Science in Developing World (OWSD).

Professor Oluokun O. Oyedapo
Department of Biochemistry, Obafemi Awolowo University, Ile Ife, Nigeria.

He is a Professor of Biochemistry and Molecular Biology, Faculty of Science, Obafemi Awolowo University, Ile-Ife, Nigeria. He attended University of Ife (now Obafemi Awolowo University, Ile-Ife) between 1976 and 1979, where he obtained B. Sc. (Biochemistry). He also obtained higher degrees (M. Sc. and Ph.D.) in Biochemistry from Obafemi Awolowo University, Ile-Ife in 1983 and 1990 respectively. He joined the service of Obafemi Awolowo University in 1985 as an Assistant Lecturer, regraded Lecturer II (1990), Lecturer I (1991), Senior Lecturer (1995), Reader (1999) and Professor of Biochemistry (2002). His area of interests are Pharmacology and Toxicology, Medicinal Plants, Pharmacognosy, Biochemistry and Phytomedicine. Presently, he has to his credit over eight five (85) scientific publications in foreign and local peer-reviewed reputable international and Nigerian based journals. Moreover, he has supervised eight (08) doctorate degrees and about twenty (20) M. Sc. degrees. He is an experienced examiner, who has served as external examiner in many Universities both in Nigeria and other parts of the world. He has served and still serving as assessor for the promotion to the grades of Professor and Associate Professor of Biochemistry and related fields and disciplines. He is a reviewer for both local and international journals. He belongs to various learned societies among which are Nigeria Society of Biochemistry and Molecular Biology and Nigerian Society of Experimental Biology.

Professor Ezekiel O. Iwalewa
Department of Pharmacology and Therapeutics, University of Ibadan, Ibadan, Nigeria.

He is a Professor of Pharmacology and Therapeutics, College of Medicine University of Ibadan. He attended the University of Ibadan, in 1980 and graduated with B.Sc. (Pharmacology) Hons degree (second class upper) in 1983. He had his M.Sc. in UI 1987 and Ph.D. from Ahmadu Bello University, Zaria in 1995. He began lecturing at ABU as Assistant Lecturer in 1988 until 1995 from where he moved to Obafemi Awolowo University, Ile-Ife (OAU) as Lecturer I. He became a full Professor at OAU, in 2010. He was appointed Professor in UI (December 2012). He has published 112 research articles, in reputable local and international journals. He has supervised 25 M.Sc., 3 M.Phil. and 10 Ph.D. theses. He is a member of many learned/professional bodies at home and abroad. He has contributed to the creation of many Pharmacology societies and presented papers in Conferences in three continents of the world. He is a Reviewer for many local and international journals and an external examiner to many Universities. His scientific area of interest is in Ethnopharmacology and Toxicology of Medicinal Plants and Natural Products as agents in Chemotherapy of Infections and Inflammations which involves screening of medicinal plants extracts and pure compound (plant derived or synthetic) for anti-inflammatory, antimalarial, antioxidants and anti-diabetics activities, determining the effects of the extracts/compounds with promising activities on NO, proteins (e.g. chaperones – heat shock proteins) at biochemical and molecular levels and the effects of extracts/compounds on such interactions in malaria and other diseases.

Professor Craig A. Obafemi
Department of Chemistry, Obafemi Awolowo University, Ile Ife, Nigeria.

He attended Christ's School, Ado-Ekiti, 1964-1970 for his West African School Certificate and Higher School certificate. He had his higher education at the University of Ibadan where he obtained his Bachelor's degree in Chemistry, 1974, Master of Philosophy degree in Chemistry, 1977 from the University of Ife (now Obafemi Awolowo University, Ile-Ife) and a Ph.D. in Chemistry from the University of Saskatchewan, Saskatoon, Canada, 1981. He became a Professor of Chemistry at Obafemi Awolowo University in 1992. He specializes in the design, synthesis, spectroscopic characterization and evaluation of biological activity of organic compounds and isolation and characterization of bioactive compounds from plant resources. He is the recipient of the International Tin Research Institute, Research Fellowship, UXBRIDGE, LONDON (1991), the Alexander von Humboldt, Stiftung Fellowship (Federal Republic of Germany) (1991-1993) and Fellow of the Chemical Society of Nigeria. His research group continued to study the quinoxaline-2,3-dione pharmacophore and results have shown that many of its derivatives possess neuropharmacological effects and potent antimicrobial activity. His group was awarded a Certificate of Recognition by Elsevier for Elsevier's top 25 cited articles for the years 2010-2011. [Ajani et al 2010]. *Bioorganic and Medicinal Chemistry*, Vol. 18 (No 1), pp 214-221]. He has published over 75 articles in international journals and graduated several Masters' and Doctoral students, some are now Professors. He was the Managing Editor of Ife Journal of Science (2006 - 2010) and is the publisher and Editor-in-Chief of Journal of Phytomedicine, Synthetic Medicinal and Business Chemistry (JPSMBC).

© Copyright (2020): Author(s). The licensee is the publisher (Book Publisher International).

DISCLAIMER
This chapter is an extended version of the article published by the same author(s) in the following journal.
Chemical Science International Journal, 23(3): 1-15, 2018.

Reviewers' Information
(1) Piotr Michel, Medical University of Lodz, Poland.
(2) Fatma Kandemirli, Kastamonu University, Turkey.
(3) Bruno dos S. Lima, Federal University of Sergipe, Brazil.

Chapter 12
Print ISBN: 978-93-90206-41-4, eBook ISBN: 978-93-90206-42-1

Studies on UV Spectrophotometric Analysis of Drugs Terbinafine Hydrochloride and Clarithromycin

R. Mrutyunjaya Rao[1*] and C. S. P. Sastry[2]

DOI: 10.9734/bpi/crdc/v4

ABSTRACT

Quality assurance for control of pharmaceutical chemicals and formulations is essential for ensuring the availability of safe and effective drug formulations to consumers. Quantitative estimation of the chemical entity of a drug is vital for maintaining and assuring the quality. Several distinct problems are encountered in the quantitative estimation of the drug in bulk samples and formulations. The interferences caused by a number of sources such as the degradation products of the drugs when they are stored for a long time, the presence of other drugs in combination products and the various additives incorporated in formulations have to be kept in view during the course of assay development for drugs in formulations. Among the various techniques for the development of assay methods, uv-visible spectrophotometry combines the advantages of low cost, easy maintenance and simplicity with the possibility of achieving high sensitivity and selectivity with good precision, accuracy and reliability. The selectivity and sensitivity of the uv-visible spectrophotometric method depends only on the nature of chemical reactions involved in color development and not on the sophistication of the equipment. The expenditure incurred on the assay determination in visible spectrophotometric methods depends on selecting the reagents (low cost, readily available) for the color development.
With above facts I am herewith enclosing my research work in estimation of terbinafine hydrochloride and clarithromycin with the help of UV spectrophotometric method as narrated below.
One simple and sensitive procedure (UV spectophotometric method) for the assay of two drugs namely terbinafine hydrochloride and clarithromycin in pure form and formulations. This method involves the formation of ion-association complex between TRB or CAM and the picric acid. In order to establish the optimum conditions necessary for rapid and quantitative formation of coloured product with maximum stability and sensitivity, the author performed experiments by measuring the absorbance at λ_{max} 350nm of a series of solutions, varying one and fixing the other parameters in each case such as type, volume and concentration of acid, organic solvent used for extraction, ratio of organic phase to aqueous phase during extraction, shaking time and temperature. The variable parameters were optimized. The results were statistically validated. The regression analysis using the method of least squares was made for the slope (b), standard deviation (S_b), intercept (a), standard deviation on intercept (S_a), standard error of estimation (Se) and correlation coefficient (r) obtained from different concentrations. The data obtained in the determination of each drug with different reagents are summarized in this section. The selectivity (or specificity) of each proposed method was ascertained through interference studies with other active and inactive ingredients usually present in pharmaceutical preparations.

Keywords: Terbenafine hydrochloride; clarithromycin; spectrophotometer and picric acid.

1. INTRODUCTION

Terbinafine hydrochloride (TRB) [1-naphthalene methanamine N-[(2E) 6,6 dimethyl-2-heptene-4ynyl]-N-methyl] is a synthetic alylamine anti-fungal compound exists in the market in the form of tablets and

[1]SRKR Engineering College, Chinna Ammiram, Bhimavaram, India.
[2]Foods and Drugs Laboratories, Department of Organic Chemistry Foods, Drugs and Water, Andhra University, Visakhapatnam-530003, India.
**Corresponding author: E-mail: rmj.rao@rediffmail.com;*

cream. It is official in USP [1], Merck Index [2] and Martindale Extra Pharmacopoeia [3]. Clarithromycin or 6-0 methyl erythromycin or [2R, 3S, 4S,5R,6R,8R,10R,11R,12S, 13R) -3-(2,6-Dideoxy-3C, 3-0-dimethyl-α-L-ribo-hexopyranosyloxy)]-11,12-dihydroxy-6- methoxy, 2,4,6,8,10,12-hexamethyl-9-oxo- 5-(3,4,6-trideoxy-3-dimethylamino β-D-xylo- hexopyranosyloxy) pentadecan-13-olide. is a macrolide antibacterial hydroxylated macro cyclic lactones containing 12 to 20 carbon atoms in the primary ring bind to the 50s sub units of bacterial ribosomes indicated to treat infections caused by bacteria. It is official in, USP [4], Merck index [5], Martindale's extra pharmacopoeia [6], Remington [7], PDR [8]. Existing analytical methods are reveal that little attention paid in developing the UV spectrophotometric methods for its determination. The present paper describes the determination of two drugs namely terbinafine hydrochloride and clarithromycin by reaction with the reagent picric acid.

Picric acid is a chemical known as symmetrical trinitrophenol and is acidic in nature and forms an adduct with aromatic hydrocarbons such as naphthalene and anthracene. It also forms picrate of the amine extractable into chloroform which is in an yellow colour but the absorption maxima is located in the UV region. Picric acid has also been used for the determination of reducing sugars as they undergo reduction to orange color picramic acid in alkaline medium [9]. Picric acid is also proposed for the estimation of cardioglycosides [10-12]. TNP is a yellow crystalline, bitter [13,14], toxic [15,16], explosive solid [17] which is widely used in the identification of activated compounds in the labs [18], picric acid is also used in medicinal formulations in the treatment of malaria, trichinosis, herpes and smallpox and antiseptics [19], preparation of charge transfer complexes [20-22] of various utilities etc.

This method involves the formation of Ion-association complex between TRB or CAM and the picric acid. In order to establish the optimum conditions necessary for rapid and quantitative formation of coloured product with maximum stability and sensitivity, the author performed experiments by measuring the absorbance at 350nm of a series of solutions, varying one and fixing the other parameters in each case such as type, volume and concentration of acid, organic solvent used for extraction, ratio of organic phase to aqueous phase during extraction, shaking time and temperature. Picric acid has also been used for the determination of reducing sugars as they undergo reduction to orange color picramic acid in alkaline medium [23]. Picric acid is also proposed for the estimation of cardioglycosides [24-26].

2. EXPERMENTAL

2.1 Instrumentation

All spectral and absorbance measurements were made on a Systronics 106 model visible spectrophotometer with 1 cm matched glass cells or Milton Roy spectronic 1201 UV-visible spectrophotometer with 1 cm matched quartz cells.

All pH measurements were made on a Systronics 335 model digital pH meter or an Elico LI 120 digital pH meter.

2.2 Reagents and Solutions

Picric acid Solution (Loba: 0.1%, 4.36×10^{-2}M)	:	100 mg of picric acid was dissolved in 100 ml of distilled water
Buffer pH – 9.8	:	Prepared dissolving 300 g of monosodium phosphate dihydrate and 9 g of NaOH in 750 ml of water

2.3 Tebinafine Hydrochloride Drug Solution

All the reagents were of analytical grade and all the aqueous solutions were prepared in double distilled water. Freshly prepared solutions were always used. One mg ml-1 stock solution of TRB HCl was prepared by dissolving 100 mg of TRB initially in 5 ml of 0.1 N HCl followed by dilution to 100 ml

with double distilled water. For pharmaceutical formulations of the drug a quantity of tablet powder or cream equivalent to 100 mg of TRB HCl was treated with 4×20 ml portions of chloroform and the chloroform extract was transferred to 100 ml volumetric flask and made upto 100 ml with chloroform to obtain 1 $mg.ml^{-1}$ stock solution. From this solution required concentrations are prepared for further experiments.

2.4 Clarithromycin Drug Solution

One mg ml^{-1} stock solution of CAM in aqueous medium was prepared by dissolving 100 mg of CAM in 5 ml of 0.1M HCl followed by dilution to 100 ml with double distilled water. Tablet powdered equivalent to 100 mg of CAM was dissolved and diluted to 100 ml with chloroform and the insoluble portion was removed by filtration to get 1 $mg.ml^{-1}$. For pharmaceutical formulations of the drug twenty five ml of above stock solution was taken and the chloroform portion was evaporated to dryness and the residue was initially dissolved in 2 ml of 0.1 N HCl followed by dilution to 25 ml with distilled water.

2.5 Recommended Procedure

Method (Picric Acid) for TRB or CAM: Into a series of 50 ml separating funnels containing aliquots of drug (TRB : 0.5-3.0 ml, 50 μg.ml-1; CAM : 0.5-3.0ml, 100 μg.ml-1) solutions, 2 ml of pH 9.8 buffer and 1 ml of 0.1% picric acid solutions were added successively. The total volume of aqueous phase in each separating funnel was adjusted to 10 ml with distilled water. To each separating funnel 10 ml of chloroform was added and the contents were shaken for 2 min. The two phases were allowed to separate and the absorbance of the separated chloroform layer was measured at 350 nm against a reagent blank prepared under similar conditions. The amount of drug was deduced from the calibration graph (Figs. 1 and 2).

Pharmaceutical formulations for TRB HCl and CAM: A quantitiy of tablet powder or cream equivalent to 100 mg of TRB HCl was treated with 4×20 ml portions of chloroform and the chloroform extract was transferred to 100 ml volumetric flask and made upto 100 ml with chloroform to obtain 1 $mg.ml^{-1}$ stock solution.

Fifty milliliters of the above stock solution (1 $mg.ml^{-1}$) was taken and chloroform portion was evaporated to dryness and the residue was transferred to a 50 ml volumetric flask by dissolving it in 5 ml of 0.1 N HCl and diluted to the mark with distilled water.

Twenty Five ml of above stock solution was transferred in to a 25 ml separating funnel and washed with 5 ml 0.05 N NaOH to get the free base formed Twenty five ml portion of this was evaporated to dryness and the residue was dissolved in 25 ml methanol to get 1 $mg.ml^{-1}$ stock solution.

Ten ml of the above stock solution was taken and chloroform portion was evaporated to dryness and the residue was initially dissolved in 2 ml of with glacial acetic acid and diluted to 10 ml with distilled water.

Tablet powdered equivalent to 100 mg of CAM was dissolved and diluted to 100 ml with chloroform and the insoluble portion was removed by filtration to get 1 $mg.ml^{-1}$.

Twenty five ml of above stock solution was taken and the chloroform portion was evaporated to dryness and the residue was initially dissolved in 2 ml of 0.1 N HCl followed by dilution to 25 ml with distilled water.

3. RESULTS AND DISCUSSION

This method involves the formation of Ion-association complex between TRB or CAM and the picric acid. In order to establish the optimum conditions necessary for rapid and quantitative formation of coloured product with maximum stability and sensitivity, the author performed experiments by measuring the absorbance at 350 nm of a series of solutions, varying one and fixing the other parameters in each case such as type, volume and concentration of acid, organic solvent used for

extraction, ratio of organic phase to aqueous phase during extraction, shaking time and temperature. The method involves the coloured species formation is as shown in Scheme 1 as shown below.

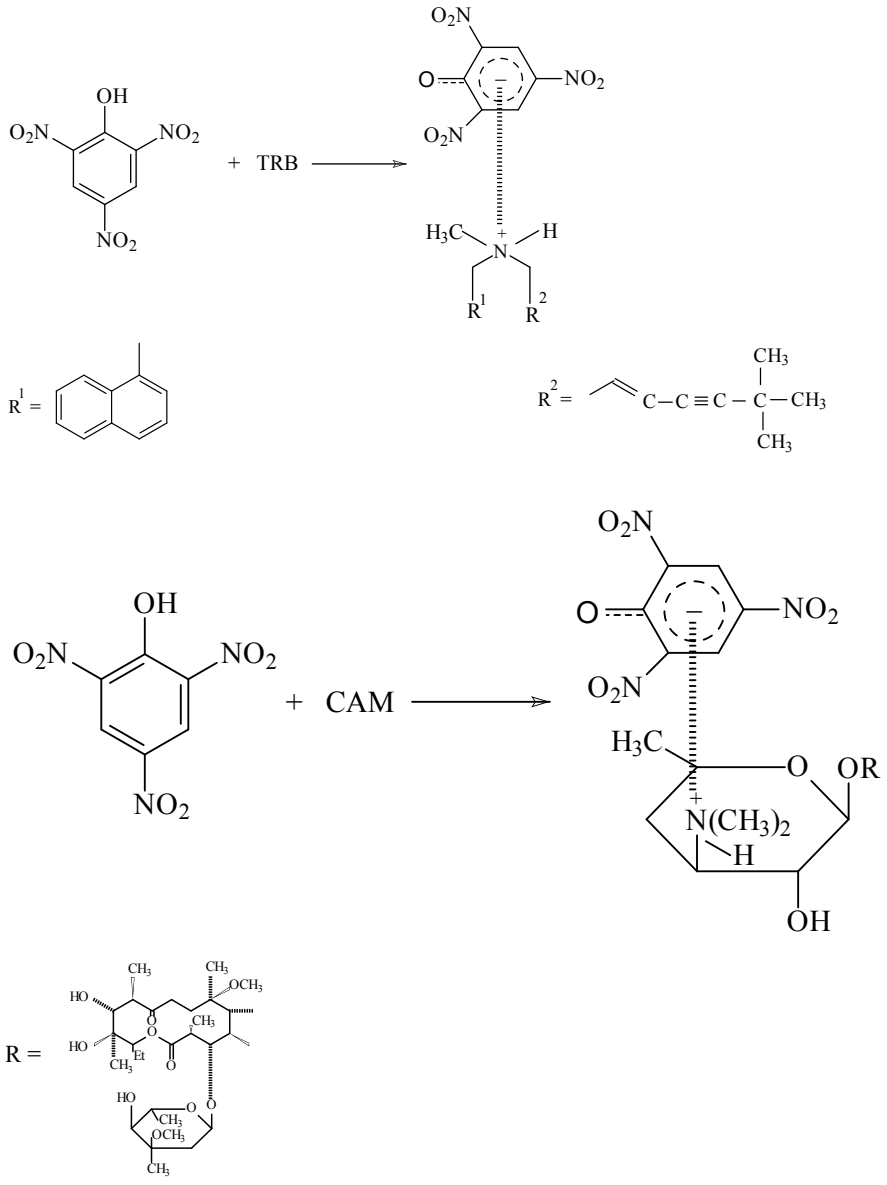

Scheme 1.

Fixation of optimum conditions for the proposed methods and optical characteristics as described below

The picric acid complex was prepared in solution as under recommended procedures given in given above and then extracted in to chloroform. After separation of chloroform and aqueous layers, the chloroform layer was collected in each case and scanned in the wavelength region 200 – 400nm against a reagent blank and the results are shown graphically in Fig. 1. The λmax value was found to be 350nm in UV region. The λmax value of picric acid in aqueous phase was almost the same by the complex in the organic phase.

- In order to test whether each one of the drug with specified reagent adheres to Beer's law, the absorbance at appropriate wavelengths of a set of solutions containing varying amounts of drug and specified amounts of reagents and treated as described in the corresponding recommended procedure were noted against appropriate reagent blank. (The Beer's law plots of the systems are presented graphically in Figs. 2 and 3. The Beer's law limits of each drug with appropriate reagents were calculated in $\mu g.ml^{-1}$ and the results are incorporated in tables. Detection limits, molar absorptivity, Sandell's sensitivity and optimum photometric range for each drug with mentioned reagents were calculated and also recorded.

The regression analysis using the method of least squares was made for the slope (b), standard deviation on slope (S_b), intercept (a), standard deviation on intercept (S_a), standard error of estimation (S_e) and correlation coefficient (r) obtained from different concentrations of each drug and the results are also summarized in Tables 1 and 2.

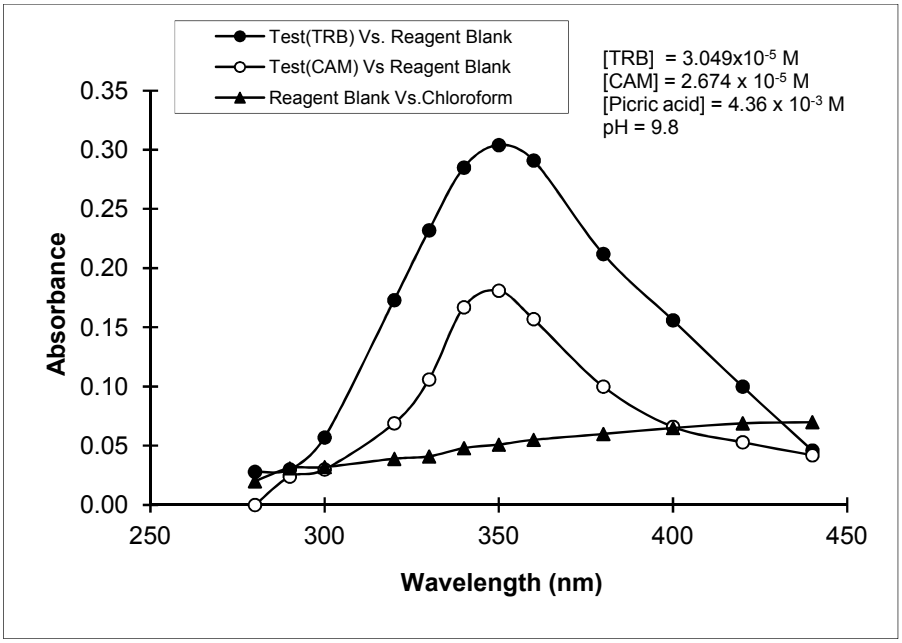

Fig. 1. Absorption spectrum of TRB and CAM-picric acid

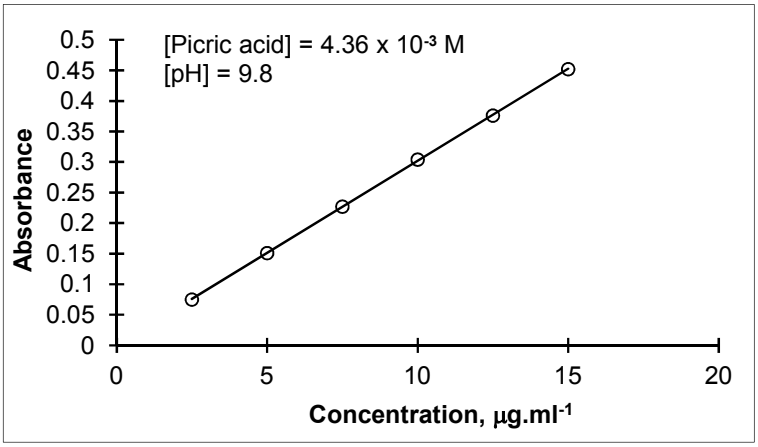

Fig. 2. Beer's law plot of TRB-picric acid M_1

Table 1. Optical and regression characteristics, PRECISION and accuracy of the proposed methods for tRB and cam

Parameter	**M_{TRB}**	**M_{CAM}**
	Picric Acid	**Picric Acid**
λ_{max} (nm)	350	350
Beer's Law Limits ($\mu g.m1^{-1}$)	2.5-15	5-30
Detection limit ($\mu g.m1^{-1}$)	1.299×10^{-1}	0.2737
Molar absorptivity ($mole^{-1}cm^{-1}$)	9.968×10^{3}	1.353×10^{4}
Sandell's sensitivity ($\mu g.cm-2$ / 0.01 absorbance unit)	3.289×10^{-2}	5.52×10^{-2}
Regression equation (y=a+bc)		
Slope (b)	3.013×10^{-2}	1.829×10^{-2}
Standard deviation on slope (S_b)	1.34×10^{-4}	8.571×10^{-5}
Intercept (a)	4.666×10^{-4}	-1.2666×10^{-3}
Standard deviation in intercepts (S_a)	1.305×10^{-4}	1.668×10^{-3}
Standard error of estimation (S_e)	1.403×10^{-3}	1.7928×10^{-3}
Correlation coefficient (r)	0.9999	0.9999
Relative standard deviation (%)*	0.3843	0.4034
% rang of error (confidence limits)*		
0.05 level	0.4034	0.4234
0.01 level	0.6330	0.6641
% Error in bulk samples**	0.2302	0.2739

**Average of six determinations considered*
*** Average of three determinations*

Table 2. Assay of CAM and TRB in pharmaceutical formulations

Formulations*	Labeled Amount mg)	Amount found by proposed methods **		Reference method for TRB	Reference method for CAM	% Recovery by proposed methods***	
		Picric acid for CAM	Picric acid for TRB			Picric acid for CAM	Picric acid for TRB
Tablets	125	123.47± 1.15 F = 1.43 t = 1.01	123.89±0.766 F = 1.74 t = 1.32	124.36± 0.72	124.04±0.96	98.78± 0.92	99.11±0.764
Tablets	250	248.70±1.94 F = 1.30 t = 0.005	248.72±1.45 F=1.94 t=1.155	249.52± 0.82	248.7±2.22	99.48± 0.77	99.48±0.458
Cream Tablet	TRB 10 CAM 250	248.17± 1.58 F = 1.54 t = 0.27	9.98±0.019 F=1.34 t=1.0	9.99± 0.016	248.4±2.00	99.26± 0.63	99.89±0.189
Cream Tablet	TRB 250 CAM 500	496.18± 1.84 F = 1.44 t = 1.09	247.5±3.63 F=1.37 t=1.174	247.86± 3.09	498.7±2.22	99.23± 0.36	99.00±1.454

** Formulations from four different pharmaceutical companies.*

*** Average ± standard deviation on six determinations, the t- and F – test values refer to comparison of the proposed method with the reference method. Theoretical values at 95% confidence limit, F= 5.05, t = 2.57.*

**** Recovery of 10 mg added to the pre-analyzed pharmaceutical formulations (average of three determinations)*

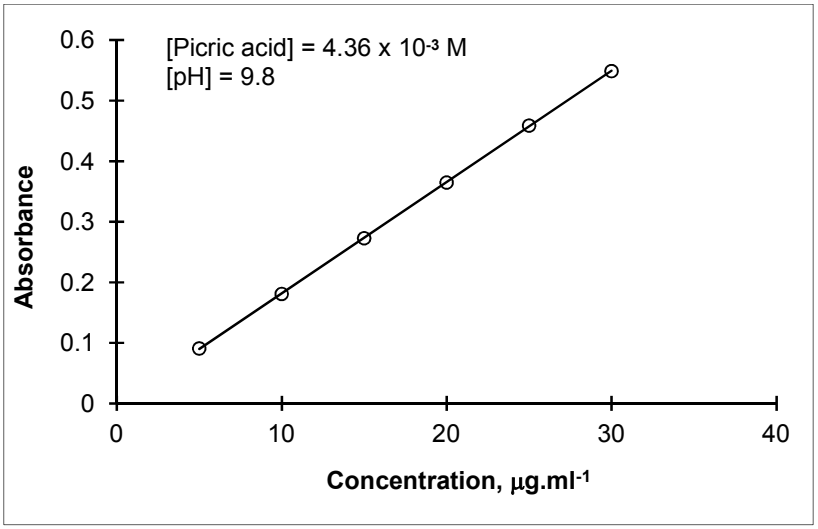

Fig. 3. Beer's law plot of CAM-picric acid M_2

4. CONCLUSION

An important step in the validation process of spectrophotometric method is the fixation of appropriate system suitability parameters to ensure successful analysis. They defined as a range of acceptance values for a series of key parameters such as precisition, accuracy, linearity of detector response and recovery as deemed appropriate for the scope of analysis.

The validity of the proposed methods for the determination of a fore mentioned drugs were established from the precision (calculating percent relative standard deviation, percent range of error at confidence limits with P=0.05 and 0.01 level from six determinations) and accuracy (percent error in pure samples, comparison of results obtained with proposed and reported methods in the case of pharmaceutical preparations and recovery experiments) studies. The sensitivity of each method was ascertained through molar extinction coefficient, sandell's sensitivity, optimum photometric range beer's law limits. The regression analysis using the method of least squares was made for the slope (b), standard deviation (S_b), intercept (a), standard deviation on intercept (S_a), standard error of estimation (Se) and correlation coefficient (r) obtained from different concentrations. The data obtained in the determination of each drug with different reagents are summarized in this section. The selectivity (or specificity) of each proposed method was ascertained through interference studies with other active and inactive ingredients usually present in pharmaceutical preparations.

ACKNOWLEDGEMENTS

The author (Dr.R.M.Rao) is grateful to University Grants Commission, New Delhi for the award of the award of Teacher Fellowship.

COMPETING INTERESTS

Authors have declared that no competing interests exist.

REFERENCES

1. Schatz F, Haberl H. Chromotograpic determination of terbinafine hydrochloride inpersence of its degradation products. Arzneim Forsch. 1989;39:527–532.
2. Budavari S, O'Neil M, Smith A, Heckelman P, Obenchain J. The Merck Index, 12th edn. Merck & Co. Inc., New York. 1996;1564.

3. The complete drug reference. Martindale extra pharmacopoeia, 32nd edn. The Pharmaceutical press, London; 1999.
4. Schatz F, Haberl H. Arzneim.-Forsch. 1989;39:527.
5. The Merck Index, Merck and Co. Inc., New York, edn. 1996;12.
6. The Complete Drug Reference, Martindale Extra Pharmacopoeia, The Pharmaceutical Press, London, edn. 1999;32.
7. United States Pharmacopoeia, USP 24, USP Convention, Inc. Rockville; 2000.
8. The Merck Index, Merck and Co. Inc., New York, edn. 1996;12.
9. Starostenko VE. Balon, farmatsyingjiyer. 1970;204.
10. Cf WM, Dehn FA, Hartman J. Amer. Chem. Soc. 1914;36:403.
11. Bell FK, Krentzors JC. J. Amer. Pharm. Assoc. Sci. Ed. 1948;37:297.
12. Kennedy EE. J. Amer. Pharm. Assoc. Sci. Ed. 1950;39:25.
13. Briggs MJ, Nguyen BT, Jorgensen LW. J. Phys. Chem. 1991;95:3315-3322.
14. Wolff ME. Burger's Medicinal Chemistry and Drug Discovery, 5th Ed., New York: Wiley-Interscience. 1996;5537.
15. OSHA, Safety and Health Topics - Picric Acid; 2010.
16. National Research Council, Drinking Water & Health, Volume 4, Washington, DC. 1981;239.
17. Meyer R. Explosives, VCH Verlagsgesellschaftmb, H. Weinheim, Germany. 1980;269-271.
18. Pfeiffer P. Organische Molekulverbindungen, 2nd Edn., Ferdinand Enke, Stuttgart; 1927.
19. Bingham, Eula, Cohrssen, Barbara, Powell, Charles, H. Patty's Toxicology, 5 th Edn. John Wiley and Sons: NY, USA; 2001.
20. Gaballa AS, Wagner C, Teleb SM, Nour EM, Elmosallamy MAF, Kaluderovic GN, Schmidt H, Steinborn D. J. Mol. Structure. 2008;876:301.
21. Babu GA, Sreedhar S, Rao SV, Ramasamy P. J. Cryst. Growth. 2010;312:12-13,1957-1962.
22. Srivastava KK, Shubha Srivastava, Md Tanweer Alam, Rituraj. An Overview of Picric Acid. Der Pharma Chemica. 2017;9(9):64-75.
23. Starostenko VE. Balon, farmatsyingjiyer. 1970;204.
24. Cf WM. Dehn FA. Hartman, J. Amer. Chem. Soc. 1914;36:403.
25. Bell FK, Krentzors JC. J. Amer. Pharm. Assoc. Sci. Ed. 1948;37:297.
26. Kennedy EE. J. Amer. Pharm. Assoc. Sci. Ed. 1950;39:25.

Biography of author(s)

R. Mrutyunjaya Rao
SRKR Engineering College, Chinna Ammiram, Bhimavaram, India.

He is working as an Emeritus Professor in Chemistry SRKR Engineering College, Bhimavaram W.G.Dt .A.P.INDIA. 2014 to present; formerly reader and HOD of Chemistry, V. S. M. College Ramachandrapuram, E. G. Dt. A.P. 1991-2013 and lecturer in Chemistry, Sri. Y. N .College Narasapuram, W. G. Dt. A.P., 1984-1990. His objectives was to Intended to build a career with leading corporate of Hi-tech environment of new technology with committed & dedicated people, which help me to explore myself and realize my potential. He completed his Ph. D (Gold Medal in 2004) from Andhra University; M. Phil (1992) from Andhra University; Masters (M.Sc.) in Organic Chemistry (1982) - with specialization Drugs, Dyes, Pesticides and Pharmaceuticals with First class from R. E. C. Warangal; B.Sc. (C. B. Z) (1978) from D.N.R college; Intermediate Bi. P.C (1974) from D.N.R College and 10th (1972) from Z. P. High school (SSC). He has supervised several projects on medicinal plants. He has published his research findings in several national and international journals of repute. He has also attended and presented his research in several conferences and seminar.

© Copyright (2020): Author(s). The licensee is the publisher (Book Publisher International).

DISCLAIMER
This chapter is an extended version of the article published by the same author(s) in the following journal.
Modern Chemistry & Applications, 6: 1-5, 2018.

Chapter 13
Print ISBN: 978-93-90206-41-4, eBook ISBN: 978-93-90206-42-1

Recent Research on Kinetics and Mechanism of Oxidation of Ethyl Diethylene Glycol by Ce(IV) Catalyzed by Ir(III) in Aqueous Sulphuric Acid Media

Kamini Singh[1], Ashish Kumar Singh[1], Jaya Jaiswal[1] and R. A. Singh[1*]

DOI: 10.9734/bpi/crdc/v4

ABSTRACT

Kinetic studies on oxidation of different types of organic compounds by cerium(IV) are well documented. Among the different metal ion catalysis, ruthenium(III) and iridium(III) have been found to catalyze even at trace quantities. The kinetics of iridium(III) catalyzed oxidation of ethyl diethylene glycol by ceric sulphate has been investigated in sulphuric acid media. The result indicates zero order kinetics with respect to cerium(IV) ion and first order kinetics with respect to ethyl diethylene glycol and iridium(III) chloride. The dielectric constant of the medium shows positive effect on the reaction rate. There is insignificant effect of ionic strength of potassium sulphate on the reaction rate indicating interaction in the rate-determining step being an ion-dipole type and not an ion type. Elevation of temperature increases the rate of reaction. Various activation parameters have been calculated and recorded. A suitable mechanism in conformity with the above observation has been proposed.

Keywords: Kinetics; mechanism; oxidant Ce(IV); ethyl diethylene glycol; Ir(III) catalyst and suplhuric acid.

1. INTRODUCTION

Kinetic studies on oxidation of different types of organic compounds by cerium(IV) are well documented [1-3]. Different metal ion catalysts like silver(I) [4], manganese(II) [5,6], copper(II) [7], osmium(VIII) [8], mercury(II) [9], chromium(III) [10], ruthenium(III) [11], iridium(III) [6], *etc.* have been utilized in cerium(IV) oxidation reactions. Among the different metal ion catalysis, ruthenium(III) and iridium(III) have been found to catalyze even at trace quantities. A strategy to potentially improve the water oxidation reaction is the use of molecular iridium and ruthenium (pre-) catalysts [12-16].

Iridium(III) catalysis in oxidation reactions by cerium(IV) in aqueous sulphuric acid media has been reported in few cases [17-20]. In different cases, different reaction mechanism have been proposed. Moreover, some previous workers have reported [21] iridium(III) catalyzed decomposition of cerium(IV) in aqueous sulphuric acid medium at elevated temperatures through the oxidation of water. The presence of such catalytic decomposition of cerium(IV) may complicate the interpretation of kinetic data. In fact, more work is needed to understand the mechanistic routes for iridium(III) catalysis in oxidation reaction by cerium(IV) in aqueous sulphuric acid medium. In present communication, the result of the kinetic and mechanism of Ir(III) catalyzed oxidation of ethyl-diethylene glycol by Ce(IV) in sulphuric acid media is reported.

2. EXPERIMENTAL

Reagent grade chemicals and doubly distilled water were used throughout. Aqueous solution of ceric sulphate was prepared by warming it in sulphuric acid and double distilled water. The strength of sulphuric acid was maintained at 0.5 N. The ceric sulphate solution standardized against ferrous

[1]Chemical Kinetics Research Laboratory, Department of Chemistry, Tilakdhari Postgraduate College, Jaunpur-222 002, India.
**Corresponding author: E-mail: rasinghtdc@rediffmail.com;*

ammonium sulphate using ferrion as an indicator. Ceric sulphate, ferrous ammonium sulphate and ferrion were all BDH, sulphuric acid was of AR-grade. Aqueous solution of ethyl diethylene glycol (BDH) was also prepared by dissolving a weighed quantity of the sample in double distilled water. Stock solution of iridium(III) chloride was prepared by dissolving the sample (Johnson and Matthey Chemical Ltd.) in a solution of HCl. The final concentration of hydrochloric acid and iridium(III) chloride were 4.00×10^{-3} and 3.80×10^{-3} mol dm^{-3}, respectively. All the kinetic measurements were carried out at constant temperature (± 0.1ºC). All the reactants were mixed in a black coated conical flask. The reaction was initiated by mixing the pre-equilibrated reactant solution taken at desired temperature (35ºC) and progress of reaction was followed by withdrawing known amount of aliquots (5 mL) of the reaction solution at regular time intervals, quenching the reaction by excess standardized ferrous ammonium sulphate solution and back titrating unreacted ferrous ion with standard Ce(IV) solution using ferrion as an internal indicator.

3. RESULTS AND DISCUSSION

The kinetics of oxidation of ethyl-diethylene glycol by cerium(IV) were investigated at several initial concentration of the reactants. The rate constant increase linearly on increasing the concentration of ethyl-diethylene glycol. It gives a straight line (Fig. 1) with unit slope, which confirms the first order kinetics with respect to ethyl diethylene glycol. The rate of reaction was found to be highly influenced by Ir(III). It was observed that with increasing Ir(III), the first order rate constant increase linearly, which proves first order dependence on Ir(III). The slope of straight line gives first-order rate constant whose values also confirms (Fig. 2). The reaction shows zero order kinetics with respect to Ce(IV). Increase in concentration of [H+] has positive effect of the medium. Negligible effect of addition of $NaHSO_4$ and Na_2SO_4 has no significant effect on the reaction rate.

The reaction were carried out at 30, 35, 40 and 45ºC and results at these temperatures led to compute energy of activation (Ea), entropy of activation (ΔS#) and free energy of activation (ΔG#) for the title reaction (Table 3).

Stoichiometry and product analysis: Several reaction mixture of [oxidant]: [ethyl diethylene glycols] at fixed H^+ concentration were prepared under the condition [glycol] << [oxidant] *i.e.* [ethyl diethylene glycol] << [Ce(IV)] and the reaction mixture was left for 72 h. Estimation of unreacted [Ce(IV)] shows that 2 moles of Ce(IV) were required for oxidation of each mole of ethyl diethylene glycol. The stoichiometric equation is as follows:

Table 1. Effect of variation of [H^+], [Ce(IV)], ethyl diethylene glycol and [Ir(III)] catalyst on reaction rate constant at 35ºC

[Ethyl D. glycol] $\times 10^2$ (mol dm^{-3})	[Ce(IV)] $\times 10^3$ (mol dm^{-3})	[H_2SO_4] (mol dm^{-3})	[Ir(III)] $\times 10^5$ (mol dm^{-3})	[(-dc/dt)] $\times 10^7$ (mol dm^{-3})	k_1 (s^{-1})
2.00	0.50	0.80	7.65	1.74	–
2.00	0.80	0.80	7.65	1.80	–
2.00	1.00	0.80	7.65	1.82	–
2.00	1.25	0.80	7.65	1.70	–
2.00	1.67	0.80	7.65	1.78	–
2.00	2.00	0.80	7.65	1.72	–
2.50	2.00	0.80	7.65	2.12	0.85
3.00	2.00	0.80	7.65	2.56	0.85
4.00	2.00	0.80	7.65	3.40	0.85
7.50	2.00	0.80	7.65	6.32	0.84
10.00	2.00	0.80	7.65	8.60	0.86
2.00	2.00	0.80	11.50	2.60	2.26
2.00	2.00	0.80	15.30	3.40	2.22
2.00	2.00	0.80	19.10	4.38	2.29
2.00	2.00	0.80	22.95	5.16	2.25
2.00	2.00	0.80	30.60	6.92	2.24
2.00	2.00	1.25	7.65	2.80	–
2.00	2.00	1.75	7.65	3.66	–
2.00	2.00	2.25	7.65	4.82	–
2.00	2.00	2.56	7.65	5.06	–
2.00	2.00	3.20	7.65	6.10	–

Table 2. Effect of ionic strength, SO_4^{2-}, HSO_4^- and different temperatures

Temperature (°C)	Ionic strength (μ) (mol dm^{-3})	Na_2SO_4 (mol dm^{-3})	$NaHSO_4$ (mol dm^{-3})	(-dc/dt) × 10^7 (mol dm^{-3})
35	3.012	0.20	0.00	1.82
35	3.612	0.40	0.00	1.84
35	4.212	0.60	0.00	1.80
35	4.812	0.80	0.00	1.78
35	5.412	1.00	0.00	1.86
35	8.412	2.00	0.00	1.84
35	3.912	0.00	0.20	2.58
35	3.912	0.00	0.40	2.66
35	3.912	0.00	0.60	2.62
35	3.912	0.00	0.80	2.68
35	3.912	0.00	1.00	2.70
35	3.912	0.00	1.50	2.66
30	3.024	0.20	0.00	1.16
35	3.024	0.20	0.00	1.72
40	3.024	0.20	0.00	2.46
45	3.024	0.20	0.00	3.72

Table 3. Thermodynamic parameters at 35ºC

k_r (s^{-1})	E_a (kJ mol^{-1})	log A	$\Delta H^{\#}$ (kJ mol^{-1})	$\Delta S^{\#}$ (Jk^{-1} mol^{-1})	$\Delta G^{\#}$ (kJ mol^{-1})
0.88×10^{-4}	85.48	10.44	82.92	−11.67	86.51

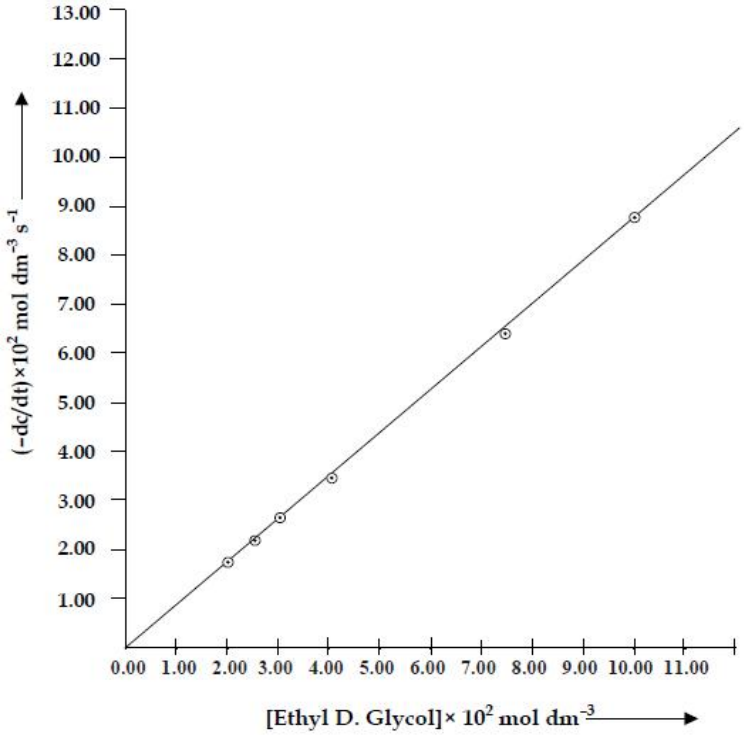

Fig. 1. Variation of substrate (ethyl diethylene glycol) at 35ºC, [Ce(IV)] × 10^3 = 2.00 mol dm^{-3}; [H_2SO_4] = 0.80 mol dm^{-3}; [Ir(III)] × 10^5 = 7.65 mol dm^{-3}; [Na_2SO_4] = 0.20 mol dm^{-3}; μ = 3.024 mol dm^{-3}

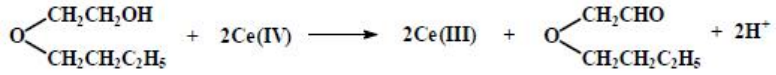

The product corresponding aldehyde was detected and identified by paper [22] and thin layer chromatography [23].

Mechanism:

$$S + H^+ \underset{}{\overset{K_1}{\rightleftharpoons}} SH^+ \quad (1)$$

$$SH^+ + [IrCl_5H_2O]^{2-} \underset{k_{-2}}{\overset{k_2}{\rightleftharpoons}} X + SH^+ + H_2O \quad (2)$$

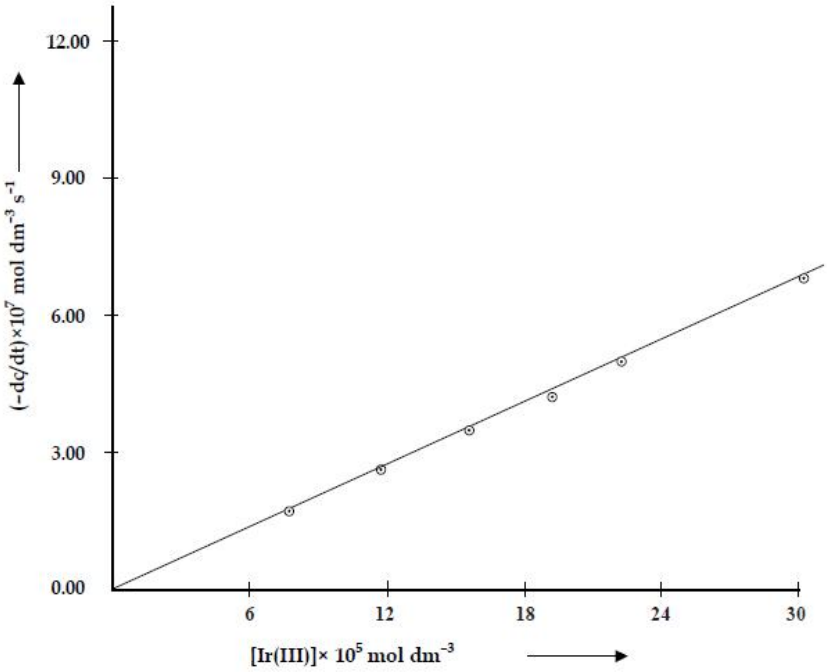

Fig. 2. Variation of catalyst at 35°C, [Ce(IV)] × 10^3 = 2.00 mol dm^{-3}; [H_2SO_4] = 0.80 mol dm^{-3}; [ethyl diethylene glycol] × 105 = 2.00 mol dm^{-3}; [Na_2SO_4] = 0.20 mol dm^{-3}; μ = 3.024 mol dm^{-3}

where S is substrate *i.e.* ethyl diethylene glycol and X is $[IrCl_5.S]^{2-}$

$$[IrCl_5S]^{2-} + H_2O \xrightarrow{k} [IrCl_4(H_2O)H]^{2-} + S^+ + Cl^- \quad (3)$$

rate determining and slowest step.

$$S^+ + Ce(IV) \longrightarrow \text{Product (P)} + Ce(III) \quad (4)$$

$$Cl^- + [IrCl_4(H_2O)H]^{2-} + Ce(IV) \longrightarrow Ce(III) + H^+ + Y \quad (5)$$

where Y is $[IrCl_5(H_2O)]^{2-}$

Considering above reaction steps, the rate of the reaction in terms of loss of concentration of Ce(IV) may be written as equation.

$$-\frac{d[Ce(IV)]}{dt} = nk[IrCl_5 \cdot S]^{2-} \quad (6)$$

On applying steady state treatment to $[IrCl_5 \cdot S]^{2-}$, we have eqn. 7 with the help of eqns. 2 and 3

$$\frac{d[IrCl_5S]^{2-}}{dt} = 0 = k_2[SH^+H][IrCl_5H_2O]^{2-} - k_{-2}[H^+][IrCl_5S]^{2-}[H_2O] - k[IrCl_5S]^{2-}[H_2O]$$

$$\text{or} \qquad k_2[SH^+][IrCl_5H_2O]^{2-} = k_{-2}[IrCl_5S]^{2-}[H_2O][H^+] + k[IrCl_5S]^{2-}[H_2O]$$

$$\text{or} \qquad [IrCl_5S]^{2-} = \frac{k_2[SH^+][IrCl_5(H_2O)]^{2-}}{k_{-2}[H^+][H_2O] + k[H_2O]} \quad (7)$$

From eqn. 1 we have

$$[SH^+] = K_1[S][H^+] \quad (8)$$

By eqns. 7 and 8 we have

$$\text{or} \qquad [IrCl_5S]^{2-} = \frac{k_2K_1[S][H^+][IrCl_5(H_2O)]^{2-}}{k_{-2}[H^+][H_2O] + k[H_2O]}$$

$$\text{or} \qquad [IrCl_5S]^{2-} = \frac{k_2K_1[S][H^+][IrCl_5(H_2O)]^{2-}}{H_2O\,\{k_{-2}[H^+] + k\}}$$

$$\text{or} \qquad [IrCl_5S]^{2-} = \frac{k_2K_1[S][H^+][IrCl_5(H_2O)]^{2-}}{k + k_{-2}[H^+]} \quad (9)$$

Considering eqns. 1 and 9, we have

$$-\frac{d[Ce(IV)]}{dt} = \frac{nkk_2K'[S][H^+][IrCl_5(H_2O)]^{2-}}{k + k_{-2}[H^+]} \quad (10)$$

where $K' = K_1/[H_2O]$

$$\text{or} \qquad \text{Rate} = \frac{nkk_2K'[S][H^+][Ir(III)]}{k + k_{-2}[H^+]} \quad (11)$$

The rate law (11) is in agreement with all observed kinetics. The rate shows that the order of the reaction is zero-order in [Ce(IV)], first order in ethyl diethylene glycol and Ir(III) and positive effect of $[H^+]$ on the rate of reaction. Here n is 2 for ethyl diethylene glycol.

4. CONCLUSION

The dielectric constant of the medium shows positive effect on the reaction rate. There is insignificant effect of ionic strength of potassium sulphate on the reaction rate indicating interaction in the rate-determining step being an ion-dipole type and not an ion type. Elevation of temperature increases the rate of reaction. Various activation parameters have been calculated and recorded. A suitable mechanism in conformity with the above observation has been proposed.

COMPETING INTERESTS

Authors have declared that no competing interests exist.

REFERENCES

1. Wells CF, Husain M. Kinetics of oxidation of isopropanol by aquocerium (IV) ions in perchlorate media. Transactions of the Faraday Society. 1970;66:679-687.
2. Sankhla PS, Mehrotra RN. Kinetics of cerium (IV) oxidation of formaldehyde in aqueous sulphuric acid solution. Journal of Inorganic and Nuclear Chemistry. 1972;34(12):3781-3788.
3. Pondit AK, Das A, Banerjea D. Kinetics and mechanism of oxidation of 8-hydroxyquinoline and its derivatives by cerium (IV) through precursor complex formation. Transition Metal Chemistry. 1991;16(3):324-327.
4. Rao MA, Adinarayana M, Sethuram B, Rao TN. Oxidation studies. 12.-effect of $(Ag]^{+}$ Cu^{2+}) on oxidation of acetic, propionic, isobutyric and pivalic acids by Ce^{4+} in sulfuric-acid medium. Indian Journal of Chemistry Section A-inorganic Bio-inorganic Physical Theoretical & Analytical Chemistry. 1978;16(5):440-442.
5. Saiprakash PK, Sethuram B. J. Indian Chem. Soc. 1973;50:211.
6. Sharma YR, Saiprakash PK. Indian J. Chem. 1980;19A:1175.
7. Reddy MR, Sethuram B, Rao TN. Kinetics of oxidation of mannitol by Ce^{4+} in H_2SO_4 medium. Current Science. 1973;42(19):677-679.
8. El-Tantawy YA, Abu-Shady AI, Ezzat II. The mechanism of Os (VIII)-catalyzed Ce (IV) As (III) reaction. Journal of Inorganic and Nuclear Chemistry. 1978;40(9):1683-1684.
9. Anantharaman R, Nair MR. Indian J. Chem. 1976;14:45.
10. Chimatadar SA, Nandibewoor ST, Sambrani MI, Raju JR. J. Chem. Soc. Dalton Trans. 1978; 573.
11. Singh MP, Singh HS, Verma MK. Kinetics and mechanism of the ruthenium (III) chloride catalyzed oxidation of butanone-2 and pentanone-3 by cerium (IV) sulfate in aqueous sulfuric acid medium. The Journal of Physical Chemistry. 1980;84(3):256-259.
12. Blakemore JD, Crabtree RH, Brudvig GW. Molecular catalysts for water oxidation. Chem. Rev. 2015;115:12974– 13005.
13. Ukuzumi S, Hong D. Homogeneous versus Heterogeneous Catalysts in Water Oxidation. Eur. J. Inorg. Chem. 2014;2014:645– 659.
14. Macchioni A. The middle-earth between homogeneous and heterogeneous catalysis in water oxidation with iridium. Eur. J. Inorg. Chem. 2019;2019:7– 17.
15. Zhang B, Sun L. Artificial photosynthesis: Opportunities and challenges of molecular catalysts. Chem. Soc. Rev. 2019;48:2216– 2264.
16. Van Dijk B, Rodriguez GM, Wu L, Hofmann JP, Macchioni A, Hetterscheid DG. The influence of the ligand in the iridium mediated electrocatalyic water oxidation. ACS Catalysis. 2020;10(7): 4398-4410.
17. Yatsimirskii KB. Kinetics and mechanisms of homogeneous redox processes catalyzed by complex-compounds of platinum elements. Journal of the Indian Chemical Society. 1974;51(1): 32-40.
18. Das AK, Das M. Indian J. Chem. 1995;34A:866.
19. Das AK. J. Chem. Res. (S). 1996;184. J. Chem. Res. (M). 1996;1023.
20. Singh RA, Gautam A. Kinetics and Mechanism of the Ir (III) Catalyzed Oxidation of Methyl Diethylene Glycol by Ce (IV) in Sulphuric Acid Medium. Asian Journal of Chemistry. 2007;19(5): 3839.
21. Ginzburg SI, Yuzko MI. Russ. J. Inorg. Chem. 1965;10:444.
22. Hartley RD, Lawson GJ. Improved methods for the paper chromatography of organic acids. Journal of Chromatography A. 1960;4:410-413.
23. Feigl F. Spot tests in organic chemistry. Elsevier, New York. 1960;369.

Biography of author(s)

Dr. R. A. Singh(D.Sc.), Associate Professor
Chemical Kinetics Research Laboratory, Department of Chemistry, Tilakdhari Postgraduate College, Jaunpur-222 002, India.

Research and Academic Experience: 29 Years

Research Area: Thermodynamics and Chemical Kinetics

Number of Published papers: 48 Papers in National and International Reputed Journals

Special Award (If any): F.I.C.C.E.

Any other remarkable point(s): F.I.S.C., F.I.C.C. & F.I.C.S.

© Copyright (2020): Author(s). The licensee is the publisher (Book Publisher International).

DISCLAIMER
This chapter is an extended version of the article published by the same author(s) in the following journal.
Asian Journal of Chemistry, 21(2): 863-868, 2009.

Chapter 14
Print ISBN: 978-93-90206-41-4, eBook ISBN: 978-93-90206-42-1

Application of Antioxidants as Effective Remedies at Hepatotoxic Action of Carbon Tetrachloride

Karlen Hovnanyan[1*], Vardan Mamikonyan[2], Anahit Margaryan[3], Kristine Sargsyan[1], Margarita Hovnanyan[1], Maria Karagyozyan[2] and Konstantin Karageuzyan[2]

DOI: 10.9734/bpi/crdc/v4

ABSTRACT

The liver, as the central metabolic organ, plays an important role in metabolism of carbohy-drates, lipids and proteins. In the environment, there are many hepatotoxic xenobiotics. CCl4 is a free radical toxic for organelles of hepatocytes. The presented work was studying the character of ultrastructural changes in CCl4-intoxicated hepatocytes as well as the tissue after treatment by grape seed extract (GSE), *α*-tocopherol (*α*-T). As a result of cell bioremediation effect and reactions against corruptive factors, the liver has a high regeneration ability. Thus, the model of liver toxicity and the LC, based on the nature of ultrastructural changes of mitochondria and other compartments of hepatocytes, GSE, as well as *α*-T and STS, have corrective effect. TEM ultrastructural characterization of the GSE influence is evidence of its success cytoprotective and antitoxic features as well as hepatocytes from xenobiotic-CCl4 induced by cirrhosis rat liver.

Keywords: CCl4; GSE; α-tocopherol; ultrastructural changes; intoxicated hepatocytes; electron microscopy.

1. INTRODUCTION

The liver, as human organ with high metabolic activity, plays an important role in metabolism of carbohydrates, lipids and proteins. As a result of cell protective cooperation and reactions against corruptive factors, liver also has a high regeneration ability [1,2]. In spite of considerable progress in hepatology [3-5], the study of corruption and regeneration mechanisms of hepatocytes on tissue, cellular and molecular levels remains to be very actual. Regeneration of the liver after resection is actually compensatory hyperplasia rather than a true restoration of the liver's original gross anatomy and architecture [6,7,8]. Among toxins, which are widely used for modulating some damage of liver (liver cirrhosis—LC, hepatitis), the most popular is carbon tetrachloride (CCl4) [9].

Aim of the presented work was to study the character of ultrastructural changes in CCl4-intoxicated hepatocytes as well as the tissue after treatment by grape seed extract (GSE), *α*-tocopherol (*α*-T), as potential prophylaxis and treatment agents with antioxidant action at liver injury, mainly in experimental model of LC.

2. MATERIALS AND METHODS

2.1 Experimental and Preparation to Assays

In this study, we used white male rats weighting between 180 - 200 g, which were subdivided into four groups: I- control group (intact animals); II-group, animals with experimental liver damages; III-group,

[1]*Scintific and Technological Center of Organic and Pharmaceutical Chemistry, National Academy of Sciences, Republic of Armenia.*
[2]*Scientific and Technological Center of Organic and Pharmaceutical Chemistry, NAS RA, Yerevan, Armenia.*
[3]*H. Buniatian Institute of Biochemistry, NAS RA, Yerevan, Armenia.*
**Corresponding author: E-mail: hovkarl@mail.ru;*

animals with experimental liver damages with GSE injection; IV-group, animals whit experimental liver damages with *α*-T. We induced liver damages by intraperitoneal injec-tion of CCl4 at a dose of 150 μg per 100 g of body weight.

2.2 Electron Microscopy Assays

For transmission electron microscope study we use liver tissue examples from control group as well as from experimental groups after CCl4, GSE, *α*-T influence. Preliminary fixation of the samples was carried out in 2.5% glutaraldehyde solution in phosphate buffer, and post fixation—in 1% solution of osmium tetroxide in the same buffer [10]. The samples were dehydrated in ethanol solutions with increasing concentration, poured and soaked by araldite mixtures of resins. After polymerization, ultrathin sections were prepared for microtome “Reichert-Ultracut” consistent with their staining solution uranyl acetate and lead citrate [11].

The study of made preparations and them photomicrography was carried out using a transmission electron microscope “Tesla BS-500” in a voltage of 80 kV.

3. RESULTS AND DISCUSSION

Ultrastructural analysis of hepatocytes in the control group white rats liver has set a characteristic feature of hepatocytes expressed the depositors function. In the cy-toplasm we can see a large number of polysomes, granu-lar endoplasmic reticulum, vesicles, rosette-shaped gly-cogen granules, which are found in the area of lipid droplets without bounding membranes, lysosomes, rarely orthodox configuration mitochondria with the normal structure of the matrix and crista as well as heterochro-matin and nucleolus in the nucleus of hepatocytes, gra-nular-fibrillar structure with normal configuration of si-nusoidal capillaries, the structure of Kupffer cells and space of Disse (Fig. 1(a) and (b)).

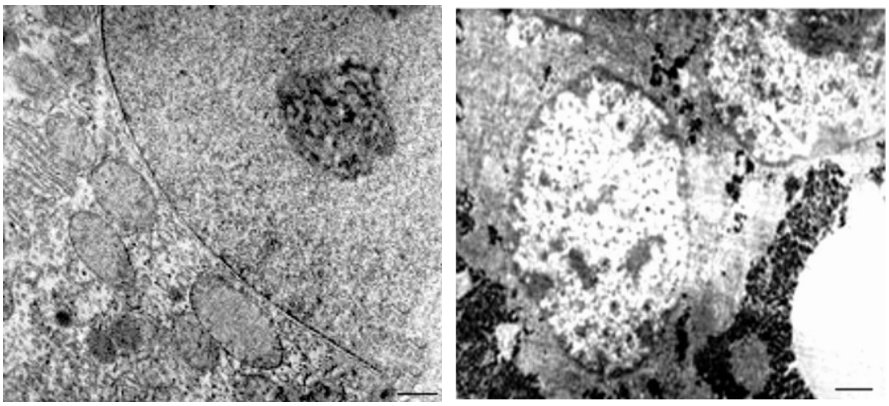

(a) **(b)**

Fig. 1. (a), (b) White rat hepatocytes (control group). TEM. Ultrathin section. Scale bare = 1 μm

Electron microscopic study of the liver of albino rats after induction of liver toxicity revealed nonspecific damage of the mitochondrial membrane, mitochondrial swelling with fragmentation and destruction of their crista (Fig. 2(a)). In the cytoplasm of hepatocytes observed vesiculation, expansion of tanks of the endoplasmic reticulum and perinuclear space with a pyknotic changed nucleus and marginated chromatin. (Fig. 2(a)), as well as hyperplasia of the granular endoplasmic reticulum (Fig. 2(b)) and the simultaneous loss of ribosomes, which results in the transformation of granular endoplasmic reticulum in smooth (Fig. 2(b)).

In the hepatocytes of the experimental animals in the areas of glycogen identified lipid droplets of various sizes and quantities, evidence of fat and vacuolar degeneration of the body. It was reveals a

sharp expansion of sinusoidal space, increase in cellular structures of connective tissue, including collagen fibrils, bundles of which fill the intercellular space, indicating the onset of the initial stage of LC (Fig. 3).

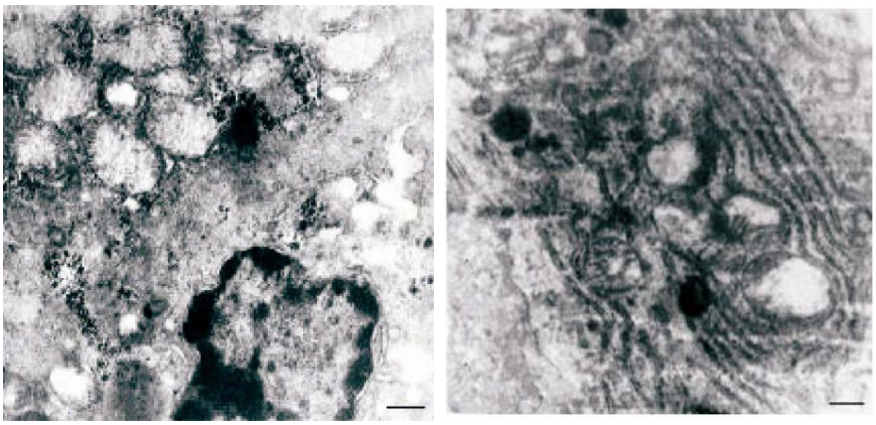

(a) **(b)**

Fig. 2. (a), (b) TEM. Experimental white rat hepatocytes with CCl_4-intoxication. Ultrathin section. Scale bare = 1 μm

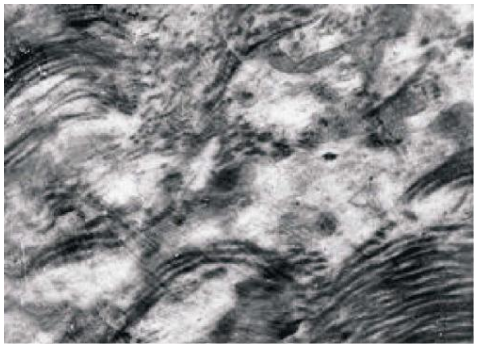

Fig. 3. TEM. Experimental white rat hepatocytes with CCl_4-intoxication. The initial stage of cirrhosis. Ultrathin section. Scale bare = 1 μm

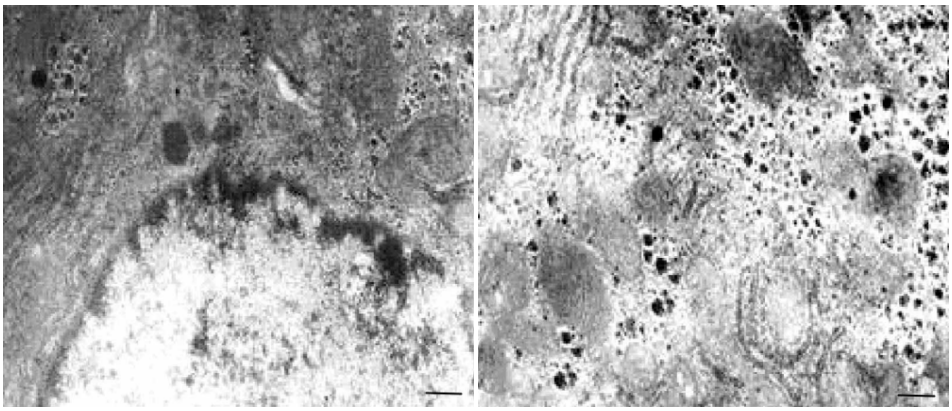

Fig. 4. (a), (b) TEM. Experimental white rat hepatocytes by CCl_4 intoxication after GSE injection (III group). Ultrathin section. Scale bare = 1 μm

The ultrastructural changes are indicators of the activation energy, glycogen and protein synthesis processes in hepatocytes in response to a damaging factor [12].

GSE influence manifested itself in a protective-restorative effect on the ultrastructure of mitochondria with a decrease in the number of hepatocytes with lipid inclusions and vacuolization (Fig. 4(a) and (b)).

The ultrastructure of hepatocytes and organization of sinusoidal cell space after GSE, as well as *α*-T was closer to the picture of intact cells (Fig. 5).

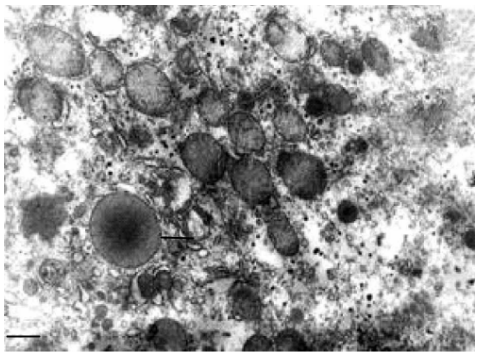

Fig. 5. TEM. Experimental white rat hepatocytes intoxication with CCl4 after *α*-T injection (IV group). Ultrathin section. Scale bare = 1 μm

4. CONCLUSIONS

Thus, the model of liver toxicity and the LC, based on the nature of ultrastructural changes of mitochondria and other compartments of hepatocytes, GSE, as well as *α*-T and STS, have corrective effect.

TEM ultrastructural characterization of the GSE in-fluence is evidence of its success cytoprotective and antitoxic features as well as hepatocytes from xenobiotic-CCl4 induced by cirrhosis rat liver.

ACKNOWLEDGEMENTS

The study was done within the framework supported by Ministry of Education and Science of the Republic of Armenia (Basic support).

COMPETING INTERESTS

Authors have declared that no competing interests exist.

REFERENCES

1. Dzhivanyan KA, Adamyan NV. About features of ultrastructure of a liver of birds in norm and after partial hepatoctomy. The Russian Morphological Sheets, Moscow. 2001;3-4:26-27.
2. Fausto N, Campbell JS. The role of hepato-cytes and oval cells in liver regeneration and repopulation. Mechanisms of Development. 2003;120:117-130.
Available:http://dx.doi.org/10.1016/S0925-4773(02)00338-6
3. Loginov AS, Block Yu. E. Chronical hepatitis and liver cirrhosis. Medicine. 1987;272.
4. Powell EE, Jonsson JR, Clouston AD. Steatosis: Cofactor in other liver diseases. Hepatology. 2005;42:5-13.
Available:http://dx.doi.org/10.1002/hep.20750
5. Simonyan AA, Margaryan AS, Hovnanyan KO, Asatryan RG, Hovnanyan MK. Effect of antioxidants on white rats with liver intoxication induced by carbon tetrachloride: Ultrastructural

analysis. Proceedings of the International Symposium under the Aegis of UNESCO "Problems of Biochemistry, Molecular and Radiation Biology and Genetics", Yerevan. 2007;74-75.
6. Taub R. Liver regeneration: From myth to mechanism. Nat Rev Mol Cell Biol. 2004;5(10):836–847.
7. Fausto N, Campbell JS, Riehle KJ. Liver regeneration. Hepatology. 2006;43(2 Suppl 1):S45–S53.
8. Riehle KJ, Dan YY, Campbell JS, Fausto N. New concepts in liver regeneration. Journal of Gastroenterology and Hepatology. 2011;26:203-212.
9. Craciun C, Ardelan A, Ciobanu C, Rusu MA, Puica C, Tamas M, Craciun V. Structuralfuntional studies regarding the effect of *Berberia vulgaris* extract on rat intoxicated liver. Proceedings of 13th European Microscopy Congress, Antwerp. 2004;3:463-464.
10. Sabatini DD, Bensch K, Barnett RJ. Cytochemistry and electron microscopy—The preservation of cellular ultrastructure and enzymatic activity by aldehyde fixation. The Journal of Cell Biology. 1963;17:19-58.
11. Venable JH, Coggeshall R. A simplified lead citrate stain for use in electron microscopy. The Journal of Cell Biology. 1965;25:407-408.
Available:http://dx.doi.org/10.1083/jcb.25.2.407
12. Sarkisov DS. Regeneration and its clinical significance. Medicine. 1970;281.

Biography of author(s)

Karlen Hovnanyan
Scintific and Technological Center of Organic and Pharmaceutical Chemistry, National Academy of Sciences, Republic of Armenia

Research and Academic Experience: Academic Experience Pathohistology and Pharmacia
Senior Staff Researcher of Electron Microscopy

Research Area: Morphology, cytology, microbiology

Number of Published papers: 205

Special Award (If any): Rudolf Virchow Medal of European Academy Sciences,

Any other remarkable point(s): He then joined the Department anatomy of pathogens microorganism (electron microscopy) at the Institute Epidemiology and Microbiology AMS name N. F. Hamaleya (Moscow). Institute Epidemiology and Virology of MS Republic of Armenia, Institute Molbiology of NAS RA, President of Armenian Electron Microsopy.

© Copyright (2020): Author(s). The licensee is the publisher (Book Publisher International).

DISCLAIMER
This chapter is an extended version of the article published by the same author(s) in the following journal.
Journal of Biophysical Chemistry, 5(1): 1-4, 2014.

London Tarakeswar

Registered offices
India: Guest House Road, Street no - 1/6, Hooghly, West Bengal, PIN-712410, India, Corp. Firm Registration Number: L77527, Tele: +91 8617752708, Email: contact@sciencedomain.org, (Headquarters)
UK: Third Floor, 207 Regent Street, London, W1B 3HH, UK
Fax: +44 20-3031-1429 Email: contact@sciencedomain.org, (Branch office)